GeoFocus volume 17

Cécile BONNET

Interactions between tectonics and surface processes in the Alpine foreland: Insights from analogue model and analysis of recent faulting

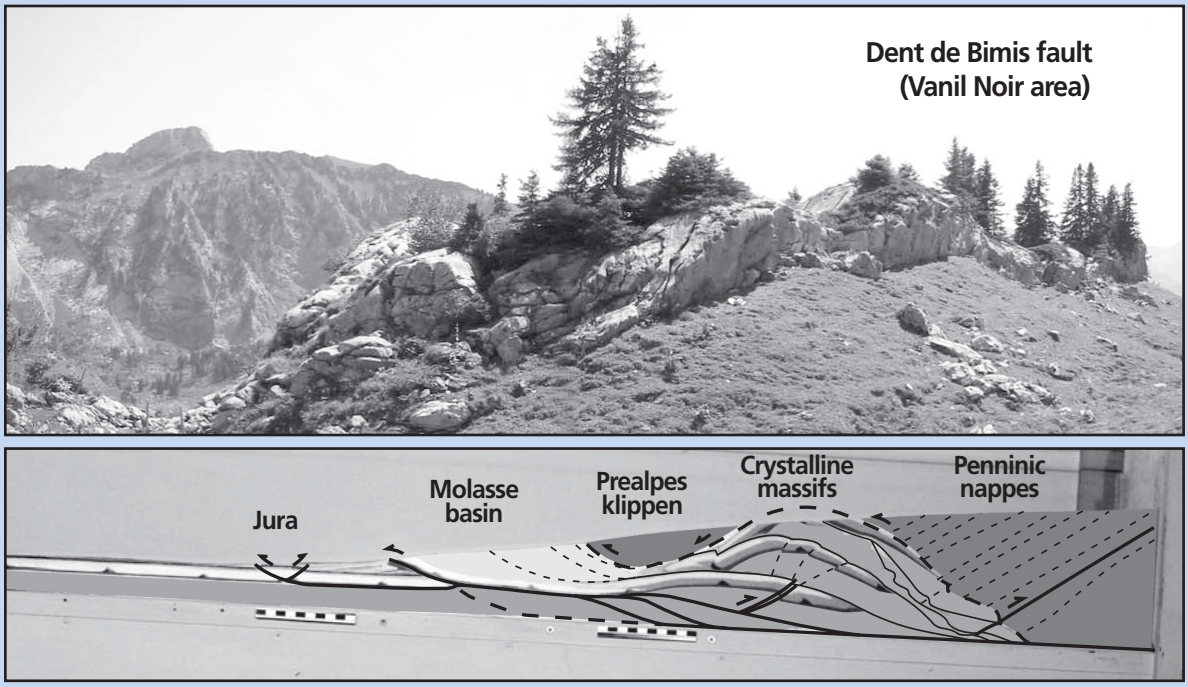

Département de Géosciences, Géologie et Paléontologie, Université de Fribourg (Suisse)

Département de Géosciences – Géologie et Paléontologie
Université de Fribourg (Suisse)

Interactions between tectonics and surface processes in the Alpine foreland: Insights from analogue model and analysis of recent faulting

Thèse

présentée à la Faculté des Sciences de l'Université de Fribourg (Suisse)
pour l'obtention du grade de *Doctor rerum naturalium*

Cécile BONNET

de Villecerf, France

Thèse N° 1551

Multiprint, Fribourg, 2007

Acceptée par la Faculté des Sciences de l'Université de Fribourg (Suisse)
sur la proposition de:

Dr. Jon MOSAR	Université de Fribourg (Suisse)	Directeur
Dr. Jacques MALAVIEILLE	Université de Montpellier (France)	Co-directeur
Prof. Maurice BRUNEL	Université de Montpellier (France)	Expert
Prof. André STRASSER	Université de Fribourg (Suisse)	Président du Jury

Fribourg, le 02 février 2007

Le Doyen:

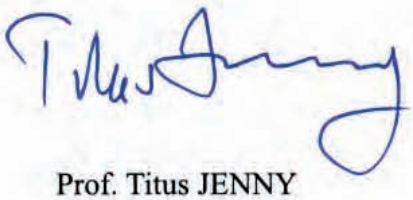

Prof. Titus JENNY

Directeur de thèse:

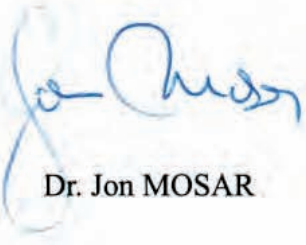

Dr. Jon MOSAR

Co-directeur de thèse:

Dr. Jacques MALAVIEILLE

A la mémoire de Martin Burkhard

CONTENTS

*****

ABSTRACT

To study the dynamics of an orogen-foreland system and more particularly the impact of surface processes on its development, we base our work on two main axes. In a first part, using analogue tapered wedge models, we investigate the interplay between tectonics, erosion and sedimentation during the orogenic growth. The basis model mimics the evolution of a wedge section extending from the orogen to its foreland basin, with both the structural and the lithological heritages simulated. In a second part, the focus is on the recent tectonic and geomorphologic processes affecting the Swiss Prealpes klippen belt and surrounding structural units (Molasse Basin and Jura fold-and-thrust belt). Remote sensing analyses allow to evaluate the impact of tectonics on the drainage pattern and landscape morphology. In addition, local field investigations in the Prealpes provide information on the nature and kinematic of brittle fractures and the paleostress fields.

Insights from analogue modeling

The series of seventeen analogue model experiments is based on a section across the north-western Alpine wedge and foreland basin. This type of analogue model obeys to the dynamics of a tapered wedge and the structures produced are determined by the wedge mechanics. The orogen grows by incremental step of shortening, while outside processes such as erosion and sedimentation may influence the criticality of the taper. This is the case in the last six experiments, where erosion and sedimentation are manually performed in varying rates. These experiments are studied in detail and allowed to investigate and quantify: sediment budget, dynamics and timing of development of the orogen and adjacent foreland basin, uplift paths of particles, etc.

The experiments show that two main mechanisms control the orogenic growth: frontal accretion and underplating. In the foreland basin, frontal accretion leads to the development of a foreland thrust belt, while in the hinterland, simple underthrusting and subsequent underplating lead to the formation of an antiformal nappe stack. The foreland basin evolution is mainly towards the front of the orogenic wedge but it differs depending on the amounts of erosion/sedimentation. Its evolution and internal structuring are governed by the wedge mechanics, thought to be the main controlling mechanism in a feedback interaction with surface processes. The basin grows to a threshold width and remains more or less constant during the subsequent evolution. This is possible because some older formed fold-and-thrust units are being eroded out of the record in the trailing part of the basin, while new units grow in its frontal part. During the development of the foreland fold-and-thrust belt, we observe the erosion of entire thrust units of freshly sedimented materials. As these types of events are untraceable in the tectonic and sedimentary record, this process leads to underestimating total shortening obtained from balancing remaining units only.

Our analogue models show the importance of feedback mechanisms of erosion/deposition on the wedge mechanics and the punctuated thrust development, as well as the cyclic behavior of surface processes. The variations in rates of erosion and sedimentation strongly modify the extent, the morphology, and the structure of the constitutive units. The timing of development and the material paths also differ depending on the rates of surface processes in the different models. It appears for instance that particles located in the converging lower plate or in the upper plate show very complex uplift paths related to the different tectonic stages.

The correlation between models and Alpine tectonic cross-sections emphasises the role of erosion and sedimentation on the dynamics and development of the orogen and adjacent Molasse Basin. Along strike changes in the geometry of the orogen can be explained by differences in surface processes. In addition, the main stages in evolution of the foreland basin and hinterland observed on the analogue models can be correlated in time and space with the major tectono-sedimentary events of the Alpine belt. These stages of evolution are for instance corroborated by the nature of pebbles in the Alpine domain which coincide with the Alpine orogenic evolution and timing. Finally, we suggest that flexural basin evolution mechanisms are secondary in the case of the Swiss Alpine Molasse Basin and that the first order basin evolution is governed by the internal mechanics of a tapered wedge type model.

Insights from morphostructural study and stress analysis in the Prealpes

The Prealpes klippen are constituted by a series of allochthonous tectonic klippen located along the northern front of the Swiss and French Alps. Their emplacement onto the Alpine foreland took place in the Early Oligocene (30 Ma). The fracture pattern in the klippen is complex since it is the final result of fold-and-thrust activity, neotectonics and certainly recent tectonics (post-nappe emplacement). To investigate the nature and kinematics of observed fractures in the Prealpes, we performed several types of analyses.

We first used remote sensing to determine the orientations of analysed structures. A morphological study of the area located between the klippen and the Molasse Plateau suggests that the hydrographic network mainly follows both glacial and structural trends. We then analysed locally the fracture and lineament orientations in three study areas located in the Swiss Chablais and in the Western Prealpes Romandes. Among different deformational models applicable to fault systems, the Riedel shear system appears to explain best the variety of obtained fault directions.

In the same three study areas, we investigated in the field the movement on fault planes in order to obtain paleostress orientations. The following chronology is suggested to explain the different deformational structures observed in the Chablais and Western Romandes Prealpes: initial layer parallel shortening, is followed by folding and thrusting with synfolding axial parallel extension generating extensional veins perpendicular to fold axis. Post-folding, local strike-slip components of faults may be observed as well as strike-slip movement reorienting the previously formed vein sets. Finally, during the last stage of deformation, large-scale faults develop, cross-cutting the existing fold-and-thrust structures.

To interpret the local stress fields, while integrating the results from the different datasets, we propose a more regional deformational model that extends from the Prealpes, through the Molasse Plateau to the Jura. The local Riedel shear zones may be combined in a general transcurrent model for the Alpine foreland. In addition, we suggest that the bulk of the brittle deformation in this transcurrent regime is recent and possibly has developed in a tectonic regime coincident with the present day stress field.

Keywords: *Alpine orogenic wedge, analogue modelling, surface processes, foreland basin dynamics, Prealpes klippen, stress analysis, transcurrent faulting, Riedel shear model*

*****

RÉSUMÉ

Afin d'étudier la dynamique d'un système orogène/avant-pays et plus particulièrement l'impact des processus de surface sur son développement, notre travail repose sur deux axes principaux. Dans une première partie, à l'aide de modèles analogiques de prisme d'accrétion, nous analysons les interactions entre la tectonique, l'érosion et la sédimentation au cours de la croissance de l'orogène. Le modèle de base reproduit l'évolution d'une section de prisme, qui s'étend de l'orogène au bassin d'avant-pays, et où les héritages à la fois structural et lithologique sont simulés. Dans une seconde partie, l'accent est mis sur la tectonique récente et les processus géomorphologiques qui affectent la klippe des Préalpes suisses et les unités structurales environnantes (le bassin molassique et le Jura). Des analyses de télédétection permettent d'évaluer l'influence de la tectonique sur le réseau de drainage et la morphologie du paysage. De plus, des analyses de terrain menées localement dans les Préalpes fournissent des informations sur la nature et la cinématique des fractures cassantes et des champs de paléocontraintes.

Apports de la modélisation analogique

Les dix-sept expériences de la série de modélisation analogique se basent sur une coupe à travers la partie nord-ouest du prisme alpin et de son bassin d'avant-pays. Ce type de modèle analogique obéit à la dynamique d'un prisme d'accrétion et les structures développées sont déterminées par la mécanique du prisme. L'orogène croît par incréments de raccourcissement tandis que les processus extérieurs tels que l'érosion et la sédimentation peuvent modifier la pente critique du prisme. C'est le cas dans les six dernières expériences où l'érosion et la sédimentation sont réalisées manuellement, à des taux variables. Ces expériences sont étudiées en détails et permettent d'analyser et de quantifier : le budget sédimentaire, la dynamique et le timing de développement de l'orogène et du bassin d'avant-pays adjacent, les trajets de soulèvement de particules, etc.

Les expériences révèlent que deux mécanismes principaux contrôlent la croissance orogénique : l'accrétion frontale et le sous-placage. Dans le bassin d'avant-pays, l'accrétion frontale conduit au développement d'une chaîne chevauchante d'avant-pays tandis que dans l'arrière-pays, le chevauchement simple et le sous-placage consécutif mènent à la formation d'un empilement antiforme de nappes. L'évolution du bassin d'avant-pays s'effectue principalement vers le front du prisme orogénique mais elle varie en fonction des taux d'érosion et de sédimentation. Son évolution et sa structuration interne sont gouvernées par la mécanique du prisme, considérée comme étant le principal mécanisme de contrôle en lien avec les processus de surface. Le bassin se développe jusqu'à atteindre une largeur seuil puis il conserve une largeur plus ou moins constante pendant la suite de son évolution. Ceci est possible grâce au fait que d'anciennes unités plissées et chevauchantes sont érodées hors de l'enregistrement sédimentaire dans la zone interne du bassin tandis que de nouvelles unités apparaissent dans sa partie frontale. Au cours du développement de la chaîne plissée chevauchante d'avant-pays, nous observons l'érosion d'unités entières de matériel récemment sédimenté. Comme ce type d'évènement ne laisse aucune trace dans l'enregistrement tectonique et sédimentaire, ce processus conduit à sous-estimer le raccourcissement total calculé uniquement à partir des unités équilibrées restantes.

Nos modèles analogiques montrent l'importance de la réponse des mécanismes d'érosion et de sédimentation sur la mécanique du prisme, ainsi que le

développement ponctué des chevauchements tout autant que le comportement cyclique des processus de surface. Les variations des taux d'érosion et de sédimentation modifient fortement l'étendue, la morphologie et la structure des unités constitutives. Le timing de développement et les trajectoires de matière diffèrent également selon les taux des processus de surface dans les différents modèles. Il apparaît par exemple que des particules situées dans la plaque inférieure qui converge, ou dans la plaque supérieure, suivent des trajectoires de soulèvement très complexes liées aux différents stades tectoniques.

La corrélation entre les modèles et des coupes tectoniques des Alpes fait ressortir le rôle de l'érosion et de la sédimentation sur la dynamique et le développement de l'orogène et du bassin molassique adjacent. Le long de l'axe, des changements dans la géométrie de l'orogène peuvent être expliqués par des différences dans les taux des processus de surface. De plus, les principaux stades d'évolution du bassin d'avant-pays ainsi que l'arrière-pays, que l'on observe dans les modèles analogiques, peuvent être corrélés dans le temps et l'espace avec les événements tectono-sédimentaires majeurs de la chaîne alpine. Ces stades d'évolution sont par exemple corroborés par la nature des galets dans le domaine alpin et ils coïncident avec l'évolution et le timing de l'orogène alpin. Pour finir, nous suggérons que les mécanismes flexuraux d'évolution du bassin sont secondaires dans le cas du bassin molassique alpin en Suisse et que l'évolution de premier ordre du bassin est gouvernée par les mécanismes internes d'un modèle de type prisme d'accrétion.

Apports de l'analyse morphostructurale et de l'analyse des contraintes dans les Préalpes

Les Préalpes sont formées par une série de nappes tectoniques allochtones situées le long du front nord des Alpes suisses et françaises. Leur mise en place sur l'avant-pays alpin a eu lieu à l'Oligocène inférieur (30 Ma). Le réseau de fractures dans la klippe est complexe puisqu'il est le résultat final de l'activité de plissement et chevauchement, de la néotectonique et certainement de la tectonique récente (post mise en place de la nappe). Afin d'étudier la nature et la cinématique des fractures observées dans les Préalpes, nous avons réalisé plusieurs types d'analyses.

Nous avons dans un premier temps déterminé les orientations des structures analysées, à l'aide d'outils de télédétection. Une étude morphologique faite sur la zone située entre la klippe et le plateau molassique suggère que le réseau hydrographique suit principalement les orientations héritées d'origines glaciaire et structurale. Nous avons ensuite analysé localement les orientations des fractures et des linéaments dans trois zones d'étude situées dans le Chablais suisse et dans les Préalpes Romandes occidentales. Parmi les différents modèles de déformation applicables aux systèmes de failles, le modèle de cisaillement de Riedel semble expliquer au mieux la variété des directions de failles obtenues.

Dans ces trois zones d'étude, nous avons analysé sur le terrain les mouvements sur les plans de faille afin d'en déduire les orientations des paléocontraintes. La chronologie suivante est proposée pour expliquer les différentes structures de déformation observées dans le Chablais et dans les Préalpes Romandes occidentales : après un raccourcissement initial parallèle aux couches, on a du plissement et du chevauchement auxquels s'associe de l'extension synchrone, parallèle à l'axe de plissement, qui génère des veines d'extension perpendiculaires à l'axe des plis. Localement, des composantes décrochantes post-plissement sont observées sur les failles, ainsi que des mouvements décrochants réorientant les ensembles de veines précédemment formées. Enfin, durant le dernier stade de déformation, des failles à grande échelle se développent, recoupant les structures plissées et chevauchantes existantes.

Afin d'interpréter les champs de contraintes locaux, tout en intégrant les résultats des différents ensembles de données, nous proposons un modèle de déformation plus régional, qui s'étend des Préalpes, à travers le plateau molassique, jusqu'au Jura. Les zones de cisaillement de Riedel locales peuvent être combinées dans un modèle général transcurrent pour l'avant-pays alpin. De plus, nous suggérons que la plupart de la déformation fragile dans ce régime transcurrent est récente et qu'elle a même pu se développer dans un régime tectonique coïncidant avec le champ de contraintes actuel.

Mots-clés : *prisme orogénique alpin, modélisation analogique, processus de surface, dynamique de bassin d'avant-pays, klippe des Préalpes, analyse de contrainte, faille de décrochement, modèle de cisaillement de Riedel*

*****

ZUSAMMENFASSUNG

Um die Dynamik eines Gebirgsvorland-Systems und insbesondere den Einfluss von Oberflächenprozessen auf dessen Entstehung zu studieren, haben wir unsere Arbeit auf zwei Hauptteile ausgerichtet. In einem ersten Teil verwenden wir analoge keilförmige Modelle (Akkretionskeile) um das Wechselspiel zwischen Tektonik, Erosion und Sedimentation während des Orogen-Wachstums zu ermitteln. Das Basismodel ahmt die Evolution der sich vom Gebirge ins Vorlandbecken erstreckenden Keilsektion nach, wobei die strukturellen und lithologischen Eigenschaften simuliert werden. In einem zweiten Teil wird auf die rezenten tektonischen und geomorphologischen Prozesse fokussiert, welche die schweizer Voralpen-Klippen und umgebende Struktureinheiten (Molassebecken und Jurafaltengebirge) beeinträchtigen. Fernerkundungsanalysen erlauben die Evaluation des Einflusses der Tektonik auf Flussnetzwerk und Landschaftsmorphologie. Zusätzlich liefern lokale Feldbeobachtungen in den Voralpen Informationen über die Art und Kinematik von Sprödbrüchen und Paläospannungsfeldern.

Erkenntnisse der Analogmodellierung

Eine Serie von 17 Experimenten zur Analogmodellierung basiert auf einem Querschnitt durch den nordwest-alpinen Keil und das Vorlandbecken. Diese Art von Analogmodellierung gehorcht der Dynamik eines Überschiebungskeils, dessen Zuschnitt durch die internen Mechanismen bestimmt wird. Das Orogen wächst stufenweise durch Verkürzung, wobei externe Prozesse wie Erosion und Sedimentation die Stabilität des Orogenkeils möglicherweise beeinflussen. Dies ist jeweils der Fall in den letzten 6 Experimenten, wo die Erosion und Sedimentation manuell in verschiedenen Mengen durchgeführt wurde. Diese Experimente werden im Detail studiert und erlauben die Untersuchung und Quantifizierung des Sedimentbudgets, der Dynamik und des zeitlichen Verlaufes der Entwicklung des Gebirges und angrenzenden Vorlandbeckens, Sockelimbrikationen, usw.

Die Experimente zeigen, dass zwei Hauptmechanismen das Gebirgswachstum kontrollieren: Frontal-Akkretion und Überschiebung. Im Vorlandbecken führt die Frontal-Akkretion zur Bildung eines Vorland Faltengebirges, während im Hinterland einfache *underthrusting* und anschliessendes *underplating* zur Bildung von antiformalen Decken führen. Die Evolution des Vorlandbeckens erfolgt hauptsächlich in Richtung der Front des Gebirgskeils, ändert sich aber in Abhängigkeit des Verhältnisses von Erosion zu Sedimentation. Die Evolution und interne Struktur wird gesteuert durch die Keilmechanik, welche vermutlich der Hauptkontrollmechanismus in einer rückgekoppelten Wechselwirkung mit Oberflächenprozessen ist. Das Becken bildet sich bis zu einem gewissen Grenzwert und bleibt dann mehr oder weniger konstant während der anschliessenden Entwicklung. Dies ist möglich, weil einige ältere tektonische Einheiten aus dem weiter zurückliegenden Becken erodiert wurden und neue Einheiten im vorderen Teil gewachsen sind. Während der Entwicklung des Vorlandes beobachtet man die Entwicklung neuer, frisch sedimentierter Überschiebungseinheiten. Da diese Art von Ereignissen weder durch tektonische noch sedimentäre Aufzeichnungen verfolgbar sind, führt dieser Prozess zu einer Unterschätzung der totalen Verkürzung, welche durch das ausgeglichene Profile erzielt wurde.

Unser Analogmodell zeigt die Wichtigkeit des Rückkopplungsmechanismus von Erosion/Ablagerung auf den Akkretionskeilmechanismus und punktu-

eller Entwicklung von Überschiebungen, sowie das zyklische Verhalten der Oberflächenprozesse auf. Die Variation der Erosions- und Sedimentationsmenge beeinflussen nachhaltig die Ausdehnung, die Morphologie und die interne Struktur der wichtigsten Einheiten. Der zeitliche Ablauf der Entwicklung und des Materialweges sind ebenfalls abhängig von der Intensität der angewendeten Oberflächenprozesse in den verschiedenen Modellen. So weisen zum Beispiel Teilchen auf der sich nähernden Platte, oder in der oberen Platte, sehr komplexe Aufstiegswege bezüglich verschiedener tektonischer Stadien auf.

Die Übereinstimmung zwischen Modellen und tektonischen Querprofilen der Alpen betonen den Einfluss von Erosion und Sedimentation auf die Dynamik und Entstehung von Gebirgen und deren angrenzenden Molassebecken. Veränderungen in der Geometrie entlang der Achse des Gebirges kann durch Unterschiede der Oberflächenprozesse erklärt werden. Zusätzlich können die im Modell beobachteten Hauptstadien der Evolution des Vorlandbeckens und des Hinterlandes mit den tektonisch-sedimentären Ereignissen der Alpen in Raum und Zeit korreliert werden. Diese Stadien der Evolution werden bestätigt durch die Natur der Gerölle im Alpengebiet, welche sowohl mit der alpinen Gebirgsbildung als auch mit deren zeitlichen Ablauf übereinstimmen. Schliesslich können wir behaupten, dass der gebogene Beckenevolution smechanismus im Fall des alpinen Molassebeckens der Schweiz nur sekundärer Natur ist, und dass die Beckenevolution eher bestimmt wird durch die internen Mechanismen des Akkretionskeils.

Erkenntnisse der morphostrukturellen Untersuchungen und Stressanalysen in den Voralpen

Die Voralpen-Klippen setzen sich zusammen aus Serien von allochthonen tektonischen Klippen, welche sich längs der nördlichen Front der Schweizer und Französischen Alpen erstrecken. Die Platznahme auf dem alpinen Vorland fand im frühen Oligozän (30 Ma) statt. Das Bruchmuster der Klippen ist komplex, da es sich um endgültige Faltungs- und Überschiebungsmechanismen, Neotektonik und mit Sicherheit auch um rezente Tektonik handelt. Um die Eigenschaften und Kinematik der beobachteten Brüche in den Voralpen zu untersuchen, führten wir mehrere Arten von Analysen durch.

Fernerkundungen dienten in einem ersten Schritt zur Bestimmung der Orientierung der analysierten Strukturen. Morphologische Untersuchungen des Gebietes zwischen den Klippen und dem Molassebecken deuten darauf hin, dass das hydrographische Netzwerk hauptsächlich glazialen und strukturellen Richtungen folgt. In einem zweiten Schritt wurden dann die lokalen Bruch- und Lineationsrichtungen in drei verschiedenen Gebieten (Chablais und westliche Voralpen (Vanil Noir, Dent-de-Lys) analysiert. Unter verschiedenster Deformationsmodellen, welche auf Bruchsysteme angewendet werden können, scheint das Riedel Schersystem am besten die Vielfalt der gemessenen Bruchrichtungen zu beschreiben.

In den Selben drei verschiedenen Gebieten wurden im Feld die Bewegungen an den Verwerfungsebenen untersucht um Paleostressorientierungen zu erhalten. Folgende zeitliche Abfolge könnte die verschiedenen beobachteten Deformationsstrukturen im Chablais Gebiet sowie in den westlichen Voralpen erklären: Eine anfängliche parallele Schichtverkürzung wird gefolgt von Faltung und Überschiebungen mit achsenparalleler Extension, was zu Dehnungsvenen senkrecht zur Faltenachse führt. Post-Faltungen (=Nachfaltung) und lokale Blattverschiebungen können beobachtet werden, sowie Scherbruch-Verschiebungen, welche zu einer Neuorientierung der zuvor geformten Venen führt. Schliesslich entstehen in einer letzten Phase der Deformation riesige Verwerfungen, welche die bereits bestehenden Faltungs- und Überschiebungsstrukturen durchqueren.

Um diese lokalen Stressfelder zu interpretieren, schlagen wir ein regionaleres Deformationsmodell vor, welches nebst den Voralpen auch noch das Molassebecken und den Jura mit einbezieht, wobei wir zusätzlich noch die Resultate von verschiedenen Datenbanken verwenden. Die lokalen Riedel-Scherzonen können kombiniert werden in einem allgemeinen *transcurrent* Bruchmodell für das alpine Vorland. Zusätzlich nehmen wir an, dass der Grossteil der Spröddeformationen in diesem *transcurrent* Bruchsystem rezent sind, und sich möglicherweise in einem tektonischen System entwickelt haben, welches mit dem heutigen Stressfeld übereinstimmt.

Schlüsselwörter: *Alpiner Gebirgskeil, Analogmodellierung, Oberflächenprozesse, Dynamik des Vorlandbeckens, Voralpen-Klippen, Spannungsanalyse, transcurrent Bruch, Riedel-Scher Modell*

*****

REMERCIEMENTS

En arrivant au terme de ces quatre années de thèse réalisée en cotutelle entre Fribourg et Montpellier, je tiens à remercier toutes les personnes qui ont contribué de près ou de loin à l'élaboration de ce travail.

En premier lieu, je remercie mon directeur de thèse, Jon Mosar, pour m'avoir proposé de travailler dans cette magnifique région que sont les Préalpes, puis d'avoir accepté avec enthousiasme le volet modélisation analogique de la thèse. Je me souviens encore de ce jour de septembre 2002 où nous avons fait connaissance à la gare de Fribourg, Jon s'éventant avec un carton qui portait mon prénom et moi un peu perdue mais déjà ravie. Merci Jon pour ton aide, ta bonne humeur, pour avoir relu mes nombreuses pages de prose et surtout pour avoir su m'écouter avec attention lorsque j'en ai eu besoin. Je remercie également Jacques Malavieille qui a co-encadré mon travail de recherche et m'a de nouveau permis de disperser du sable dans la salle de modélisation analogique à Montpellier. Si nous avons obtenu aussi rapidement d'aussi bons résultats expérimentaux, c'est sans aucun doute grâce au doigté du modélisateur expérimenté.

Je tiens ensuite à exprimer ma profonde reconnaissance à Christian Caron qui a scrupuleusement veillé au bon déroulement de la thèse, autant du point de vue financier que matériel. Merci de m'avoir offert un poste d'assistante à l'Institut de Géologie grâce auquel j'ai eu autant de plaisir à m'occuper des travaux pratiques de cartographie que de participer aux diverses excursions où tu désignes chaque sommet par son petit nom…

Le volet modélisation analogique de cette thèse se base sur l'excellent travail d'Anna Sommaruga et du regretté Martin Burkhard. Je les remercie tous les deux pour les discussions enrichissantes que nous avons eues et me souviendrai longtemps de la journée de terrain ensoleillée passée à essayer de suivre Martin, en compagnie de quelques autres géologues, dans la région des Diablerets.

Merci à Maurice Brunel et André Strasser, respectivement expert et Président du jury qui m'ont fait le plaisir et l'honneur de juger ce travail.

Merci à Raymond Plancherel, passionnant structuraliste avec qui j'ai beaucoup apprécié de discuter, sur le terrain tout autant qu'à l'université. Merci à Jeroen Smit pour les conseils avisés et les remarques très pertinentes sur mon travail. Merci à Cécile Allanic avec qui je partage de très bons souvenirs d'excursion.

A Montpellier, je remercie toutes les personnes qui m'ont aidée et surtout Stéphane Dominguez, toujours présent et disponible depuis le DEA ainsi que Christian, Nicolas et Julien pour leur aide technique dans le cadre des expériences de modélisation analogique. Merci infiniment aux secrétaires Céline, Nathalie et Marie-France qui ont facilité mes séjours à Montpellier en réglant les divers problèmes rencontrés avec rapidité et une égale gentillesse.

A Fribourg, je remercie toutes les personnes rencontrées au long de ces quatre années. L'équipe de tectonique et notamment Martin Bochud, Luc Braillard et enfin Corinne Saudan, très agréable colocataire de bureau qui m'a fait découvrir le Chablais valaisan; les enseignants (actuels et anciens) de l'institut: Michèle Caron qui m'a accueillie avec toute sa générosité, merci à Bernard Grobéty et Juergen Von Raumer pour leur intérêt scientifique et leurs conseils, et également Jean-Pierre Berger, Elias Samankassou et Silvia Spezzaferri; les doctorants et tout particulièrement Claire (Dame

Blanc) et sa contagieuse résistance patriotique, Katja Von Allmen et Pierre Vonlanthen; l'équipe technique dont Nicole Bruegger, Daniel Cuennet et Christoph Neururer; les anciennes doctorantes Florence Dapples et Claude Colombié; et enfin, les étudiants géologues et géographes et notamment Gianfranco, Riccardo, Stefan, Jean-Pierre, Christina, Daniel, Eva, Sarah, Annick et Patrik.

Une pensée particulière va à mes amis Barbara, Raphaël, Elodie, Nadine, Matthieu, Anne, Christelle, Quentin et Cédric, mes colocataires Yannick et Samba et les taekwondoïstes Luca, Valérie et Song. Merci à Carolina qui m'a fait confiance en me proposant un travail.

Je remercie du fond du cœur ma famille pour son soutien. Et enfin, merci Kuno d'être passé par là avant moi et d'ainsi me comprendre et m'aider… Merci simplement pour ta présence qui m'a été indispensable.

*****

1 - INTRODUCTION

This dissertation is the final result of a four years dual-PhD research performed in the universities of Fribourg (Switzerland) and Montpellier (France). It consists of two distinct parts, both for the subject and the study methods. The first part is a study of analogue modelling that investigates the impact of surface processes (erosion and sedimentation) on an orogenic wedge evolution. The aims of the work, the experimental setup, and the procedure are synthesised in three papers (submitted or to be submitted) that present the different results and discussions obtained. The second part of the dissertation is an investigation of the nature and kinematics of brittle fracturation and paleostress fields in the Prealpes klippen in Switzerland. To better understand the recent processes affecting the prealpine belt, we combined remote sensing analyses (using a Geographic Information System) and fieldwork, in order to interpret the results in a regional stress model. The series of analogue experiments was performed in Montpellier, while the study of the Prealpes klippen was led in Fribourg.

1.1 INSIGHTS FROM ANALOGUE MODELLING

Following the tapered wedge principle, the basis analogue model represents a section of an orogenic wedge, with both the structural and lithological heritages simulated. To investigate the influence of surface processes on the orogenic evolution, the model is submitted to manual erosion and sedimentation during shortening. Indeed, to maintain a critical wedge, the tectonic processes compete with the surface processes. The involved mechanisms are comparable in the model and in Nature since the orogen develops by frontal accretion in the foreland and by underplating in the hinterland. In the first paper, we compared the two-dimensional development of an experiment performed with intermediate conditions of erosion and sedimentation, with a section of the Western Alps. During the experiment, we also studied both the evolution of the sediment budget and the variation in length of the foreland basin. In the second paper, we compared the strongly different evolutions of six experiments performed with variable amounts of erosion and sedimentation. The correlation between models and three Alpine tectonic cross-sections highlights the role of surface processes on the dynamics and development of the orogen and adjacent foreland basin. We finally analysed the complex uplift paths of particles located in the lower and upper plates and linked their trajectories to main tectonic stages. In the third paper, the punctuated cycles of erosion/deposition and the tectonic structures developed in the analogue foreland basin are correlated to the stages of evolution of the Alpine Molasse basin. In the light of this comparison, the pertinence of the flexural basin evolution model usually proposed to explain the development of the Molasse Basin of the Swiss Alps is discussed.

1.2 FRACTURE PATTERNS AND STRESS IN THE PREALPES

The Prealpes klippen belt in Switzerland and France is formed by a series of allochthonous tectonic nappes of which the Prealpes Medianes are the most important. The latter detached from their homeland and were subsequently emplaced into their present position in front of the Helvetic nappes and the External crystalline basements (post-Early Oligocene, 30 Ma).

While the fold-and-thrust development is rather well understood, the more recent tectonic events (neotectonics and present tectonics) remain largely unknown. Besides some suspected reactivation of thrusting, there is also a "general feeling" that brittle faults are due to recent tectonic activity. To investigate the nature and kinematics of fracturation in the Prealpes, we performed different types of analyses (morphologic, fault and lineament orientations and paleostress) in three study areas located in the Swiss Chablais (in collaboration with Corinne Saudan) and in the Western Prealpes Romandes. The results of these analyses are locally interpreted thanks to mechanical models that may be integrated to a regional deformation model implying the different units constitutive of the Alpine foreland.

*****

2 - Interactions between tectonics, erosion and sedimentation during the recent evolution of the Alpine orogen - Analogue modeling insights

Bonnet, C., Malavieille, J., & Mosar, J.

submitted to *Tectonics* (09.2006)

Abstract

Based on a section across the north-western Alpine wedge and foreland basin, analogue modelling is used to investigate the impact of surface processes on the orogenic evolution. The basis model takes into account both structural and lithological heritages of the wedge. During shortening, erosion and sedimentation are performed to maintain a critical wedge. Frontal accretion leads to the development of a foreland thrust belt; underplating leads to the formation of an antiformal nappe stack in the internal zones. Important volumes of analogue materials are eroded out of the geological record which in the case of the Alps suggests that the original lengths and volumes may be underestimated. The foreland basin evolves differently depending on the amounts of erosion/sedimentation. Its evolution and internal structuring is governed by the wedge mechanics, thought to be the main controlling mechanism in the development of the Molasse basin in a feedback interaction with surface processes.

2.1 Introduction and scope of the study

In the Alps, a number of tectonic developments illustrate the importance of the feed-back mechanisms linking surface processes, tectonic processes and structural heritage. A first example is the Molasse foreland basin growing in the northern part of the orogen in response to the development of the mountain belt. The basin does not only reflect the Tertiary history of the Alps but it also influences the mechanics of the wedge during its formation. Indeed, the size of the basin controls the taper of the wedge and consequently the wedge mechanics such as for instance the sequence of thrusting. A second example, farther to the South, is the exhumation of the External Crystalline Massifs. The uplift of these basement units is largely driven by the subduction mechanism but it appears nevertheless that erosion of the overlying Penninic lid controls also the localization, the velocity and magnitude of the exhumation. A last example is the Jura development. It started during the Miocene, because of a major "jump" of the Alpine thrust front by about 100 km towards the North under the Molasse foreland basin. The propagation is due to a combined effect of the structural and lithological heritages of the wedge and a high sedimentation rate. The presence of a large thickness of Molasse deposits in the Alpine foreland allowed the activation as décollement level of the Triassic evaporite layers accumulated at the base of the European cover. These examples of classical Alpine tectonic features show the necessity to study the complex interactions between erosion, sedimentation and tectonics to understand the dynamics of a thrust wedge.

Geodynamics of orogenic wedges has been for a number of years a major subject of study (Davis et al. 1983, Dahlen et al. 1984, Mattauer 1986, Molnar & Lyon-Caen 1988, Willett 1992, Beaumont et al. 1996,

KONSTANTINOVSKAIA & MALAVIEILLE 2005). The case of the Alpine mountain belt is a very well established and documented example of internal dynamics (ESCHER & BEAUMONT 1997). Some studies have focused on the mechanics of the Alpine orogenic wedge (PFIFFNER et al. 2000) and others dealt with the complex interactions between tectonics and surface processes and also their consequences on both the dynamics of the orogenic wedge and the evolution of topography (STORTI & MACCLAY 1995, KOOI & BEAUMONT 1996, SCHLUNEGGER et al. 1997b, SCHLUNEGGER et al. 1998, SCHLUNEGGER 1999, BEAUMONT et al. 2000, KÜHNI & PFIFFNER 2001, SCHLUNEGGER & HINDERER 2001, PERSSON & SOKOUTIS 2002, PFIFFNER et al. 2002, SCHLUNEGGER & HINDERER 2003, CEDERBOM et al. 2004). Indeed, depending on their rates and localization in space and time, erosion and sedimentation modify the morphology and the internal structure of the wedge. Different approaches have been applied to the study of the Alpine orogenic wedge. Geology and geophysics provide a global view of the wedge at a lithospheric scale, but this image is a "snap shot" in time. Numerical and analogue modeling offer the possibility for a complete and direct observation of scaled models simulating geologic features developed over geologic timescales and often in subsurface. Thus, modeling appears to be appropriate to study and quantify dynamically the impact of surface processes on the evolution of the wedge. It allows systematic tests on models varying mechanical and geometrical parameters that are difficult to analyze.

To study the evolution of the Alpine mountain belt and investigate the influence of surface processes on tectonics, a series of scaled analogue experiments has been performed. This type of analogue models obeys the dynamics of a critically tapered wedge and the structures produced inside the wedge are determined by the wedge mechanics. The criticality of the taper may be influenced by outside processes such as erosion and sedimentation. Our experimental approach is new since our models take into account the regional structure of the wedge, in contrast to a number of global and simplified models of the Alps proposed to this day. In our experiments we control geometrical and mechanical boundary conditions and we can vary each study parameter. It allows us to analyze the role and interactions of the initial structures, the rheologies, the erosion and the sedimentation on the Alpine orogenic evolution.

In a first step we test the structural setup, based on a restored section across the Western Alps (BURKHARD & SOMMARUGA 1998). Then the geometries of the developed structures and their evolution in space and time will be linked with the involved tectonic processes and compared with the Alpine development. A semi-quantitative analysis of the experimental sediment budget and its evolution through time are linked to the dynamical framework of the growing wedge. Finally we discuss the interactions between surface processes, structural and lithological heritages and tectonic processes, as well as their feedback on the dynamics of the Alpine wedge.

2.2 THE NW OROGEN-FORELAND BASIN SYSTEM AND MODELING

2.2.1 Geological framework of the NW Alps

After a short summary of the Alpine orogenic history, proceeding for 140 Ma, the cross section of the Western Alps chosen as a reference for the experiments will be presented. The uncertainties and noteworthy points of the structural development along this cross section will also be raised and discussed.

The Alpine evolution has been divided into three main periods, following a history based on the tectono-metamorphic activity and summarized from DAL PIAZ et al. (1972), TRÜMPY (1973, 1980), HUNZIKER et al. (1989), HUNZIKER et al. (1992), STECK & HUNZIKER (1994), ESCHER & BEAUMONT (1997), ESCHER et al. (1997): the *Eoalpine* orogenic events, Cretaceous to Early Paleocene in age (140-60 Ma), the *Mesoalpine* orogenic events, of Late Paleocene to Early Oligocene age (60-30 Ma) and the *Neoalpine* orogenic events, of Late Oligocene and younger age (30-0 Ma).

The *Eoalpine* event started in the Late Jurassic-Early Cretaceous with the south-dipping subduction of the Alpine Tethys and Valais Oceans along the northern margin of Adria (MOSAR et al. 1996, SCHMID et al. 1996, STAMPFLI et al. 1998a, MOSAR 1999). The stacking of Austroalpine nappes probably took place at an early stage of the subduction. The involved materials (basement and cover nappes and pieces of oceanic floor) were strongly deformed and high-pressure mineral assemblages were formed. Following the Eoalpine events, the Late Cretaceous-Early Paleocene phase was characterized by the exhumation and uplift of the whole nappe stack.

The *Mesoalpine* orogenic event caused the deformation of the central part of the Briançonnais and the internal part of the European continental crust by continental subduction to the southeast. This resulted in the formation and stacking of basement nappes. During this process, the Mezosoic cover (forming the main body of the Prealpine cover nappes) was expelled towards the northwest. For this reason, the Prealpine nappes escaped the intense ductile deformation and metamorphism of the basement units. Progressively from the SE to the NW, the basement units (Mont Chetif, X-basement-Gotthard and Mont Blanc-Aar nappes) started to take shape and their corresponding cover nappes were individualized. The tectonic inversion of previous normal faults played a major role during this event. At the end of the Mesoalpine period, the internal European crustal units were thrust by tectonic Underplating below the external Briançonnais ones. Simultaneously, the first Helvetic nappes began to take shape.

The *Neoalpine* orogenic event started around 30 Ma ago. Probably due to the addition of frontal imbricates, the originally shallow SE dipping thrusts in the nappe stack became progressively steepened to reach finally subvertical to overturned dips. This verticalisation triggered the development of intensive S and SE-vergent backfolding and backthrusting together with dextral strike-slip movements in the more internal part of the Western Alps. The northwest and southeast movements produced a generalized uplift, exhumation (retrograde metamorphism) and erosion with deposition of Molasse sediments in peripheral foredeep basins. The onset of large-scale S- to SE-vergent movements, combined with a continuing NW-vergent ductile shearing, initiated the present wedge shape of the Western Alps.

2.2.2 Experimental setup: geological constraints given on models by the restored cross section of the NW Alps

The framework of the experimental study is based on a transversal section across the Western Alps (Fig. 2.1A) (Burkhard & Sommaruga 1998) that extends from Besançon in the NW to Torino in the SE (Schmid et al. 2004). This transect (Fig. 2.1B) provides the maximal extension of the Penninic lid, composed by the Penninic Nappes and the Prealpes klippen. The uplift of the External Crystalline basement Massifs isolated the Prealpes klippen from their homeland, the Penninic nappes further South. Following to the North are the Molasse foreland basin and the Jura fold-and-thrust belt which reflect the more recent developments of the Alpine orogenic wedge. The section provides a solid basis for modeling since the structures are very well constrained in terms of stratigraphy, geometry and ages.

Along this transect, a present day cross section (Fig. 2.1B) based on seismic-reflexion profiles (Sommaruga 1997), surface-geology and thrust-system considerations has been elaborated (Burkhard & Sommaruga 1998). As underlined by the authors, the description of the characteristic units and evolutionary steps of the North Alpine Molasse basin fits perfectly with the idealized foredeep as proposed by Bally (1989). (1) A crystalline basement is dipping gently from the foreland toward the orogen. (2) Localized grabens filled with Carboniferous and Permian clastics, are considered by the majority of Alpine authors as the last expression of the Variscan orogeny. (3) A passive margin series deposited at the southern margin of the European plate above a major "post-Variscan" erosional unconformity is constituted by Middle Triassic to Upper Cretaceous shallow-marine carbonates. It includes the future Jura, Molasse, "Autochthonous" and Helvetic domains and has a total thickness varying from 1 to 2.5 km (Wildi et al. 1991, Loup 1992). (4) Tertiary clastic wedges are deposited above a well developed foreland unconformity which can be traced from the external Jura southward into the most internal Helvetic domain (Boyer & Elliott 1982, Herb 1988, Homewood et al. 1989). (5) The lateral continuity between Helvetic and Molasse parts of the foreland basin has been obscured by incorporation into the evolving orogenic prism. The tectonic activity progressively advanced from the internal parts toward the northwest including Penninic, Helvetic and Subalpine Molasse thrust systems (Pfiffner 1986, Burkhard 1988).

From the present day balanced cross section, Burkhard & Sommaruga (1998) reconstituted the recent history of the orogen (i.e. from Eocene to Present) (Fig. 2.1C). As the structural and lithological heritages play a major role on the kinematics of the belt, the tectonic and stratigraphic features involved in the Alpine development are taken into account in the experimental set up. To better understand the influence of the heritages along this section, we will detail the relevant points of the Western Alps evolution since the Middle Eocene (46 Ma), starting point of the "Neogene orogeny" (Trümpy 1973).

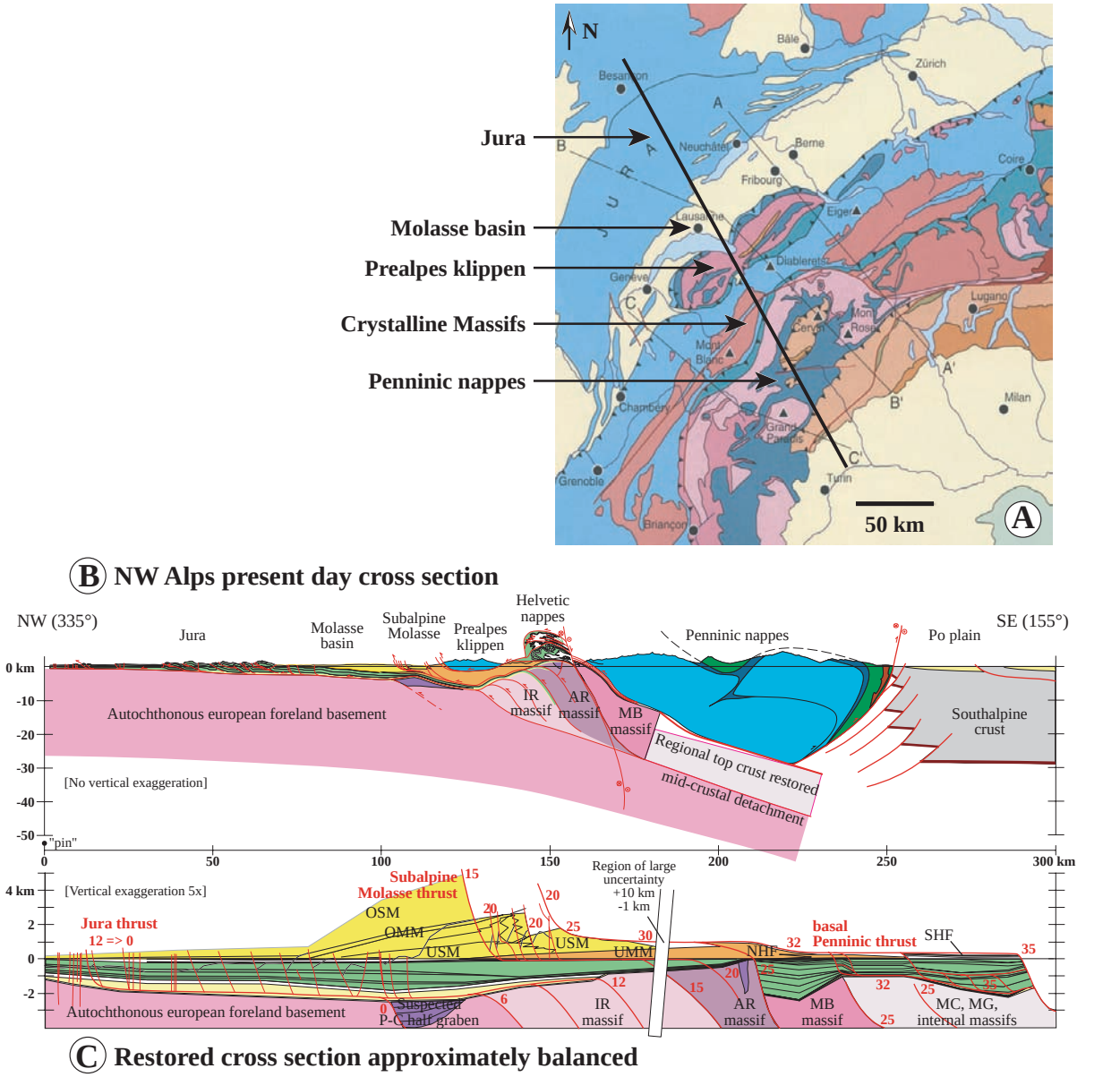

Fig. 2.1 *Location map and transverse section across the NW Alps used as experimental basis model, A) location of the section and succession of structural units on a tectonic map of the Alps (*Schmid *et al. 2004), B) Present-day cross section across the NW Alps (modified after* Burkhard & Sommaruga *1998) showing the converging European plate made of successive basement units (various shades of pink) and their Mesozoic cover (light yellow and green) and the Apulian upper plate mainly made of Penninic nappes (blue) from which the Prealpes klippen are detached, C) restored cross section approximately balanced (modified after* Burkhard & Sommaruga *1998) showing the prestructured basement units (various shades of pink) and sedimentary basins of the Helvetic domain (green), the weak layer of Triassic evaporites at the base of the cover (light yellow), the estimated volumes of overlying Molasse deposits (orange and yellow) and the basal Penninic thrust (red) at the base of the overriding lid. Relative timing of thrusting is indicated by red numbers (in Ma). SHF and NHF = respectively South and North Helvetic Flysch, UMM = Lower marine Molasse, USM = Lower freshwater Molasse, OMM = Upper marine Molasse, OSM = Upper freshwater Molasse, IR = Infra-Rouges massif, AR = Aiguilles Rouges massif, MB = Mont-Blanc massif, MC = Mont-Chetif, MG = Mont-Gotthard.*

Following the closure and subduction of the Alpine ocean, an aerial orogeny developed due to the continental subduction of the European plate under the Apulia/Adria plate (Schmid et al. 1996, Escher et al. 1997, Stampfli et al. 1998a). In the late Eocene (*c*. 40 Ma), the foreland sedimentation started in the most internal (Helvetic) domain with a shallow (<600 m deep) and narrow (<100 km wide) underfilled trough before being covered by the rapidly advancing Penninic (including Ultrahelvetic) thrust front (Burkhard & Sommaruga 1998). In the latest Eocene (*c*. 40 to 30 Ma), the thrust front and the "pinch-out" (Fig. 2.1) advanced very

quickly northwestward and the basin grew slightly to about 100 km. In the early Oligocene (*c*. 30 to 22 Ma), both thrust front and "pinch-out" migrated at the same decreased rate, maintaining constant the basin width. At this time interval, the basin (UMM and USM sediments) underwent a definitive transition from underfilled to overfilled since the increased total subsidence is totally compensated by sedimentation (Burkhard & Sommaruga 1998). The crystalline basement units started also to take shape, strongly influenced by the tectonic inversion of previous normal faults (Escher et al. 1997). From 22 to 12 Ma, the thrust front seemed to be in a fixed position southeast of Lausanne. The lack of information concerning this period is due to the fact that corresponding sediments (OSM) have been removed by erosion. Some distal erosional remnants in Jura synclines as well as the degree of burial below younger Molasse series (Schegg 1994, Schegg et al. 1997, Cederbom et al. 2004) testify to a strong ongoing subsidence trend with probably more than 2.5 km of Upper freshwater Molasse (OSM) deposited in the Lausanne area (Burkhard & Sommaruga 1998). Thrusting may have taken place within the Subalpine Molasse zone at this time interval. Fission tracks determinations (Schaer et al. 1975, Hurford 1986, Burkhard 1990) indicate that the uplift of the Central Alps must have started in the early Miocene at a time, when the Molasse basin was still subsiding. Burkhard (1990) proposes also that the steepening (backfolding) of this area is older than 15 Ma because of a lack of a discontinuity in the paleo-isotherm pattern across the steep Helvetic "root zone". An important consequence is that during the thrusting of the Jura, there exists already an Aar massif culmination that has about half its present amplitude. The décollement in the Triassic evaporites plays a major role for the development of the thin skin frontal fold-and-thrust belt of the Jura. Cenozoic and Mesozoic series of the Western Swiss Molasse basin and the Jura fold belt have been severely deformed over this main décollement zone (Burkhard & Sommaruga 1998). Seismic-reflexion lines and drill holes show that the thickness of the evaporitic cushion varies from 0.5 to 1.4 km. The onset of main Jura deformation is generally proposed to start in the Late Miocene, after the Serravalian (Naef et al. 1985, Laubscher 1987, Burkhard 1990, Laubscher 1992) and apparently put a halt to the subsidence history of the Molasse basin (Burkhard & Sommaruga 1998). Conversely, the end of deformation is still debated: the Jura tectonic activity would have ended in the Tortonian (Laubscher 1987), or the Jura folding and thrusting could still going on today (Naef et al. 1985). The development of the Jura belt is still debated too. The first assumption (Laubscher 1973, Boyer & Elliott 1982), called "Fernschub theory", involves a distant push from the Alps by which the Jura and Molasse displace and deform (thin skinned thrusting and associated folding) over a basal décollement horizon (Philippe et al. 1996). The second theory (Aubert 1945, Pavoni 1961, Rigassi 1962, Wegmann 1963, Ziegler 1982), reinforced by seismic data and neotectonics (Guellec et al. 1990, Gorin et al. 1993, Pfiffner 1994, Signer & Gorin 1995, Pfiffner et al. 1997d) presents the autochthonous folding of the Jura cover as a consequence of basement thrusting and/or wrench-faulting. More recently, some authors (Mosar 1999, Lacombe & Mouthereau 2002) proposed a compromise between these two end member hypothesis to explain the tectonic evolution of the Molasse Basin-Jura Mountains system. For them, the most probable mechanism comprises both thin-skinned tectonics along a basal décollement within the Triassic evaporites and basement involvement possibly along a deeper detachment. The latter accounts for inversion of underlying Permo-Carboniferous and accommodates stacking of basement thrust units beneath the External Crystalline Massifs (Lacombe & Mouthereau 2002). In this model, the involvement of the crystalline basement began recently in the outermost parts of the Alpine foreland thrust belt, either during the latest stage of frontal thin-skinned thrusting or just after it ceased. The geodynamic development of the Alpine foreland has been continuous through time and goes on consequently at the present day.

A noteworthy point in the Alpine foreland development is the unusual evolutionary sequence of folds from the Molasse Basin to the External Jura. It is often admitted that fold and thrust belts evolve by progressive "in-sequence" deformation from the hinterland to the foreland (Bally et al. 1966, Dahlen et al. 1984). While the folds beneath the Molasse basin are located in a more internal position of the Alpine foreland belt than the Jura folds, they represent typically early stage buckle folds and their Triassic cores seem to be filled with well-organized evaporite duplexes. An explanation is the load of the Tertiary sediments, which prevented the Molasse basin buckle folds to further evolve into thrust-related folds (Burkhard & Sommaruga 1998, Sommaruga 1999).

Uncertainties remain as to the detailed geometry of the structures below the Prealpes klippen in Western Switzerland. They are at the origin of the previously detailed theories proposed to explain the tectonic evolution of the Jura fold-and-thrust belt and the

Molasse Basin. Indeed, despite the results of the deep seismic-reflection campaign of the Swiss NRP20 program (Mosar et al. 1996, Pfiffner et al. 1997a) there remains some ambiguity in the interpretation of individual reflectors and even first order features (Burkhard & Sommaruga 1998). These uncertainties concern especially the basement structure and the thickness of Molasse in the alpine foreland for which different solutions have been proposed. The large discrepancies between models with a moderate thickness of autochthonous and subalpine Molasse and a rather shallow depth for the basal décollement of the Prealpes (Mosar 1999) and models with an important thickness of Molasse and a deeply rooted basal décollement of the Prealpes (Escher et al. 1997, Burkhard & Sommaruga 1998) are related to the interpretation of surface and subsurface geology. Projecting fold axes over long distances into a section of the Rhône valley results in a deep synformal structure beneath the trailing Prealpes linked to a plunging antiform in the frontal part of the nappe stack. Using structural evidence from the Prealpes in the near vicinity of the Rhone valley and information from drill hole data lead to the conclusion that the basal décollement of the Prealpes is shallow and rather flat. Based on different types of seismic data it is suggested that the basement rises to form a structural high beneath the western Prealpes Romandes (Switzerland) and the eastern Chablais Prealpes (Switzerland and France) (Mosar 1999). Seismic lines show a possible inversion of a Permo-Carboniferous graben beneath the transition from the Molasse to the Prealpes klippen (Subalpine flysch) in the Rhône valley area (Gorin et al. 1993, Sommaruga 1997, Burkhard & Sommaruga 1998, Sommaruga 1999). In the western Prealpes romandes and the Chablais Prealpes the basal décollement surface shows important changes in depth along strike of the regional fold and thrust trend, rising for example from a depth of -1 km NE of Montreux to an altitude of +1 km near the northern shores of Lake Leman. This type of basement high, the earthquake activity, and an uplift rate higher than surrounding areas, have been explained by the development of a new thrust in the European basement below the frontal Prealpes (Mosar et al. 1996, Mosar 1997). Its formation postdates the development of the other structures and is thus post-Oligocene (Mosar 1999).

2.2.3 Apparatus and experimental procedure

A number of analogue modeling investigations using granular materials have shown the similarity between deformation in model wedges and structures observed in fold-and-thrust belts and/or submarine accretionary wedges (e.g., Davis et al. 1983, Malavieille 1984). Subsequent studies have been led to systematically investigate the role of main experimental parameters such as for instance basal friction, layer thickness, sediment rheology, brittle-ductile coupling, relative strength of the backstop material, taper geometries and ratio of sediment input to output (non exhaustive list of publications: Byrne et al. 1988, Mulugeta 1988, Liu et al. 1992, Lallemand et al. 1994, Storti & MacClay 1995, Gutscher et al. 1998a, 1998b, Cobbold et al. 2001, Persson & Sokoutis 2002, Smit et al. 2003, Konstantinovskaia & Malavieille 2005). Our original study investigates the structural evolution of a section across the Western Alpine accretionary wedge, under given experimental conditions of erosion / sedimentation, taking into account the regional structure of the wedge. The experimental setup of our analogue model is constrained by the restored section proposed by Burkhard & Sommaruga (1998). While we test the structural setup, we may compare the experimental evolution to the Alpine wedge evolution. The 2-dimensional model cross section provides a live observation of phenomena such as for instance subduction, thrust propagation, uplift/exhumation and folding.

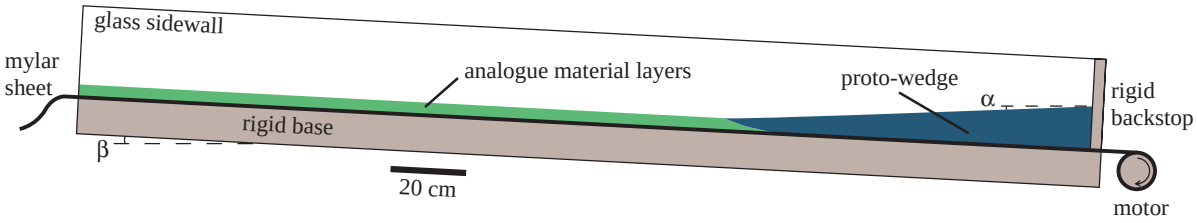

Fig. 2.2 *Experimental sandbox device and basis set up simulating the development of a foreland basin in front of a growing orogen, based on a Coulomb wedge model (on the scheme, surface (α) deeps 2° to the left, and base (β) 3° to the right, corresponding respectively to 2° to the N and 3° to the S in an Alpine setting). Prestructured analogue materials are pulled on a Mylar sheet against a rigid backstop leading to the development of a thrust wedge.*

The experiments were performed under normal gravity in a classical sandbox device, close to the set up elaborated by MALAVIEILLE (1984). The device (Fig. 2.2) is formed by a flat basal plate bound by two lateral glass walls. A motor pulls on the plate a 10 cm wide Mylar sheet with a rough surface simulating a high basal friction. Analogue materials are deposited on the sheet to fit the succession of units present on the restored cross section of the Western Alps. The shortening leads to the development of the analogue thrust wedge against a rigid backstop, with no subduction window at its base. Replaced in the Alpine setting, the layers of analogue materials mimic the subducting European plate, while the proto-wedge represents the Penninic lid that will be deformed against the rigid backstop simulating the strong lithosphere of the Apulian upper plate. Cohesion and size are scaled with a factor of 10^5 (for scaling and characterization of model materials see also LALLEMAND et al. 1994, GUTSCHER et al. 1996, GUTSCHER et al. 1998a, KUKOWSKI et al. 2002; for additional references see LOHRMANN et al. 2003). To maintain a compromise between a maximal experimental shortening and an appropriate visualization of the developed structures, the vertical scale is 2.5 times exaggerated in the experiment. For the vertical scale, 1 cm in our experiment is roughly equivalent to 1 km in nature and for the horizontal one, 1 cm corresponds to 2.5 km. The length of the basal plate (about 2.80 m) offers a maximum convergence of 160 cm that corresponds to 60% of shortening or about 400 km at the natural convergent orogenic wedge scale. One camera records all stages of the experiment allowing structural interpretations and semi-quantitative analysis to be made.

We wish to insist on the fact that our approach restricts to a first order study. The initial state and boundary conditions of this simulation of the Alpine setting and development remain approximate. The "critical wedge" theory (DAVIS et al. 1983, DAHLEN 1984, DAHLEN et al. 1984) predicts that the geometry of a growing wedge (defined by its surface slope α and its basal slope β) is a function of the material strength and the basal friction. Deformation in accretionary wedges (with negligible cohesion) is consequently scale independent. As orogens are on the verge of gravitational failure (DAVIS et al. 1983), they adopt a distinct geometry with a low-tapered pro-wedge facing the subduction plate, and a high-tapered retro-side (WILLETT et al. 1993). The model Coulomb wedge used in the experiments (Fig. 2.2) presents the geometry of the Alpine proto-wedge proposed in cross sections of the literature (MOSAR 1999, LACOMBE & MOUTHEREAU 2002): the surface of the wedge (α) deeps 2° to the North and the base (β) 3° to the South, which corresponds to the dip of the subducting European plate. The easiest solution to simulate the basal dip was to incline the experimental device which is a major simplification since we do not consider lithospheric flexure. The behavior of the deep ductile part of the crust was not considered here since only its upper part is involved in the deformation. Indeed, as can be seen on most deep seismic-reflection profiles crossing the Alps (GUELLEC et al. 1990, MUGNIER et al. 1990, PFIFFNER et al. 1990), a mid-crustal detachment level is located above the well-layered lower crust (BURKHARD & SOMMARUGA 1998).

The analogue materials have frictional properties satisfying the Coulomb theory (DAVIS et al. 1983, DAHLEN 1984, DAHLEN et al. 1984) and they mimic a non-linear deformation behavior of crustal rocks in the brittle field (LOHRMANN et al. 2003). The three kinds of used materials (sand, silica powder and glass beads) are chosen for their contrasted behaviors and are employed both mixed and separately to fit the behavior of the different Alpine units. The aeolian sand used in this study is rounded with a grain size of 200 to 315 μm and a density of 1690 kg/m^3. The internal coefficient of friction is 0.57 and the cohesion Co = 20 Pa. Décollement levels are created by introducing in the model some layers of glass beads with a grain size between 50 and 105 μm. They are a Coulomb material and their density is almost the same as that of dry sand. However due to their close to perfect roundness their coefficient of internal friction is about 23% smaller (0.44), with cohesion almost negligible. Resistant layers in the models are made of pure dry silica powder or of a mix with sand. Silica powder has a significantly higher cohesion (150 Pa) than sprinkled sand (20 Pa) and may simulate stronger (resistant) material. The solid units, i.e. the orogenic lid and the basement units (Fig. 2.3), are a very cohesive mix of silica powder and sand in variable proportions. The overriding lid is a homogeneous unit that represents mainly the Penninic. Indeed, as the lid is passively transported and eroded, its internal structure does not seem to play a role in the tectonic development of the wedge. Consequently, we did not judge necessary to discern the Penninic cover from its basement. The different crystalline units simulate from left to right, i.e. from NW to SE, the Autochthonous European foreland basement, the "Infra-Rouges", Aiguilles Rouges, Mont-Blanc and Mont-Chétif, Gotthard massifs. In contrast, the more "deformable" cover units are composed of sprinkled sand only. The surficial layer

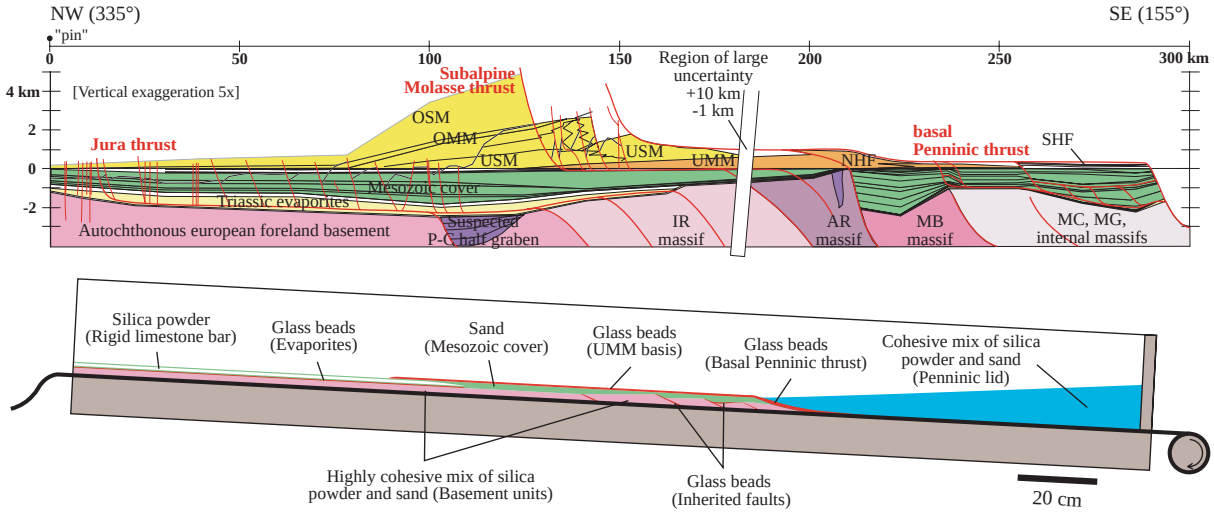

Fig. 2.3 *Structural setup based on the restored section across the Western Alps by* Burkhard & Sommaruga *(1998) (see additional legends Fig. 2.1). On the right side, the upper plate represented by a homogeneous solid lid (blue) will override on a basal thrust (red) the lower plate constituted by a succession of solid basement units (pink) and their more "deformable" cover (green), both prestructured by inherited faults (red). A rigid layer (white) located in the core of the cover mimics a calcareous horizon and is underlined by a weak level (red) simulating evaporites at the base of the Mesozoic cover.*

(Fig. 2.3) corresponding to the Mesozoic cover of the European margin is constituted from North to South by the Jura, the Autochthonous, the Helvetics and the Ultrahelvetics. In the core of the cover layer, a level of cohesive pure silica powder (Fig. 2.3) simulates a rigid calcareous horizon (Tithonian limestones of the Jura). Thin (< 2 mm) layers of glass beads are employed as weak zones (inherited faults) or décollement levels in the series. For instance the basal layer of basement units is pre-cut by thin levels of glass beads to model the inherited normal faults deeping South and bordering the basement units (Fig. 2.3). In our experiment, these décollement levels play as reverse faults, as in the Alpine orogen. Another glass bead layer is placed at the base of the sand, under the pure silica powder level (Fig. 2.3). It mimics the Triassic evaporites that behave as décollement level for the cover during the shortening. The last thick (< 8 mm) décollement level of glass beads allows the orogenic lid to override the basement and cover units (Fig. 2.3). It corresponds to the basal Penninic thrust followed to the North by the base of the first marine Molasse deposits (UMM).

The most important characteristic of our series of analogue modeling experiments is the simulation of the regional structure of the wedge. At the initial stage, the basis model is constituted by defined units inherited from the former complex evolution of the orogen. The structural heritage is both tectonic with faults of inherited basins that can be reactivated as reverse faults and stratigraphic with the succession of contrasted lithologies.

While descriptions and estimates of the post-collisional sediment budget history of the western and central parts of the Alps have been proposed by some authors (Kuhlemann 2000, Kuhlemann et al. 2001, Kuhlemann et al. 2002, Kuhlemann & Kempf 2002), we decided not to impose given rates of erosion and sedimentation in our experiments. Our aim was rather to favour a tectonic control for the rates and localization of erosion and sedimentation. In the models, surface processes were imposed to keep the mechanical equilibrium of the wedge, i.e. we eroded and deposited sediments to maintain a constant slope of the wedge during shortening. We considered that the Alpine orogenic wedge obeys at a first order to simple diffusion laws of erosion and sedimentation and we applied constant erosion on the units independently of their lithological nature. Yet at a large timescale, we were careful to obtain realistic rates of erosion and sedimentation. For instance, at the end of the experiment, the deposited volumes still in the geological record constitute 10% to 20% of the eroded volumes, as proposed in the literature (Kuhlemann op. cit.). The scaled volumes of analogue materials involved in the sediment budget history may be then directly compared to the values proposed for the Alpine sediment budget.

2.3 EXPERIMENTAL RESULTS

In the framework of this study, we performed a series of sixteen experiments. The ten first led to the satisfying basis model presented previously (Fig. 2.3). We varied unit's lengths, angles, rheologies and localization of décollement levels to constrain the geometry and mechanical behavior of the different tectonic units and depositional realms. In the last six experiments, we varied the rates of sedimentation and erosion to better understand the influence of surface processes on the evolution of a mountain belt. In the following, we describe the evolution of one of these last experiments, for which the imposed conditions of erosion and sedimentation led to a two-dimensional development fitting the most properly the geometry proposed of the studied cross section of the Western Alps.

To simplify the description of the experiment, we chose to express the displacement of the subducting plate in terms of time increments. The 152 cm of subducting plate convergence in the model, corresponding to 380 km of natural displacement of the European plate, are performed between the time increments t_0 and t_{38}. The key stages of the tectonic evolution are presented (Fig. 2.4) with the structural interpretation draped on the pictures.

The rates and localization of erosion and sedimentation vary during the experiment in response to the tectonic development of the model. To simulate the submarine episode of the orogen before continental subduction, the initial stage of the experiment (t_0 to t_5) was achieved with no erosion/sedimentation. Then the orogen becomes aerial (t_6) and until the end of the experiment, we erode analogue materials and deposit sand so as to maintain the mechanical equilibrium of the wedge. Erosion is performed to preserve the initial slope of the wedge, both on the lid and on the recently deposited foreland sediments. Simultaneously in the foreland, the successive layers of sedimentary filling are added to obtain the equilibrium profile.

From the beginning, the mechanism of model shortening leads to the climb of the lid onto the top of the basement ramp. The geometrical response is a continuous and marked internal deformation of the lid due to retrothrusting (t_{10} Fig. 2.4). The nucleation of retrothrusts takes place at the transition from flat to ramp of the basal thrust of the lid. Backthrusts are active as long as they are located on this mobile transition point. They are then passively displaced on the top of the ramp, becoming inactive (t_{16} Fig. 2.4). At an advanced stage of the experiment (t_{29} Fig. 2.4), we may notice that some ancient retrothrusts are reworked by new ones generated at a transition from flat to ramp inside the basement units.

The displacement of the orogenic front is first accommodated by several small thrust slices in the foreland sediments, very close of the lid (t_{10} Fig. 2.4). The deformation is then propagated to the foreland (t_{13} Fig. 2.4) due to the activation of the décollement level, simulated by a glass bead layer at the base of the foreland basin. The displacement of the orogenic front is accommodated by retrothrusting and a piggy back basin grows in the rear of the frontal pop up structure (t_{16} Fig. 2.4). To maintain a constant slope of the lid, we filled this basin with sand.

From the stage t_{16} (Fig. 2.4), the structural heritage controls the deformation of the subducting plate. The different décollement weaknesses, simulating the inherited normal faults and surrounding basins, are activated as reverse faults in the basement units. These faults propagate across the basal décollement level and appear at the surface as a succession of foreland sediment slices. Then the basement imbricates thrust each other according to a process called underplating (t_{23} Fig. 2.4). This mechanism allows material of the lower-subducting plate to be accreted into the upper plate (PLATT 1986, GUTSCHER et al. 1996, KUKOWSKI et al. 2002).

At stage t_{29} (Fig. 2.4), the homogeneous part of basement of the subducting plate is spontaneously underplated, following the evolution of the pre-structured basement units. The resulting thrust affects both the sedimentary cover and the overlying foreland sediments. It initiates a fold-and-thrust development in the foreland. The combined effect of tectonics and erosion leads to localization of the uplift on basement units and the isolated front of the lid constitutes a nappe (t_{29} Fig. 2.4). At this stage of evolution, the piggy back basin located on the frontal part of the lid is completely eroded. On the final stage picture (t_{38} Fig. 2.4), the development of the fold-and-thrust belt in the foreland constitutes the last event of the orogenic evolution. The different units have been largely eroded and more particularly the foreland basin, the Penninic lid and also its frontal isolated nappe. The underplating of the basement units has led to the formation of an antiformal nappe stack.

In conclusion the evolution of the experiment may be described by three major tectonic phases. From t_0

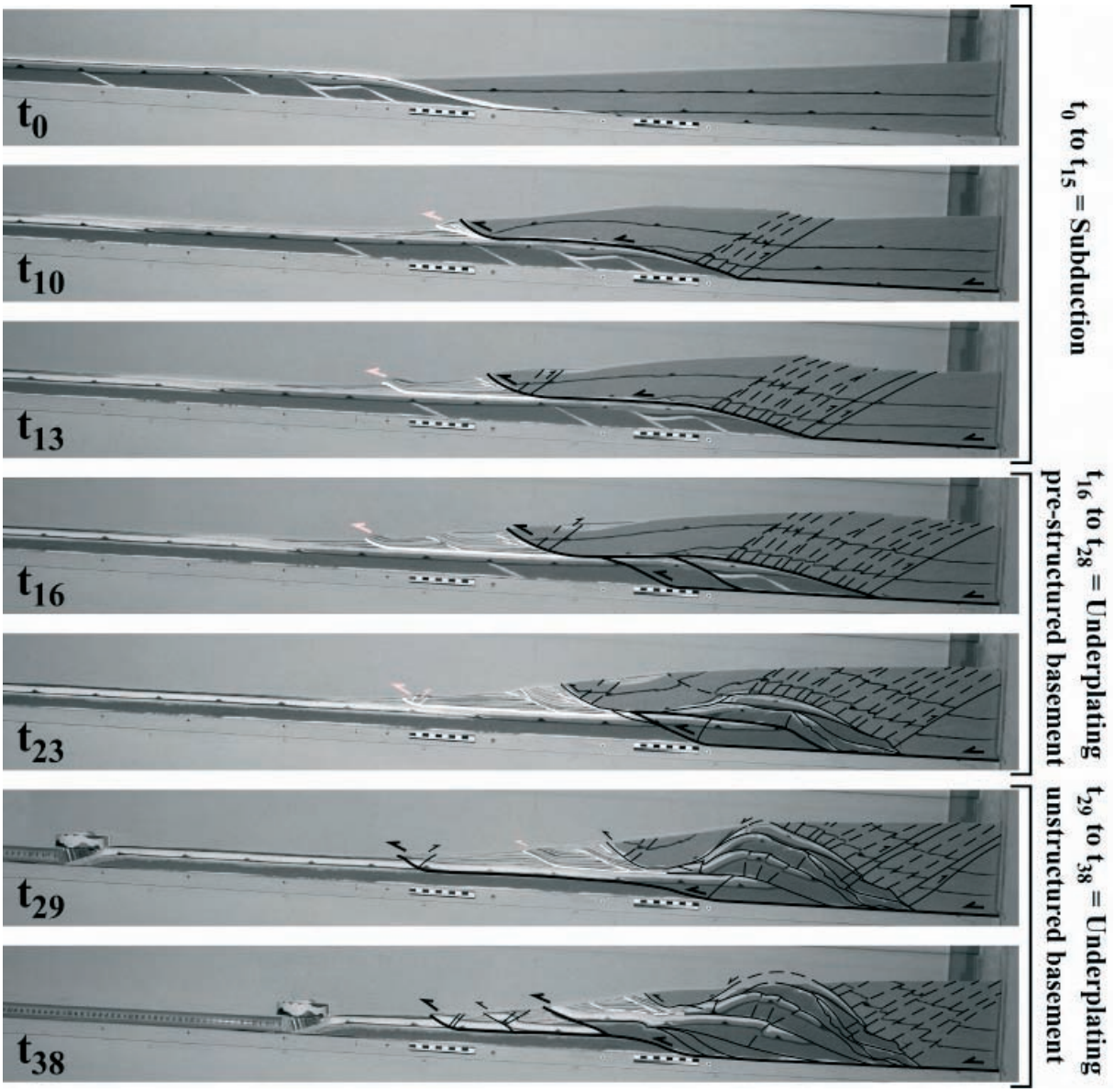

Fig. 2.4 *Key stages of the analogue model evolution from time increment t_0 to t_{38}. Structural interpretation is draped on the pictures: thrusts affecting only the foreland sediments (white), other faults, i.e. affecting the lid, the basement units and the cover (black), faults accommodating major displacements (thick), minor displacement (thin) and inactive faults (dashed lines). t_0 = initial stage; t_{10} = climb of the lid onto the top of the basement ramp causing an intense internal deformation of the lid due to backthrusting; t_{13} = first slice of recently deposited foreland sediments thanks to the activation of the basal décollement level in the basin; t_{16} = inversion of the inherited basement normal faults and propagation to the surface as a second foreland sediment slice; t_{23} = underplating of the basement imbricates and development of a third foreland sediment slice; t_{29} = spontaneous underplating of the homogeneous part of the basement, initiation of a fold-and-thrust development in the foreland and detachment of a nappe from the lid due to the uplift of basement units; t_{38} = final stage picture showing the developed foreland fold-and-thrust belt, the remains of the detached nappe and the antiformal basement nappe stack.*

to t_{15}, the lid climbs up onto the top of the basement ramp due to the subduction of the converging plate. Then, from t_{16} to t_{28}, the wedge grows by underplating of the pre-structured basement units. In the following chapters, this phase will be called "underplating of the Crystalline Massifs" in reference to the cross section by BURKHARD & SOMMARUGA (1998). The final tectonic phase, from t_{29} to t_{38}, is marked by the spontaneous underplating of the unstructured part of the basement. Similarly, in reference to the Alpine setting, this phase will be called "underplating of the Autochthonous European basement".

2.4 Discussion

Under the action of erosion and sedimentation, the experiment develops a two-dimensional geometry that can be compared with the studied section of the Western Alps. The similarities between experimental and natural tectonic structures will be highlighted before discussing the interactions between tectonics and surface processes. The study of the thrust front propagation will first reveal the major mechanisms involved in the orogenic development. We will see then that the evolution in length of the sedimentary foreland basin is closely linked to these major mechanisms. Finally, thanks to a semi-quantitative study of the sediment budget in the analogue model, the feedback mechanisms linking erosion, sedimentation and tectonic processes will be more precisely investigated.

2.4.1 Experimental results (tectonic and structural) versus observed structures

A comparison between the model at a very advanced stage of its evolution (t_{34}) and the basis cross section (Fig. 2.5) reveals that the first order tectonic structures developed present similar geometries. To highlight the similarities, the successive units constituting the model are color coded as in the cross section by Burkhard & Sommaruga (1998).

The antiformal geometry of the basement nappe stack is similar to the scheme (Fig. 2.5) elaborated by Burkhard & Sommaruga (1998). These authors propose that thrust ramps and stacking with more than 36 km of combined horizontal shortening are responsible for the formation of the External Crystalline Massif culmination. In addition, to accommodate the whole proposed total shortening, they show on the present day cross section trapped Mesozoic cover between the basement imbricates (Fig. 2.6A). Such features are also identifiable in the experiment: a considerable shortening is distributed on the different thrust planes and some cover units appear between the basement nappes (Fig. 2.6B). Burkhard & Sommaruga (1998) propose some 50 km total northwestward transport of the Morcles nappe with its crystalline core, the Mt Blanc massif (Fig. 2.6A). In the experimental stack, the cover of the two most internal basement units underwent similarly an extensive displacement. The

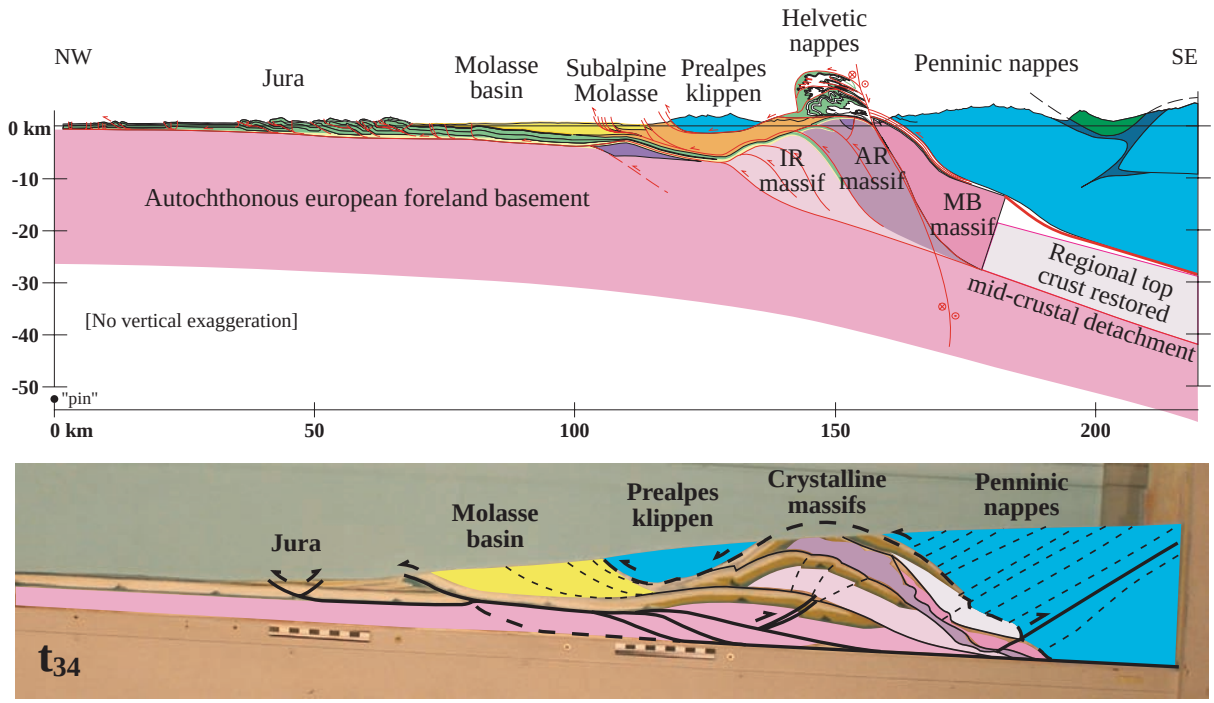

Fig. 2.5 *Comparison between the cross section modified after Burkhard & Sommaruga (1998) (see additional legends Fig. 2.1) and the analogue model at an advanced stage of its evolution (t_{34}). Both profiles are similarly color coded and the varying units are from left (NW) to right (SE): the fold-and-thrust belt of the Jura (just initiated in the experiment), the slightly deformed Molasse basin (yellow), the Prealpes klippen (blue) separated from the lid due to the uplift of the Crystalline massifs (various shades of pink) that constitute an antiformal nappe stack and the Penninic nappes (blue), remains of the lid deformed by diffuse backthrusting.*

transport of this cover nappe even brought its upper part to the surface, where it is eroded (Fig. 2.6B).

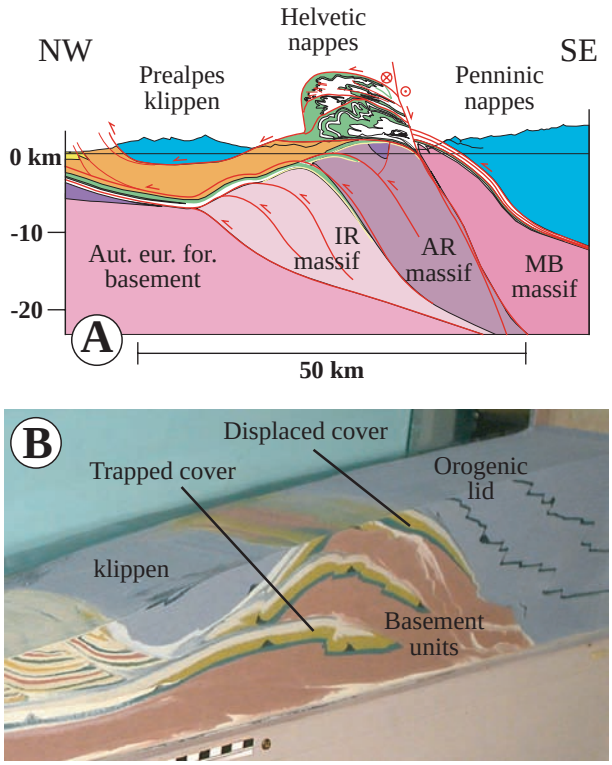

Fig. 2.6 *Common features between the antiformal nappe stack in A) the scheme by* Burkhard & Sommaruga *(1998) (IR = Infra-Rouges massif, AR = Aiguilles Rouges massif, MB = Mont-Blanc massif) and B) the analogue experiment: trapped cover between the basement imbricates; considerable shortening accommodated on the different thrust planes; and extensive displacement of the cover of the two most internal basement units (corresponding to the Helvetic nappes).*

The uplift of the basement nappe stack causes a klippen to detach from the main body of the lid. This tectonic unit, very similar to the Prealpes klippen (Fig. 2.5) in terms of geometry, dimensions and mechanism of formation, illustrates well how the mechanisms of nappe emplacement are strongly influenced by erosional processes. A major difference is yet that the experimental klippen not only thrust the foreland sediments, but also lies directly on some slices of cover trapped between the basement imbricates. This observation raises the still currently debated question of the geometry and the thickness of Molasse below the Prealpes klippen.

Despite a difference in extent of the foreland sediment basin, the geometry of the latter is quite analogous in the model and the nature (Fig. 2.5). The sediments are slightly deformed due to the brief activation of successive small thrust propagating from the base of the basin, in response to the thrust of the lid. The variations in length of the foreland basin are discussed in the following chapter.

The most external unit and also the last appeared in the model during a new stage of frontal accretion, is the foreland fold-and-thrust belt (Fig. 2.5). After a long steady state period, the wedge became unstable because of its large thickening due to the growth by underplating and subsequent uplift of basement units. To diminish the surface slope of the taper, the wedge extends into the foreland. The fold-and-thrust development is the combined result of the presence of a glass bead layer below the basement cover and the thickness of sediment deposits in the basin. The weak layer modifies the mechanics and the dynamics of the wedge and the weight of sediments favors its activation as décollement. These mechanical changes induce the forward migration of the deformation front, from a position close to the tip of the orogenic lid to a more distal position. This event could be compared to the major “jump” of the Alpine thrust front by about 100 km northwestward (Burkhard & Sommaruga 1998), approximately from Lausanne to the external Jura, that occurred after the Serravalian (c. 12Ma). This phenomenon is attributed to the presence of an important accumulation of Triassic evaporite in the Alpine foreland series. We observed subsequently in the experiment that the foreland basin migrated farther to the external domain. The remnant sedimentary basin is passively incorporated in the wedge and is largely eroded from this time.

2.4.2 Interactions between mechanics and surface processes

In this chapter, the experimental data are analyzed and presented in graphs scaled to the nature. While the scaled values often differ from the data provided in the literature, they give a well known frame of reference to the experiment and may be immediately compared with the structures and events of the Alpine setting. The data presented on the various graphs may be impinged by small errors related to different sources like the experimental procedure, the mechanical properties of the used materials and the transition between the machine and the graphical representation. Because of the uncertainty related to the estimation of the errors and because they remain small to negligible and may be either cumulated or subtracted, no error bars have been presented on the graphs. Rather we briefly

discuss the different types of errors hereafter. The experiments have been performed with incremental displacements of the basal Mylar sheet (stop at each 2 cm), measured on a graduated ruler with a maximal error of 5% (1 mm for each increment, but with a total length of the experimental setup of 280 cm). Despite its mechanical resistance, the long Mylar sheet may be slightly stretched due to the increasing force of traction necessary to pull the growing wedge. Since there is no evidence of a consistent and/or proportional relationship between the length of the Mylar sheet and the displacement of materials, it seems that stretching of the sheet is negligible. Friction on the lateral glass walls during displacement of the material is diminished thanks to the application of a lubricant before material deposition. A slight diffusion leading to a less precise reading of markers can, however, not be excluded. Another kind of error results from the graphical analysis. The localization of a point, and the drawing of a line or surface by the same person are not exactly reproducible from one stage to the other. The error estimated on distances is less than 1% and on areas less than 2%. Finally, the error due to the change of scale between the analyzes performed on photographs and the studied features on the machine is estimated to 1.3%. Compared to the approximations at the base of the model setup and to the simple laws used in the experimental procedure, the different errors of measurements are considered negligible.

2.4.2.1 Propagation of the thrust fronts

During the experiment, we studied the progression of three specific thrust fronts separating the main tectonic units. The active thrust front which corresponds to the last initiated thrust in the foreland is illustrated by the red arrow on the final stage picture (t_{38}) (Fig. 2.7). The first orogenic front represents the most external point of the orogenic lid in direction of the foreland and is shown by the single black arrow (Fig. 2.7 and 2.8). From the stage t_{29}, it corresponds to the thrust front of the isolated nappe detached from the lid. A second orogenic front appears when the division of the lid into two distinct nappes occurs and is illustrated by the double black arrow (Fig. 2.7 and 2.8). It corresponds to the front of the remaining lid. We measured the distance of the three fronts from a pin located in the undeformed part of the converging plate cover (white star Fig. 2.7), at each increment of displacement of the subducting plate (Fig. 2.8). To favor a direct comparison of the experimental thrust propagation to the Alpine setting, we named "active Alpine thrust", the active thrust front, and respectively, "Penninic front" and "2nd Penninic front" the two orogenic fronts (Fig. 2.7 and 2.8).

The propagations of both "Penninic" fronts are very regular (black curves Fig. 2.8) due to the passive transport of the lid on the subducting plate. The active "Alpine" front (red curve Fig. 2.8) shows a punctuated behavior with the development of successively active frontal thrust slices at the leading edge of the wedge (green arrows Fig. 2.8). The cyclic formation of thrust slices is expressed by a two-speed displacement of the active front illustrated by the two different slopes of the curve (Fig. 2.8).

Frontal accretion is responsible for thrust activation in the foreland basin. Thus for example at the stage t_{23} (Fig. 2.8), a new thrust slice affecting the foreland sediments develops. The punctuated development of thrusts in the foreland combined with syn-deformational erosion of the sediments lead to a major cyclic foreland sediment disappearance. This observation supports the conclusion proposed by Burkhard & Sommaruga (1998) that the present-day Molasse basin is only a small remnant of a much larger foreland basin in a very advanced stage of its evolution.

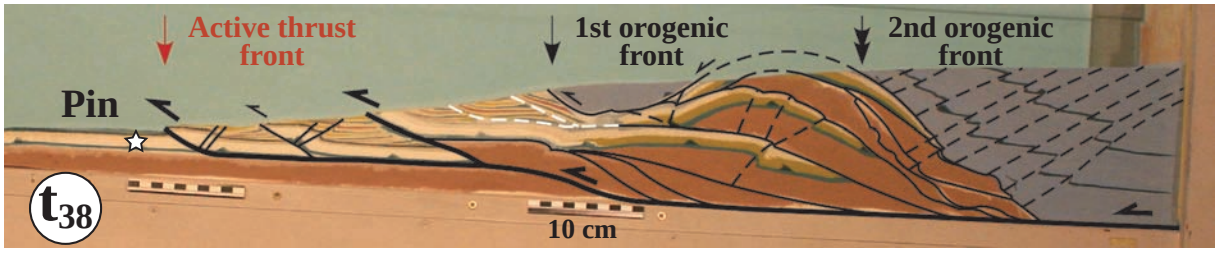

Fig. 2.7 *Location of the three studied thrust fronts separating the main tectonic units on the experimental final stage picture (t_{38}). The active thrust front (red arrow) is the last initiated thrust in the foreland. The first orogenic front represents the most advanced point of the lid (single black arrow), and the second orogenic front (double black arrow) corresponds to the front of the remaining lid, after the detachment of the frontal nappe (at t_{29}). Displacements are measured from a mobile pin (white star) located in the undeformed part of the converging plate cover.*

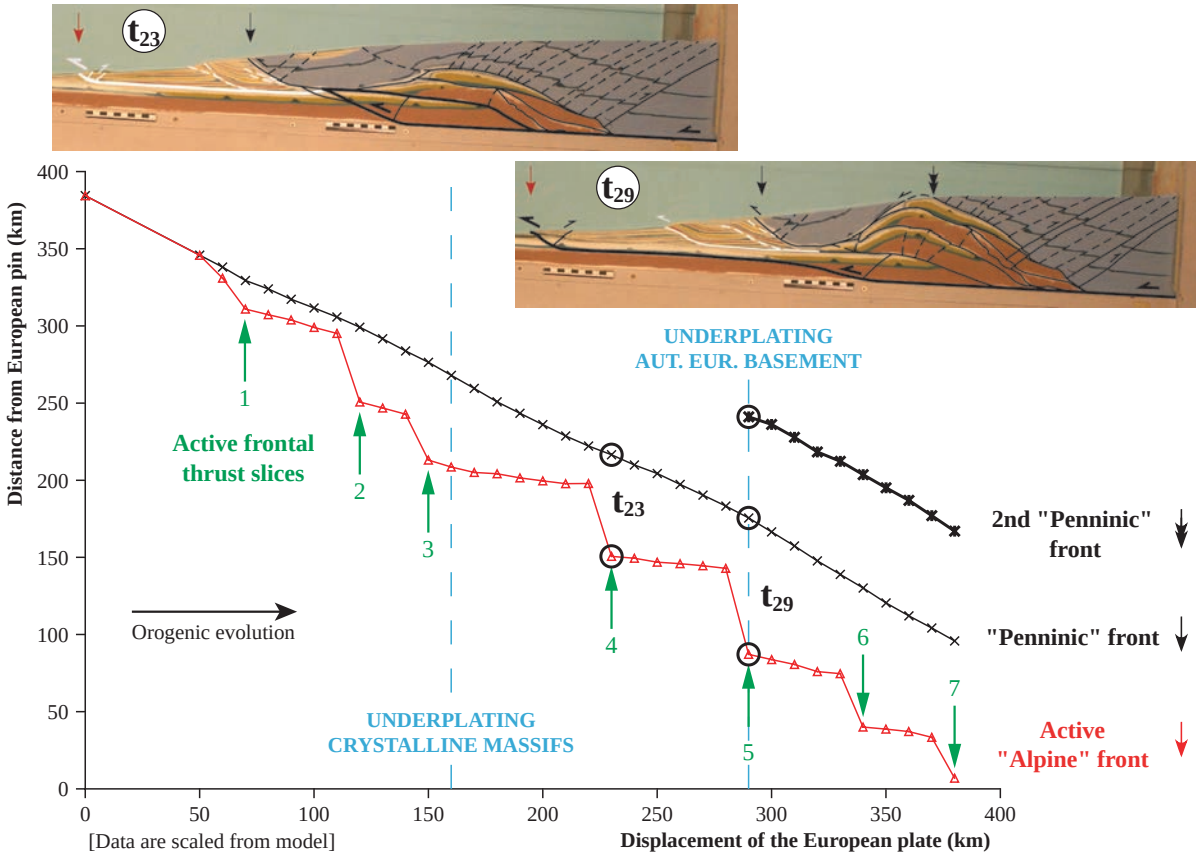

Fig. 2.8 *Propagation of the three studied fronts measured from the European pin (see Fig. 2.7) at each step of displacement of the subducting plate. The first and the second orogenic (or "Penninic") fronts (black curves) move very regularly due to the passive transport of the lid on the converging plate. The propagation of the active ("Alpine") thrust front (red curve) is in contrast punctuated by the apparition of successively active frontal thrust slices (green arrows). At* t_{23}*, the active front "jumps" to the foreland leading to the development of a new thrust slice of deposited sediments. At* t_{29}*, the active front "jumps" again to the foreland but the thrust is generated by the spontaneous failure of the basement also affecting the cover.*

The basin would have been cannibalized since the early Tortonian. In the field, this volume of eroded Molasse sediments would disappear from the geological record without leaving a trace. This is suggested by burial data provided by vitrinite reflectance (Schegg et al. 1997). As assumed by Burkhard & Sommaruga (1998), we believe that the original lengths and the total Alpine shortening on restored cross sections are underestimated. The foreland Molasse basin is most likely the structure on which the underestimation of shortening is the strongest. The erosion of a large thickness of sediments has definitively removed the structures accommodating the displacement.

At the stage t_{29} (Fig. 2.8), a new frontal thrust slice appears in the foreland but it now also affects the autochthonous cover. With no pre-existing fault simulated by glass beads, the thrust is generated by the spontaneous basement underplating of the subducting plate, called "Autochthonous European basement" in reference to the cross section by Burkhard & Sommaruga (1998). The mechanics of the wedge is then modified because the deformation is propagated to the foreland.

We observe in the model that frontal accretion and underplating are active simultaneously. Frontal accretion in the external parts will lead to the development of a foreland fold-and-thrust belt, while underplating in the internal zones leads to the formation of the antiformal basement nappe stack. The development of the nappe stack is initiated by the tectonic heritage of the basement, but is maintained and reinforced by the surface processes. Erosion of the lid favors and localizes the exhumation of basement imbricates and sedimentation in the foreland inhibits the lateral growth of the stack.

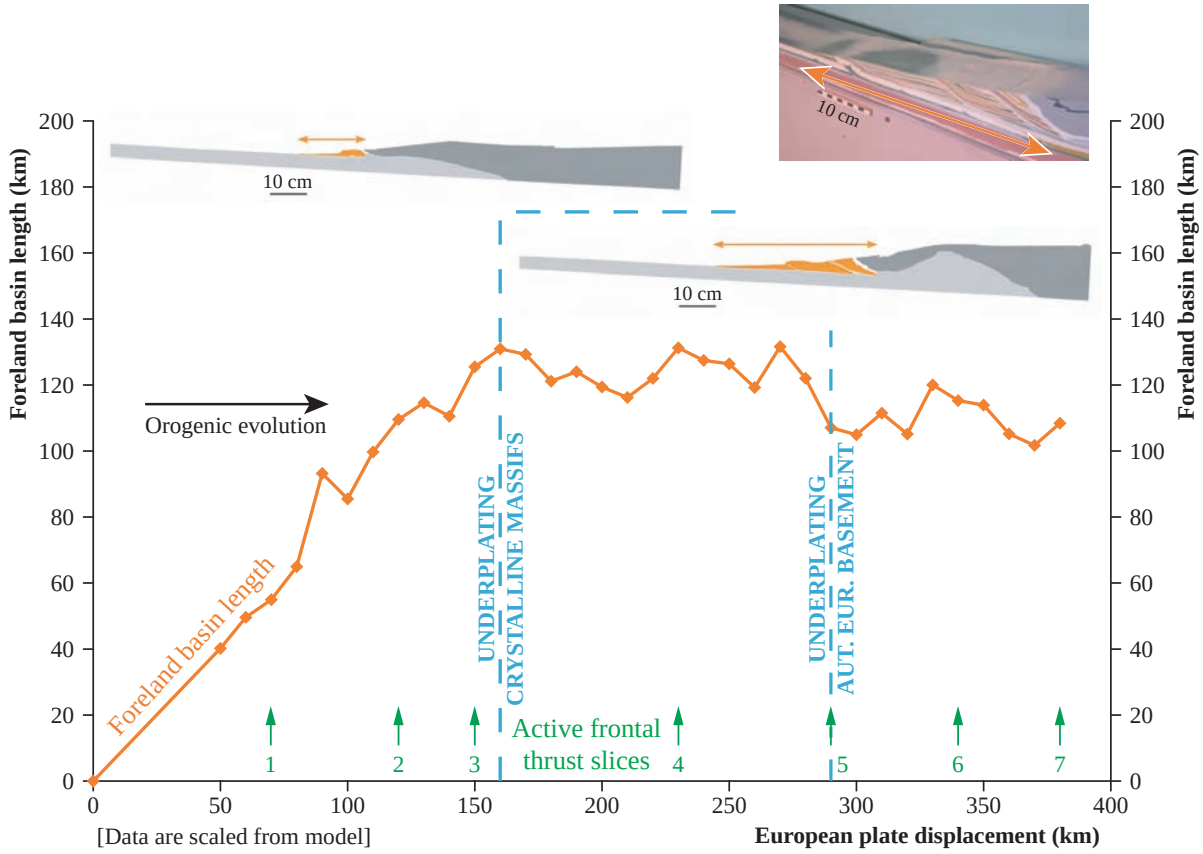

Fig. 2.9 *Length of the sedimentary foreland basin (orange curve) measured at its base (picture) at each step of displacement of the subducting plate. Two stages, each one illustrated by a scheme, are distinguishable: first, the basin is massively filled and reaches its maximal length of 130 km at 160 km of converging plate displacement. A more or less final basin width is reached with the initiation of underplating and subsequently remains constant throughout the final stages of the experiment.*

2.4.2.2 Evolution of foreland basin width

During the experiment, we measured the length of the sedimentary foreland basin at its base (picture Fig. 2.9). This measurement provides the maximal geographical extent of the basin at each stage of its evolution and takes also into account the foreland sediments thrust by the lid.

We propose that the history of the basin is divided into two stages. First, the basin is massively and constantly filled to recover the equilibrium profile of the wedge. Indeed, as the lid thrust the subducting plate, its frontal part advances and is uplifted. To maintain the initial slope of the wedge, the front of the lid is eroded and layers of sand are successively deposited in the foreland. The wedge spreads and the basin reaches its maximal length of about 130 km (Fig. 2.9), after a displacement of 160 km of the European plate. The second stage starts with the underplating of the basement and shows a continuous slight decrease in length of the basin (Fig. 2.9). The exhumation of the basement units modifies the development of the wedge: it does not grow anymore in length but in thickness. The layers of sand simulating the foreland sediments in the basin become shorter and thicker. At the end of the basin evolution (Fig. 2.9), its length is approximately 110 km. The two schemes (Fig. 2.9) represent this two-stage evolution and illustrate the large variation in length of the sedimentary foreland basin.

2.4.2.3 Sediment budget: a semi-quantitative study of the experimental results

Our semi-quantitative estimates of the sediment budget on the cross section (Fig. 2.10) are expressed, scaled to the nature, in square kilometers. The data are given at each step of displacement of the subducting plate. The sedimentation rate corresponds to the surface of the last sand layer deposited in the foreland basin. The erosion rate includes all the eroded materials: first it involves mainly materials from the lid, then are added basin sediments and ultimately small percentages of basement units and their cover. Both

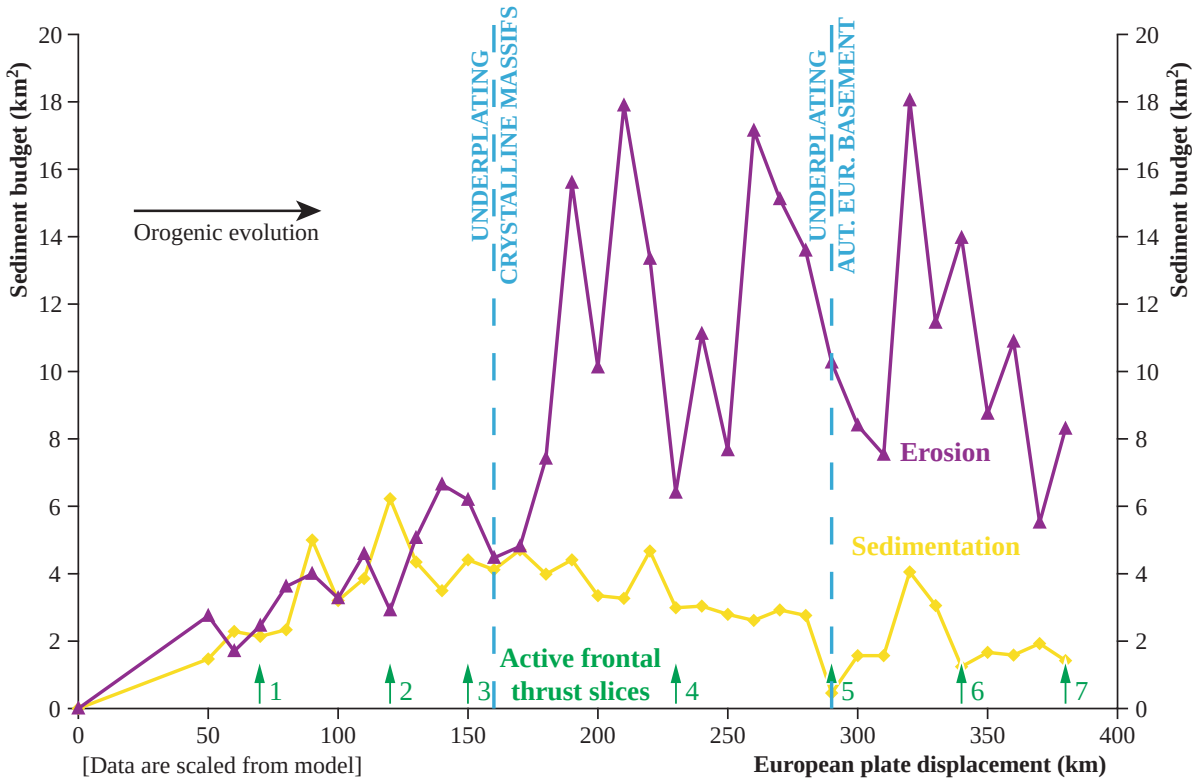

Fig. 2.10 *Sediment budget (i.e. variations in rates of erosion and sedimentation) measured in the experiment at each step of displacement of the subducting plate. The sedimentation rate (yellow curve) increases until reaching its maximum before diminishing gently. In contrast, the erosion rate (violet curve) strongly fluctuates around a high average value after having reached its maximum. The underplating of basement units seems to govern the rates of surface processes: the initiation of underplating modifies the trend of the curves of erosion and sedimentation with a domination of the erosive phenomenon until the end of the experiment.*

curves are not cumulative ones but they rather express the temporal evolution of the erosion and sedimentation rates.

The sedimentation rate (Fig. 2.10) shows the same evolution as the basin length previously described: after a rapid increase it diminishes gently. In contrast, the erosion rate (Fig. 2.10) increases slowly, and after the initiation of underplating, strongly fluctuates around a high average value. The trend of the curves of erosion and sedimentation are then inverted and the erosive phenomenon dominates. Indeed, the rapid uplift of the pre-structured basement units brings on an over-elevation of the lid. To recover a stable taper, the erosion undergoes a major increase in rate. In contrast, after the initiation of underplating, the orogenic wedge does not grow anymore and the volume of sediment deposits diminishes gradually. In nature, the barrier created by this uplift would probably restrain the sedimentary flux in the foreland leading to an additional decrease of the sedimentation rate. Therefore, it appears that the rates and the localization of sedimentation and erosion obey to the direct influence of the tectonic development to maintain the dynamics of the wedge. The cyclic secondary variations in rates of erosion, but also in sedimentation are most likely linked to the punctuated activation of new frontal thrusts in the foreland (green arrows Fig. 2.10) and reflect a response to the mechanical adjustments inside the wedge.

At the end of the experiment, we have estimated the whole eroded surface of the lid and the sedimented materials present on the geological record. The sediments constitute approximately 15% of the eroded materials in the lid and 43% of the original Penninic lid still remain. These estimations seem to be in a good agreement with the values proposed for the Alps (Kuhlemann et al. 2002). A more detailed discussion of model results compared with the Alpine sediment budget will be presented in a complementary work (Bonnet et al. 2007).

2.5 Conclusions

The analogue model used in this study is based on few simple first order assumptions: four different kinds of lithologies are simulated, the structural heritage is uniformly modeled by glass bead levels and we have taken into account only the upper part of the crust but not the lithospheric flexure. In addition, the experimental procedure is performed with first order laws of erosion and sedimentation since erosion is done to maintain average Coulomb equilibrium profiles, independently of the lithologies. Despite these simplifications, the development of the model fits well the natural cross section in terms of geometry.

Modeling reveals that two major types of mechanisms are active simultaneously: frontal accretion in the external parts leading to the development of a foreland thrust belt and underplating in the internal zones leading to the formation of an antiformal nappe stack. The basement imbricates in the antiformal stack are progressively steepened during its development. In the internal part of the Alpine belt, the originally shallow SE dipping axial surfaces and thrusts in the nappe stack also steepen to attain finally subvertical to overturned dips. The reason for this geometry, as for example proposed by Escher et al. (1997), is the addition by accretion through tectonic underplating of frontal imbricates resulting in the rotation of the older trailing thrust sheets.

In the experiment, important volumes of analogue material are eroded out of the geological record. Indeed, the combined effect of punctuated frontal thrust development (due to frontal accretion) and syn-deformational erosion of the foreland sediments leads to a major cyclic sediment disappearance. Some of the tectonic structures accommodating the convergence are definitively eroded at the end of the experiment and there is no remnant of their original lengths. Observation reinforces the conclusion proposed by Burkhard & Sommaruga (1998) that the present-day Molasse basin is only a small remnant of a much larger foreland basin in a very advanced stage of its evolution. As a consequence, the original lengths and the total Alpine shortening on restored cross sections are most likely underestimated.

It appears in the experiment that to maintain the dynamics of the wedge, the surface processes obey to the direct influence of tectonic events. For instance, the initiation of basement underplating totally inverts the respective importance of erosion and sedimentation. The over-elevation of the lid due to the rapid uplift of basement imbricates is controlled by a major increase of the erosion rate. In contrast, as the orogenic wedge does not grow anymore, the volume of sediment deposits diminishes gradually. In nature, the barrier created by this uplift would probably restrain the sedimentary flux in the foreland leading to an additional decrease of the sedimentation rate. In contrast, we saw that erosion and sedimentation influence in return the tectonic development. For instance, the erosion of the lid favors a localized exhumation on pre-structured basement imbricates and controls the uplift rate. The sedimentation in the foreland changes also the dynamics of the wedge. Sediment deposits inhibit the lateral development of the stack but favor the activation as décollement of the weak layer at the base of the cover, leading to the growth of the fold-and-thrust belt. To sum up, the tectonic development constrains the sediment budget in space, time and rate and vice versa. As a consequence, our experimental approach shows the necessity to combine studies of erosion, sedimentation and tectonics.

It is largely admitted that the principal mechanism forming the Molasse foreland basin is the flexural bending of the European down-going plate under the thrust load advancing from the south (Price 1973, Dickinson 1974, Turcotte & Schubert 1982). However, as said in the initial postulates, we neglected the effect of the subducting European lithosphere flexure. Despite this simplification, we obtain realistic structural developments such as the antiformal nappe stack, the foreland sediment basin and the frontal fold-and-thrust belt. We conclude that the lithospheric flexure may not be the main controlling mechanism in the evolution of the Molasse foreland basin. The feed-back mechanisms linking surface processes to tectonic processes may be mainly responsible for the development of the foreland sediment basin. To reinforce this assumption, it would be interesting to perform new experiments taking into account the lithospheric flexure, simulated for instance by a flexible basal plate. It would be thus possible to discriminate the respective impacts of the combined effect of tectonics and surface processes on one hand, and the flexure of the lithosphere on the other hand.

While the constituents of the Northern Alpine system are the results of the convergence between Adria and Europa, they are laterally discontinuous (Laubscher 1992). Discontinuities in the very deep structures are proposed to explain such lateral variations, but we also believe that the surface processes are in part responsible. A comparison between the geometries developed

on a unique basis model but with variable amounts of sedimentation and erosion would discriminate the influence of surface processes on lateral variations of the Alpine structures. Such a comparison between all the experiments performed during this study has been done and will be presented in a separate paper.

Another perspective of work would be the comparison of the experimental results with major tectonic stages and structures of the Alpine development. In this aim, we studied material paths and linked their trajectories of exhumation with the tectonic stages described in this article. We would like to replace the timing of the experimental tectonic evolution in an alpine framework and compare our experimental sediment budget with sediment/erosion budgets in alpine-type settings. It would allow us possibly to discriminate the impacts of the climatic and the tectonic signals on the sediment budget, notably during the 5 last Ma.

*****

3 - SURFACE PROCESSES VERSUS KINEMATICS OF THRUST BELTS: RATES OF EROSION, SEDIMENTATION, AND EXHUMATION - INSIGHTS FROM ANALOGUE MODELLING

BONNET, C., MALAVIEILLE, J., & MOSAR, J.

submitted to *Bulletin de la Société Française de Géologie* (03.2007)

ABSTRACT

The mechanical equilibrium of an orogenic wedge is maintained thanks to interactions between tectonic processes and surface processes. To better constrain the influence of erosion and sedimentation on the orogenic evolution, we performed a series of analogue models based on the tapered wedge principle, varying the amounts of erosion and sedimentation. The models develop by frontal accretion in the foreland basin and by simple underthrusting and subsequent underplating in the hinterland. The variations in rates of erosion and sedimentation strongly modify the extent, the morphology, the structures, the timing of development and the material paths in the different models. Under certain conditions, entire structural units can be formed and subsequently eroded out of the geological record, leading to important underestimations when restoring sections. Particles located in the converging lower plate or in the upper plate show very complex uplift paths related to tectonic stages. The correlation between models and three Alpine tectonic cross-sections emphasises the role of erosion and sedimentation on the dynamics and development of the orogen and adjacent Molasse basin. Along strike changes in the geometry of the orogen can be explained by differences in surface processes.

3.1 INTRODUCTION

Based on theoretical models, it has been shown that orogens adopt a distinct geometry with a low-tapered pro-wedge facing the subducting plate, and a high-tapered retro-side (WILLETT et al. 1993). The tapered wedge geometry is established because orogens tend to be on the verge of gravitational failure (DAVIS et al. 1983). According to these models, the velocity field of the crust and, hence, the exhumation paths of rock particles, depends on erosion at the surface (e.g., HORTON 1999). Consequently, any changes in erosion rates potentially result in a modification of the strain pattern (SCHLUNEGGER & HINDERER 2001) and thus the internal evolution of the wedge. Based on analogue models, we performed a series of analogue experiments including erosion/sedimentation to investigate the foreland/hinterland evolution. In a simple set-up we investigate the influence of erosion and sedimentation on the internal structure of the wedge while maintaining a constant taper angle. The models were designed for direct comparison to the setting and tectonic evolution of the western Alps. How does the erosion/sedimentation change the tectonic structure, and what conclusions are to be drawn on the evolution of an orogenic wedge such as the Alps? In addition we chose to make a prestructured model setup in order to simulate realistic conditions of a deforming plate margin edge such as the Helvetic domain. How important is this prestructuring in the tectonic evolution of an orogenic belt, and are their main tectonic events related to differences of behaviour of the prestructured and non prestructured domains during the evolution of the wedge? Our models are capable of reproducing

first order tectonic structures as known from the Alpine orogen. In turn, modelling results make it possible to draw conclusions on the evolution of the Alpine foreland (structural development, basin evolution, exhumation, etc) and make links between the along strike changes in the geometry of the orogen and differences in surface processes.

3.2 Analogue modelling experiments

To better describe the evolution of a mountain belt and to investigate the combined influence of surface processes and tectonics on the kinematic evolution of a thrust belt, we performed a series of seventeen experiments. The basic geometric setup simulates a section of a growing orogen in a convergent system, when the orogenic lid begins to override the subducting plate formed by prestructured basement and cover units (Fig. 3.1). This prestructured setup is justified since we want to investigate the inversion of a former passive margin setting and rim basin realm such as formed by the Ultrahelvetic and the Helvetic domains. During the orogenic evolution of the Alps the inversion of the Ultrahelvetic tilted block margin leads to the formation of the Flysch basin, whereas the inversion of the platform-type rim basin of the Helvetic leads to the formation of the Molasse Basin (Stampfli & Marthaler 1990b). Such margin domains are typically prestructured by half-graben like basin and tilted blocks on the margin (Trümpy 1980, Wildi et al. 1989b, Wildi et al. 1989a, Funk & Loup 1992) and it is therefore important to consider, even in a simplified way, the existing geometries if realistic results from modelling are to be obtained. This is necessary moreover if we want make meaningful comparisons with the Alpine orogeny. The eleven preliminary experiments led to the establishment of both the basic model and the experimental procedure, as presented in the following. By successive improvements, we constrained the geometry and mechanical behaviour of the different tectonic units and depositional realms to achieve a model that can be considered as analogous to the European Alpine platform and the Alps. Based on this model of orogenic development, the last six experiments (called 42 to 47) were performed with variable rates of sedimentation and erosion to better understand their impact on thrust wedge growth.

3.2.1 Experimental set up, basic model and experimental procedure

To study the development of orogenic wedges in relation to the processes of erosion and sedimentation, our simulation is based on the very well established and documented example of the Alpine mountain belt. The basic model (Fig. 3.2) has been designed from a restored section across the Western Alps proposed by Burkhard & Sommaruga (1998). The lengths of units, angles, rheologies and localization of décollement levels in the experiments are directly inspired by their work. The classical sandbox device (Fig. 3.2) we used is close to the set up of Malavieille (1984) and Konstantinovskaia & Malavieille (2005). It is made by a flat basal plate bound by two lateral glass walls. A motor pulls a 10 cm wide Mylar sheet with a rough surface thus simulating a high basal friction, over the plate. A thrust wedge is developed against the rigid

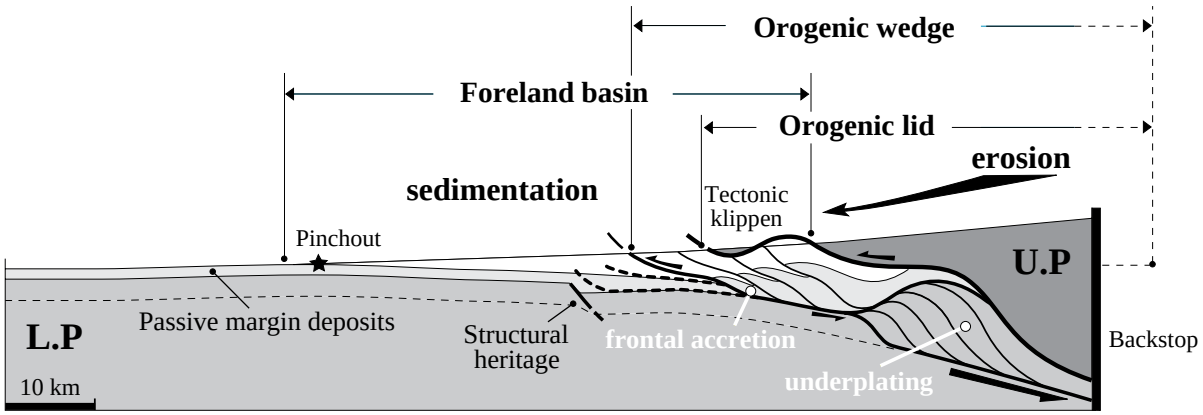

Fig. 3.1 *Components of a foreland system and their interaction with surface processes and tectonic mechanisms. The orogenic lid is dark grey, the foreland basin white and the converging lower plate (basement + cover) is light grey. U.P = Upper Plate and L.P = Lower Plate. Surface processes are erosion and sedimentation. Tectonic mechanisms controlling the orogenic growth are frontal accretion and underplating.*

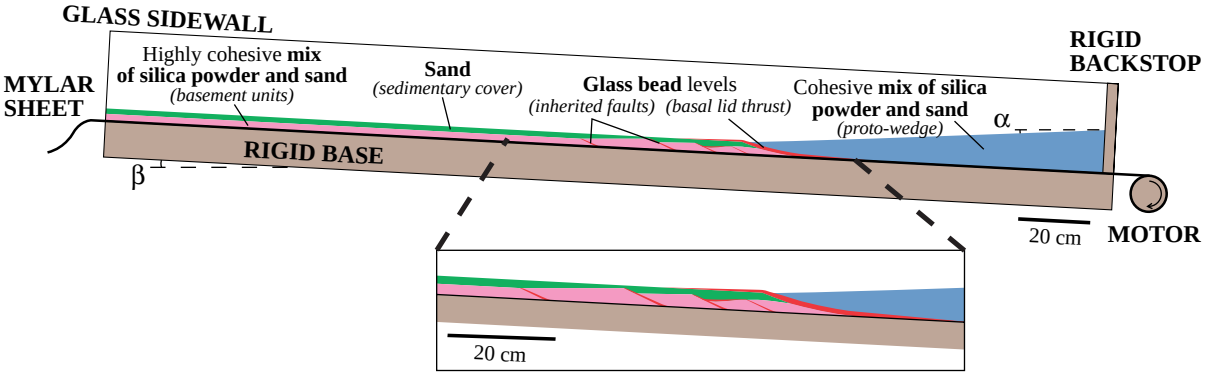

Fig. 3.2 *Experimental sandbox device and basic model of a growing orogen and its foreland basin, based on a model Coulomb wedge (on the scheme, surface α deeps 2° to the left and base β, 3° to the right). Prestructured analogue materials are pulled on a Mylar sheet against a rigid backstop, leading to the development of a thrust wedge. On the right side, the upper plate consists in a homogeneous solid lid (blue) that will override on a basal thrust (red) the lower plate constituted by a succession of solid basement units (pink) and their more "deformable" cover (green), both prestructured by inherited faults (red).*

backstop by the analogue materials deposited on the sheet due to the movement of the Mylar sheet. The latter simulates the rigid lithosphere of the upper plate without a subduction window at its base. Cohesion and size are scaled (scaling, with a factor of 10^5, and characterization of model materials are discussed in Gutscher et al. 1998), Gutscher et al. 1996, Kukowski et al. 2002, Lallemand et al. 1994 and Lohrmann et al. 2003). The basal plate measures about 2.80 m that offers a maximum convergence of 160 cm, or about 400 km at the natural orogenic wedge scale. One camera records all stages of the experiment allowing structural interpretations and semi-quantitative analysis to be made.

The "critical wedge" theory (Davis et al. 1983, Dahlen 1984, Dahlen et al. 1984) predicts that the geometry of a growing wedge (defined by its surface slope α and its basal slope β) is a function of the material strength and the basal friction. The surface of the model Coulomb wedge (α) used in the experiments (Fig. 3.2) dips 2° to one side and its base (β) dips 3° into the opposite direction (angle of subduction). Angles have been based on Alpine sections discussed in Mosar (1999) and Lacombe & Mouthereau (2002). The geometry of two natural boundary conditions has been simplified in the models: the lithospheric flexure is not considered (the flat basal plate was simply inclined) and, assuming the possibility of thrusts to develop at a mid-crustal detachment level (Burkhard & Sommaruga 1998), only the upper part of the crust is involved in the model deformation.

The six experiments described here, are built on the same basic model (Fig. 3.2), despite variations in length and thickness of some given layers. Two main units are distinguishable in the models: on the right side, the homogeneous orogenic lid represents the upper plate that overrides, on the left side, a succession of pre-cut basement units and their cover forming the subducting plate. The analogue materials have frictional properties satisfying the Coulomb theory (Davis et al. 1983, Dahlen 1984, Dahlen et al. 1984) and they mimic a non-linear deformation behaviour of crustal rocks in the brittle field (Lohrmann et al. 2003). The orogenic lid is made of a cohesive mix of silica powder and sand. The aeolian sand used in this study is rounded with a grain size of 200 to 315 μm and a density of 1690 kg/m^3. The internal coefficient of friction is 0.57 and the cohesion Co = 20 Pa. The pure dry silica powder has a significantly higher cohesion (150 Pa) than sprinkled sand (20 Pa), allowing the simulation of stronger (more resistant) material. The lid is separated from the subducting plate by a thick layer (< 8 mm) of glass beads that simulates a major basal thrust. Glass beads have a grain size between 50 and 105 μm and are a Coulomb material of density similar as that of dry sand. Due to their close to perfect roundness, their coefficient of internal friction is about 23% smaller (0.44), with cohesion almost negligible. The basement units of the lower plate are also composed of sand and silica powder, but the latter is in a higher proportion to model very strong lithologies. They are pre-cut by thin layers of glass beads simulating inherited normal faults. These weak zones bordering old basins can be reactivated as reverse faults during the compression. Finally, a layer of sprinkled sand represents the sedimentary cover of the subducting plate. The novelty of our approach is consequently that the analogue model takes into account both the tectonic and stratigraphic inheritance of the wedge.

Except for experiment 42, in all other experiments we performed both erosion and sedimentation. Even when varying the rates of the surface processes, the experimental procedure was based on the assumption that the tectonic development of the model governs the rates and localization of erosion and sedimentation. In each experiment (except 42), surface processes were imposed to maintain the initially chosen mechanical equilibrium of the wedge ($\alpha+\beta = 5°$ as discussed prior). Erosion is performed both on the lid and on the recently deposited materials to maintain the slope of the wedge constant. Simultaneously in the foreland, the successive layers of basin filling are added to obtain the equilibrium profile. We simulated first order simple diffusion laws of erosion and sedimentation, and applied constant erosion on the units, independently of their lithological nature. The varying rates of imposed erosion and sedimentation are indicated for the six described experiments (Fig. 3.7). In addition experiments present minor differences with the initial set up (Fig. 3.3) of the basic model adopted. In experiment 42, basement units and cover form two flat, parallel layers. The thin levels of glass beads located in the lower plate cut the basement units, but also the sedimentary cover to finally reach the surface. In contrast, in all the other experiments, top of basement is not flat, and basement units are offset along normal faults forming the inherited basins filled with the sedimentary cover. Except in experiment 42, we introduced in the sedimentary cover of the lower plate a flat layer of pure silica powder to simulate a more resistant lithology. The strong layer is meant to mimic the thick and massif limestone series in the late Jurassic series of the Alpine foreland. A thin level of glass beads (< 2 mm) with the same length than the layer of silica powder is also placed between the base-

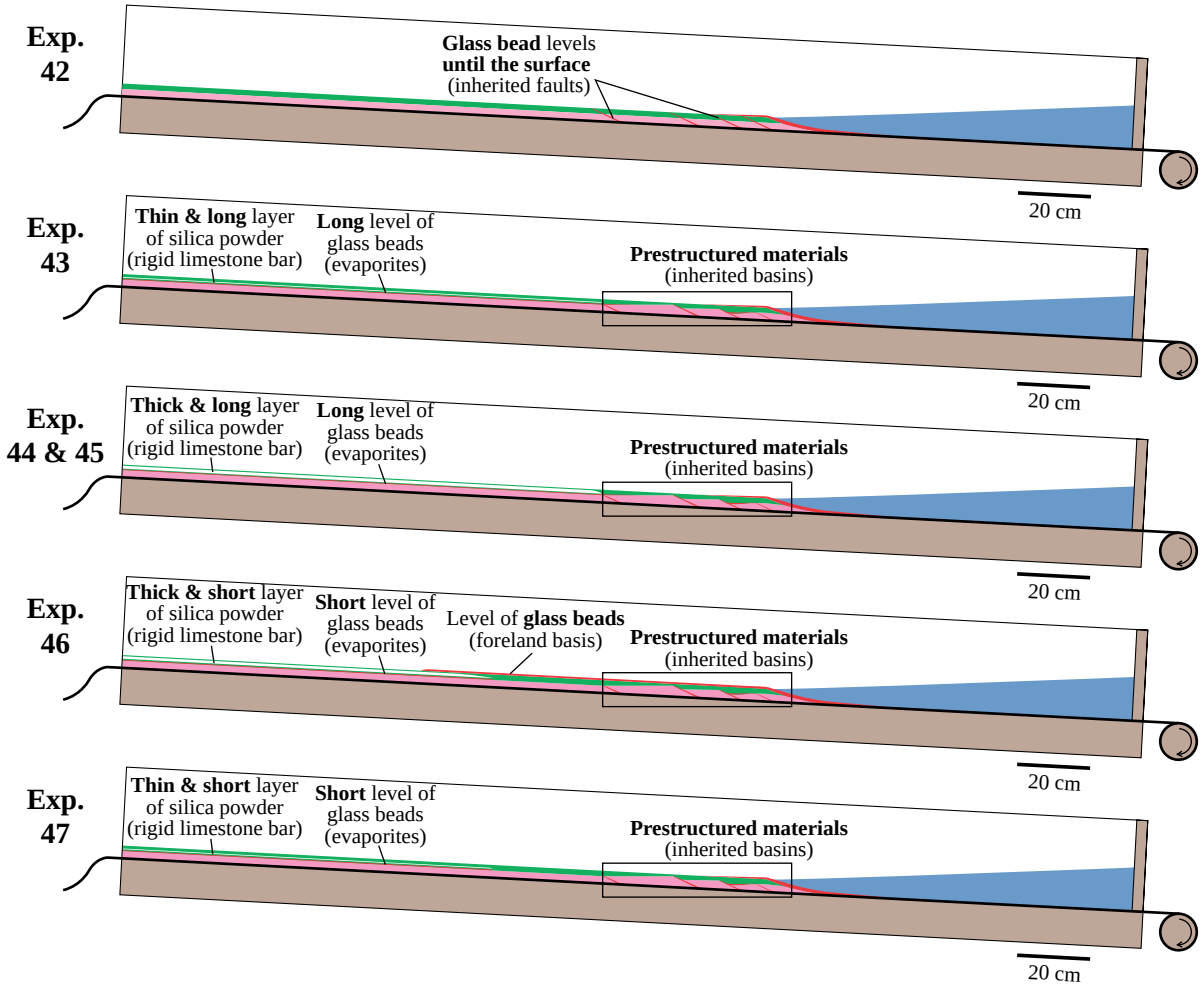

Fig. 3.3 *Initial set up of the six presented experiments. The main differences concern the structure of the converging lower plate. The internal part of the plate is either prestructured by inherited basins cutting only the basement or by inherited faults reaching the surface (red levels). With the exception of the experiment 42, a cohesive layer (white) simulating a rigid lithology is placed in the core of the cover, underlined by a weak level (red) of same length simulating evaporites at the base of the cover. This cohesive layer may be thin (< 2 mm) or thick (< 7 mm) and also long (reaching the first inherited basin) or short. In the experiment 46, a glass bead level is added on the right half of the cover's length to simulate a major weakness at the base of the future foreland basin.*

ment and the cover in the subducting plate. It mimics a weak level of evaporites acting as a décollement level for the cover. The length of both the silica powder and the glass bead levels vary following the experiments as well as the thickness of silica powder (see dimensions Fig. 3.3). In the experiment 46, we added a level of glass beads (< 2 mm) on the right half of the cover's length to simulate a major unconformity at the base of the future foreland basin. This level favours the overriding of the lid on the lower plate. The two-dimensional development of this experiment (46) presents a geometry of orogenic wedge that is in good agreement with the geometry of the present day section across the Western Alps (BURKHARD & SOMMARUGA 1998) at the origin of our basic model. In addition, in the experiment 46 we performed more detailed analysis (sediment budget (BONNET et al. 2006), evolution in length of the basin (BONNET et al. 2006), exhumation paths of analogue materials, etc). The evolution of this reference experiment will be described in more details.

3.2.2 Main stages of the reference experiment

To simplify the description of the experiments, we chose to express the displacement of the subducting plate in terms of time increments. For instance, the reference experiment (46) is performed between the time increments t_0 and t_{38}, for a total shortening of

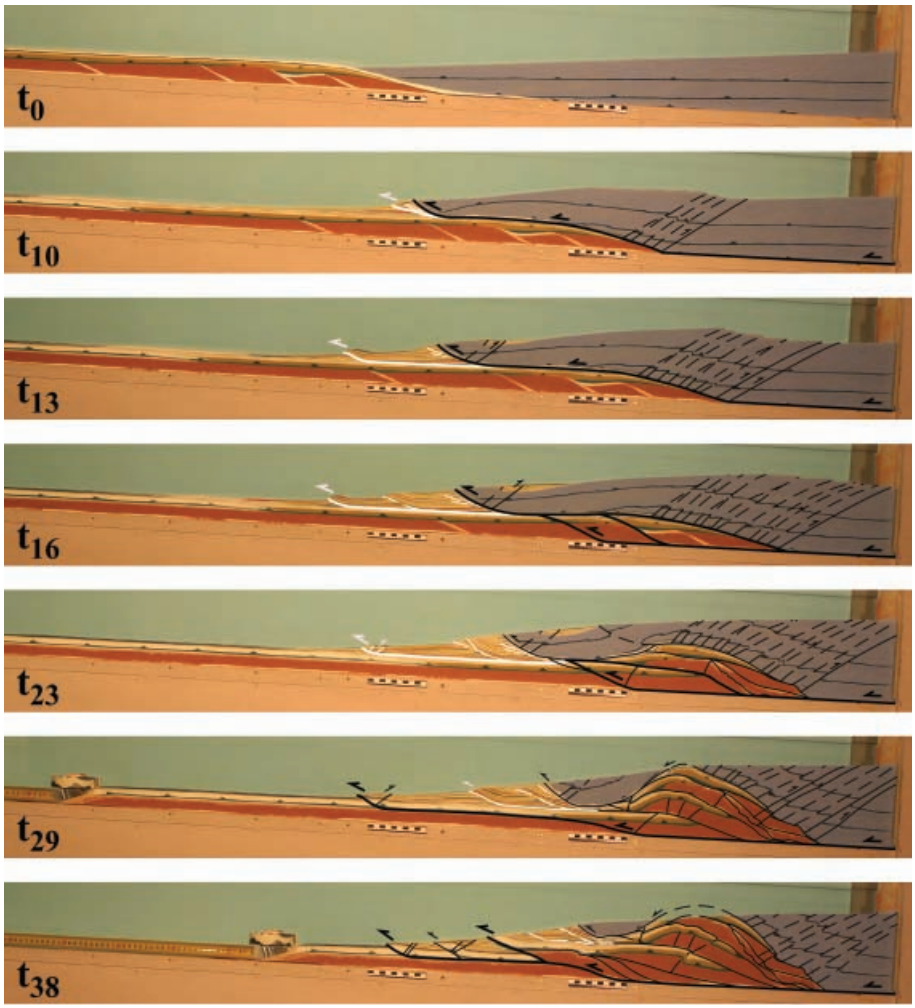

Fig. 3.4 *Key stages of the reference model evolution from time increment t_0 to t_{38}. Structural interpretation is draped on the pictures: thrusts affecting only the foreland sediments (white), other faults (black), faults accommodating major displacements (thick), minor displacement (thin) and inactive faults (dashed lines). t_0 = initial stage; t_{10} = climb of the lid onto the top of the basement ramp causing an intense internal deformation of the lid due to backthrusting; t_{13} = first slice of recently deposited foreland sediments thanks to the activation of the basal décollement level in the basin; t_{16} = inversion of the inherited basement normal faults and propagation to the surface as a second foreland sediment slice; t_{23} = underplating of the basement imbricates and development of a third foreland sediment slice; t_{29} = spontaneous underplating of the homogeneous part of the basement, initiation of a fold-and-thrust development in the foreland and detachment of a nappe from the lid due to the uplift of basement units; t_{38} = final stage picture showing the developed foreland fold-and-thrust belt, the remains of the detached nappe and the antiformal basement nappe stack.*

152 cm (corresponding to 380 km at the natural orogenic scale). The key stages of the tectonic evolution are presented with the structural interpretation draped on the pictures (Fig. 3.4).

Shortening in the model leads to the climb of the lid onto the top of the basement ramp. The geometrical response is a continuous and marked internal deformation of the lid mainly accommodated by diffuse backthrusting (t_{10} Fig. 3.4). As the orogen starts showing some relief (t_6) and until the end of the experiment, we remove analogue materials (erosion) and deposit sand to maintain the mechanical equilibrium of the wedge. The displacement of the orogenic front is first accommodated by several small thrust slices in the foreland sediments, very close of the lid (t_{10}). The deformation propagates then to the foreland (t_{13}) through the glass bead level located at the base of the sedimentary deposits and activated as a décollement. The displacement of the orogenic front is accommodated by retrothrusting (t_{16}). From the stage t_{16}, the structural heritage controls the deformation of the subducting plate. The inherited weaknesses (normal faults) in the basement units are activated as reverse faults. They propagate across the basal décollement level and appear at the surface as a succession of foreland sediment slices. Then the basement imbricates thrust each other due to underplating (t_{23}) (PLATT 1986). At stage t_{29}, the homogeneous part of basement (not prestructured) of the subducting plate is spontaneously underplated. The resulting thrust affects the sedimentary cover and the overlying foreland sediments and initiates a fold-and-thrust development in the foreland. The combined effect of tectonics and erosion leads to localization of the exhumation on basement units. Their uplift isolates the front of the lid that constitutes a synformal nappe (t_{29}). The last event of the orogenic evolution is the development of the fold-and-thrust belt in the foreland (t_{38}). At this stage, the different units have been largely eroded and more particularly the foreland basin and the orogenic lid including its frontal klippe. The underplating of the basement units has led to the formation of an antiformal nappe stack.

3.3 RESULTS OF MODEL ANALYSIS AND TECTONIC IMPLICATIONS

When erosion and sedimentation operate in the experiments, the wedge development presents a classical geometry of mountain belt with a basement nappe stack in the internal zones and a foreland highly deformed by thrusting. The two types of tectonic mechanisms involved (frontal accretion and underplating) will be described based on the reference experiment. Then, all the experiments performed with surface processes and the single one without will be compared to investigate the influence of erosion and sedimentation on the mountain belt evolution. Independent variations in rates of erosion and sedimentation strongly modify the structural development of the wedge. To highlight the diversity of geometries obtained, three natural profiles across the Western to the Central Alpine arc will be compared to model sections. Finally, we will describe the complex two-dimensional trajectories of particles located in the different tectono-sedimentary units of the model, during the development of the thrust wedge. To better constrain the influence of erosion and sedimentation on material paths, we will compare the results of experiments performed with and without surface processes.

3.3.1 Frontal accretion vs. underplating

Two main types of tectonic mechanisms are simultaneously involved in the experiments performed with surface processes (experiments 43 to 47). In the external parts, frontal accretion leads to the development of a foreland thrust belt, while underplating in the internal zones results in the formation of an antiformal nappe stack (Fig. 3.1 and 3.5).

Frontal accretion affects the recently deposited foreland sediments and starts very early in the experiments (see stage t_{10} in the experiment 46, Fig. 3.4). This mechanism is expressed by the successive activation of frontal thrust slices in the foreland basin and favours the growth of the wedge perpendicularly to the orogenic axis. When the sediments thrust by frontal accretion exceed the initial surface slope ($\alpha = 2°$) of the wedge, they are eroded. Frontal accretion therefore leads to a cyclic syndeformational removal of an important volume of foreland sediments. For instance, in the experiment 46 (Fig. 3.6), the slice of foreland sediments trapped between the thrusts 1 and 2, activated respectively at t_{13} and t_{15}, has almost disappeared at t_{23}, when a third thrust appears in front. Both in the models and in nature, at an advanced stage of evolution, a number of structures accommodating some displacement are totally eroded. This is the case for the thrusts 1 and 2, whose small remnants observable at stage t_{23} (Fig. 3.6) do not provide any indication on their original lengths. Because of this erosion of

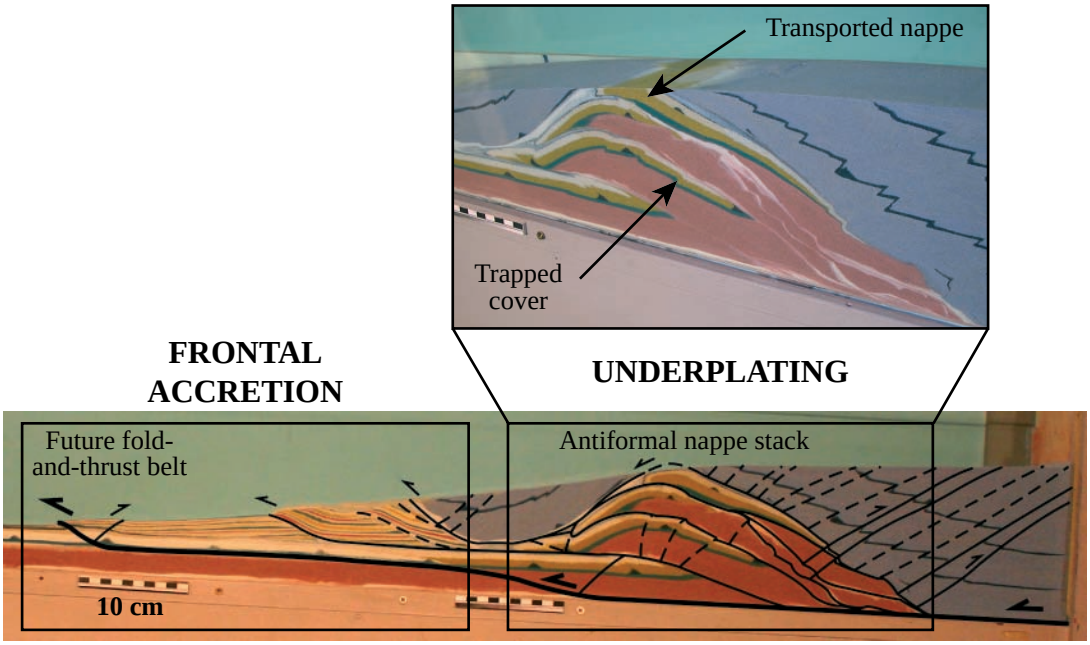

Fig. 3.5 *Tectonic mechanisms involved in the development of an orogenic wedge: frontal accretion of foreland sediments in the external parts and underplating of basement imbricates in the internal zones. Frontal accretion is initiated early (t_{10}) in the experiment and results in a large erosion of the recently deposited sediments before being in addition responsible for the fold-and-thrust development in the foreland. Underplating starts later (t_{16}) and leads to the development of an antiformal basement nappe stack.*

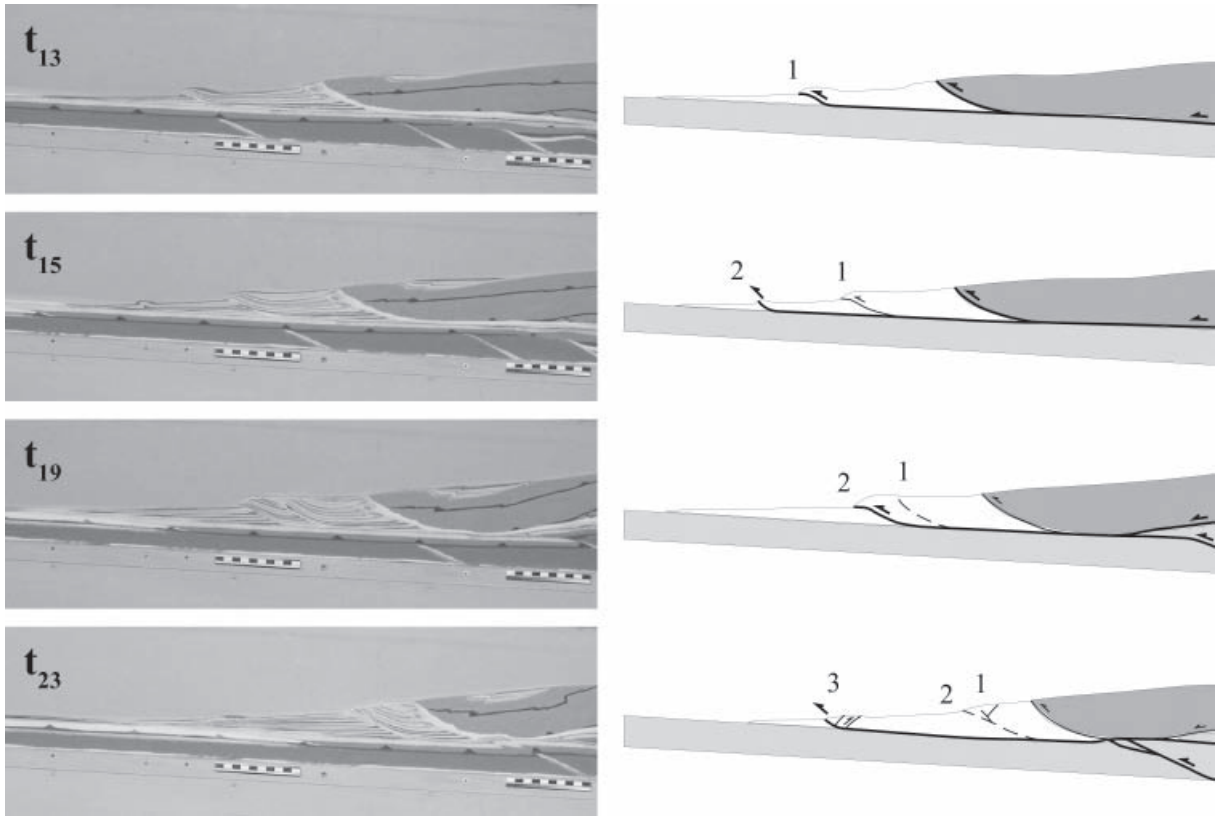

Fig. 3.6 *Cyclic syndeformational removal of foreland sediments due to frontal accretion. On the structural schemes, the main units and faults are drawn: the lid (dark grey), the basement and cover are grouped (light grey), the foreland sediments (white), the faults accommodating major displacements (thick lines), minor displacement (thin) and the inactive faults (dashed lines). From t_{15}, the foreland sediment slice delimited by the thrusts 1 (t_{13}) and 2 (t_{15}) is gradually eroded and when the thrust 3 propagates (t_{23}), this tectonic unit has almost disappeared.*

tectonic structures, the total shortening is most likely strongly underestimated in a number of mountain belts. This lack of data may cause major mistakes in the restoration of balanced cross sections. In addition, frontal accretion is also responsible for the development of a fold-and-thrust belt in the foreland (just initiated in Fig. 3.6).

When the displacement of the lower plate can no longer be mechanically accommodated by subduction of thrust units at depth, shortening is taken up by underplating. This mechanism allows material of the lower subducting plate to be accreted to the upper plate, contributing to wedge growth. In the experiments, the structural heritage of the lower plate (weak levels of glass beads in the basement) defines the size and favours the initiation of underplating, but the process then continues spontaneously in the homogeneous part of the basement due to burial (t_{29} Fig. 3.4). Underplating leads to the formation of an antiformal nappe stack (Fig. 3.5) where the displacement is accommodated along thrust ramps, favouring localized rapid syn-convergence exhumation. In the experiment 46, the geometry of the nappe stack is very close to the one proposed by BURKHARD & SOMMARUGA (1998) for the Alpine Crystalline Massifs. In their profile, some cover is trapped between the basement imbricates and, similar to the Helvetic nappes, the cover of the two most internal basement unit undergoes a large transport.

Exp.	Erosion	Sedimentation
42	no	no
43	high	very low
44	very low	very high
45	low	high
46	low	low
47	high	high

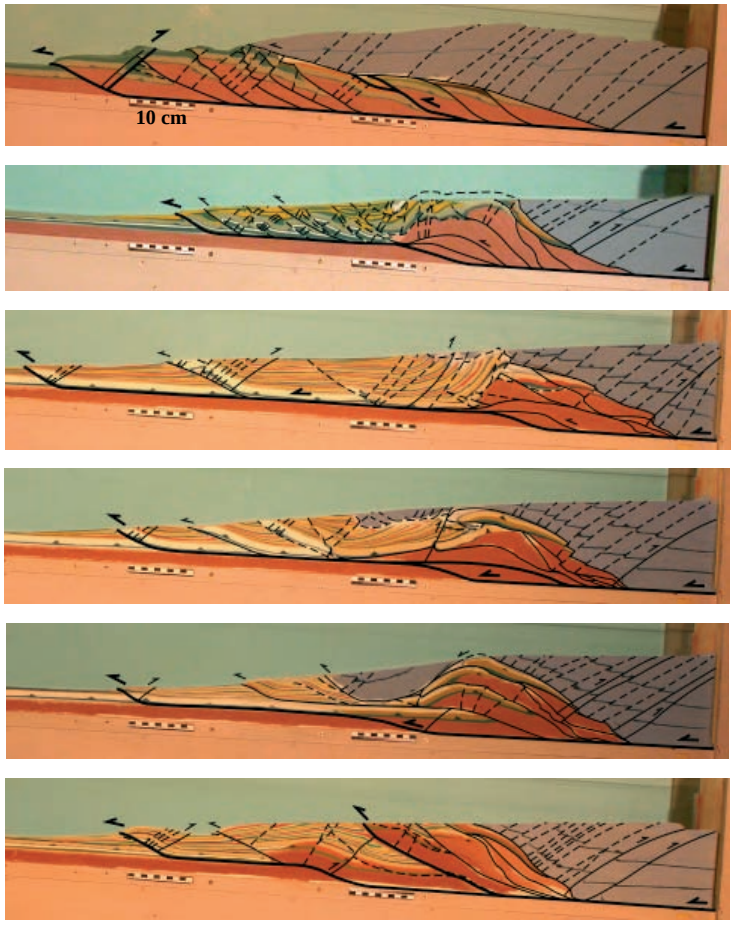

Fig. 3.7 *Six experiments performed with variable amounts of erosion and sedimentation are compared (each section undergoes the same shortening). Three kinds of faults are distinguished: faults accommodating main displacements (thick black lines), minor displacement (thin lines) and inactive faults (dashed lines). A high friction wedge is obtained without surface processes (experiment 42). Erosion (43 to 47) increases the underplating and localizes the uplift of basement imbricates. Low erosion preserves a maximal extent of the lid and consequently favours the detachment of its front (45 & 46), while basement imbricates are steeper with a high erosion rate (43). A very low sedimentation (43) favours the creation of a number of small thrust slices briefly active in the foreland basin. In contrast, high sedimentation (44, 45 & 47) is expressed by few thrusts active for a long time and intense backthrusting. A very high sedimentation rate inhibits the development of the antiformal stack (44). Intermediate conditions of sedimentation and erosion (46) lead to a realistic exhumation of the basement units and to the development of both a sedimentary foreland basin and a future fold-and-thrust belt.*

3.3.2 Variations of erosion and sedimentation rates

A comparison of experiments with variable rates of erosion and sedimentation reveals that surface processes play a major role during the evolution of a mountain belt. Indeed, without surface processes we obtain an unrealistic high friction wedge. Models that include erosion/sedimentation and changes in rates of surface processes lead to major structural differences in the orogenic development. Thus, we suggest that the diversity of structural styles and morphologies encountered along the Alpine arc (illustrated by the three cross sections Fig. 3.10) may be in part explained by such local variations in efficiency of surface processes.

3.3.2.1 Insights from different experiments

A comparison of six experiments that underwent the same amount of shortening (around 300 km at the natural scale) but variable amounts of sedimentation and erosion (Fig. 3.7) shows the wide range of structures (experiment 42 vs. experiments 43 to 47). Without surface processes (experiment 42), we obtain a classical high friction wedge. In response to shortening, basement imbricates first thrust each other using inherited weaknesses. Then, the unstructured part of the basement spontaneously underthrusts. Erosion increases the underplating and localizes the uplift of basement units that constitute a nappe stack. High erosion (experiment 43) appears to favour the development of steeper basement imbricates in the antiformal stack. In contrast, a very high sedimentation rate (experiment 44) strongly inhibits the development of such an antiformal stack. In this case, the still horizontal imbricates are underplated on two levels, forming a flat nappe stack. Erosion favours also an important displacement of the cover of the two most internal basement units, overriding the antiformal nappe stack (experiments 43 to 47). This transport (stage A Fig. 3.8) is possible due to the presence of a décollement level at the base of the cover, similar to the Triassic evaporite level in the Alpine setting.

Very low sedimentation (experiment 43) favours the creation of a number of small thrust slices briefly active in the domain of frontal accretion (Fig. 3.9). High sedimentation results in the development of only a few thrusts in the foreland basin sediments (experiments 44, 45 and 47). They are typically intensely retrothrust and active for a long time (Fig. 3.9).

Intermediate conditions of sedimentation and erosion (experiment 46) lead to a realistic exhumation of the basement units and to the development in the foreland of both a sedimentary basin and, at an advanced stage of evolution, a fold-and-thrust belt. The localized

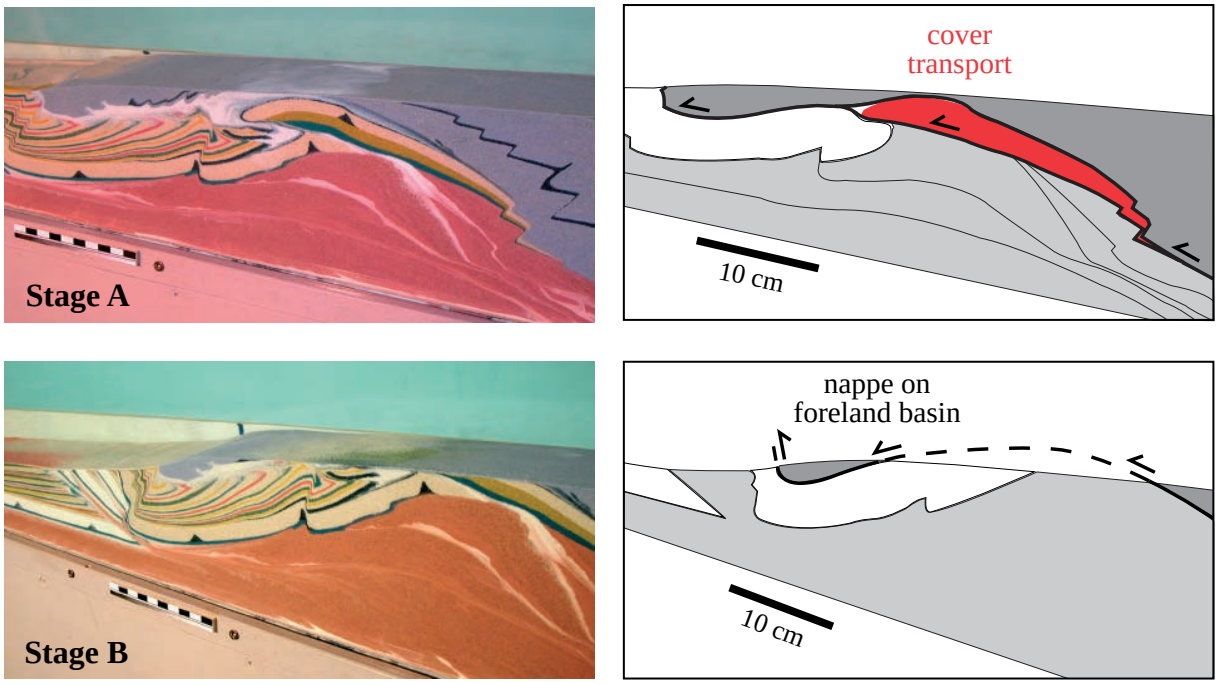

Fig. 3.8 *At the stage A (experiment 45), the cover (red on the scheme) of the two most internal basement units is transported on the top of the antiformal nappe stack. This displacement is possible due to the effect of erosion combined with the presence of a décollement level at the base of the sedimentary cover (experiments 43 to 47). At the stage B, due to the combined effect of low erosion and high sedimentation, the nappe detached of the lid lies uniquely on foreland basin sediments (experiment 45).*

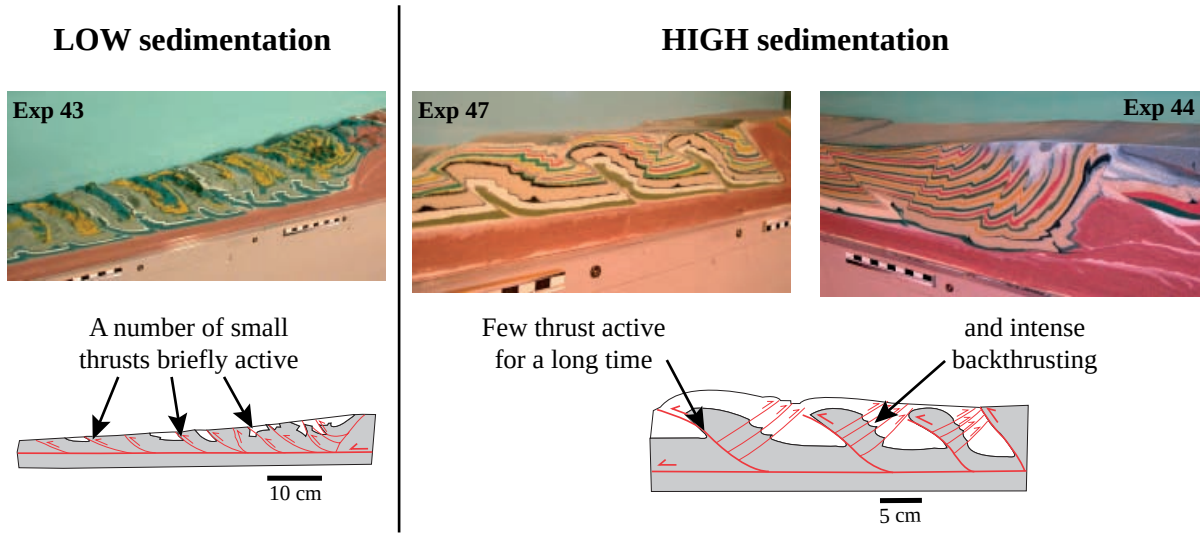

Fig. 3.9 *Contrasted structures in the foreland due to low or high sedimentation rates.*

uplift of the basement nappe stack results in the detachment of a klippen from the lid. Low erosion preserves a maximal extent of the lid and consequently favours the detachment of its front (only experiments 45 and 46). In experiment 46 the nappe overthrusts both the foreland sediments and the antiformal stack. As the sedimentation rate is higher in the experiment 45, the nappe lies entirely on foreland basin sediments (stage B Fig. 3.8).

3.3.2.2 Comparison with Alpine cross sections

Natural orogen-foreland basin systems are not homogeneous along strike due to structural and mechanical heterogeneities, but also due to external parameters such as surface processes. For instance, the width and depth of the North Alpine Foreland Basin (NAFB) strongly increases along its axis, from SW to NE (Homewood 1986), most likely linked to the varying volumes of sediment deposits. To better constrain the influence of erosion and sedimentation on the development of the Alps and adjacent northern foreland basin, we compared models with variable rates of surface processes to three Alpine tectonic cross-sections (Fig. 3.10).

In the first model with very low sedimentation and high erosion (experiment 43), the foreland basin is subdivided by thrust-related anticlines into smaller sub-basins. In the Western Alps, along a profile from the Jura to the Belledone massif (profile XX' Fig. 3.10), these structures correlate well with anticlines such as the Salève and Ratz. Separated by these narrow sub-basins, the southern border of the folded Jura is located very close to the Alpine front. In the internal part of the foreland, portions of the Molasse basin are overthrust by autochthonous Mesozoic cover such as the Bornes-Aravis massifs. The most external analogue basement imbricates show a rather shallow dip to the foreland, similar to the northern imbricates of the Belledone massif (Lacombe & Mouthereau 2002). Finally, only very small remnants of the Penninic klippen remain both in the model and in the Western Alps cross-section (Sulens-Annes klippen).

In the second model with low erosion and sedimentation (experiment 46), the internal part of the foreland basin is disturbed by a succession of small thrusts, comparable to those developed along a more central Alpine profile (profile YY' Fig. 3.10), where the NAFB is an apparently unique basin deep of 3-4 km. Without structural heritage, new basement imbricates develop in the frontal part of the analogue wedge, corresponding to a forward evolutionary stage of the presumed current Alpine underplating. Autochthonous sedimentary series and foreland basin-sediments

Fig. 3.10 *Comparison of geometrical structures between three simplified cross-sections of the central-western Alps and three analogue experiments performed with variable rates of erosion and sedimentation. Location of sections on a structural map of the Western Alpine foreland: section from the Jura to the Belledonne massif (modified from Jouanne et al. 1995 and Lacombe & Mouthereau 2002) (Profile XX' compared with experiment 43), section from central Jura to Mont-Blanc massif (modified from Burkhard & Sommaruga 1998 and Mosar et al. 1996) (Profile YY' compared with experiment 46) and section from Molasse basin to Aar massif (modified from Spicher 2005) (Profile ZZ' compared with experiment 47).*

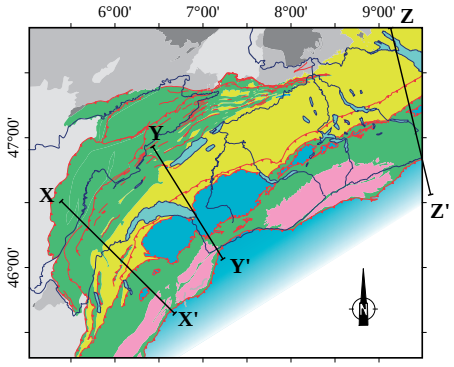

Molasse deposits / N+S Helvetic Flysch

Mesozoic cover

Basement units (included Permo-Carboniferous grabens)

Penninic nappes

Profile X-X'

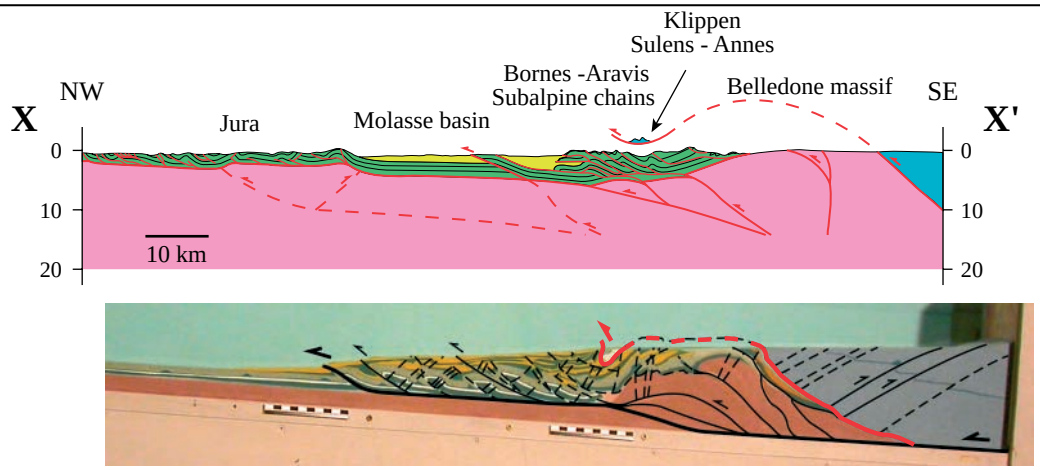

Profile Y-Y'

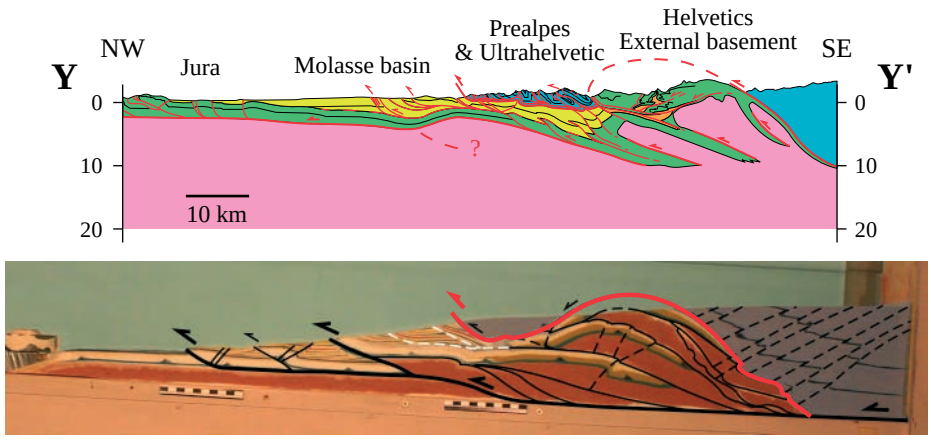

Profile Z-Z'

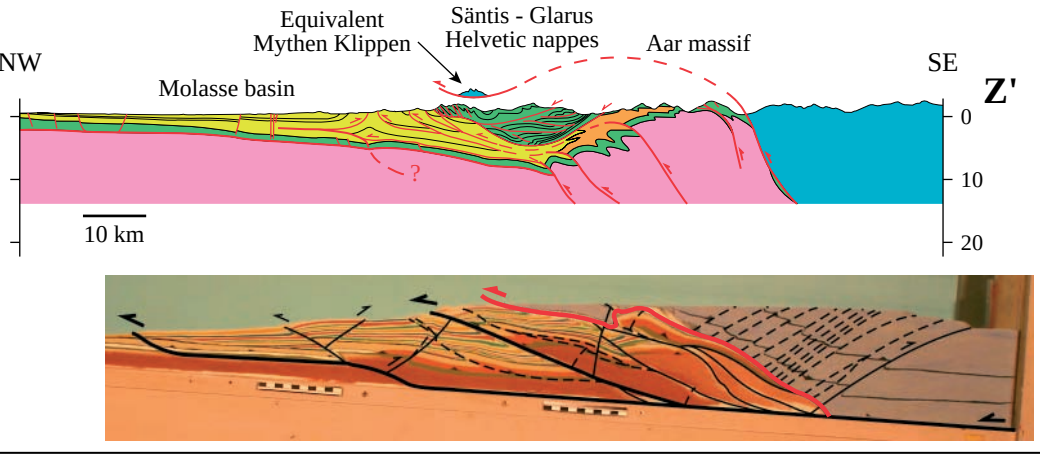

(equivalent of the North Helvetic Flysch) are involved in the large basement thrusts bringing basement units (equivalent of the Helvetics External basement) on top of sedimentary cover. Due to the uplift of the antiformal basement nappe stack, the lid cover is separated in two pieces leaving an important allochtonous Penninic klippen equivalent of the Prealpes klippen belt.

In the third model, a broader and thicker foreland basin develops because of high sedimentation associated with high erosion (experiment 47). Similar to the Central Alps (profile ZZ' Fig. 3.10), the NAFB reaches its maximum width (more or less 100 kilometres) and thickness (5-6 km). The successive layers of foreland sediment deposits are little deformed, and the layers of Molasse remain subhorizontal in the central and northern parts of the basin, and are only affected by steep normal faults. The basement imbrication style is quite different, because the steep imbricates are only slightly underthrust, stay next to one another, and do not constitute an antiformal stack. A frontal basement imbricate develops similarly to model 2 and develops a triangle structure, as in the Central Alps cross section. Small remnants of the Penninic klippen remain both in the model and in the cross-section, as in model 1.

Results from modelled orogen-foreland basin systems provide insights into the dynamics and development of the Molasse basin and its orogenic hinterland in relation to surface processes. The analogue modelling experiments demonstrate that variations along strike of the Alpine structural development clearly depend in part on the different local rates of erosion and sedimentation.

3.3.3 Material paths

The study of material paths (trajectories) in mountain belts may provide useful data on the understanding of their kinematics. It is known that surface processes strongly influence the timing, localization and amplitude of rock displacements in the varying members of an orogenic wedge. After a brief outline on exhumation and uplift of rocks, we will study the two-dimensional trajectories of points located in the lower converging plate and then the differing paths of points located in the upper plate. By the comparison of their trajectories in experiments performed with and without erosion/sedimentation, we aim to better understand the influence of surface processes on material transfer in the wedge.

One way to investigate orogen dynamics is to look at the ages recorded by different thermochronometers across it (Willett & Brandon 2002). Geochronological data such as fission tracks or U Th/He methods are very useful for deciphering the cooling and exhumation history of rocks. To avoid confusion, the terminology used for material displacement during mountain building, follows that of England & Molnar (1990). Exhumation of rocks means the approaching of a rock particle to the Earth's surface, which is, e.g. recorded by cooling rates calculated from thermochronologic data (e.g., Foster & John 1999), whereas uplift of rocks means the displacement of rocks with respect to the geoid, or less accurately with respect to the mean sea level.

In our study, we have compared the two-dimensional trajectories of five points located in the different members of the model, evolving with or without erosion/sedimentation. In the following, we will first study the trajectories of three points located in the lower subducting plate (3.3.3.1) and then the paths of two points in the lid (3.3.3.2). The experimental data are directly scaled to nature in the various graphs to favour a direct comparison with the evolution of a mountain belt. These data may include small errors related to different sources, such as the experimental procedure, the mechanical properties of the used materials and the transition between the device and the graphical representation. As these errors due to measure are small relative to the size of the studied processes, they are neglected.

3.3.3.1 Major experimental tectonic stages through the trajectories of points located in the subducted plate

To describe and investigate the mechanism of underplating leading to the uplift of basement units, the displacement of three points located in the subducting plate is analysed. Two points are chosen at the top of the basement units and a third one inside the cover (Fig. 3.11). To make the graph easy to read, the three points are named depending on their location along the reference Alpine cross section (Burkhard & Sommaruga 1998). The horizontal transport of the points is expressed in terms of incremental displacement relative to a pin, located in the undeformed part of the converging cover (X-axis). The motion of this mobile pin (represented by a white star on the final stage picture) shows the incremental convergence of the lower plate. The vertical component of displacement (Y-axis) is represented by the depth or

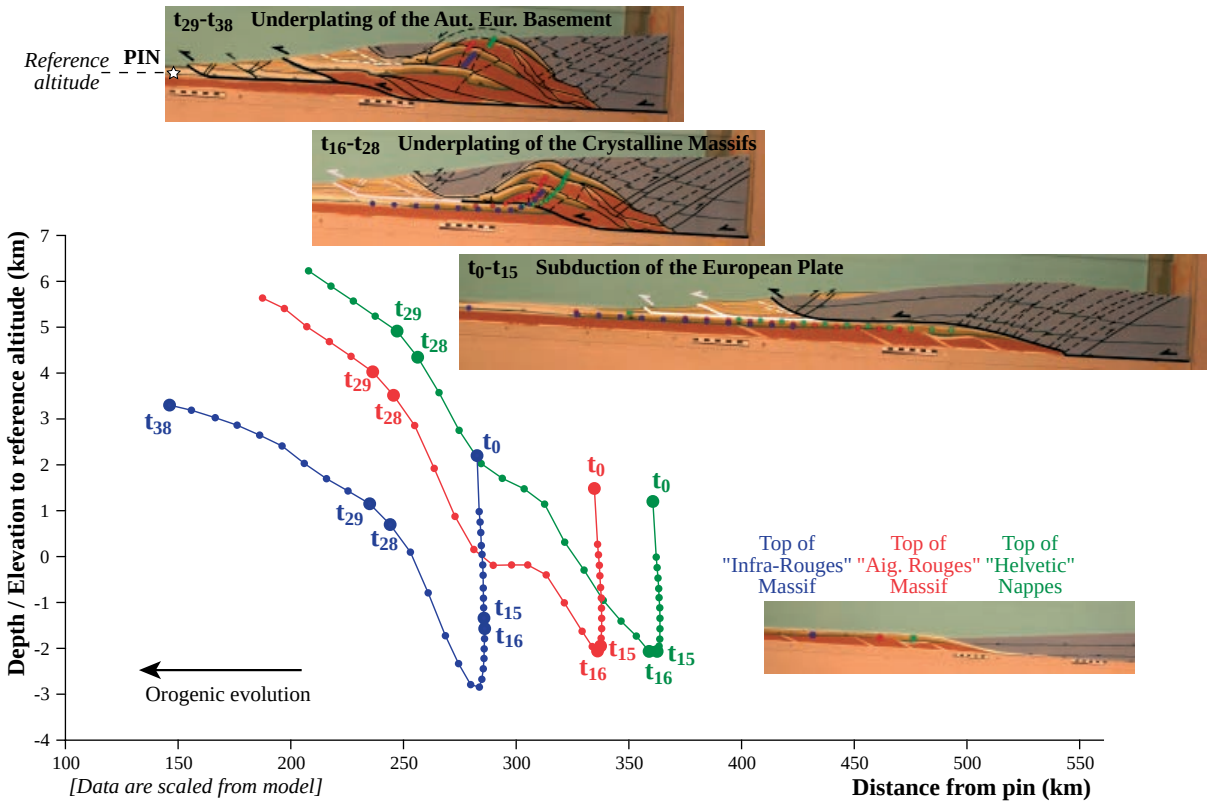

Fig. 3.11 *Trajectories (measured relative to a fixed reference) of three points located in the converging plate, during an experiment performed with surface processes (experiment 46). The studied points are named in reference to the Alpine setting (picture): two are situated at the top of the basement units and the third is inside the cover. The horizontal component of the movement is measured relative to a pin located in the undeformed part of the lower plate (white star) and the vertical component to the reference altitude of the pin at the end of the experiment (dashes). Three stages of evolution appear, each one governed by a major tectonic mechanism. From t_0 to t_{15}, the points are driven to depth quickly following the subduction of the lower plate. From t_{16} to t_{28}, due to the underplating of the basement units, the green and the red points undergo a rapid uplift, shortly followed by the blue one. From t_{29} to t_{38}, the uplift of the points continues but is slower, because the underplating now concerns the homogeneous and most external part of the basement.*

elevation of the points to the reference altitude of the pin (dashes on the final stage picture), at the end of the experiment (Fig. 3.11). This measure of vertical transport to a mean elevation may be compared to apatite and zircon fission-track analyses. The localization of the studied points has been accurately drawn on pictures of the successive stages of shortening and the displacement in both directions has been systematically measured. Each curve representing the displacement of the described points must be read from right to left, following the orogenic evolution. It appears that the process may be described in terms of three stages (see pictures Fig. 3.11), each one governed by a major tectonic mechanism. During the phase t_0 to t_{15}, the points are driven to depth quickly due to the subduction of the lower plate. During the phase t_{16} to t_{28}, the green and the red points undergo a rapid uplift. The blue dot is initially still involved in the subduction, before being uplifted too. The major mechanism responsible for this rapid uplift is the underplating of the basement units, called “Crystalline Massifs” in reference to the Alpine cross section of Burkhard & Sommaruga (1998). During the t_{29} to t_{38} phase, the uplift of the points slows down. The green and the red dots are completely eroded at the end of the experiment. The major mechanism involved is still the underplating but it now affects the homogeneous and most external part of the basement, called “Autochthonous European foreland basement”. The mechanics of the wedge is then modified because deformation propagates toward the foreland. Detailed inspection of the curves shows that the path of two close points (the green and the red ones for instance) do not present exactly the same pattern. While the two points are quickly uplifted between t_{16} and t_{28}, this uplift is not regular (Fig. 3.11). The varying slope of the trajectories indicates the differences in uplift rates of points that may end up very close in a final stage. The secondary variations are linked to the local structural and lithological heritages, leading to a different tectonic response.

A different way of investigating transfer of material

in mountain belts is the analysis of P,T,t paths. In this case, it is not the displacement of a rock with respect to a fixed reference (corresponding to the uplift) that is measured, but the displacement with respect to the surface (Fig. 3.12) (i.e. the exhumation). We decided to express the distance between a rock and the topographic surface in terms of thickness of rocks (including sediments and basement). The distance between a study point and the surface vertically corresponds to the sedimentary thickness (Y-axis Fig. 3.12) measured at each increment of displacement, relative to the pin located in the converging plate (X-axis). For the three points in the lower subducting plate, the curves representing their two-dimensional displacement measured to a reference altitude (uplift, Fig. 3.11) or to the topographic surface (exhumation, Fig. 3.12) seem to be very similar. The curves showing the exhumation paths present yet more irregularities, especially to the end, due to the variable erosion of the lid topographic surface. Another very interesting fact is the timing of the events linked to the underplating. Based on the depth/elevation of the points relative to the reference altitude, the subduction phase ends at t_{15} and underplating initiates at t_{16}, by an immediate uplift of the red and green points. But the graph presenting the exhumation paths shows that the sedimentary thickness is still at a maximum from t_{16} to t_{18} and decreases only after this time. This discrepancy illustrates the fact that underplating and subsequent basement uplift induce a large but slightly delayed increase of the erosion rate on the lid. Changes in the slope of the "exhumation" curves (Fig. 3.12) reflect changes in rates. Similar changes in rates of exhumation are also observed on data sets of cooling ages from the different tectonic units in the Alps (Hunziker et al. 1989, Hunziker et al. 1997, Kühni & Pfiffner 2001). Results from our model investigation may help unravel the complexity of these curves.

To investigate the role of surface processes on the uplift of basement units, we studied the trajectory of a point during the experiment performed without erosion and sedimentation (experiment 42). This point is located exactly at the same position as the red one analysed in the experiment 46 (top of the second most internal basement unit) and is represented consequently with the same colour (scheme Fig. 3.13). The paths of the yellow and the pink points located in the lid (scheme Fig. 3.13) will be described in the following chapter. The trajectory of the red point is simple and may be cut into two phases: from t_0 to t_{13}, the point is driven to depth quickly due to the subduction of the lower plate and from t_{14} to t_{34}, it slightly and regularly goes up as a result of little underthrusting of the basement units.

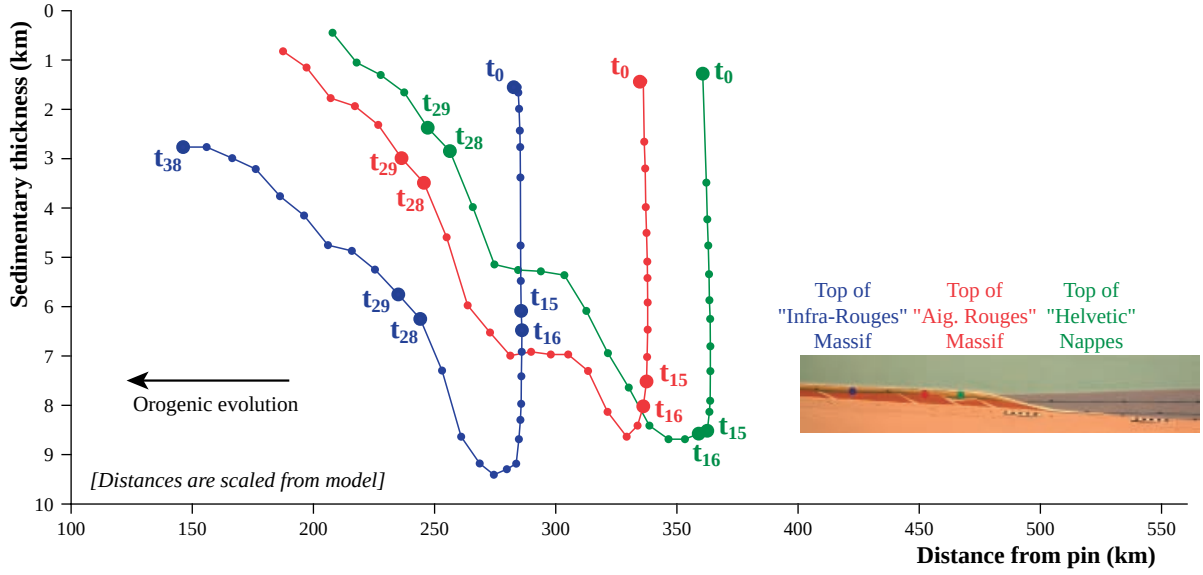

Fig. 3.12 *Trajectories (measured with respect to the surface) of three points located in the converging plate, during an experiment performed with surface processes (experiment 46). In contrast to Fig. 3.11, the vertical component of the movement represents the distance between the study point and the surface, in terms of thickness of sediments on the analysed material. The three stages of evolution are reproduced from Fig. 3.11 (t_0 to t_{15} = subduction of the lower plate, t_{16} to t_{28} = underplating of the basement units, t_{29} to t_{38} = underplating of the homogeneous and most external part of the basement). The uplift of basement units due to their underplating (from t_{16}) causes an increase of erosion on the lid. As the sedimentary thickness on the studied points is still maximal during some increments of displacement, it appears that the erosive response is slightly delayed.*

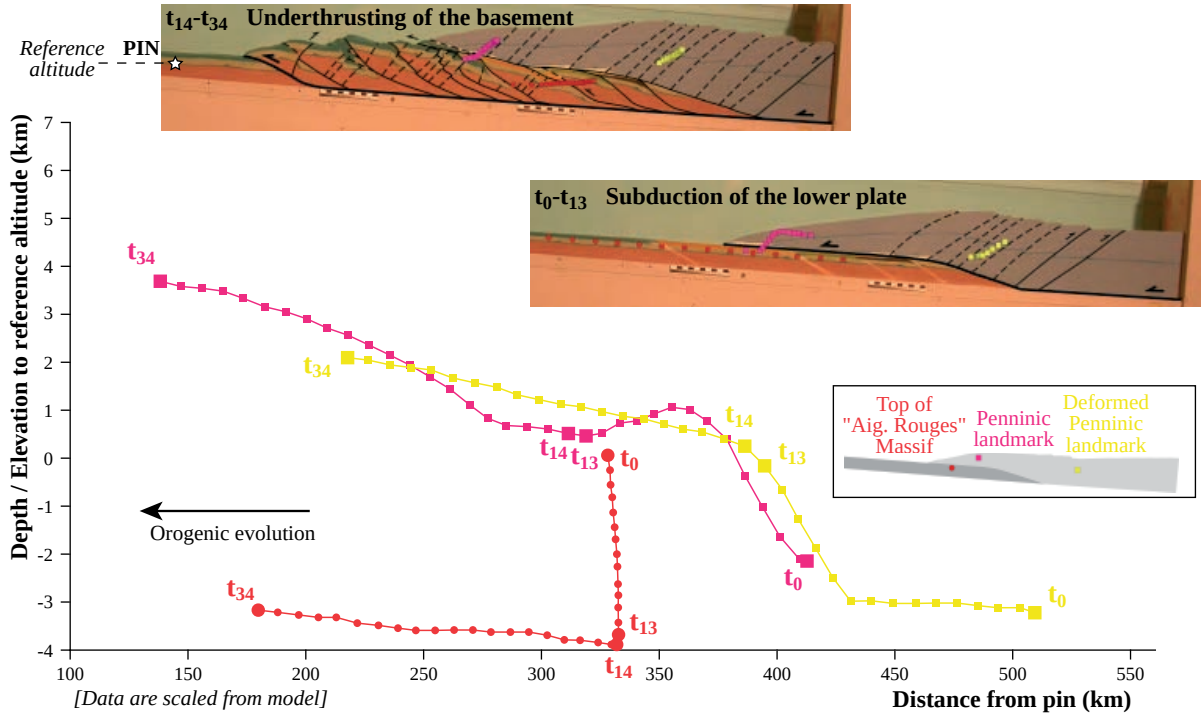

Fig. 3.13 *Trajectories (measured relative to a fixed reference) of one point located in the converging plate and two in the upper plate, during an experiment performed without surface processes (experiment 42). The horizontal component of the movement is measured relative to a pin located in the undeformed part of the lower plate (white star) and the vertical component relative to the reference altitude of the pin at the end of the experiment (dashes). The trajectory of the point in the converging plate may be divided into two phases: from t_0 to t_{13}, the point goes down quickly due to the subduction of the lower plate and from t_{14} to t_{34}, it is slightly and regularly uplifted as a result of minor underthrusting of the basement units.*

With and without surface processes, the points located at the top of basement units in the lower plate are first pulled to depth before going up to the surface. The initial phase is governed by the process of subduction and the second one by the underthrusting of basement units (experiment 42, Fig. 3.13), changing to underplating (experiment 46, Fig. 3.11) under the action of erosion. The comparison of these two experiments shows that the erosion of the lid initiates the uplift of basement units. Associated with sediment deposit in the foreland, erosion localizes and controls their exhumation with respect to the surface.

3.3.3.2 Complex uplift paths of points located in the lid

During the experiments, the lid is passively transported on the converging lower plate and is internally deformed by backthrusting, as its surface is gradually eroded. To better describe the evolution of the lid and estimate its internal rate of deformation, we studied the uplift paths of two inner points spatially remote (Fig. 3.14). The most internal point (yellow point on scheme) is located in the core of the lid and is named "deformed Penninic landmark" in reference to the Alps and because it is largely affected by retrothrusting. The second one (pink point) is situated close over the basal thrust of the lid, half way up the basement ramp and is named "Penninic landmark". The graph of their trajectories presents the same axis and scales as the graph showing the material paths in the lower plate (Fig. 3.11). While they are continuously uplifted, their paths appear to be quite different notably during the first half of model evolution (Fig. 3.14). Indeed, from the beginning, the external pink point climbs up onto the top of the basement ramp yielding the "bump" shape of the curve, whereas the internal yellow point is passively transported (t_{10}). From the stage t_{12}, the situation inverts: the internal yellow point climbs up onto the top of the basement ramp and the pink one, having passed the ramp, is passively transported on the succession of basement units (t_{16}). In addition, the uplift of the yellow point increases due to internal retrothrusting of the lid. The final phase is common for both points: they are passively uplifted due to basement underplating (t_{38}). However the proximity of the deformation front favours a higher uplift of the pink point.

In the experiment without surface processes (experiment 42), the trajectories of two points of the

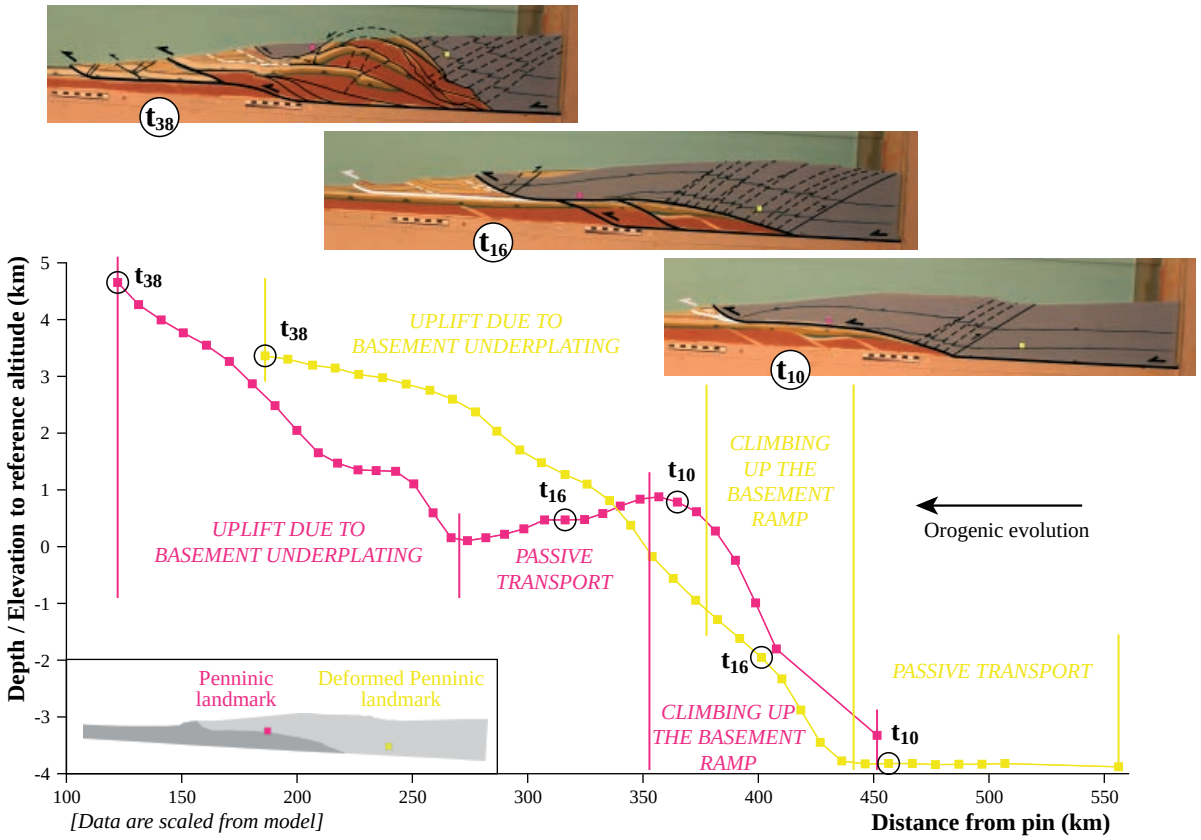

Fig. 3.14 *Trajectories (measured relative to a fixed reference) of two points located in the lid, during an experiment performed with surface processes (experiment 46). The horizontal component of the movement is measured relative to a pin located in the undeformed part of the lower plate (white star Fig. 3.11) and the vertical component to the reference altitude of the pin at the end of the experiment (dashes Fig. 3.11). The point located in the front of the lid (pink) climbs up onto the top of the basement ramp, is then passively transported on the succession of basement units and finally is uplifted due to basement underplating. The point more internally located in the lid (yellow) is passively transported, then it climbs up onto the top of the basement ramp before being passively uplifted due to basement underplating.*

lid located approximately at similar places than in experiment 46 (scheme Fig. 3.15) are comparable (Fig. 3.15). The external point (pink) first climbs up the basement ramp, while the internal one (yellow) is passively transported (t_8). Then, the latter is also uplifted due to the combined effect of climbing up the ramp and retrothrusting and the pink point is passively transported on the top of basement units (t_{14}). Finally, the two points are slightly uplifted due to basement underthrusting (t_{34}). The major difference between experiments 42 and 46 is the amplitude of uplift. Without erosion (experiment 42, Fig. 3.15), the maximal vertical displacement of the points is 6 km scaled to nature, while the value reaches 8 km when erosion is performed (experiment 46, Fig. 3.14). The underplating of basement units, initiated by erosion, increases noticeably the uplift of the thrusting lid.

3.4 Conclusions

The series of analogue modelling experiments shows that the two main mechanisms controlling the orogenic growth are cyclic frontal accretion and underplating. In the external parts of the model, frontal thrust slices are successively activated in the recently deposited foreland sediments. This frontal accretion leads to major removal of foreland basin sediments and to a consequent erosion of the inner structures accommodating displacement. This phenomenon may lead to serious underestimation of total shortening in actual mountain chains. Simultaneously in the internal zones, basement units are underthrust along weak levels simulating inherited structural control. Enhanced by erosion, this mechanism produces underplating that leads to the development of an antiformal nappe stack. This geometrical feature accommodates large displacement along very active thrust ramps.

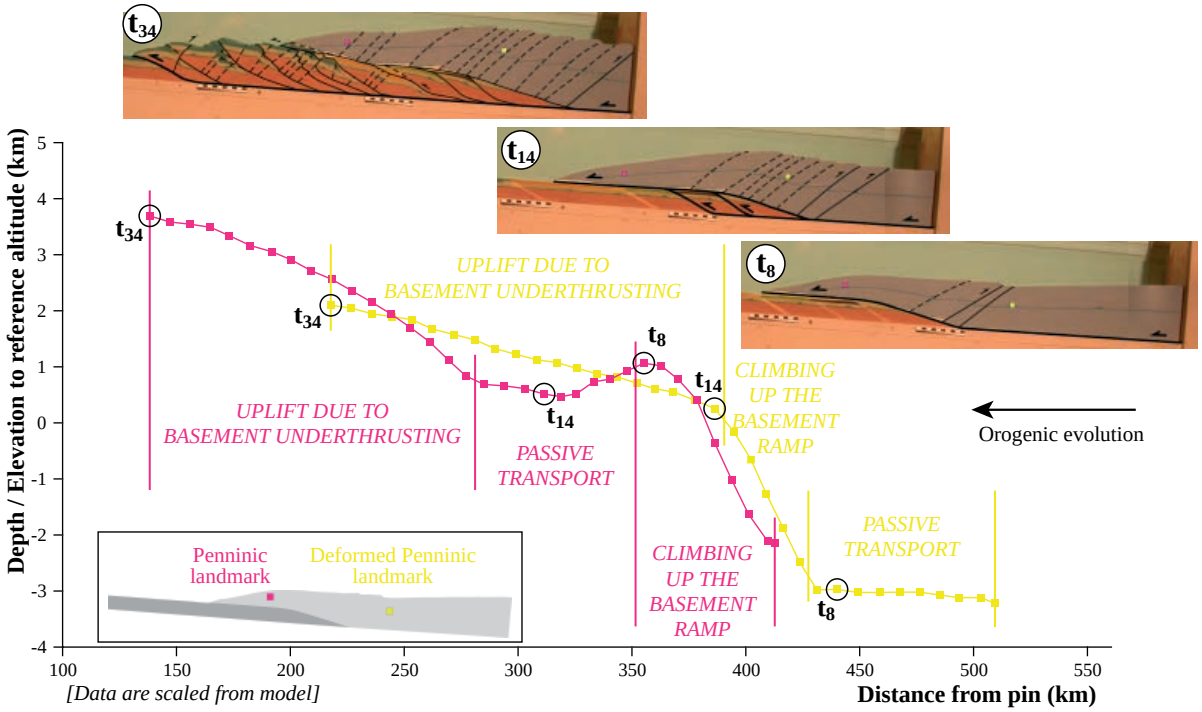

Fig. 3.15 *Trajectories (measured relative to a fixed reference) of two points located in the lid, during an experiment performed without surface processes (experiment 42). The horizontal component of the movement is measured relative to a pin located in the undeformed part of the lower plate (white star Fig. 3.13) and the vertical component to the reference altitude of the pin at the end of the experiment (dashes Fig. 3.13). The two-dimensional trajectories of both points are similar to the trajectories described in the experiment performed with surface processes (see Fig. 3.14). The only difference is the amplitude of uplift, increased by the underplating of basement units and therefore by erosion.*

Surface processes play a major role in the development of a mountain belt. They interact with tectonic processes to maintain the mechanical equilibrium of the wedge. The variations in rates of erosion and sedimentation strongly modify the extent, the morphology, the structures, the timing of development and the material paths in a mountain belt. For instance, erosion of the lid increases the underplating of basement units and localizes the exhumation, resulting in an antiformal nappe stack. In response, the uplift of material due to the underplating of basement units at depth leads to an increase of localized erosion. It also appears that the higher the erosion rate the steeper are the basement imbricates in the antiformal stack. However, a very high sedimentation rate in the foreland basin strongly inhibits development of an antiformal stack. In contrast, very low sedimentation rates favour the creation of a number of small thrust slices briefly active. Intermediate conditions of erosion and sedimentation lead in the foreland to the development of a sedimentary basin and a fold-and-thrust belt.

The influence of surface processes on material paths has been studied using the trajectories of three particles located in the converging lower plate and two in the upper plate. In the lower plate, the complex uplift paths are related to the tectonic stages (subduction and underplating). In the lid, the trajectories are linked to thrusting movement of the upper plate, before being affected by underplating of the lower plate basement units. Two experiments performed with and without surface processes show quite similar trajectories for particles in the upper and lower plates. The main difference is that erosion increases the amplitude of underplating and consequently the amplitude of particle uplift. In addition, two neighbouring points may follow very dissimilar trajectories. Local differences in structures and/or lithologies may lead to major variations in the tectonic development. Studies of exhumation paths in mountain belts often show trajectories of rocks constrained by few data points only. They are probably “smoothed” models trajectories of particles likely more complex in reality, as suggested by our model results.

The role of erosion and sedimentation on the dynamics and development of the Alpine orogen and adjacent Molasse basin has been emphasised by a comparison between tectonic cross-sections and models performed with variable rates of surface processes. For

instance, with low sedimentation, as in the Western Alps, the foreland basin is shallow and subdivided by thrust-related anticlines into smaller sub-basins. In contrast, in the Central Alps, a broader and thicker foreland basin develops because of high sedimentation and the successive layers of foreland sediment deposits are little deformed. In the experiments, new basement imbricates develop in the frontal part of the wedge that may correspond to a forward evolutionary stage of the presumed current Alpine underplating indicated by present seismic activity and measured convergence (MOSAR 1999, CALAIS et al. 2002). Both, in the models and along the three Alpine cross-sections, remnants of the cover lid are represented by allochthonous klippen, of various sizes depending on the erosion rate. Along strike, the Alpine basement massifs are imbricated with styles, varying from simple underthrusting to underplating and the development of an antiformal nappe stack.

Another insight from models has significant implications for geologists who study active mountain belt using kinematics of active faults to obtain estimates of middle term shortening rates. During active shortening of the model wedges, most of the horizontal displacement on faults is accounted for by few very active thrusts located at the frontal part, whereas, inside the body of the wedge, faults that reach the surface are not very active and the major part of deformation is essentially accounted for by vertical movements. Such rather unexpected deformation partitioning between horizontal displacements in the external domains and vertical movements in the inner parts of the wedge is a direct consequence of simultaneous frontal accretion and underplating at depth. These mechanisms seem to have occurred both in fossil orogens (for example the Alps, this study) and in active mountain belts, such as Taiwan (e.g., SIMOES et al. 2006) and the Himalaya (e.g., AVOUAC 2003).

*****

4 - Swiss Molasse Basin dynamics: Insights and lessons from analogue modeling

Mosar, J., Bonnet, C., & Malavieille, J.

submitted to *Basin Research* (12.2006)

Abstract

To investigate the mechanisms and processes controlling the evolution of a foreland basin at the front of a tapered wedge orogen, we ran analogue models simulating erosion and sedimentation. The prestructured setup is inspired from the Alpine domain and surface processes were performed to maintain the critical wedge geometry. During the experiments, we observed the development of internal tectonic geometries and punctuated thrusting as well as the cyclic behavior of surface processes. The models highlight also the importance of feedback mechanisms of erosion/deposition on the wedge mechanics. The comparison of the analogue foreland basin development with the evolution of the Alpine Foreland Basin showed strong correlations. We observed for instance in the experiments the transition of an underfilled "Flysch" type basin to an overfilled "Molasse" type basin and the similarity between the first-order analogue sedimentary cycles and those affecting the Alpine Foreland Molasse Basin. The sedimentary events documented in the Alps, but not seen in the analogue model evolution, are certainly due to external processes and mechanisms not modeled here, as for instance the climate changes. Finally, we suggest that the sedimentary processes in the Swiss Foreland Molasse Basin are governed at first order by the internal mechanics of the tapered wedge, and only secondarily by the flexural basin evolution mechanisms.

4.1 Introduction

The Molasse Basin in Switzerland forms a foreland basin that has evolved in response of the formation of the Alpine orogen. Following an initial stage of an underfilled Flysch basin, the foreland basin evolved into an overfilled Molasse basin, while at the trailing end the orogen kept growing involving cover nappes of the Helvetic platform domain and their equivalent basement units which formed an antiformal stack. This latter led to the Present day elevated topography of the Western Alps. In order to investigate the feedback mechanisms between surface processes such as erosion and sedimentation and tectonic processes at the front of the Alpine orogenic wedge and inside the Molasse Basin (Fig. 4.1), we performed a series of scaled analogue models based on the tapered wedge principle. In our analogue modeling we set out to investigate mechanisms and processes related to the period concerning the evolution of the Molasse Basin.

The main goals of this research are to investigate the physical responses of an orogenic wedge to erosion and sedimentation, the evolution of the foreland basin, and to take the Swiss Alps as an example. How are surface processes related to tectonic process in a tapered wedge model, and how does the foreland basin evolve? How do our results relate to the Alpine geodynamic setting, what are the insights gained on the operating mechanism and what are the lessons?

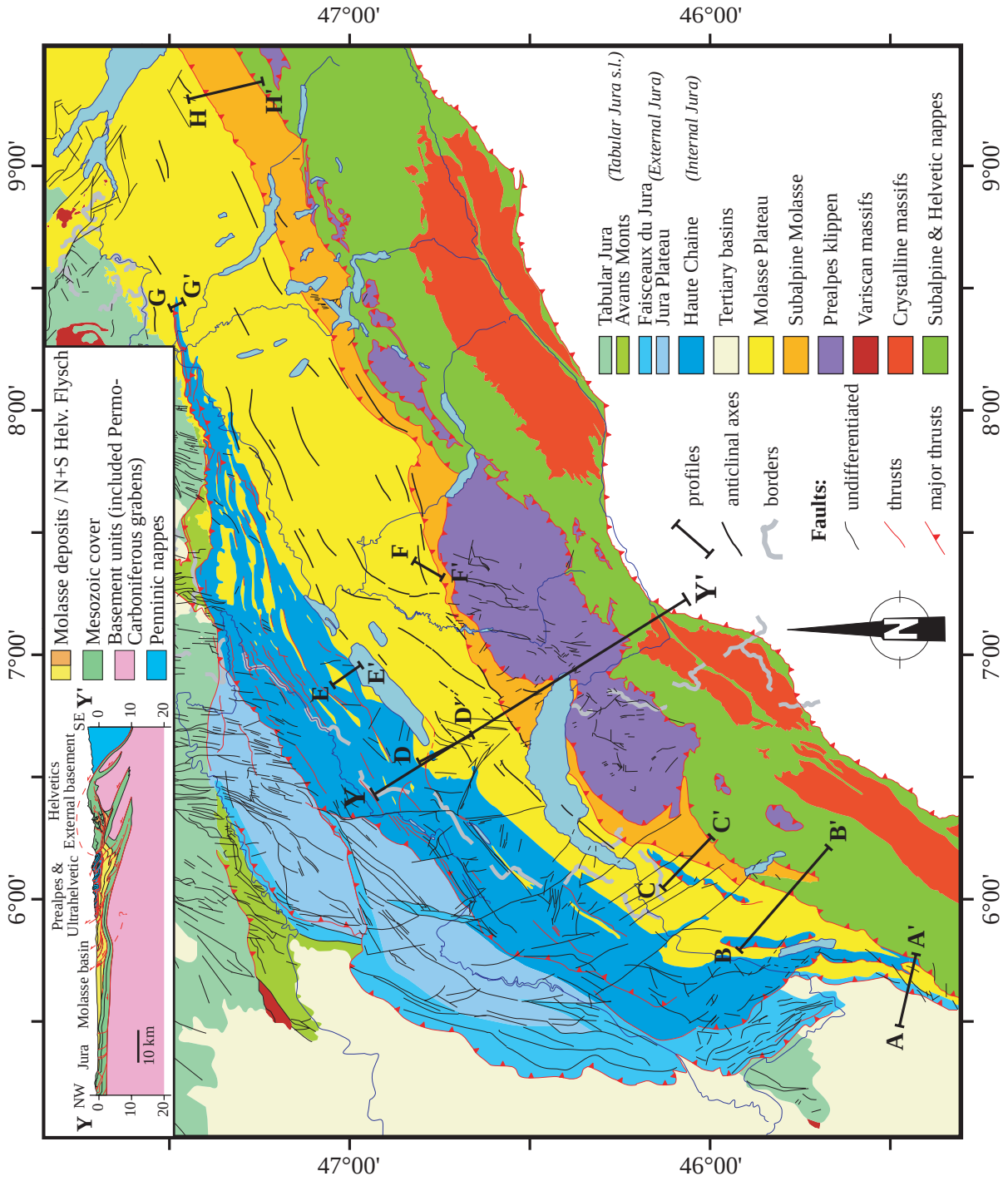

Fig. 4.1 *Simplified tectonic map of the Western and Central Swiss Alps. Faults fracturing the Prealpes, Molasse Plateau and Jura are indicated, as well as the anticlinal axes in the Molasse Plateau. Lines AA' to HH' on the map indicate the location of detailed tectonic profiles in the Molasse Basin (see Fig. 4.6). Line YY' on the map localizes a simplified section (top left) showing the overall tectonic structure across the central-western part of the Alps and foreland (modified from* Burkhard & Sommaruga *1998 and* Mosar *et al. 1996). From north to south, the main tectonic structures are the Jura fold-and-thrust belt, the Plateau formed by the Molasse Basin, the Subalpine Molasse imbricates which are thrust by the Prealpes klippen, the Helvetic nappes and their crystalline basement imbricates, and finally the orogenic lid formed by the different tectonic units of the Penninic.*

4.2 Analogue tapered wedge model

Analogue tapered wedge models are able to produce foreland basins that tectonically deform by folding and thrusting while sedimentation is going on. The punctuated thrusting in the foreland fold-and-thrust part of the orogenic wedge model is governed by the mechanics of the wedge. The geometric and kine-

matic evolution of the wedge is strongly dependent on the amounts of sediments shed into the foreland basin, as well as the volumes eroded, both in the growing wedge, and the basin. The novelty of our approach is that the analogue model takes into account both the tectonic and lithological heritages based on an Alpine paleogeographic setting (cross section Fig. 4.1).

4.2.1 Model setup

Our model is set up to understand processes of development of a foreland Molasse type basin in front of a growing orogen. The set up (Fig. 4.2) was chosen to represent the European platform with its prestructured basement units and sedimentary basins of the Helvetic domain. These units are successively incorporated into the accretionary prism after the Flysch to Molasse basin stage transition. The overriding lid is mainly considered to be the equivalent of the Penninic units. The setup was inspired from paleoreconstructions (Stampfli et al. 1997, Stampfli et al. 2001) and a balanced crustal-scale section across the Western Swiss Alps by Burkhard & Sommaruga (1998). The surface slope angle α and the basal detachment dip β, of 2° respectively 3°, were chosen in accordance with present day geometries in the Western Swiss Alps (Mosar 1999, Lacombe & Mouthereau 2002). Test runs with a thicker wedge, and incidentally with other initial setups, led to geometries and scenarios not applicable to the Alpine domain. The deep behavior of the ductile part of the crust is neglected since mainly its upper part is implied in the deformation. Indeed, as can be seen on most deep seismic-reflection profiles crossing the Alps (Guellec et al. 1990, Mugnier et al. 1990, Pfiffner et al. 1990), a mid-crustal detachment level is located above the well-layered lower crust (Burkhard & Sommaruga 1998).

The model is run on a 3 m long sandbox device very similar to the set up of Malavieille (1984) and Konstantinovskaia & Malavieille (2005). The obtained maximal convergence is 160 cm, which, when scaled to the natural size of the orogenic wedge, corresponds to some 400 km. The prestructured analogue materials are deposited on a 10 cm wide Mylar sheet pulled by a motor on a rigid base. The Mylar sheet has a rough surface leading to the development of a high basal friction wedge against the rigid backstop. Incremental experimental steps are recorded by a camera across the lateral glass walls. The backstop simulates the rigid lithosphere of the upper plate and no material may go out of the system. Cohesion and size are scaled with a factor of 10^5 (scaling and characterization of model materials are also discussed in Lallemand et al. 1994, Gutscher et al. 1996, Gutscher et al. 1998a, Kukowski et al. 2002, Lohrmann et al. 2003). The vertical scale (1:1) and the horizontal one (1:2.5) differ in order to improve the resolution of the developed structures; the vertical scale has been 2.5 times exaggerated in the experiment. The analogue materials used have frictional mechanical properties satisfying the Coulomb theory (Davis et al. 1983, Dahlen 1984, Dahlen et al. 1984) and they mimic a non-linear deformational behavior of crustal rocks in the brittle field (Lohrmann et al. 2003). The orogenic lid consists of a cohesive mix of silica powder and sand. The aeolian sand used is rounded with a grain size of 200 to 315 µm and a density of 1690 kg/m^3. The internal coefficient of friction is 0.57 and the cohesion Co = 20 Pa. The pure dry silica powder has a significantly higher cohesion (150 Pa) than sprinkled sand (20 Pa) and is used alone or mixed, to mimic rheologically stronger (more resistant) material. The lid is separated from the subducting plate by a thick layer (< 8 mm) of glass beads that simulates a major basal thrust or décollement level. The glass beads are a Coulomb material with a density similar to that of dry sand but

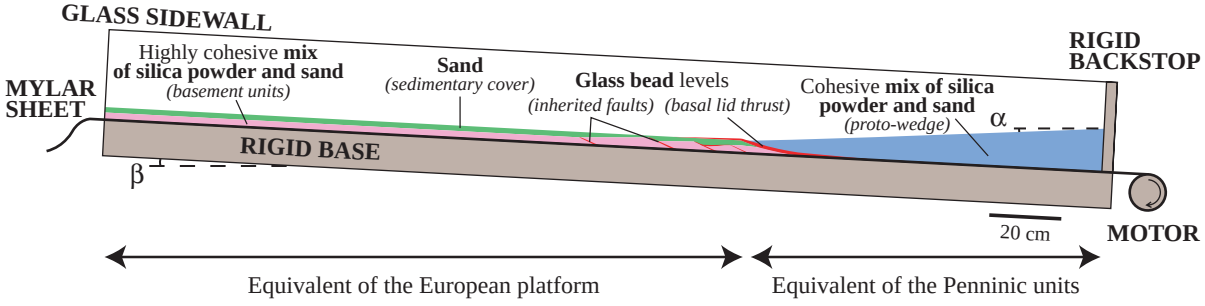

Fig. 4.2 *Analogue model setup. The model is scaled to represent the European platform (left) subducting beneath the overriding Apulian lid (right). The orogenic lid is mainly considered to be the equivalent of the Penninic units, while the European platform consists of basement units and sedimentary basins of the Helvetic domain, both prestructured by inherited normal faults. The surface slope angle α measures 2° and the basal detachment dip β 3°, according to present day geometries in the Western Swiss Alps.*

their grain size is between 50 and 105 μm. Due to their close to perfect roundness, their coefficient of internal friction is about 23% smaller (0.44), with an almost negligible cohesion. The basement units of the tectonically underplated European platform are very strong lithologies and were therefore chosen to be composed of sand with a higher rate of silica powder than those of the orogenic lid unit. The pre-existing structures, such as the inherited normal faults bordering former extensional basins, are simulated by levels of glass beads. The sedimentary cover of the subducting plate consists in sprinkled sand.

To achieve the critical taper angle, surface processes such as erosion and sedimentation compete with tectonic processes such as thrusting and underplating. While internal deformation is driven by the continuous shortening of our model, the surface processes are operated from the outside. In the experiments, after each incremental step of shortening the ideal wedge geometry was maintained by eroding and sedimenting in areas which were in a super- or sub-critical stage, respectively. Erosion and sedimentation were done according to simple, first-order laws and constant erosion was applied on the units, independently of their lithological nature. Sedimentation though mainly in the foreland basin, may also happen in the more internal parts of the wedge. Simultaneously, erosion can occur throughout the model, including the Molasse Foreland Basin. Thus, recently deposited materials may be cannibalized, recycled and re-sedimented in the basin.

4.2.2 Results from modeling

The several major types of results briefly discussed here are all related to the feedback processes between tectonics and erosion-sedimentation.

4.2.2.1 Inherited structures and initial basin geometry

Considering the inherited margin and basin geometries in the Alpine domain is important to understand the inversion of the margin prior and during entrance into the accretionary prism (Stampfli et al. 1998b), but also to understand the evolution of the flexural basin of the North and South Helvetic Flysch. Reactivation of former extensional faults, both affecting cover series and basement units, is important to understand this transition from underfilled to overfilled basin (Lihou & Allen 1996). As is demonstrated from model results presented here and is known from the geological record, considering the inherited structures in a model is necessary to better assess the spatial and temporal evolution of the foreland fold-and-thrust belt and its implication on the basin evolution. Thus, all the major basement units including their sedimentary cover units have been built into the model (Fig. 4.2).

4.2.2.2 Stages of structural development

During the development of our models, three major phases of evolution could be discriminated. The main stages are described based on the model run most representative for the Central-Western Alps (experiment 46, Fig. 4.3). During the first stage of evolution, the converging lower plate is passively subducted beneath the orogenic lid. Because of its continuous climb up onto the top of the basement ramp, the lid internally deforms by backthrusting. The displacement of the orogenic front causes the successive thrusting of the recently deposited foreland sediments by frontal accretion. When the displacement of the lower plate cannot be anymore mechanically performed by subduction, the inherited normal basement faults invert, and propagate to the surface as a new foreland sediment slice. During this second stage of evolution, from simple underthrusting, the basement imbricates are subsequently deformed by underplating. This process in the internal parts of the models leads to the formation of an antiformal nappe stack. In reference to the section across the Western Swiss Alps by Burkhard & Sommaruga (1998) that inspired this modeling, this second phase will be called “underplating of the Crystalline Massifs”. The underplating of the basement continues during the third stage of evolution, but from this time on, it generates new spontaneous nappes in the unstructured part of the lower plate. Similarly, in reference to the Alpine setting, this phase will be called “underplating of the Autochthonous European basement”. In the foreland, the resulting thrust involves both the sedimentary cover and overlying deposited sediments and initiates the development of an external fold-and-thrust belt. The uplift of the underplated imbricates forming the basement nappe stack isolates the front of the lid that constitutes a klippen from its more internal trailing homeland.

4.2.2.3 Basin evolution or erosion versus sedimentation

To describe the experiments, the evolution is expressed by the incremental displacement of the lower European plate (in kilometers scaled to nature)

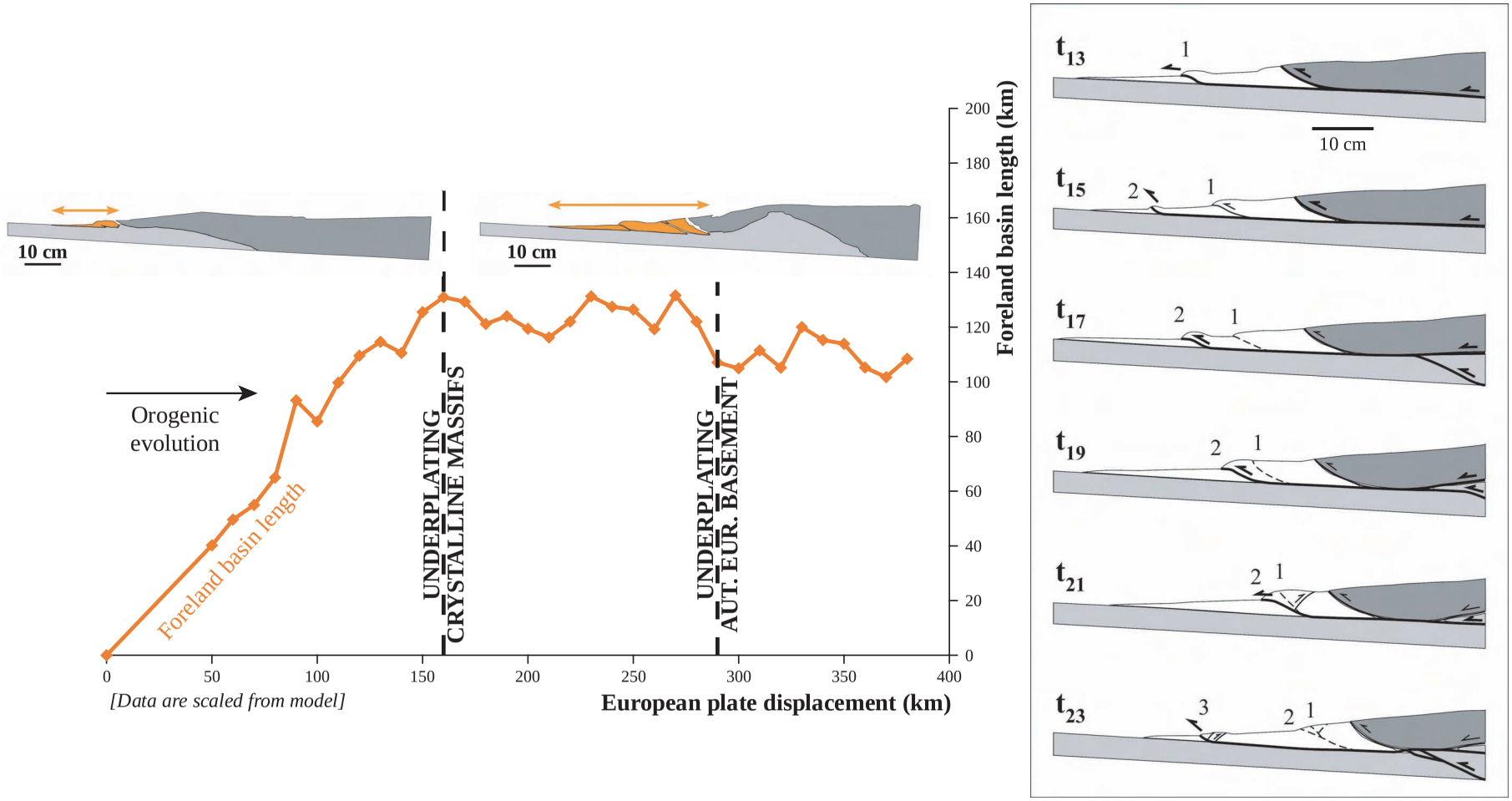

Fig 4.3 *Evolution of the foreland basin: insights from an analogue model with low sedimentation and erosion (experiment 46). After an initial stage of growing, the overall width of the Molasse Basin remains more or less constant (orange curve). The basin evolves into sub-basins due to the punctuated formation of thrust-related folds (called 1 to 3, right scheme). In the deforming Molasse foreland basin, such fold-thrust units may totally disappear, as for example at time* t_{23} *for the slice of sediments between the thrusts 1 and 2.*

or in terms of time increments. Between two time increments, the plate displacement is about 10 km. The experimental results clearly emphasize the importance of where erosion takes place. Erosional unloading of the hangingwall, above for example the active basement anticlinal stack, allows the thrust system to remain active (see also PERSSON & SOKOUTIS 2002). Erosion localizes strain and thus may enhance/favor exhumation of basement massifs. The geometry of the basin is linked to the amount of sediments deposited into the basin, and in turn is linked to erosion in the model. We have calculated the amounts of eroded and deposited material and the evolving basin width in a model with low sedimentation and erosion (experiment 46, Fig. 4.3 and 4.5).

After an initial stage of growing, the basin attains a rather constant width (Fig. 4.3 left). The maximal width of the foreland basin is reached when the underplating of the prestructured basement units starts ("underplating of the Crystalline Massifs"). Then, the steady state occurs simultaneously with the underplating of the basement, pre-cut and not ("underplating of the Autochthonous European basement"). Despite showing a rather constant width, the basin may remain very active in terms of tectonics. Indeed, the foreland basin evolves into sub-basins due to the punctuated formation of thrust-related folds (Fig. 4.3 right). This

Exp.	Erosion	Sedimentation
42	no	no
43	high	very low
44	very low	very high
45	low	high
46	low	low
47	high	high

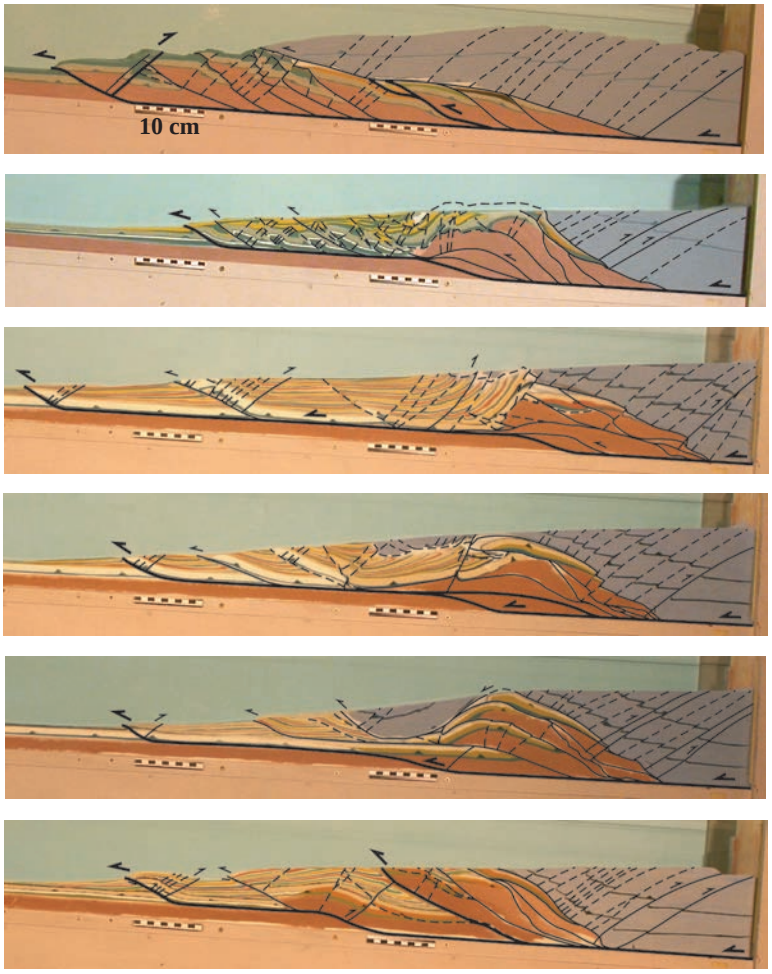

Fig. 4.4 *Different model settings at the same shortening stage, but with more or less erosion and sedimentation, show varying basin and hinterland developments. Small sub-basins with important folding and thrusting develop in the foreland thanks to a very low sedimentation (experiment 43). In contrast, a unique wide and deep basin with few tectonic structures forms with a high sedimentation (experiments 44, 45 and 47). The basement units constitute a nappe stack formed by underplating when surface processes are active (experiment 43 to 47 vs. experiment 42). This development may be inhibited due to a very high sedimentation (experiment 44), while a high erosion rate favors the steepening of the basement imbricates (experiments 43 and 47). A klippen detached of the lid is preserved if erosion remains low (experiments 45 and 46). The detachment of the foreland deposits above the autochthonous cover series is facilitated by an additional décollement level placed at the base of the sedimentary basin (experiment 46). At this stage of development, the most external thrust in the foreland constitutes the initiation of a fold-and-thrust belt comparable to the Jura.*

process of frontal accretion leads to a syndeformational vanishing of an important volume of foreland sediments, as shown by the total erosion of some subbasins (for instance at t_{23} the sediment slice between the thrusts 1 and 2 has almost disappeared, Fig. 4.3 right). These units are subsequently unaccounted for in the sedimentary record.

We performed different sets of models which show the differing basin evolutions as a function of basin infill (Fig. 4.4). Indeed, varying the amounts of erosion and sedimentation strongly influences the overall basin geometry. Large amounts of sediments produce a wide and deep basin with few tectonic structures (experiments 44, 45 and 47), whereas smaller basins with more folding and thrusting develop with less sedimentation (43). A maximal extent of the orogenic lid is preserved in situations of low erosion, leading to the detachment of its front (45 and 46). A high erosion rate favors the steepening of basement imbricates (43 and 47). Surface processes (experiments 43 to 47 vs. experiment 42) favor the development by underplating of the basement nappe stack, but a very high sedimentation rate inhibits this development (44). Intermediate conditions of erosion and sedimentation lead to the formation of an antiformal nappe stack in the hinterland and to a sedimentary basin bordered by a fold-and-thrust belt in the foreland (46).

Our semi-quantitative estimates of the sediment budget (i.e. variations in rates of erosion and sedimentation) are based on a model performed with low sedimentation and erosion (experiment 46, Fig. 4.5). While in a first phase, sedimentation (black continuous curve) and erosion (dashed curve) present similar rates, subsequently, with the initiation of underplating of basement units, the erosive phenomenon largely dominates. Until the end of the experiment, the sedimentation rate gently decreases, and erosion shows strong fluctuations around a high average value. The cyclic behavior of erosion (grey arrows) occurs with the same frequency as punctuated thrusting in the foreland (white stars). The cyclicity observed in the sediment budget evolution is inherent in the process and is caused by the wedge mechanics in response to surface processes.

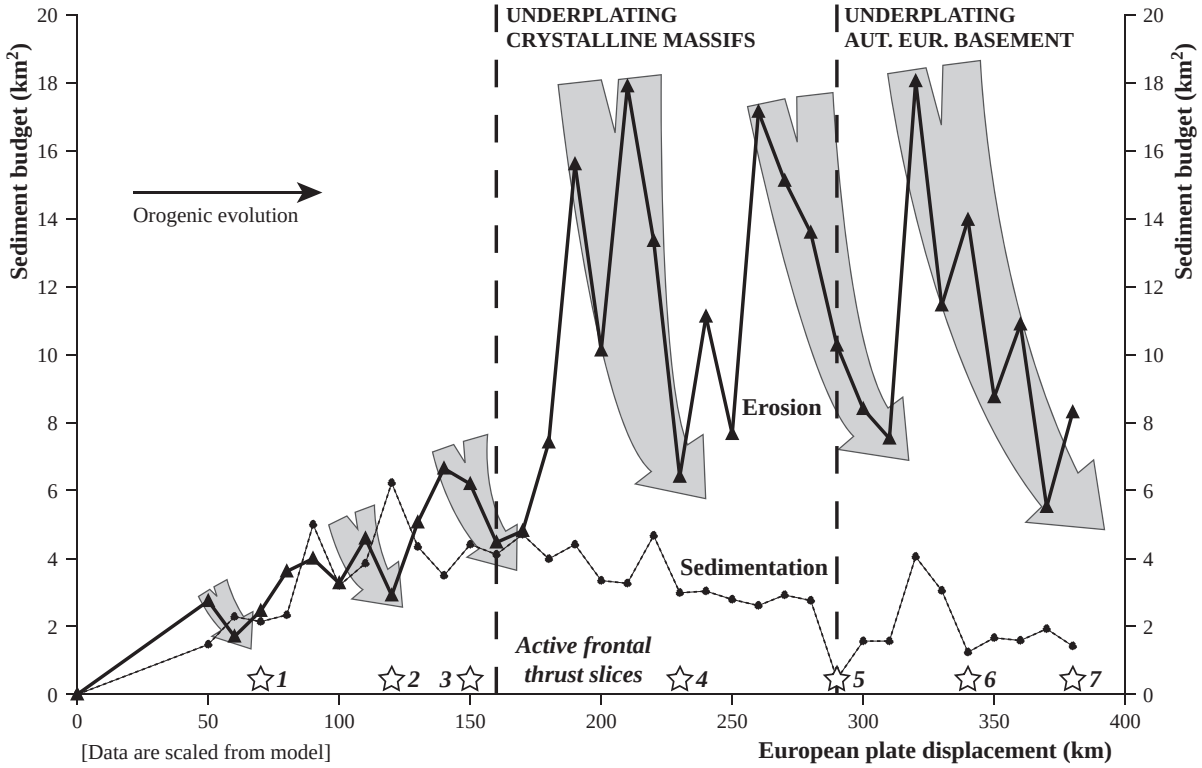

Fig. 4.5 *Graph of total displacement showing punctuated thrusting and major phases in erosion/sedimentation evolution. The semi-quantitative estimates of the sediment budget (experiment 46) are expressed, scaled to nature, in square kilometers. The curves represent the temporal evolution of the rates of erosion (affecting the lid, basin sediments, basement units and their cover) and sedimentation (corresponding to the surface of the last sand layer deposited in the foreland basin). During the subduction phase, both sedimentation (dashed curve) and erosion (black continuous curve) increase. With the underplating of basement units, the sedimentation rate diminishes gently, while the erosion rate strongly fluctuates around a high average value. Due to the wedge mechanics, erosion presents a cyclic behavior (grey arrows) with the same frequency as punctuated thrusting in the foreland (white stars).*

4.3 Sedimentation in the Molasse Basin of Switzerland

The Molasse Basin of Switzerland has been investigated over many decades and is considered a classic foreland basin (Homewood & Caron 1982, Homewood & Lateltin 1988). Starting in Tertiary times, the basin developed in response to and witnessed the arrival of the orogenic wedge onto the European platform, following the closure of the Alpine Tethys. The orogenic lid which overrode the meridional edge of the European margin and than moved northward onto the Helvetic platform is formed by the Penninic units (Escher & Beaumont 1997, Escher et al. 1997). The arriving upper plate thus inverted the lower passive margin and rim basin of the European margin, which was progressively incorporated into the overriding upper plate, including cover and basement.

From an underfilled Flysch basin in front of the closing/subducting Alpine Tethys, the foreland evolved into a Molasse type basin at the front of an actively growing orogen (Pfiffner 1986, Burkhard 1990, Burkhard & Sommaruga 1998, Kempf & Pfiffner 2004). The Molasse sediments range from Late Eocene to Miocene in age. The oldest Flysch deposits in the Swiss Foreland Basin are turbidites of early Eocene age (Lihou 1996). The underfilled Flysch stage continued until the middle of Oligocene when the Alpine Foreland Basin became progressively filled. Sedimentation changed from deep marine to shallow marine and continental, and the Foreland Basin setting changed from the underfilled Flysch stage to the overfilled Molasse stage (Sinclair 1997a). Late Miocene, Pliocene and Pleistocene sediments are not known, though they were probably deposited but subsequently eroded out of the basin record (see Berger et al. 2005 and references therein).

4.3.1 Sedimentation and sedimentary budgets

The Molasse consists essentially of detrital sediments derived mostly from the rising Alps and to a smaller extent from the North. Four general groups can be distinguished: the oldest, the UMM – Lower marine Molasse, the USM Lower freshwater Molasse, the OMM – Upper marine Molasse, and the OSM – Upper freshwater Molasse (Fig. 4.7). They represent two major cycles in sedimentation linked to the evolution of the mountain belt, but also with connections to the Paratethys, to the North with the Rhine graben, and to the West with the Rhone river system. The development of the different continental facies is related to the formation of an important drainage system, large rivers with important alluvial fans, flood plains braided streams, lakes and coal-swamps. Large conglomeratic fans are well developed mainly along the foot of the active mountain and record the nature of the eroded rocks in the hinterland (Trümpy 1980, Sissingh 2006a, 2006b). The marine environments are shallow brackish, current-swept seas, papralic deltas and tidal flats.

Arrivals and provenance of pebbles and clasts show which terranes are being actively eroded in the hinterland. Noticeable is the arrival of clasts and conglomerates of the Penninic Prealpes Supérieures nappes during the Chattian in the Mont Pélerin Fm.. An important increase in crystalline clasts is observed beginning with Late Oligocene and peaking in the Early to Middle Miocene (Schlunegger et al. 2001). They are interpreted to have their origin in the core of the Penninic cover: the beginning of the External massifs exhumation is around 20Ma, but due to the important cover, no crystalline pebbles are eroded at this time. Only later in post-Miocene times (?) do these pebbles appear (Schlunegger et al. 1998). Also, arrival of clasts from the Helvetic units seems not to be before 15Ma that is Early-Middle Miocene.

The main post-collisional sedimentary history starts with an uplift of the external massifs (Kuhlemann et al. 2001, Kuhlemann et al. 2002, Kuhlemann & Kempf 2002, Berger et al. 2005). Sediment accumulation rates were doubled probably due to continental collision (Willett et al. 1993) and slab breakoff sensu lato of the subducting European plate occurred under the Alps (von Blanckenburg & Davies 1995). The sediment discharge reached steady state after a response time of 2-3 Ma. The Miocene sediment budget shows an increase between 24 and 21 Ma related to the buildup of topography and relief in the Swiss and Western Alps. At 21 Ma the sediment discharge rates of the entire Alps dropped dramatically (Kuhlemann & Kempf 2002). This event occurred coeval with the reduction of thrust advance rates in the Swiss Molasse zone to at least one third (Homewood et al. 1986, Burkhard & Sommaruga 1998). The decrease in sediment discharge rates is in conflict with model predictions (Sinclair et al. 1991, Schlunegger 1999, Schlunegger & Hinderer 2001, Schlunegger et al. 2001) that postulate an increase in topography. Schlunegger (1999) and Schlunegger et al. (2001)

propose that at this time, reduced sediment discharge was caused by the exposure of more resistant rocks in the distant hinterland ("Alpine core" of SCHLUNEGGER et al. (2001)). Between 18 and 17 Ma, a short-termed, drastic increase of sediment discharge rates might be related to uplift of the Lepontine dome, or alternatively, to differential uplift of the Aar massif (SCHLUNEGGER et al. 1997c, SCHLUNEGGER et al. 1998, SCHLUNEGGER 1999). The generally low sediment discharge rate in the entire Alps between 16 and 12 Ma records further extension linked to crustal thinning. The inversion of the Western Swiss Molasse Basin between 11 and 10 Ma (KAELIN 1997), changing the drainage pattern to an easterly direction, is related to folding and thrusting of the Swiss Jura mountains. This process appears not to have increased sediment discharge rates from the Swiss and Western Alps as a whole. Thrusting and uplift of the Jura mountains does not mean that the base level at the northern margin of the Swiss Alps changed substantially, if at all. The sediment discharge of the entire Alps was rather uniform between 11 and 6 Ma with a drainage systems into an eastern direction (SCHLUNEGGER et al. 1998, KUHLEMANN 2000). After 5 Ma, strong erosion in the Alpine orogen and in the Western North Alpine Foreland Basin is indicated by a spectacular increase in sediment discharge from the Swiss and Western Alps. This increase is also documented by an important amount of sediments removed from the Molasse Basin. It has been shown that a thickness of 1-4km of Molasse sediments has been eroded (SCHEGG et al. 1997, SCHEGG & LEU 1998, CEDERBOM et al. 2004). The bulk of this erosion appears to occur since the early Pliocene (CEDERBOM et al. 2004). The most likely cause could be an isostatic rebound of the mountain belt in response to an important change in climate (CEDERBOM et al. 2004).

4.3.2 Basin evolution and tectonics

The evolution of the Molasse Basin is tightly linked to the evolution and progression of the frontal parts of the Alpine orogen (HOMEWOOD et al. 1986). Especially relevant are the development of the External crystalline basement imbricates and the formation of the Helvetic nappes (LAUBSCHER 1992, ESCHER et al. 1993, SCHMID et al. 1996, ESCHER et al. 1997, STAMPFLI et al. 1998b, MOSAR 1999, SCHMID et al. 2004). At the onset of the Late Oligocene at around 30 Ma, or slightly before, a major event in the internal part of the Alpine belt causes the originally shallow SE dipping axial surfaces and thrusts to become progressively steepened, to attain finally subvertical to overturned dips. The reason for this may have been the addition of frontal imbricates resulting in the rotation and steepening of the older thrust sheets (ESCHER et al. 1997). The main events, both in the tectonics and the basin evolution are discussed (Fig. 4.7). It is largely admitted that the principal mechanism forming the Molasse Foreland Basin is the flexural bending of the European down-going plate under the thrust load advancing from the South (PRICE 1973, DICKINSON 1974, TURCOTTE & SCHUBERT 1982). This led to the characteristic downwarp flexure responsible for the wedge-shaped geometry of the basin and an upward flexure, the forebulge, located in the foreland. Based on uplift and earthquake data, some authors have argued that the Molasse Basin is still active and that incipient basement nappes are developing under the Molasse Basin mainly due to continued convergence and the necessity of the orogenic wedge to remain critical (MOSAR 1999, LACOMBE & MOUTHEREAU 2002).

From a tectonic point of view, the Molasse Basin in Switzerland is often regarded as a largely undeformed sedimentary basin in front of an active mountain belt. Gentle folds are thought to represent early stages of buckle folds with Triassic cores filled with well-organized evaporites pillows and duplexes (SOMMARUGA 1997, 1999). The load of the Tertiary sediments in the basin is thought to inhibit and/or prevent these folds to further evolve into thrust-related folds (BURKHARD & SOMMARUGA 1998). Seismic and structural investigations show that, in fact, the Molasse in the Swiss Plateau area and towards its western termination is folded and thrust. Generally the folds are gentle and show a NE-SW orientation with local changes to more N-S orientations such as in the Fribourg area. The autochthonous Mesozoic series are folded throughout the Molasse Basin, mainly over salt-cored structures (salt-pillows - MURALT et al. 1997, SOMMARUGA 1999). In numerous other instances throughout the Molasse Basin, fault-related folds may even bring the Mesozoic series to the surface indicating the formation of important imbricates. Examples are the Salève anticline near Geneva (section CC' Fig. 4.6) (SIGNER 1992, GORIN et al. 1993, WILDI & HUGGENBERGER 1993), the Chamblon fold near Yverdon (JORDI 1990, 1993, MURALT et al. 1997) or the Sünikon-Regensberg anticline near Weiach (section GG' Fig. 4.6) (Naef and Mertz in BOLLIGER 1999). Syndepositional folding and thrusting is clearly documented in the vicinity of Lake Annecy, at the western termination of the Molasse Basin in France (BECK et al. 1998). Folds of the Jura mountains give way to the Subalpine fold-and-thrust belt. Large fault-related structures such as the Semnoz,

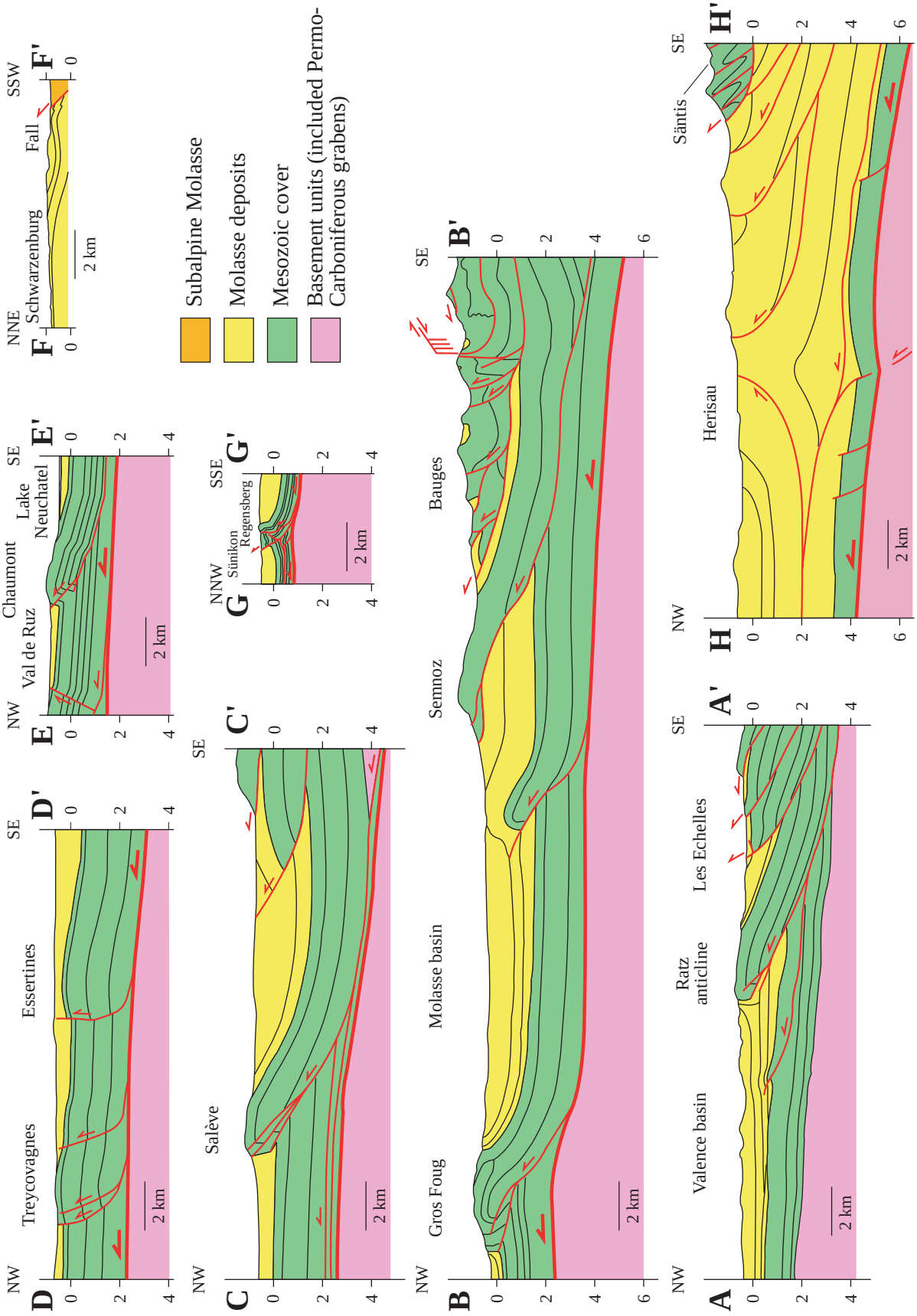
Subalpine Molasse
Molasse deposits
Mesozoic cover
Basement units (included Permo-Carboniferous grabens)
NNE
Schwarzenburg
Fall
SSW
F
F'
2 km
NW
Val de Ruz
Chaumont
Lake Neuchatel
SE
E
E'
NNW
Sünikon
Regensberg
SSE
G
G'
NW
Treycovagnes
Essertines
SE
D
D'
NW
Salève
SE
C
C'
NW
Gros Foug
Molasse basin
Semnoz
Bauges
SE
B
B'
NW
Valence basin
Ratz anticline
Les Echelles
SE
A
A'
NW
Herisau
Säntis
SE
H
H'

Fig. 4.6 *Simplified tectonic profiles in the Molasse Basin showing changing internal structure from east to west across the Alpine foreland. The sections can be compared with profiles from different settings of analogue models. In the Western Alps, fault-related folds bring the Mesozoic cover to the surface, subdividing the foreland basin into smaller sub-basins. Such anticlinal structures such as the Ratz (section AA' modified from Beck et al. 1998), Semnoz, Gros Foug (both section BB' modified from Beck et al. 1998) and Salève (section CC' modified from Beck et al. 1998) anticlines correlate well with the structures developed in the foreland basin of the model section 43, with high erosion and very low sedimentation. At the southern edge of the Jura Mountains, the younger series of the Molasse are involved in the folding and thrusting of the Mesozoic cover (sections DD' modified from Sommaruga 1999 and EE' modified from Sommaruga 1997). The thin Molasse deposits are deformed both in the Plateau and in the core of the internal Jura synclines. The formation of such syndepositional anticlines is very similar to the foreland fold-and-thrust development of the experiment 46, performed with low erosion and sedimentation. In the Fribourg-Singine area, near the transition between the Molasse Plateau and the Subalpine thrust Molasse (section FF' modified from Frasson 1947), the Molasse deposits are intensely folded. At the front of the klippen in the experiment 46, the sediment deposits are similarly deformed by synsedimentary tectonics. At the eastern termination of the Jura Mountains, the Sünikon-Regensberg anticline brings highly faulted Mesozoic cover to the surface (section GG' modified from Naef and Merz in Bolliger 1999). This anticline may be compared to the more external foreland thrust of the experiment 45 (low erosion and high sedimentation) which is affected by a number of backthrusts. In the most central Alpine section, a new basement imbricate develops, leading to the formation of triangle structure (section HH' modified from Spicher 2005). Similarly in the experiment 47, the last frontal basement imbricate appears spontaneously (without basement structural heritage) bearing large backthrusts.*

Riaz or the Gros Foug anticlines separate stripes of Molasse (sections AA' and BB' Fig. 4.6) (Guellec et al. 1989, Guellec et al. 1990, Wildi & Huggenberger 1993, Jouanne et al. 1995, Jouanne et al. 1998). The development of these syndepositional anticlines leads to the separation of sedimentation areas and hence the individualization of different sub-basins. Similarly, in the northern part of the former Molasse Basin – now the meridional edge of the Jura mountains – the younger series of the Molasse are involved in the folding and thrusting of the Jura mountains, as clearly documented by sections for example in the Val de Travers area, west of Neuchatel (sections DD' and EE' Fig. 4.6) (Sommaruga 1997, Burkhard et al. 1998, Burkhard & Sommaruga 1998, Sommaruga 1999, Valley et al. 2004). To the South, near the transition to the Subalpine thrust Molasse, one can locally observe intense folding, such as near Lucerne (Matter et al. 1980), or in the Fribourg-Singine area (section FF' Fig. 4.6) (Marescot 2000), or even more gentle large scale folds such as in the Lake Leman area between Montreux and Lausanne. Data from the coal bearing Molasse in the Subalpine Molasse show very differing facies and types of coal veins suggesting the existence of three independent sedimentation basins: the Paudèze, the La Miannaz and the Oron basins (Berger J.P. personal communication). The three separate basins in the area near Lausanne could reflect a piggy-back type basin evolution linked to synsedimentary folding and faulting.

It appears also that the Molasse series are folded and faulted independently from the Mesozoic substratum. This is in contrast with the general idea that the Molasse series are folded together with the Mesozoic autochthonous. Unpublished and confidential data from interpretation of seismic lines suggest that in many instances the Molasse series may be folded independently from the substratum, which implies the existence of a décollement level or local thrust at the base of the Molasse series. A similar situation has, however, been described in the Subalpine Molasse domain and the transition zone to the autochthonous Molasse. Here, the Subalpine Molasse is intensely imbricated and develops triangular structures above the Mesozoic autochthonous in the Molasse series (section HH' Fig. 4.6) (Müller et al. 1988, Pfiffner et al. 1997c). In the Subalpine Molasse, the series of the lower Molasse are intensely imbricated and thrust, and show important folding such as SW of Fribourg, in the Moudon area and near Lake Leman. All these data show that the Molasse Basin is structurally implicated in the development of the Alpine foreland and that the development of these structures is syndepositional.

4.3.3 Flexural models of the Molasse Basin

Peripheral basins such as the Alpine Molasse Basin, as well as the former Flysch Basin, have often been described as resulting from flexural down-bending of the lithosphere in response to tectonic loading by an arriving orogenic wedge. The depocenters subsequently evolve and migrate according to the progression of the wedge, as well as the erosion rates and the mechanical properties of the lithosphere (Allen & Allen 2005). Foredeeps generally evolve from an underfilled flysch-type basin to a filled or overfilled molasse-type basin. Flexural deflection of the lithosphere produces a significant foreland flexural bulge that is for example believed to be responsible for the Siderolitic deposits in the Jura mountains, and which migrates with time, defining the pinchout line of the Foreland Basin.

The Flysch to Molasse Basin transition in the Middle Oligocene reflects important modifications in the thrust/foreland basin system: increased exhumation and initiation of backthrusting is linked to increased sediment supply, and a slowing of the basin migration across the foreland (Sinclair 1997a, Sinclair 1997b). The cause for this transition is often regarded as the movement of the orogenic wedge and its foredeep over the shoulder of the inherited passive margin. In the case of the Alpine foreland evolution, alternative models underline the importance of the slab breakoff as triggering mechanism for this transition (Davies & von Blanckenburg 1995, Sinclair 1997a). Other models relate the transition to imposed boundary conditions within the model setup: elastic thickness and wedge advance rate are regarded as minor causes that mainly retard or promote the Flysch to Molasse transition. The dominant mechanism is thought to be denudation (Hoth et al. 2004). Flexure induced subsidence is mainly governed by the advance/growth (exhumation) rate of the orogenic wedge in the hinterland. Numerical models of the interaction between fold-and-thrust belt deformation, foreland flexure and surface mass transport (Simpson 2006) show that the geometry of the fold-thrust system is linked to the rate of surface processes and conditions the basin width.

4.3.4 Insights and lessons from analogue modeling on the Alps and Molasse Basin

Surface processes - erosion and sedimentation - are key mechanisms in maintaining the wedge critical, and thus contribute in determining the internal geometries. Model results reveal that during the foreland evolution, folds and thrusts develop in the substratum, forming more or less independent sub-basins, but also that the Molasse sediments are detached from their substratum. They develop thrusts and folds independently, though contemporaneously, from the structures in the substratum.

A series of results and insights from analogue modeling highlights the evolution of the Alpine Molasse Basin in new ways:

(i) Basin width is constant after growing during the initial stages of development and than reaching a threshold width with the initiation of underplating of crystalline basement units.

(ii) Basin evolution, i.e. development of basin-internal thrusts and folds, is mainly towards the front of the orogenic wedge.

(iii) Basin evolves into sub-basins due to the punctuated formation of thrust-related folds. Locally, the Molasse cover appears to be detached from its substratum and developed distinct fold-thrust units. During the course of evolution some of these basins may completely disappear by erosion. These units are subsequently unaccounted for in the sedimentary record. As a consequence the total length of the basin may significantly be underestimated.

(iv) Sedimentation and erosion show an inherent cyclicity caused by the wedge mechanics and that is linked to the punctuated forward propagation of the thrusts.

(v) The model evolution shows several stages of development with an increase of sedimentation and

Fig. 4.7 *Sedimentary processes in the Alpine Molasse Basin versus semi-quantitative erosion/sedimentation budget from analogue modeling, and their correlation with tectonic processes. The main sedimentation events from the N and the S into the Molasse Basin and the major unconformities are indicated. The sedimentary events are correlated with tectonic "events" (modified from Sissingh 1997). The distribution of the major Molasse Basin formation was modified and simplified from Burkhard & Sommaruga (1998). The sediment discharge from the Alps is based on studies from Kuhlemann et al. (2002). The main history of the sediment discharge from the Alps starts with an increase of sediment accumulation between 30 and 28 Ma, explained by the continental collision (Willett et al. 1993) and slab breakoff of the subducting European plate under the Alps (von Blanckenburg & Davies 1995). After a steady state of 2-3 Ma, the sediment discharge of the Alps shows a two-fold increase possibly triggered by tectonic and magmatic events in the orogen. The first peak (peak 1, between 24 and 21 Ma) is related to an increase of the relief due to ongoing uplift in the Western Alps. The second peak (peak 2, between 18 and 17 Ma) is probably linked to the uplift of the Lepontine dome (inside the Penninic lid), or, alternatively, to differential uplift of the Aar massif (Schlunegger et al. 1997a). The peaks are separated by a dramatic drop of the sediment discharge of the entire Alps at 21 Ma, caused by the exposure of more resistant rocks in the distant hinterland (Schlunegger 1999, Schlunegger & Hinderer 2001, Schlunegger et al. 2001). From 16 to 6 Ma, the sedimentation discharge of the entire Alps is rather uniform with a lower rate between 16 and 12 Ma linked to crustal thinning as a far-field effect of strong continental extension in the Pannonian basin. After 5 Ma (peak 3), strong erosion in the Alpine orogen and in the Western North Alpine Foreland Basin is indicated by a spectacular increase in sediment discharge from the Swiss and Western Alps. This latter aspect is related to the important changes in climate (Cederbom et al. 2004). Results from erosion/sedimentation budgets from analogue modeling show an increase in sedimentation – that can be correlated with the underfilled Flysch Basin stage – followed by a series of 3 major cycles of sedimentation. The first 2 cycles correlate with the two major cycles of deposits in the Molasse Basin, whilst the 3rd one is not recorded in the Molasse Basin.*

TIME SCALE
SEDIMENTATION FROM THE NORTH
MOLASSE FACIES / GEOMETRY
SEDIMENT DISCHARGE FROM THE ALPS
SEDIMENTATION FROM THE SOUTH
MODEL
(Ma)
TERTIARY
Miocene
Oligocene
Eocene
Paleoc.
Pleistocene
Pliocene
Messinian
Tortonian
Serravallian
Langhian
Burdigalian
Aquitanian
Chattian
Rupelian
Priabonian
Bartonian
Lutetian
Ypresian
Thanetian
Selandian
Danian
Sedimentary cycle sets of the NAFB
Post-Molasse
Late Molasse
Early Molasse
Pre-Molasse
Alpine foredeep
Main tectonic events
Uplift & tilting
Jura thrusting & folding
Base Pliocene
Base IV
Mid.-Mioc.
Intra-Burdig.
Base Burdig.
Intra-Chattian
Main rifting
Initial rifting
Base Mid.-Eocene
Unconformities
Marine communication with (RG=Rhine graben; BG=Bresse graben; MG= Molasse graben)
RG
BG
MG
Volcanism
NE
SW
No deposition ?
OSM
OMM
USM
UMM
NHF
SHF
eroded
No deposition covered by advancing thrust front
BASEMENT UNITS
OVERFILLED MOLASSE BASIN
UNDERFILLED FLYSCH BASIN
(km³/Ma)
(1)
(2)
(3)
(distance from foreland pin (km))
Marine communication with (RG=Rhine graben; BG=Bresse graben; MG= Molasse graben)
Compressive front/ foredeep migration
Main tectonic events
Uplift & tilting
Imbrication of sub. molasse "Miocene revolution"
Rapid thrust wedge uplift
Subsidence
Normal faulting & subsidence
Base IV
Jura thrusting & folding
Mid.-Mioc.
Intra-Burdig.
Base Burdig.
Intra-Chattian
Intra-Rupelian
Paleocene
Base Mid.-Eocene
Pebbles from (C= Crystalline massifs; H= Helvetics; P= Praalpes)
(C&H)
(P)
2 to 4 km eroded*
OSM
OMM
USM
UMM
New frontal thrust slice
Main tectonic events
Klippen detachment
...prestructured basement
...unstruct. basement
UNDERPLATING
Erosion
Sedimentation
(km²)
Eur. plate displacement (km)

a growth of the basin width followed by three major cycles of sedimentation. These stages favorably compare with the transition from underfilled to overfilled basin and the major sedimentation cycles in the Molasse Basin.

The foreland evolution has been linked to the tectonics in the hinterland. The major stages of evolution are corroborated for example by the nature and provenance of pebbles in the Alpine domain and coincide with the Alpine orogenic evolution and timing. In the Alpine Foreland Basin, several studies clearly suggest that folding of the Mesozoic and sedimentation in the Molasse Basin are contemporaneous. Also, in some occasions the Molasse basinal sediments are detached from the Mesozoic substratum and are deformed independently. The main stages in evolution of the foreland basin and the hinterland observed on the analogue models can be correlated in time and space with the major tectono-sedimentary events in the Alpine belt (Fig. 4.7).

The stage of a growing foreland basin corresponds to the arrival of the orogenic lid and is equivalent of the passive's margin incorporation into the accretionary prism. The transition from underfilled Flysch type basin to an overfilled Molasse type basin correlates with the beginning of imbrication of the prestructured basement massifs and is equivalent of the stacking of the outer crystalline massifs. This transition is thus inherent in the wedge evolution and no external agent need is necessary to explain this stage. The subsequent evolution in the basin is mainly reflected by the punctuated imbrication of the frontal accretion and the associated cyclic increase in erosion. This cyclicity in erosional/depositional "sequences" can be compared with the successive Tertiary depositional cycles. These latter have been tentatively correlated by many authors (op. cit.) with tectonic/orogenic phases, in which foredeep events are coeval with specific orogenic events. Based on insights from the model results, it appears that these depositional cycles, together with the erosional events and tectonic phases, are directly related to the internal mechanical evolution of the orogenic wedge.

The third erosional event in the model is, however, accounted for in the sedimentary record of the Molasse Basin. Indeed no sediments younger than Middle/ Late Miocene are unknown, although we know of an important drainage system during the Miocene to Present (Berger et al. 2005). The very important increase in erosion rates since the Late Pliocene in the Western Alps (Kuhlemann et al. 2001) is not modeled. These rates are related to erosive denudation driven by important changes in climate. This discrepancy can be explained by the fact that processes external to the wedge mechanisms will influence to varying degrees the timing, rates and geometries of the Molasse Basin evolution, either by directly influencing the erosional processes or by indirectly altering the internal dynamics of the wedge.

A series of processes and mechanisms, not taken into account in our modeling and potential candidates to explain the discrepancies in erosional budgets for the latest period of the foreland basin evolution, includes:

(i) The convergence rates of the orogenic wedge which are directly related to convergence rates of tectonic plates (Apulia indentor) could possibly translate into increased uplift. Plate velocity curves show indeed a slight increase of the African plate relative to the European plate around 15 Ma.

(ii) Loading/unloading by icecaps and glaciers which induce an additional isostatic response can be another mechanism.

(iii) Flexural loading and visco-elastic relaxation due to changes in the load of the European plate are another mechanism not explored by our models to date.

(iv) Sea-level changes, though important, probably only contribute in a minor extent to the basin development and the sedimentation.

(v) Changes in climate, however, will drive or inhibit erosion and thus indirectly influence wedge mechanics and exhumation rates (Kuhlemann et al. 2001, Hay et al. 2002). They appear as one of the most probable mechanisms of the late stage erosion in the Alps and have extensively been discussed in the literature.

4.4 Conclusions

Analogue models based on a prestructured setup, inspired from the Alpine domain, have been performed to show the importance of surface processes (such as erosion and sedimentation) on the evolution of a tapered wedge "orogen" and its foreland basin as well as the internal tectonic geometries developing. The evolution of the foreland basin from an initial stage to a constant width basin mimics the transition of an underfilled flysch type basin to an overfilled molasse

type basin. The transition between these two stages is clearly related to changes occurring inside the mechanical wedge. In the present models, it is the imbrication and stacking of prestructured basement units the marks of this transition. Punctuated thrusting in the frontal accretionary zone is linked to cyclic variations in sedimentation and mainly erosion. These first-order sedimentary cycles correlate to the cycles observed in the Alpine Molasse Basin. The third and youngest cycle in the models has no equivalent in the Molasse Basin, where no sediments younger than Late Miocene are observed. In addition, the very recent and dramatic increase in erosion documented in the Alps is not seen in the analogue model evolution. These discrepancies are explained by the influence of external processes and mechanisms not directly related to the mechanical wedge evolution modeled in this study. The most notable of these processes is believed to be important climate changes that influence erosion rates.

Flexural models consider the foreland basins as passively evolving units that do not deform internally. Space for sediments is created by the evolving flexure of the substratum (autochthonous) which is considered as a plate with elastic properties. The plate flexes in response to loading by the Alpine wedge in the case of the Molasse Basin in Switzerland. The interface between the advancing load – considered the backstop – and the basin sediment remains "inactive". A number of papers (op. cit.) have considered the development of the Molasse Basin as dominantly governed by this type of models. Though successful in explaining features such as onlaps, and progressive outward migration of the pinchout point (outward migration of the sedimentary wedge), they fail to reproduce/explain punctuated cycles of erosion/deposition as well as tectonic structures in the basin. The successive sedimentary events are recognized but are imposed on the model evolution, rather than being inherent to the models. We suggest that the first order sedimentary processes are governed by the internal mechanics of a tapered wedge type model. Flexural basin evolution mechanisms are believed to be secondary in the case of the Molasse Basin of the Swiss Alps. These mechanisms mainly condition the position and spatio-temporal evolution of the forebulge and create/reduce the large-scale depositional space. Onlapping surfaces and outward migrating sedimentary series can well be explained by a tapered wedge model only.

A series of competing mechanisms such as flexure, isostatic loading/unloading, climate changes and plate tectonics operate simultaneously during the evolution of the orogenic wedge and the development of its Molasse type Foreland Basin. Our analogue models show the importance of feedback mechanisms of erosion/deposition on the wedge mechanics and the punctuated thrust development as well as the cyclic behavior of surface processes. We suggest that the main features of the Molasse Basin are directly related to the internal wedge mechanics. Inherited structures and surface processes are strongly determining the future geometry and are to be built into the models to obtain meaningful similarities with orogenic belt such as the Alps as a whole.

*****

5 - TRANSCURRENT FAULTING IN THE PREALPES KLIPPEN BELT

5.1 INTRODUCTION

The Prealpes are constituted by a series of allochthonous tectonic klippen located along the northern front of the Swiss and French Alps, in the NW of the Helvetic nappes and External crystalline basement of the Alps (Fig. 5.1). They have been detached from their mostly Briançonnais basement located on the meridional border of the Tethyan margin (STAMPFLI & MARTHALER 1990a, STAMPFLI et al. 1991), before being thrust to the NW to their present day position (MASSON 1976, SARTORI 1987, ESCHER et al. 1988, MOSAR et al. 1996, STAMPFLI et al. 1998b). While a large number of studies have been undertaken on the Prealpes klippen belt, we are today still lacking a clear understanding of the Prealpes tectonic evolution post-dating the nappe emplacement (post-Early Oligocene, 30 Ma). However, some structures have been found to be linked to events post-dating the emplacement of the Prealpes onto the Alpine foreland. These structures are for instance some out-of-sequence thrusting to the N and to the W-NW (Prealpes and underlying Subalpine flysch), brittle faults cutting the whole nappe structure and a high structural relief in the Prealpes to the North and South of Leman Lake. The aim of this study is to gain new insight into recent processes affecting the Prealpes klippen belt as for instance its geomorphologic history and tectonic evolution through the investigation of brittle faulting and paleostress field. We wish then to enlarge our analysis to understand the relations between the Prealpes and overridden structural domains, i.e. from south to north the Subalpine and Helvetic nappes, the Subalpine Molasse, the Molasse Plateau and ultimately the Jura fold-and-thrust belt.

We present the results of a systematic effort to investigate the nature and kinematics of observed fracturation in the Prealpes and foreland. The investigations have been first led in the two prealpine major lobes, the Chablais Prealpes south of Leman Lake and the Romandes Prealpes between the Rhone valley and Thun Lake. In the Swiss Chablais, we studied at a local scale the Taney area (Fig. 5.2A), while we focused on the Vanil Noir area (Fig. 5.2B) and the Dent de Lys area (Fig. 5.2C) in the Prealpes Romandes. We then enlarged our study to a more regional scale in order to understand the transition between the Prealpes klippen, the Molasse substratum and further north, the Jura fold-and-thrust belt.

5.1.1 Aims of the study

The major aim of this work is to investigate the families of fractures observed in the Prealpes to possibly attribute them at best to an appropriate tectonic event. Fracturation in the klippen is complex since it is the final result of fold-and-thrust activity, neotectonics and certainly recent tectonics. To characterize fracturation and fault systems of the Prealpes area, we will describe and analyse the lineaments and faults at different scales.

The second aim is to characterize fracture orientations and movements on fault planes to determine associated stress and strain fields. We want to establish if several superposed events are at the origin of the present fracture pattern in the Prealpes and discuss the timing of fracturation development. The analysis

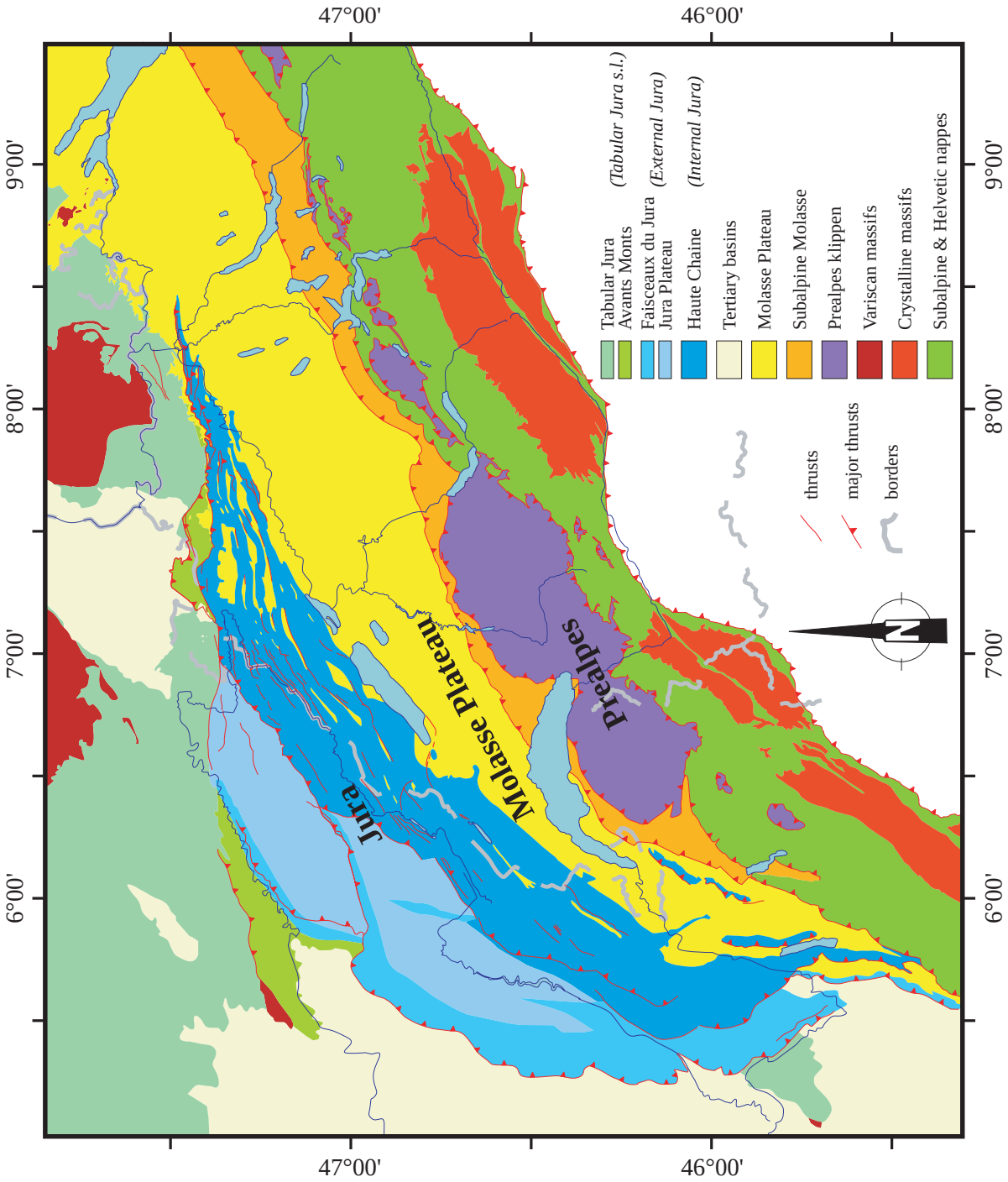

Fig. 5.1 *Simplified tectonic map of the Western Alpine orogen and foreland showing the location of the structural units including the Prealpes, which are the subject of this study. The Prealpes are formed by a series of allochthonous tectonic klippen located along the northern front of the Swiss and French Alps, to the NW of the Helvetic nappes and the External crystalline basement of the Alps.*

of paleostress is based on measurements of faults and slickenlines. The data were collected in three areas of the Western Prealpes Romandes showing quite different tectonic settings, and also in the Taney area (Swiss Chablais Prealpes). To determine paleostress patterns, we will use analysis methods as stress inversion and right dihedra. The local interpretation of the lineaments and observed faults thanks to mechanical models will allow interpreting, in a regional context, the global fracture pattern of the Prealpes.

The final aim of this study is to establish the different morphologic zones forming the Prealpes and adjacent Molasse Plateau, and relate them to a tec-

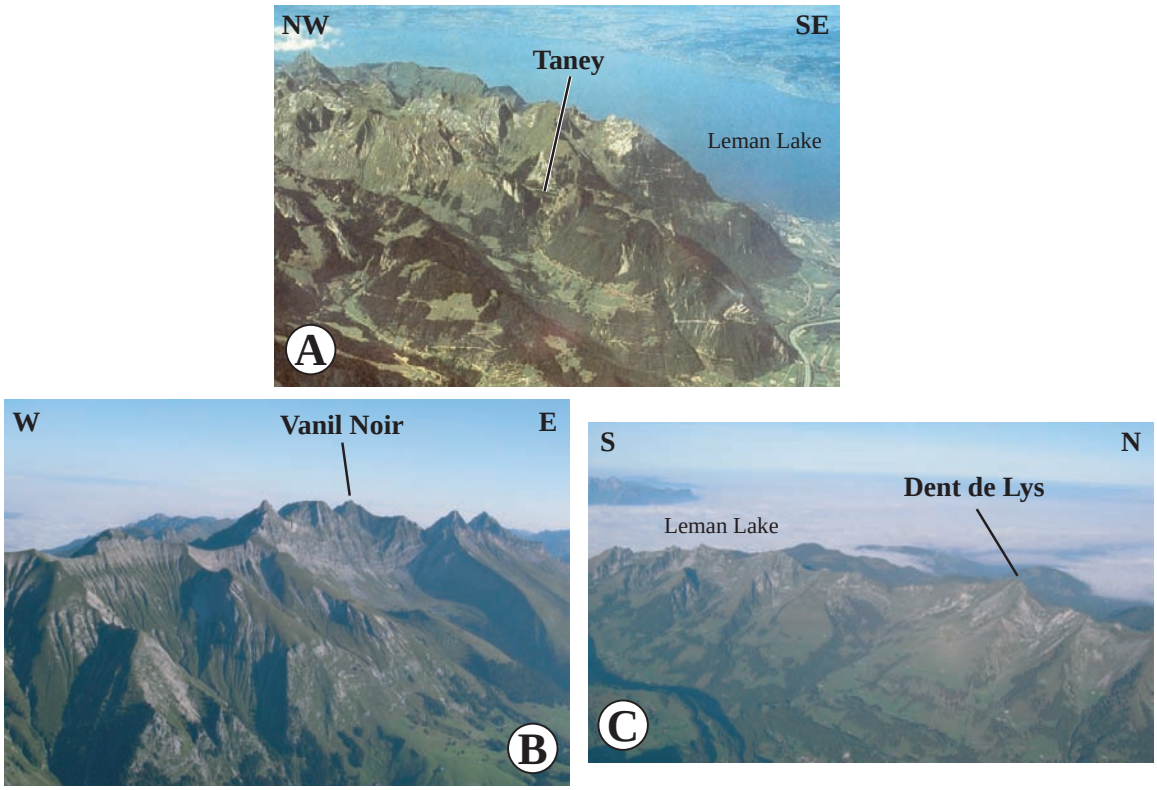

Fig. 5.2 *Photographs of the three study areas: A) The Swiss Chablais Prealpes with focus on the Taney area (Burri 1987) and in the Western Prealpes Romandes B) The Vanil Noir ridge and C) The Dent de Lys ridge.*

tonic framework. Indeed, morphology results of the interactions between notably tectonics, climate and lithologies. Faults modify topography by a mechanical action (fracturation linked to movements) but also by a physico-chemical action (fluid circulation weakening rocks). This tectonic activity may for instance be revealed by linear segments of drainage pattern, brutal topographic changes, slope variations and erosional features. Combining fieldwork and remote sensing data (Digital Elevation Models (Fig. 5.3), aerial pho-

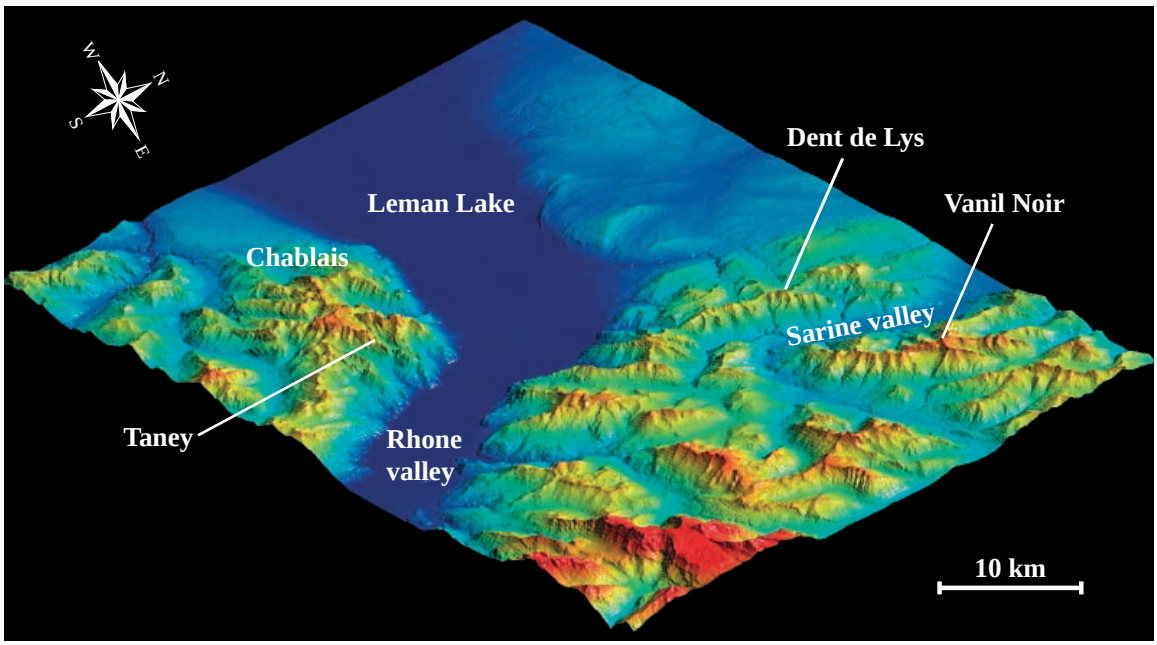

Fig. 5.3 *Digital Elevation Model (MNT25) showing the three study areas. The Taney area in the Swiss Chablais, west of the Rhone valley, and in the Western Prealpes Romandes, north-east of the Leman lake, is located the Dent de Lys area separated from the Vanil Noir area by the Sarine valley.*

tographs, geomorphologic maps and drainage pattern) we will carry out geomorphologic analyses. It will allow us to associate location and orientation of major morphologic structures to structural trends of the large brittle faults and the fold/thrust systems. In addition, we will analyse in detail the orientation of the hydrographic network in three distinct geologic areas (Molasse Plateau, Nappes Superieures area and Western Prealpes Romandes).

5.1.2 Methodology

5.1.2.1 Data

The first step of this work was to setup a GIS database and compile all the data available for the Prealpes and proximal zone of the Molasse Plateau. The official reference system for cadastral surveying (defined and introduced in 1903) is CH 1903. The system comprises the definition of a reference ellipsoid (Bessel 1841) fixed in position and orientation to the old fundamental point (old observatory in Bern) and the Swiss map projection ("Swiss Grid").

The numerical and georeferenced data provided by Swisstopo consist of geologic maps at 1:25000 Châtel-St-Denis, Gruyères, les Mosses, Monthey and Montreux ("Basic data: GA25, © FOWG, Bern"), the corresponding topographic maps and Château-d'Oex map at 1:25000 ("CP25, © 1998 swisstopo"), orthophotographs ("swissimage, © 1998"), the hydrographic network, that is a layer of the digital landscape model of Switzerland at 1:25000 ("VECTOR25, © 1998 swisstopo") and a Digital Elevation Model (MNT25). Orthophotographs are digital color aerial photographs with corrections of inclination and influences of both the camera and terrain. They are consequently presented in one uniform scale and one uniform radiometry that allow to directly read off distances at the ground resolution (between 0.25 and 0.5 m). The hydrographic layer of VECTOR25 has been simplified to keep a continuous and natural hydrologic network. For instance, human constructions such as pipelines, pressure tunnels or canalisations are ignored.

To complete this set of data, a number of published and unpublished maps at 1:5000, 1:10000 and 1:25000, taken from diploma, thesis and articles were scanned and georeferenced. In the Prealpes Romandes, the geomorphologic maps are from Balmat (1982), Fierz (1994), Baudraz (1997); and the geologic maps from Campana (1941), Chenevart (1945), Spoorenberg (1952), Dousse (1965), Chatton (1974), Brasey (1989), Doerfliger (1989), Fierz (1994). The oriental part of the French map at 1:50000 of Thonon-Châtel (Badoux 1965c) was also used for the Swiss Chablais Prealpes.

The fieldwork provided data for the structural analysis such as the dip of bedding, distribution of fractures, fold geometry and orientation of calcite vein sets as well as measures of kinematic indicators on fault planes for the paleostress analysis. In the field, the correlation between the varying maps compiled to elaborate a new regional geologic map has been controlled. The observed geologic and morphologic features are also documented by a number of photographs taken in the field.

5.1.2.2 Structure analysis

The first type of structures analysed to characterize fracturation consists of lineaments. These linear geomorphologic features are the surface expression of zones of weakness or structural displacement in the crust of the Earth (Hobbs 1904). Both in the Prealpes Romandes and the Swiss Chablais Prealpes, lineaments were studied at a very local scale (kilometric), and may for instance correspond to aligned surface sags and depressions (such as dolines), abrupt topographic changes (cliffs for instance), erosional features (karsts), or tectonic features as fault surface ruptures (Appendix 5.I). Three mountainous domains were given special attention: the "Taney area lineaments" for the Swiss Chablais Prealpes, the "Vanil Noir area lineaments" and the "Dent de Lys area lineaments" for the Prealpes Romandes. The morphological aspect of such local scale lineaments is illustrated in this last area by the analysis of a small karst zone (Fig. 5.4 and Appendix 5.II). We graphically represented this kind of lineaments as lines on maps, drawn from orthophotographs with the software ArcView 3.2. We verified the presence of lineaments in the field (when possible) to avoid analysing a pasture's fence as a major fracture trend!

The second type of analysed structures used to characterize fracturation consists of mapped geologic faults. They are reproduced from the set of geologic maps previously cited and completed by observed faults in the field. Thrust faults are differentiated from the other faults because their complex and variable orientations were not measured.

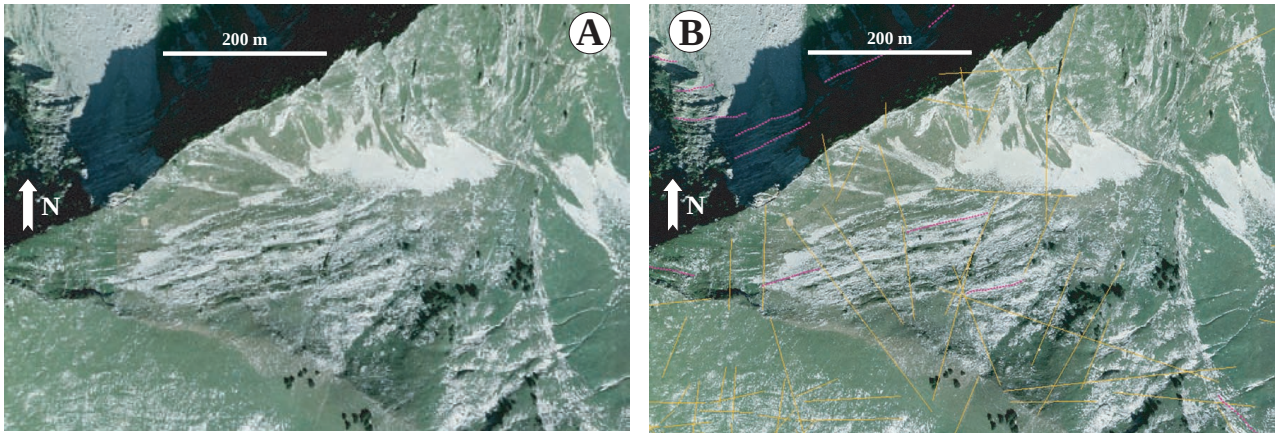

Fig. 5.4 *A) Orthophotography of the Dent de Lys lapiaz, east of the Dent de Lys summit, canton of Fribourg, Switzerland ("swissimage, © 1998") and B) Lineament analysis draped on the orthophotography (pink curves = stratification; yellow lines = lineaments).*

5.1.2.3 Orientation analysis

The orientation analysis concerns the previously described lineaments and geologic faults (Western Prealpes Romandes and Swiss Chablais Prealpes), but also the hydrographic network from the Western Prealpes Romandes to the Molasse Plateau, farther north. Two procedures were used to determine the orientations.

The first procedure, only applied on the lineaments and geologic faults of the Prealpes Romandes, was labor-intensive and involved many steps. First, the curves representing faults in ArcView 3.2 were cut out as successive linear segments to measure their various orientations. The feature orientations to the North were obtained by the software Canvas, where the layers were exported. Feature lengths were considered because the longer a feature on map, the higher its kinematic importance is. The measures of feature orientation and length were then exported in an Excel table to weigh feature orientations by their length (orientation values of long lines put a higher number of times). Finally, with the software TectonicsFP, the orientations of features were represented in rose diagrams.

The second procedure to determine feature orientations uses the script L-STAT (Kim 2004) on ArcView 3.2. Not only the lineaments and geologic faults of the Romandes and Swiss Chablais Prealpes were concerned, but also the hydrographic network in different tectonic zones (Molasse Plateau, Nappes Superieures area and Western Prealpes Romandes) to compare their morphologies. The script calculates directly the orientation distribution of features, both for lines and curves, and weights the lengths. The orientations are then drawn in a 360° rose diagram. Having used the two techniques, it was possible to make a comparison between different methods of analysis. In addition, we compared weighed and non weighed diagrams and tested the validity of our kinematic assumption.

5.1.2.4 Stress analysis

The stress analysis is based on the fault plane and striation values collected in the field. *In situ* work consisted in measuring fault planes with slickenfibre lineations providing the sense of movement of the faults. The field data then have been analysed using TectonicsFP for Windows™ (Ortner et al. 2002). For each dataset, we recorded the dip direction/dip of the fault plane, the trend/plunge of the fault lineation and the relative sense of slip of the stria (dextral, sinistral, normal or reverse). The kinematic history of a single fault is defined by the striations on the fault surface. For a population of faults, the orientation of the fault planes and their associated striae allow to determinate the three principal stress axes (σ_1, σ_2, σ_3) (Angelier & Mechler 1977). The determination of stresses from measurements of striations in the field is based on several hypotheses. It is assumed that slip takes place in a direction parallel to that of the maximum shear stress on the plane of movement (Ramsay 2000). Consequently, the striation of the fault plane is considered as representing the direction of maximal shear stress (Peresson 1992). The stress field is estimated homogenous within the outcrop containing the sampled faults. Finally, the movement on a fault does not hold any influence on the slip sense of other faults (Ramsay 2000).

5.2 PREALPES GEOLOGY

5.2.1 Tectonics

The Prealpes are formed by several klippen located along the northern front of the Alps. The two major lobes are situated on both sides of the Rhone valley (Fig. 5.5): the Chablais Prealpes, south of the Leman Lake and the Prealpes Romandes, east of the lake. The nappe transport occurred during the Alpine orogeny and led to the actual thrust of the Prealpes on top of the Autochtonous and Subalpine Molasse to the North, and on the Helvetic nappes to the South (Fig. 5.5). The Prealpes Medianes are the largest member of the nappe stack (Fig. 5.5). Their meridional part is overthrust by the Brèche nappe and the whole is overridden by a group of nappes called Nappe Superieure s.l. (CARON 1972, 1976, CARON & DUPASQUIER 1989). The paleogeographic origin of the Prealpes Medianes is in the Sub-Briançonnais and Briançonnais sedimentation realm (TRÜMPY 1960, CARON 1972, 1973, TRÜMPY 1980, BOILLOT et al. 1984). The Prealpes Medianes Nappe was transported over a distance exceeding 100 km (MASSON 1976) on a basal décollement in evaporites located at the base of the Middle and Late Triassic. Most tectonic and all of its very low-grade metamorphic features were acquired during the incorporation into the Alpine accretionary wedge between 45 and 27 Ma (MOSAR et al. 1996).

The Prealpes Medianes are subdivided into Medianes Plastiques, forming the frontal part (NW) of the nappe and Medianes Rigides, forming its trailing part (SE) (LUGEON & GAGNEBIN 1941). These names reflect the change in structural style from a fold-dominated northern part ("Plastiques") to large imbricated structures in the southern part ("Rigides"). A domain located between the Medianes Rigides and Plastiques, the Gastlosen range, has intermediate characteristics both tectonic and sedimentological (LUGEON & GAGNEBIN 1941, BAUD 1972, PLANCHEREL 1979, MOSAR et al. 1996).

The Prealpes Medianes Plastiques consist of successive large-scale fault-related folds. Their trends vary from E-W in the eastern part of the nappe to NNE-SSW and even N-S in the western part of the fold-and-thrust belt (GAGNEBIN 1922, JEANNET

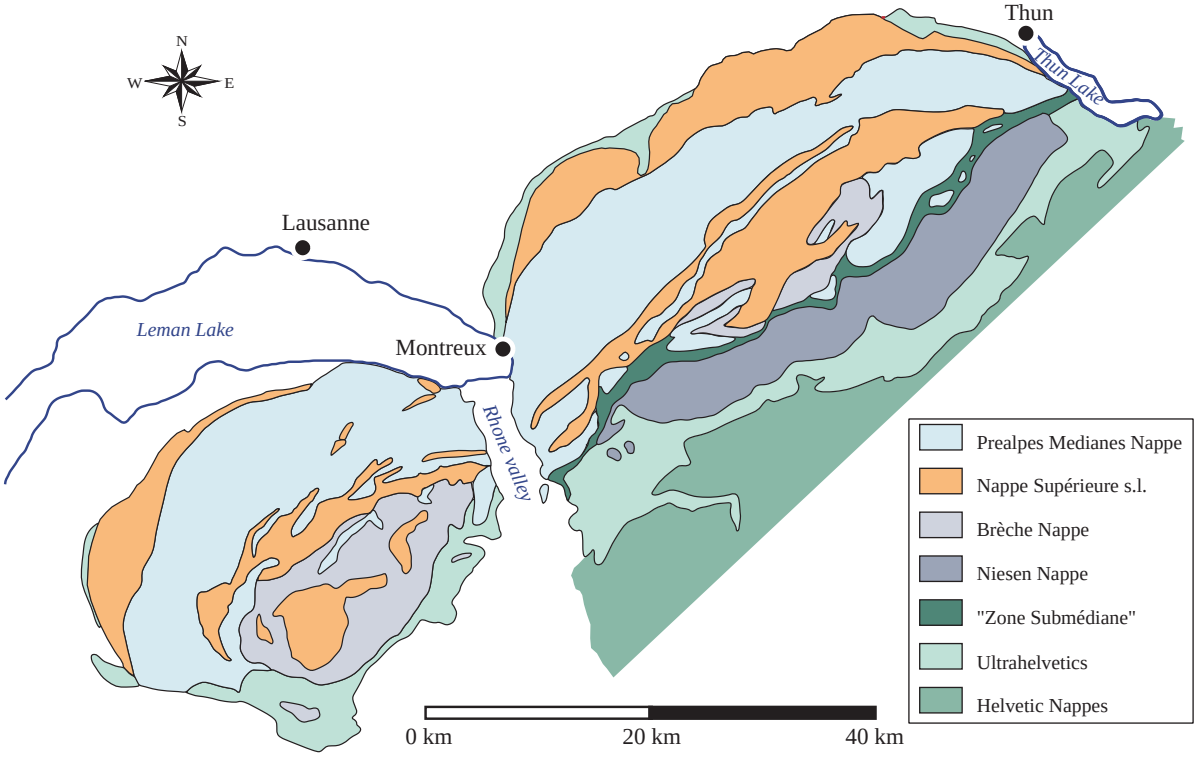

Fig. 5.5 *Structural map of the Prealpes modified after CARON (1973). The complete series of nappes forming the Prealpes klippen can be observed in the Prealpes Romandes, east of the Leman Lake. The succession of units is from top to bottom: a) the Nappe Superieure (CARON 1972, TRÜMPY 1980), b) the Brèche Nappe, c) the Prealpes Medianes Nappe and d) the Niesen Nappe (present uniquely in the Prealpes Romandes) (CARON 1972, 1973, BERNOULLI et al. 1979, MATTER et al. 1980, ACKERMANN 1986) and two mélange zones developed during the nappe transport that are the Ultrahelvetics and the "Zone" Submédiane (WEIDMANN et al. 1976).*

1922, Badoux et al. 1960, Badoux & Mercanton 1962, Badoux 1965c, Plancherel 1979, Müller & Plancherel 1982, Mosar 1988b, 1988a, Mettraux & Mosar 1989, Mosar 1989, Mosar 1991, Mosar & Borel 1992, 1993, Mosar 1994, Mosar et al. 1996, Mosar 1997). The folds and their genetically linked thrust-planes die out laterally and are relayed by other folds, thus forming en échelon structures. They can be viewed as transfer zones located where local strike-slip faults are expected to develop (Mosar & Borel 1992). The Prealpes Medianes Rigides are formed by one major, in some places one or two minor, imbricated thrust slices dipping to the N/NW (Mosar 1997). The large- and small-scale tectono-metamorphic events proceeded continuously and diachronically from the South to the frontal part of the nappe in the North. They were complete before the Prealpes arrived on the future Helvetic nappes (Mosar 1988a, 1989, Mosar 1991, Mosar & Borel 1992).

The "Zone Submédiane" structural unit (Weidmann et al. 1976) is located at the base of the Prealpes Medianes and separates them from the Niesen Nappe (Fig. 5.6A and 5.6B). Elsewhere the sole of the Prealpes is in contact with the underlying units (the Helvetic nappes in the South and the Subalpine Molasse and flysch to the North) by means of the "Ultrahelvetics" (Badoux 1963, Homewood 1977, Jeanbourquin 1991, Jeanbourquin & Goy-Eggenberger 1991, Jeanbourquin 1992, Jeanbourquin et al. 1992, Lempicka Münch & Masson 1993, Mosar et al. 1996). In the surroundings of Charmey, the transition between the Prealpes Medianes Nappe and the Subalpine Molasse and flysch is illustrated by a cross section (Fig. 5.7).

The Jura fold-and-thrust belt represents the most external part of the Alpine chain and consequently the most recently deformed unit. Its development started 11 Ma ago, during the Late Miocene and probably continued at least until the Pliocene around 3 Ma ago (Naef et al. 1985, Laubscher 1987, 1992). It is characterized by a typical thin-skinned tectonic style controlled by the presence of a basal décollement horizon within Triassic evaporites (Fig. 5.7) (Jordan & Nüesch 1989). Two main structural zones are distinguished: the external plateau Jura and southern, the internal folded Jura (Fig. 5.7) where fault-propagation folds and fault-bend folds are common (Suppe & Medwedeff 1990). These Mesozoic layers were covered by the Molasse sedimentation which currently appears as remnants in the core of some synclines, but which constitutes especially the Molasse Plateau and the Subalpine Molasse (Fig. 5.7).

The Molasse sediments (Matter et al. 1980, Homewood 1986) are composed of shallow marine deposits alternating with thick sequences of continental detrital sediments, beginning with the Early Oligocene and continuing until the end of the Middle Miocene. Four major subdivisions can be recognised from bottom to top: a Lower Marine Molasse (UMM), a Lower freshwater Molasse (USM), an Upper Marine Molasse (OMM) and finally an Upper Freshwater Molasse (OSM). The internal deformation and shortening within the Molasse Plateau and its underlying Mesozoic cover (Fig. 5.7) is relatively weak (Pfiffner 1986, Burkhard 1990, Jordan 1992). Only the Subalpine Molasse has seriously been affected by thrusting and folding and a tectonic slice stack brings the USM, UMM and subalpine flysch and wildflysch to outcrop, as a succession of complex alternations (Fig. 5.7) (Weidmann 1988). It is therefore reasonable to suggest that the Molasse sediments transmitted part of the Alpine push to the Jura belt and were thereby translated towards the NW, together with the underlying post Middle Triassic cover (Escher et al. 1997).

At the southern part of the cross section, the Prealpine stack thrusts the cushion formed by the Ultrahelvetics (Fig. 5.7). They represent a chaotic and complex deformed zone of lenses and small nappes of Mesozoic cover (Jeanbourquin 1994), originating from the South of the Helvetic. The contact between the Prealpes and the Subalpine Molasse is complicated by the presence of the Gurnigel Nappe. This nappe is regarded as a digitation of the lowermost unit of the Nappe Superieure (Caron 1972, Lemoine 1984), i.e. of Piemont origin. The nappe thrusts to the North in an early stage of nappe transport and subsequently was overthrust by the Prealpes Medianes Nappe in a final stage of deformation (Middle-Late Oligocene) (Wissing & Pfiffner 2002).

5.2.2 Stratigraphy and paleogeography

The Prealpes Medianes are the most important unit of the Prealpes klippen belt. Their sedimentation realm has been interpreted in terms of a rim basin located in the Sub-Briançonnais domain, to the N-NW of the Briançonnais upper plate rift shoulder (Stampfli & Marthaler 1990a, Mosar et al. 1996, Mosar 1997). This rim basin presents two major sedimentation realms clearly differentiated since the Early Jurassic (Lias). To the N-NW, in the Medianes Plastiques, a

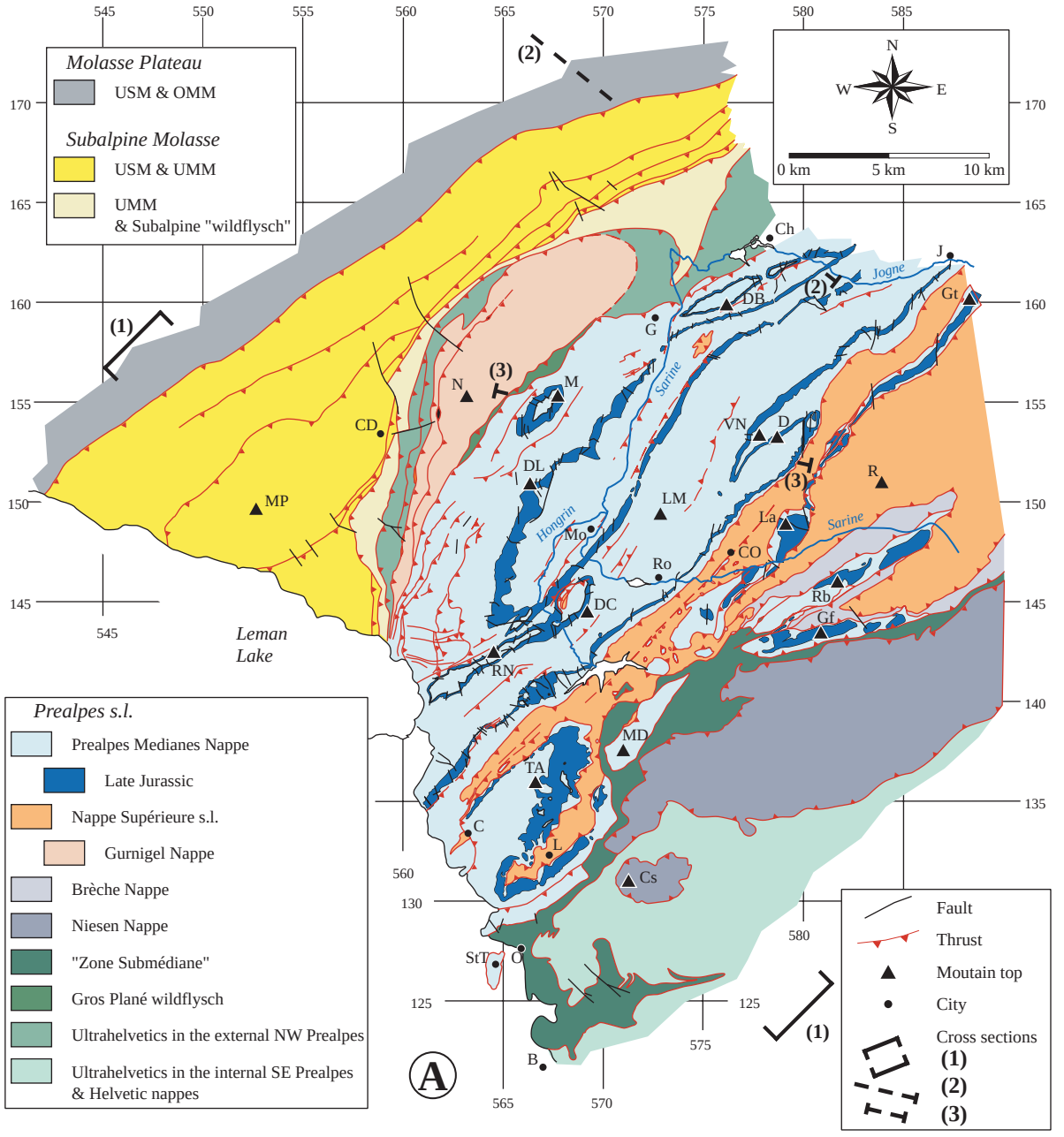
Molasse Plateau
USM & OMM
Subalpine Molasse
USM & UMM
UMM
& Subalpine "wildflysch"
N
W
E
S
0 km
5 km
10 km
Leman
Lake
Jogne
Sarine
Hongrin
Prealpes s.l.
Prealpes Medianes Nappe
Late Jurassic
Nappe Supérieure s.l.
Gurnigel Nappe
Brèche Nappe
Niesen Nappe
"Zone Submédiane"
Gros Plané wildflysch
Ultrahelvetics in the external NW Prealpes
Ultrahelvetics in the internal SE Prealpes
& Helvetic nappes
Fault
Thrust
Moutain top
City
Cross sections
(1)
(2)
(3)
A

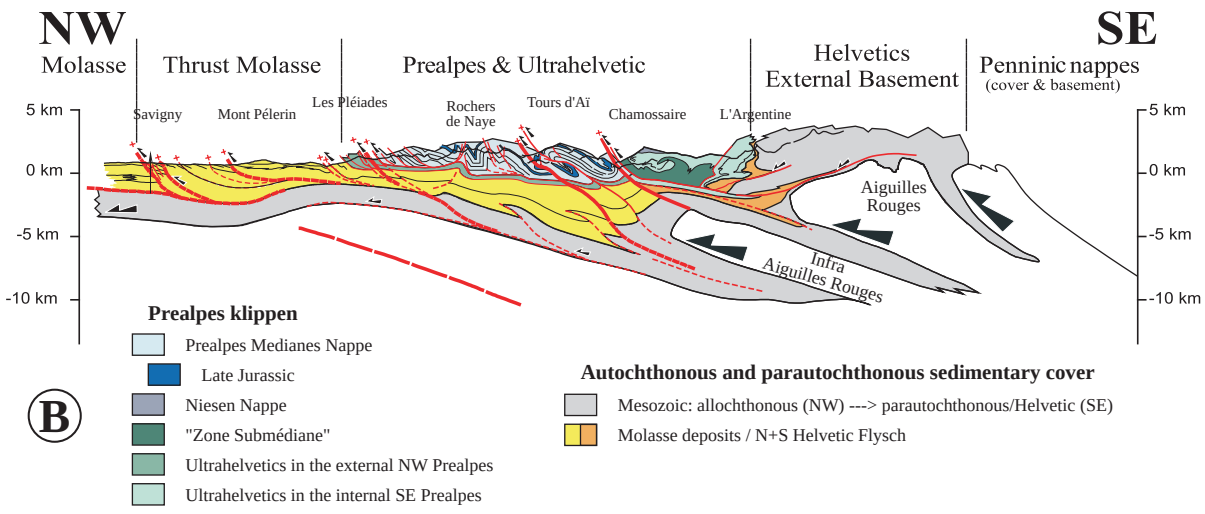
NW
Molasse
Thrust Molasse
Prealpes & Ultrahelvetic
Helvetics
External Basement
Penninic nappes
(cover & basement)
SE
Savigny
Mont Pélerin
Les Pléiades
Rochers
de Naye
Tours d'Aï
Chamossaire
L'Argentine
Aiguilles
Rouges
Infra
Aiguilles Rouges
5 km
0 km
-5 km
-10 km
Prealpes klippen
Prealpes Medianes Nappe
Late Jurassic
Niesen Nappe
"Zone Submédiane"
Ultrahelvetics in the external NW Prealpes
Ultrahelvetics in the internal SE Prealpes
Autochthonous and parautochthonous sedimentary cover
Mesozoic: allochthonous (NW) ---> parautochthonous/Helvetic (SE)
Molasse deposits / N+S Helvetic Flysch
B

Fig. 5.6 *A) Structural map of the Western Prealpes Romandes (modified after Mosar 1997) showing the main structural units, the major thrusts and folds. B=Bex; C=Corbeyrier; CD=Châtel St. Denis; Ch=Charmey; CO=Château d'Oex; Cs=Chamossaire; D=Dorena; DB=Dent de Broc; DC=Dent de Corjon; DL=Dent de Lys; G=Gruyère; Gf=Gummfluh; Gt=Gastlosen; J=Jaun; La=Laitemaire; L=Leysin; LM=Les Millets; M=Moléson; MD=Mont d'Or; Mo=Montbovon; MP=Mont Pélerin; N=Niremont; O=Ollon; R=Les Rodomonts; Rb=Rübli; RN=Rochers de Naye; Ro=Rossinière; StT=Saint Triphon; TA=Tours d'Aï; VN=Vanil Noir and B) NW-SE cross section across the alpine foreland extending from the Molasse basin to the Penninic units (see location cross section 1 Fig. 5.6A). The thick limestones (200 m) of Late Jurassic age are highlighted on the map and section since they form important cliffs which are a major morpho-tectonic feature highlighting the succession of fault-related anticlines and synclines.*

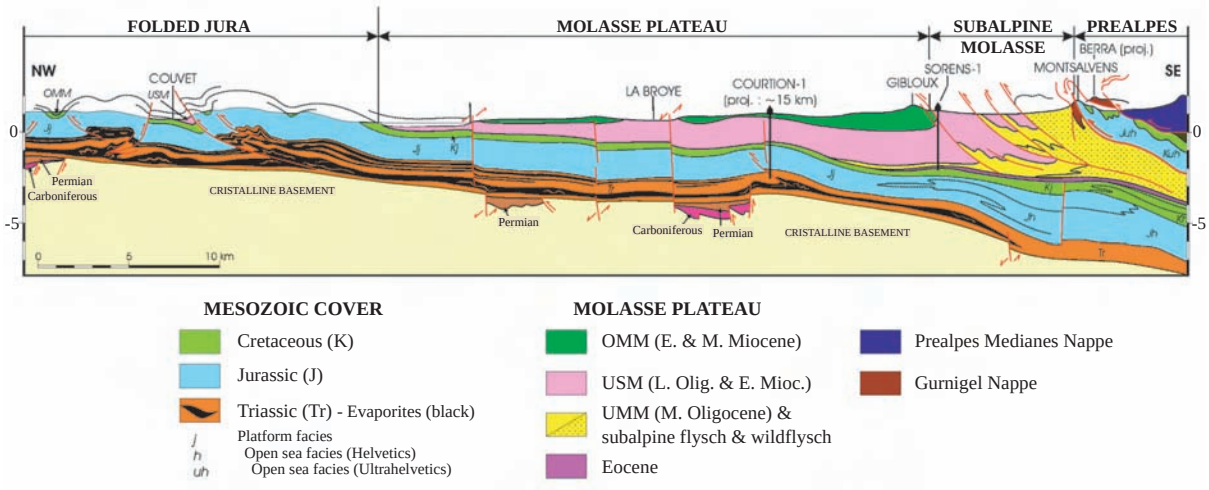

Fig. 5.7 *Cross section (see location cross section 2 Fig. 5.6A) from the Prealpes (SE) to the folded Jura (NW) showing the structural styles of the different crossed units (folded Jura, Molasse Plateau, Subalpine Molasse and Prealpes) modified from Matter et al. (1980).*

large basin is marked by an important thickness of sediments. To the South, this subsiding domain turns into a ramp that gives way since the Middle Jurassic (Dogger) to a platform and lagoonal environment. This meridional part of the Prealpes Medianes is called Prealpes Rigides (Baud & Septfontaine 1980, Mosar 1994, Mosar et al. 1996, Mosar 1997).

5.3 Prealpes Romandes

5.3.1 Presentation of the study area

5.3.1.1 Structural and tectonic features

The two zones of the Western Prealpes Romandes, subjects of this fracturation study, are located in the Prealpes Medianes Plastiques. They are included in a bigger zone of morphologic study (about 300 km^2) situated between 560000 and 585000 of longitude and 143000 and 160000 of latitude (Swiss geographic coordinate system). The investigated mountainous domain to the East is the Vanil Noir area and to the West, the Dent de Lys area (Fig. 5.6A). Both belong to a succession of structural sub-units of the Western Prealpes Romandes (Fig. 5.6 and 5.8).

The fracture and lineament analysis covers a zone of about 8.5 km^2 along the Dent de Lys ridge (summit at 2014 m), i.e. the eastern part of the Gros Mology-Molard-Les Avants anticlinorium. The studied Vanil Noir area covers almost 30 km^2 and comprises the eastern flank of the Tsavas-Millets anticline, the Vanil Noir-Dent de Corjon-Rochers de Naye syncline and the Dorena anticline. The Vanil Noir summit reaches 2389 m and is amazingly located in the core of the syncline (Appendix 5.III). While the Dent de Lys and Vanil Noir areas present the same lithologies (limestones, marls and dolomites) ranging from the Upper Triassic to Early Cretaceous in age, morphologies of the landscape differ. The Vanil Noir area is formed by large folds (Fig. 5.9A), while the Dent de Lys area consists of a large monoclinal and fractured calcareous slab (Fig. 5.9B). It will thus be possible to compare the influence of the structure and the morphology on the fracturation in these two areas.

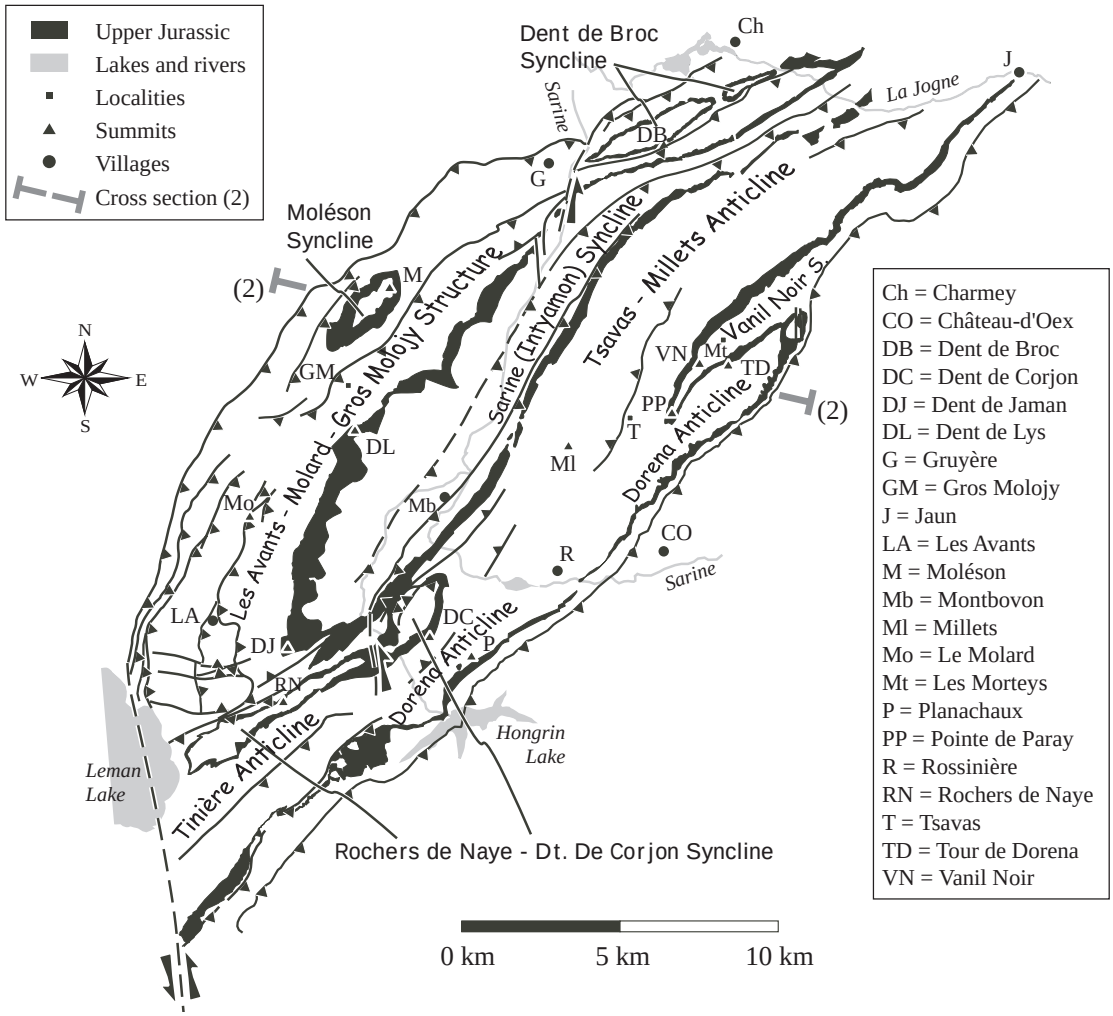

Fig. 5.8 *Structural scheme of the Western Prealpes Medianes Plastiques Romandes modified after* Mosar *(1997). The successive structural sub-units described by* Mosar *(1997) are from the external NW border towards the SE in direction of the Prealpes Medianes Rigides: (a) The external imbricates (*Schardt *1893,* Jeannet *1922,* Badoux *1965b,* Mosar *1994). (b) The Gros Mology-Molard-Les Avants anticlinorium that forms the transition from the external imbricates to the "main body" of the Medianes Plastiques. The Dent de Lys is one of the highest summits of the ridge formed by the eastern flank of this anticlinorium. (c) The broad and deep Sarine (or Intyamon) syncline. (d) The Tsavas-Millets anticline that runs on the NW flanks of the Vanil ridge. (e) The Vanil Noir-Dent de Corjon-Rochers de Naye syncline forms a high mountain ridge that runs SE of the Sarine valley and extends till Leman Lake. (f) The Dorena and Tinière anticlines. (g) The Château-d'Oex syncline and further south the intermediate domain of the Prealpes Medianes (Gastlosen-Tours d'Aï) followed by the Medianes Rigides.*

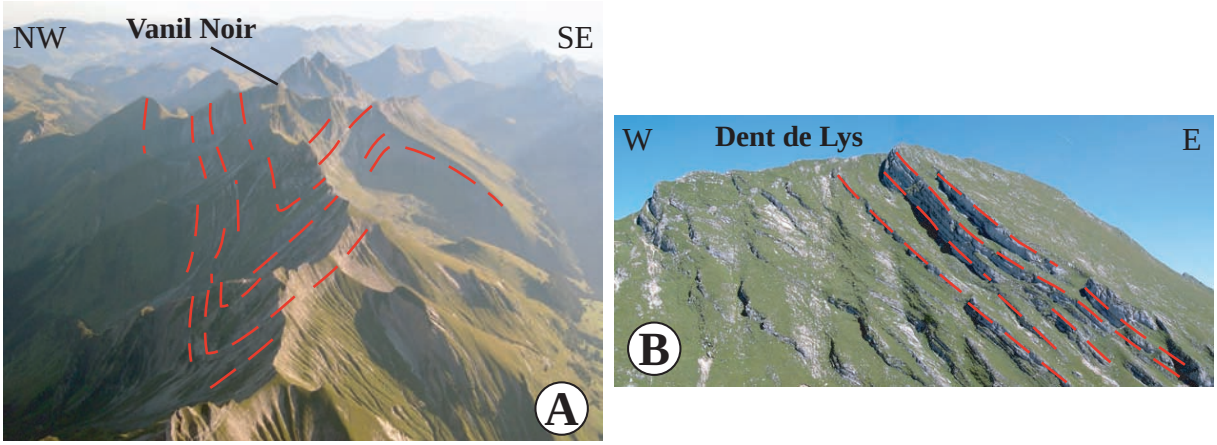

Fig. 5.9 *A) Picture of the folding Vanil Noir area and B) Picture of the Dent de Lys calcareous slab. The summits are indicated and the stratification is underlined by dashed red lines.*

5.3.1.2 *Stratigraphy, sedimentology and rheology*

The sediments of the Dent de Lys and Vanil Noir area (Appendix 5.III) are presented in four simplified stratigraphic columns located along a NW-SE cross section (Fig. 5.10). They are formed by limestones, dolomites and marls from the Upper Triassic to Tertiary in age (Trümpy 1960, Badoux & Mercanton 1962, Baud & Septfontaine 1980, Trümpy 1980, Baud et al. 1989, Plancherel 1990, Borel 1995). The stratigraphic subdivision used in this study is based on a structural classification depending on the relative competence of the series (Mosar 1997). This subdivision is consequently morphologic, since competent lithologies appear as cliffs and more "ductile"/erodable lithologies as erosional depressions. The different units are named according to the corresponding geologic stage or system. This choice implies a non respect of a strict chronostratigraphic scale (Plancherel 1979).

The Upper Triassic starts the stratigraphic series of the Dent de Lys and Vanil Noir area. It is represented by evaporites, dolomites and lumachelles and appears as small dispersed outcrops in the core of the eroded anticlines (Les Avants-Molard-Gros Molojy structure in the N-NW and Tinière and Tsavas-Millets anticlines in the South and East) (Mosar 1997). Isolated, or associated with dolomites, cornieules are most of the time found along thrust planes (Masson 1972, Jeanbourquin 1988). These evaporitic layers constitute the basal detachment of the Prealpes Medianes and are characteristic of the thrust planes in the klippen (Baud 1972, Masson 1972).

Tectonic geomorphology: The triassic rocks are intensively tectonised and consequently easily alterable. For this reason, they form large depressions filled by Quaternary deposits (Plancherel 1979).

The Early Jurassic (Lias) consists of a maximum 200 m thick succession of oolitic, spathic and siliceous limestones. It appears around the Triassic outcrops and forms the core of the southern part of the Dorena anti-

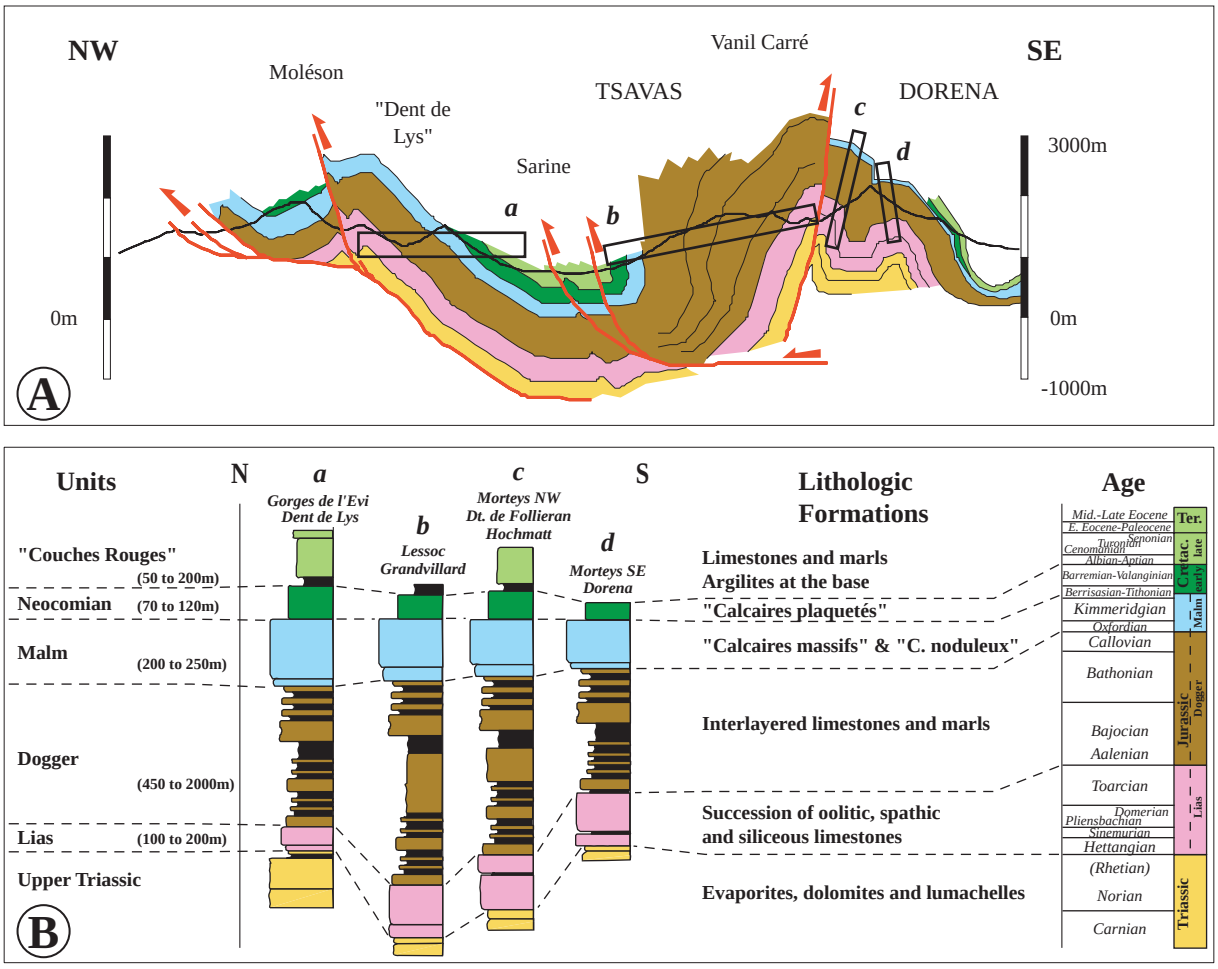

Fig. 5.10 *A) NW-SE section across the Western Prealpes Romandes (see location cross section 3 Fig. 5.6A) showing the structural style of the Medianes Plastiques B) Simplified stratigraphic columns (location indicated on the cross section) illustrating the morphology of the successive units and also their variable thickness, both modified after Mosar (1997).*

cline.

Tectonic geomorphology: The calcareous nature of the Early Jurassic (Lias) determines its specific structural behaviour since it forms pronounced reliefs surrounded by the soft levels of the underlying Triassic and overlying Middle Jurassic (Dogger). Furthermore, the competent nature of these rocks causes brittle deformation (many fault planes with striations can be observed) despite the presence of small scale folds (PLANCHEREL 1979).

The Middle Jurassic (Dogger) is the thickest studied formation (450 to 2000 m) and consists of interlayered limestones and marls. It is widely represented since it cores many of the anticlinal structures together with the liassic formations, and forms the core of the northern part of the Dorena anticline (Fig. 5.11A).

Tectonic geomorphology: The Middle Jurassic appears clearly in the morphology because it forms monotonous slopes between the Early Jurassic (Lias) and the Late Jurassic (Malm) resistant lithologies. This lithology constitutes the base of the high cliffs dominated by the Late Jurassic massive limestones. The transition between Middle and Late Jurassic is difficult to place because of an increase of calcareous layers at the top of the Dogger. While the whole Dogger behaves in a "plastic" way, the numerous calcareous layers act as brittle levels (PLANCHEREL 1979). The alternate limestone and marl layers control the tectonic style of the Middle Jurassic formation. We can observe folds near faults, tension gashes and calcite veins. For instance, a recent fault affecting the Middle Jurassic has been identified near the Vanil Noir, at a place called Tête de l'Herbette (Fig. 5.11B and Chapter 5.3.2.4).

The Late Jurassic (Malm) formation is 200 to 250 m thick and its base consists of a layer of Calcaires noduleux overlain by an important thickness of Calcaires massifs. It forms the top of the cliffs bordering some synclines such as from the NW to the SE: the Moléson syncline, the Sarine (Intyamon) syncline, the Rochers de Naye-Dent de Corjon syncline, the Vanil Noir syncline and the Hongrin syncline (Fig. 5.8). The thrust slice of the Gastlosen is also formed by Late Jurassic limestones.

Tectonic geomorphology: The competent cliffs are intensively faulted and, emphasized by erosion, large rockfalls are frequent (Fig. 5.11C). Late Jurassic rocks present a lot of fault planes but they are often karstified (Fig. 5.11D), that erases the markers of movement as striations. In this lithology, a complex network of karst caverns developed. For instance in the vallon des Morteys, NE of the Vanil Noir summit, a system of karst caverns is overprinted on the set of cross faults (Appendix 5.IV). Neotectonics indicators have been found in circular galleries displaced along brittle faults (BRASEY 1989). The circular shape of these caverns hints to a development below water level. Since these caverns are located around 2000 m altitude, high above valleys, we have to conclude to important erosion since.

Pelagic calcareous sedimentation continues during the Early Cretaceous (Neocomian) but as limestones are remarkably bedded (Fig. 5.11E), they are called Calcaires plaquetés. Folding of the limestones due to this bedding (Fig. 5.11F) complicates the thickness estimation of the formation that may be between 70 and 120 m.

Tectonic geomorphology: Neocomian rocks form on the flanks of the synclines a transition zone between the Late Jurassic cliffs and the smooth shapes of the younger Couches Rouges and flyschs (PLANCHEREL 1979). Neocomian rocks are karstified, as the Late Jurassic, predominantly in the high areas (Vallon des Morteys and En Lys area). While this lithology is less massive than the Late Jurassic formation (Malm), it forms the highest summits in the canton of Fribourg (Vanil Noir and Vanil de l'Ecri). It is also affected by big faults as for instance the fault near the Vanil Noir called Pas de la Borière (Fig. 5.11G).

When the lithologic series is complete as is the case in the core of the synclines (stratigraphic columns *a* and *c* Fig. 5.10B), the Neocomian is successively overlain by a level of argilites, limestones and marls of the Couches Rouges formation. This unit is of Late Cretaceous to Tertiary in age and measures between 50 and 200 m. The Couches Rouges formation follows the Neocomian lithology and fills the

Fig. 5.11 *Simplified stratigraphic column from the Prealpes Plastiques Romandes showing lithologies ranging from the Upper Triassic to Tertiary and illustrated by photographs A) The core of the northern part of the Dorena anticline constituted by the Middle Jurassic formation, B) Recent brittle fault with extensive cataclasites and calcite veins affecting the Middle Jurassic formation close to the Vanil Noir summit, C) Large rockfall affecting the Late Jurassic formation of the southern flank of the Vanil Noir syncline, D) Late Jurassic rocks are often karstified erasing all the striations of the numerous fault planes, E) Limestones remarkably bedded of the Early Cretaceous thus called Calcaires plaquetés, F) Bedding of the Early Cretaceous limestones implies an important folding of the formation, G) The highest top of the canton of Fribourg (Vanil Noir summit) is formed by the Early Cretaceous limestones and is also affected by big faults (Pas de la Borière), H) Curved calcite fibres collected in a quarry near Ennay, in the Sarine valley.*

TIME SCALE
Cenozoic
Mesozoic
Neogene
Paleogene
Cretaceous
Jurassic
Triassic
Pleistocene
Pliocene
Miocene
Oligocene
Eocene
Paleocene
Late
Early
Late
Middle
Early
Late
(Ma)
23.03
65.5
145.5
199.6
UNITS
"Couches Rouges"
Neocomian
Malm
Dogger
Lias
Upper Triassic
PICTURES
H
E, F, G
C, D
A, B
H)
10cm
0cm
G)
NNE
SSW
Vanil Noir
fault
Bimis
D)
SE
NW
B)
15 cm
N
S
F)
W
E
C)
SE
NW
E)
NW
SE
A)
S
N

core of the Sarine syncline, the Rochers de Naye-Dent de Corjon syncline and the Vanil Noir syncline, with their numerous small-scale folds. In the SE, along the Gastlosen, transgressive Couches Rouges are closely associated with their Late Jurassic (Malm) substratum (PLANCHEREL 1979).

Tectonic geomorphology: Couches Rouges are intensively faulted and a lot of quarries (notably in the Sarine valley) or road building sites provide numerous fresh outcrops where calcite fibres indicate sense of movement (Fig. 5.11H and Chapter 5.3.2.4).

The SE zone of the Dent de Lys and Vanil Noir area is overthrust by the Simme nappe belonging to the group of nappes called Nappe Supérieure s.l. (CARON 1972, 1976, CARON & DUPASQUIER 1989). The Cretaceous flyschs of the Simme nappe only appear as remnants in the synclines of the Prealpes Medianes Plastiques.

5.3.2 Results of the feature analyses

5.3.2.1 Morphologic features

In the area extending north and east of the Leman Lake, the hydrographic network presents varying orientations from the Molasse Plateau to the Western Prealpes Romandes. From north to south, three morphological zones with different drainage patterns have been distinguished: the Molasse Plateau, a mélange zone called "external units area", and the Western Prealpes Romandes (Fig. 5.12). We used the script L-STAT (KIM 2004) of ArcView 3.2 to analyse the orientations of the drainage pattern. Understanding the varied morphologies of the hydrographic network, the main or particular trends of the drainage pattern, may help relate to the structural and lithological heritages of the area.

The hydrographic network of the Molasse Plateau between the Western Prealpes Medianes front and the Neuchatel Lake is arranged as a "trellis pattern" type, in which small tributaries are essentially same size on opposite sides of long parallel subsequent streams (HOWARD 1967), here oriented NE-SW. On the Molasse Plateau, the major hydrographic trend is NE/SW (see the rose diagram Fig. 5.12) and corresponds to the trend of the structures modelled by the ice flow. The major part of the sedimentary material brought by the Alpine alluvial fans was evacuated to the SW by the Rhone River or to the N-NE by the Rhine River and the last part constituted the plurikilometric-thick Molasse sediments of the plateau. The ice flow, bordered by the Jura fold-and-thrust belt to the NW and by the Alps to the SE, cut the Molasse sediments parallel to the chain.

The hydrographic network of the external unit area can be clearly distinguished from the surrounding ones since it is radial and very dense (Fig. 5.12). The flow is centripetal because the concerned areas consist of isolated hill tops surmounting the Molasse Plateau. In addition, the "soft" levels of erodable lithologies (flyschs, wildflyschs, marls, limestones and dolomites) favour a densification of the drainage pattern. However, some anomalies disturb the uniform presence of the flow. First, a non irrigated zone exists around the summit Moléson (Fig. 5.6, 5.12 and 5.13) due to the high resistance to erosion of the main constitutive lithology, the thick limestones of Late Jurassic age. The second anomalous feature is the linear orientation of two rivers called Veveyse de Châtel and Veveyse de Fégire (Fig. 5.12). Their trend is N110-N120 and we believe that the rivers follow a major fracture direction. This orientation is the most represented on the external unit rose diagram (Fig. 5.12). It raises the question of the importance of tectonic influence on the hydrographic network in this area.

In the Western Prealpes Romandes, the drainage pattern is less dense than in the external units but presents varied morphologies due to local influences of the lithologies (karst areas), structures (large parallel folds for instance) and tectonics (fracture pattern). Three zones are remarkable by their lack of hydrographic network, as for the Moléson (Fig. 5.13), and they correspond to the principal mountain ranges. These karst areas, dominated by large Upper Jurassic (Malm) slabs, are the Vanil Noir, Dent de Lys and Dent de Broc areas (Fig. 5.12). While all the trends are represented in the hydrographic network, two major orientations can be distinguished: N010°-N020° and NE-SW (Fig. 5.12). These orientations correspond to the structural trends, i.e. the fold/thrust system orientations. For instance, the Sarine syncline follows the N010°-N020° trend and the Hongrin syncline the NE-SW orientation (Fig. 5.12).

This study of the hydrographic network illustrates the variety of drainage morphologies at the transition between the Prealpes klippen and the Molasse Plateau. In addition, as we attributed clearly a structural or a lithological origin to the preferential orientations of the drainage, the influence of these heritages in the

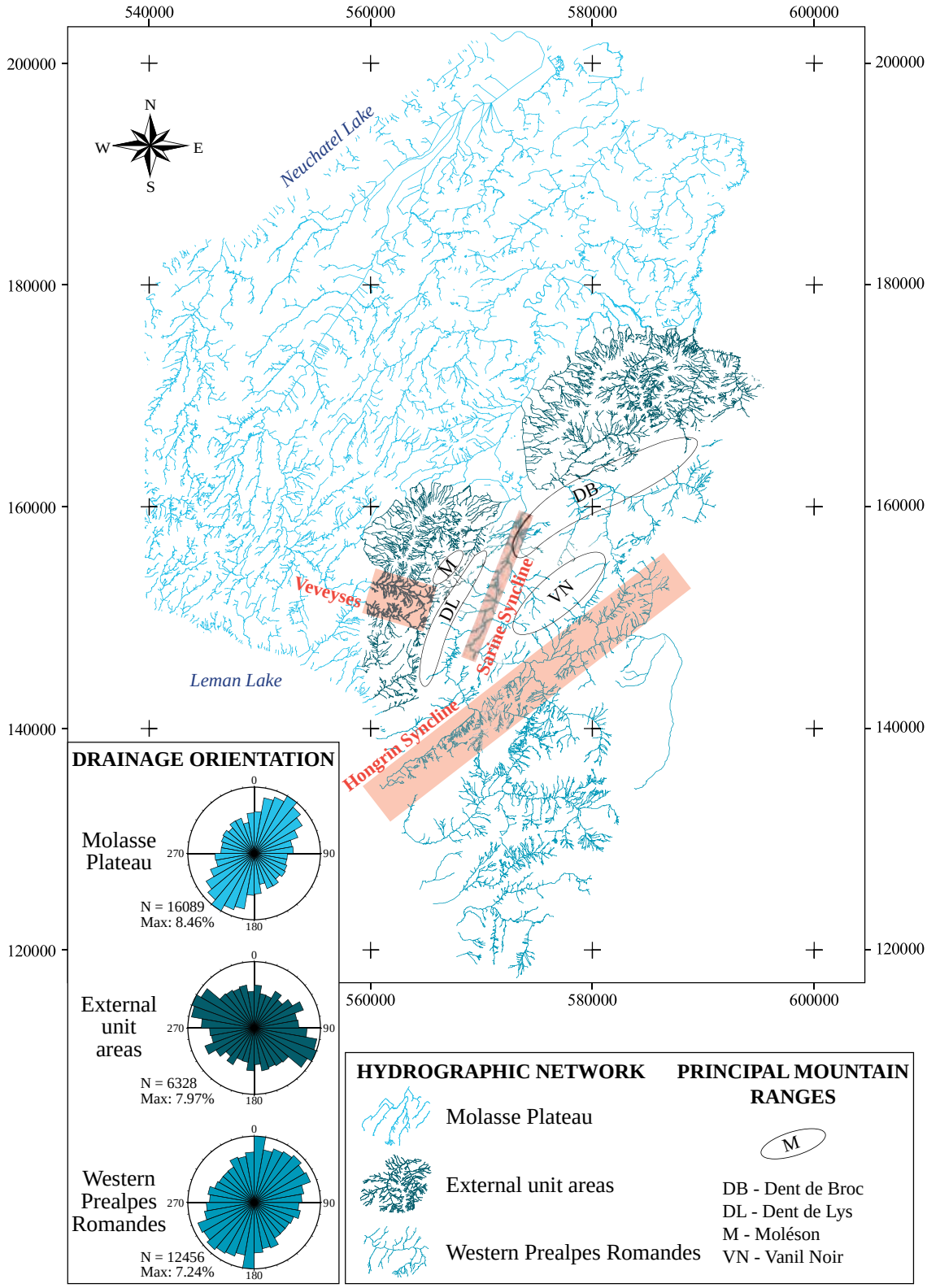

Fig. 5.12 *In the area south and east of the Leman lake, three zones morphologically different of the hydrographic network ("VECTOR25, © 1998 swisstopo") appear from N to S: the Molasse Plateau, a mélange zone called "external units area" (the Ultrahelvetics, the Gurnigel Nappe, the Gros Plané wildflysch and the most external part of the Prealpes Medianes, composed of tectonic imbrications and fault-related folds described notably by* MOSAR *1994) and the Western Prealpes Romandes. For each domain, a rose diagram shows the orientations of the drainage pattern with the number of data and also the maximal value expressed as percent. The principal mountain ranges are karst areas and present consequently no hydrographic network. Red rectangles indicate anomalous orientations of the drainage pattern that follows the folding structures or the fracture pattern.*

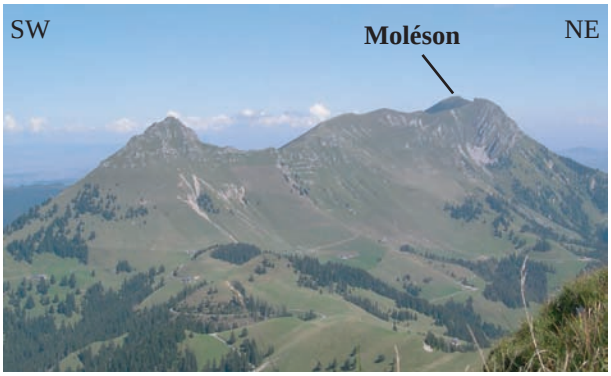

Fig. 5.13 *In the dense drainage pattern of the external unit area, the Moléson constitutes an anomalous non irrigated zone because of its poorly erodable constitutive lithology (thick limestones of the Late Jurassic).*

area is evident. The lithological heritage prevails for instance in the karst areas, recognisable by an absence of drainage, and in the external unit areas where the drainage is dense due to the presence of erodable lithologies. For its part, the structural heritage governs the development of the hydrographic network in the Western Prealpes Romandes since the rivers follow the fold and thrust system orientations. On the Plateau, the Molasse deposits modelled by the ice flow parallel to the chain control the drainage pattern. Finally, some rivers seem to follow major fracture directions instead of the local network.

In the Alps, the shape of the valleys has been deeply influenced by the action of the Quaternary glaciers, which overdeepened many of the valleys originally incised by rivers (Pfiffner et al. 1997b). On the Digital Elevation Model of the Western Prealpes Romandes (Fig. 5.14) the glacial activity is evident across the U-shaped valleys (Sarine and Jogne for instance), the glacial troughs and the cirques as Vallon des Morteys, NE of the Vanil Noir or smaller ones, SW of the summit (Fig. 5.15A and Appendix 5.V). In addition, various types of morainic deposits are observable in the field. The morphologic analysis of the area suggests that the location and orientation of the major morphologic structures and trends (hydrographic and/or glacial) are determined by the structural trends of the fracture pattern (Fig. 5.15B) and the fold/thrust system.

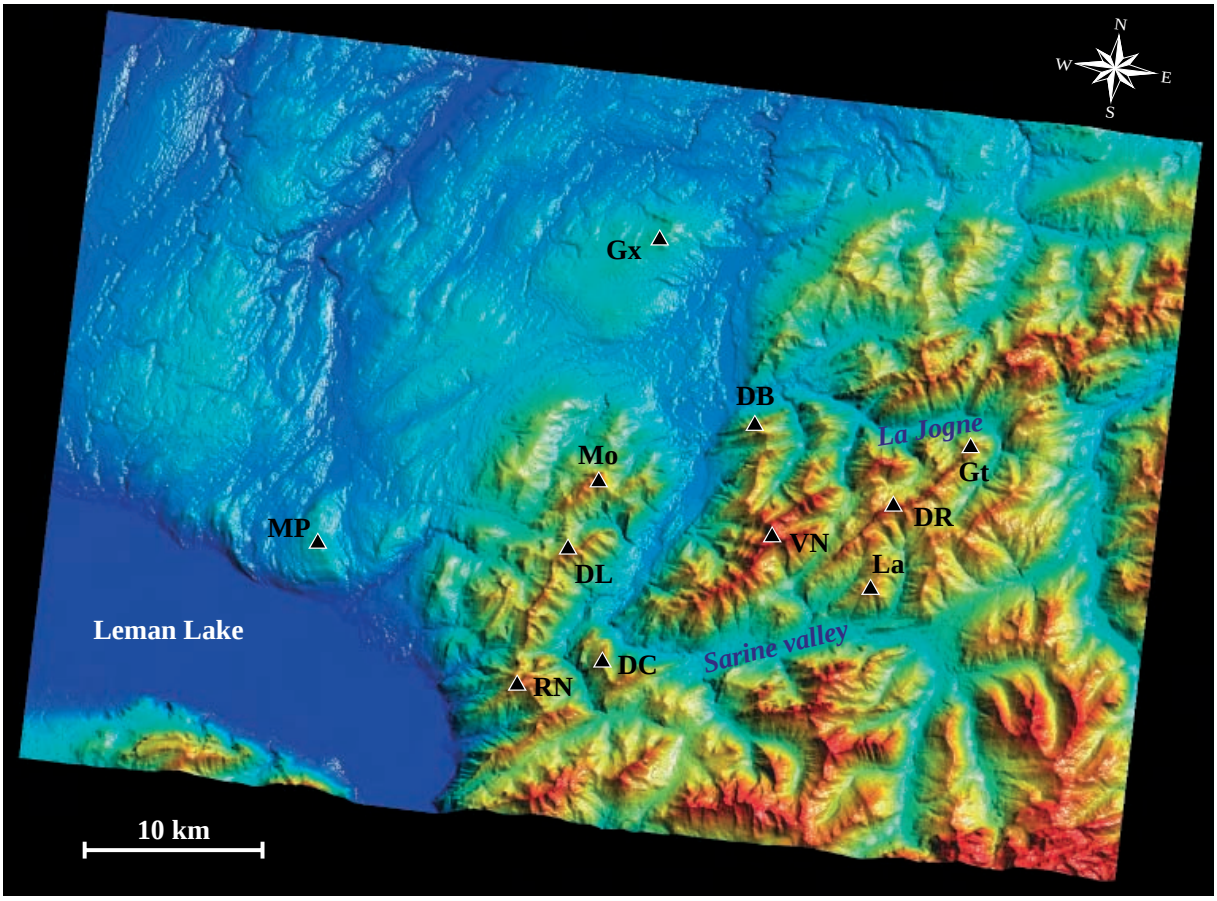

Fig. 5.14 *Digital Elevation Model of the Western Prealpes Romandes (MNT25) with principal mountain tops (DB=Dent de Broc; DC=Dent de Corjon; DL=Dent de Lys; DR=Dent de Ruth; Gx=Gibloux; Gt=Gastlosen; La=Laitemaire; Mo=Moléson; MP=Mont Pélerin; RN=Rochers de Naye; VN = Vanil Noir). The Sarine and Jogne rivers present typical morphologies of glacial valleys and the different summits are surrounded by glacial troughs and cirques.*

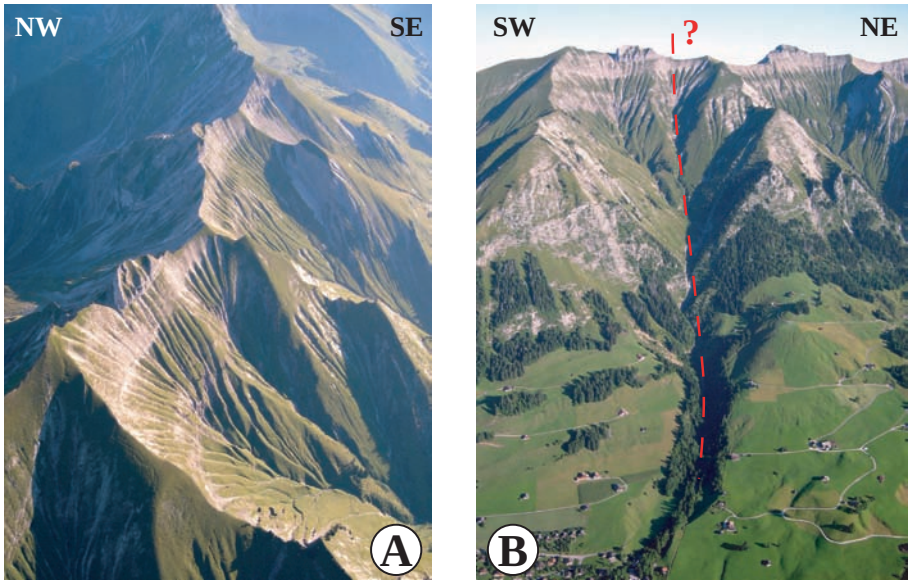

Fig. 5.15 *The two points of view of the Vanil Carré (see cross section Fig. 5.10A), located SW of the Vanil Noir illustrate A) The surrounding glacial troughs and B) The probable influence of the fracture pattern on the morphologic structures.*

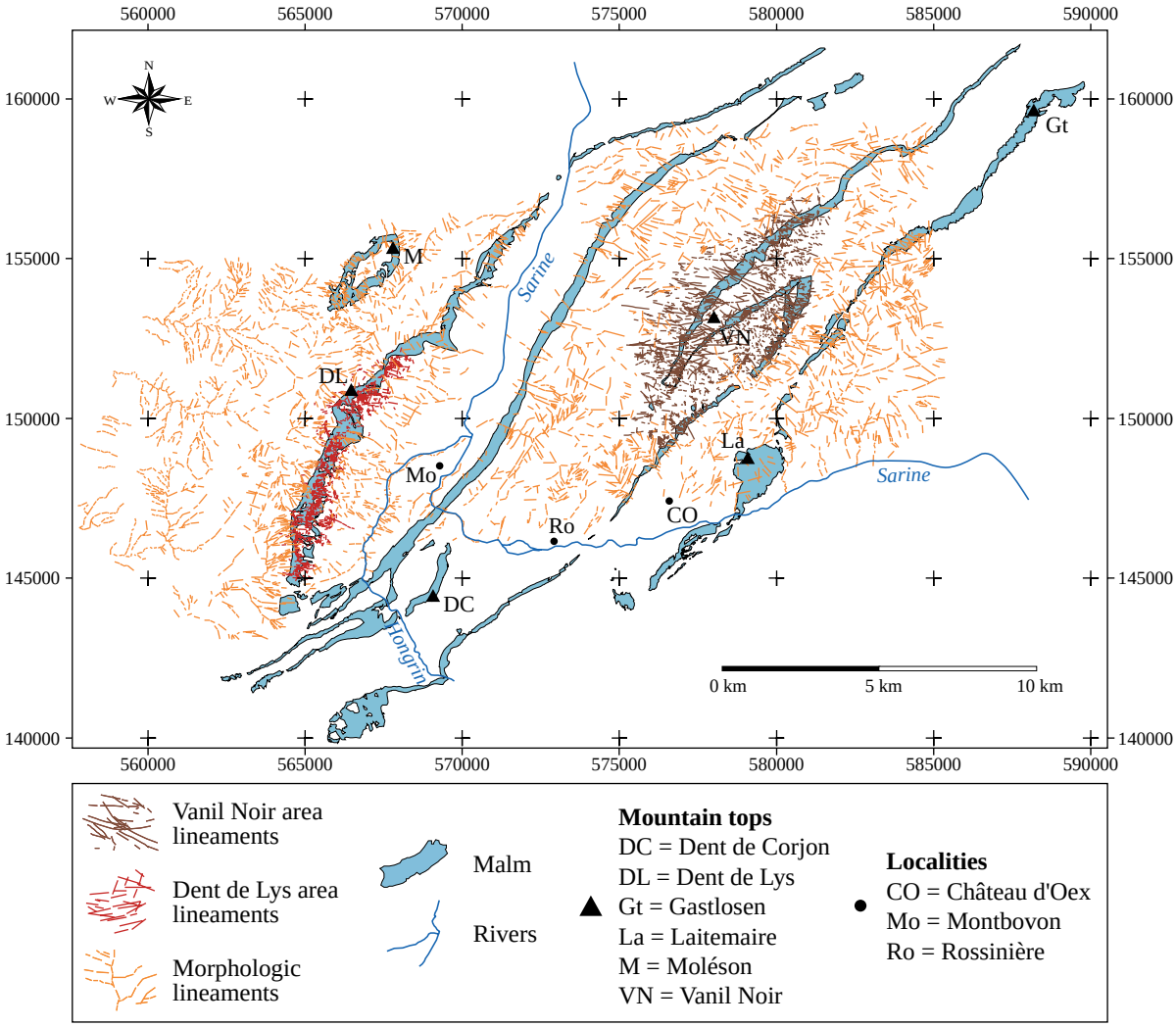

Fig. 5.16 *Map of the Western Prealpes Romandes area lineament pattern. At a local scale (kilometric), the lineaments are plotted from orthophotographs in two mountainous domains dominated by large Upper Jurassic (Malm) slabs: the Vanil Noir area and the Dent de Lys area. At a regional scale (plurikilometric), the "morphologic lineaments" are drawn from topographic maps (1:25000) in a large zone surrounding the two study areas and correspond to particularly linear parts of the drainage pattern (straight streams and valley segments). As the human presence largely disturbs tectonic and morphologic heritages, no lineament has been drawn in the valleys.*

5.3.2.2 Lineament and fracture analysis

The determination and representation of faults and lineaments in the Western Prealpes Romandes include 1568 geologic faults that have been reproduced from maps and 6989 observed and reported lineaments. The lineament and fault patterns have been analysed with the ArcView 3.2 software. The lineaments have been plotted and classified into two sets: the "morphologic lineaments" drawn at a plurikilometric scale from topographic maps (1:25000) and the lineaments plotted from orthophotographs at a more local scale (kilometric), in the Vanil Noir area and the Dent de Lys area (Fig. 5.16). The "morphologic lineaments" analysed at a bigger scale (plurikilometric) are drawn from topographic maps (1:25000), in a large zone surrounding the Dent de Lys and Vanil Noir areas. They correspond to particularly linear parts of the drainage pattern that follow straight streams and valley segments. Their establishment was facilitated by the use of a software called ERMapper that allows visualizing the topography (MNT25) with a rotating 3D-perspective. The set of analysed geologic faults essentially comes from geologic maps and is completed by observed faults in the field in the same geographical domains as for the lineaments (Fig. 5.17). Most of the time, both faults from geologic maps and linear geomorphologic features observed on the orthophotographs are identifiable and thus can be controlled in the field, as illustrated in the Dent de Lys area (Fig. 5.18A and 5.18B).

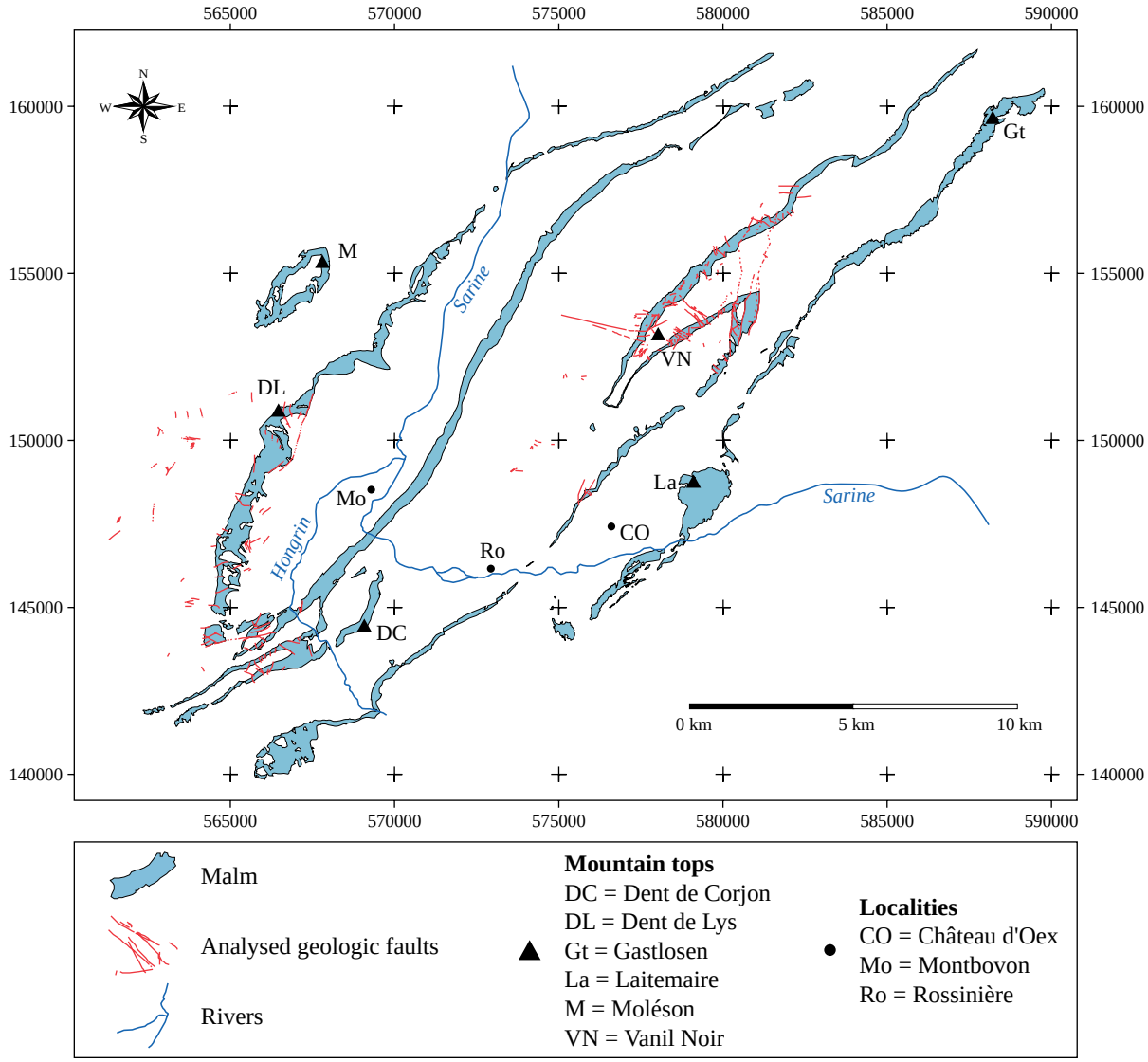

Fig. 5.17 *Map of the analysed geologic fault pattern in the Western Prealpes Romandes area. The faults are reproduced from a set of geologic maps completed by observed faults in the field, in the Vanil Noir area and in the Dent de Lys area. Thrust faults are neither indicated nor analysed because of the difficulty to measure their complex and variable orientations.*

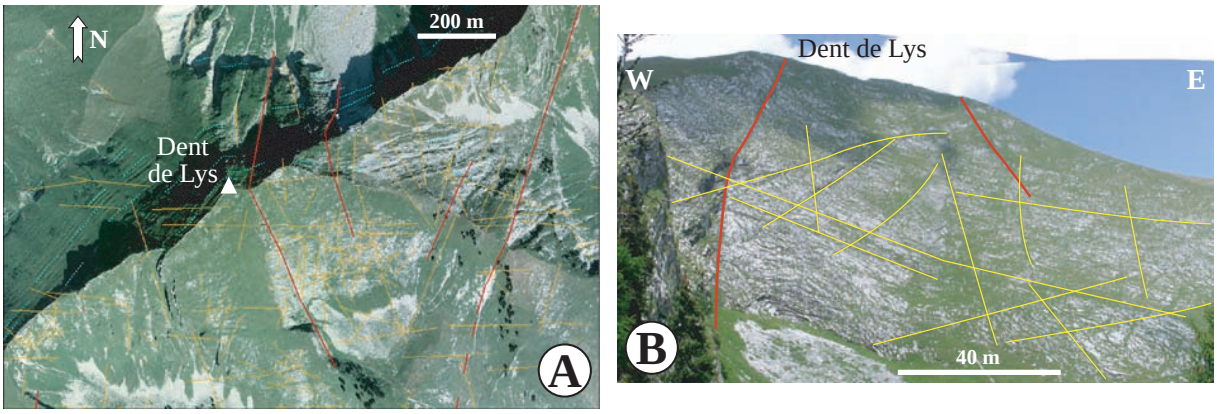

Fig. 5.18 *A) The faults (red) and the lineaments (yellow) are plotted on an orthophotograph in the Dent de Lys area and B) are recognisable in the field.*

The orientations of the faults and lineaments in the Vanil Noir and Dent de Lys areas are obtained with the "first procedure" (described in the Chapter 5.1.2.3) and are presented as rose diagrams (Fig. 5.19). We chose a bipolar and centre to centre representation to isolate at best the orientation peaks. In addition the orientation interval of 8° allows to distinguish the peaks while conserving a legible diagram. For both areas, there is a marked difference in the preferential orientation of the faults from the geologic maps (red diagrams Fig. 5.19) and the lineaments mapped from the orthophotographs (yellow diagrams Fig. 5.19). In the Vanil Noir area, the geologic faults show a dominant N-S orientation, while the lineaments show a main directional component E-W. The N-S geologic fault orientation represents the trend of strike-slip faults, easily observed in the field and consequently massively reported on the geologic maps. In the Dent de Lys area, the lineaments are also largely oriented E-W, but the two main families of faults (N020° and N070°) correspond to the joint and conjugate fault system affecting the calcareous slab. The lineaments present a statistically more robust distribution of orientations than the faults since their datasets are largely higher. The comparison between non weighed (left diagrams Fig. 5.19) and weighed (right diagrams Fig. 5.19) data shows a high similarity. The major peaks follow the same trends, but when feature length is taken into account (weighed data), peaks are better constrained. Because of the high number of lineaments in the Vanil Noir area, we did not apply the fastidious "first procedure" and the diagram remained consequently non weighed (darker rose diagram Fig. 5.19). At a more regional scale, i.e. from the Mont-Pélerin (west) to the East of the Vanil Noir (Fig. 5.19), the "morphologic lineaments" (representing mainly the drainage pattern) follow a principal orientation WNW-ESE. In the final rose diagram (blue diagram bottom right Fig. 5.19) representing the addition of all the datasets (faults+lineaments), the E-W trend dominates. As these varying added features reflect the fracturation, it appears that both in the Molasse s.l. and the Western Prealpes klippen s.l., the main orientation of fractures is almost E-W.

5.3.2.3 Comparison of methods and analyses

To validate the chosen approaches and types of analyses, the techniques used for the orientation analysis have been inter- and intra-compared (Fig. 5.20). The presented example shows the distribution of fault orientations in the Vanil Noir area, analysed by four different ways: (1) with the script L-STAT (Kim 2004) on ArcView 3.2, directly on the drawn curved faults, (2) with the same script on the faults manually cut out as segments, (3) with the non weighed measures of the cut out segment orientations reported in TectonicsFP, (4) with the same data weighed.

The script L-STAT presents the advantage to quickly and automatically analyse the orientation of curved features and provides directly weighed statistics of orientation. In addition, it avoids forgetting to report measures as with the long "first procedure" using TectonicsFP (Chapter 5.1.2.3). Indeed, in the case of the faults in the Vanil noir area, 20 measures lack since only 324 on the original 344 datasets appear on the non weighed rose diagram (central diagram Fig. 5.20). All the orientation analyses concerning the Vanil Noir and Dent de Lys areas had to be performed on linear features. We should consequently cut out manually the curves. To test the validity of this simplification, using L-STAT on ArcView 3.2, we compared on the one hand 254 geologic faults of the Vanil Noir area and on the other hand 344 segments issued from their

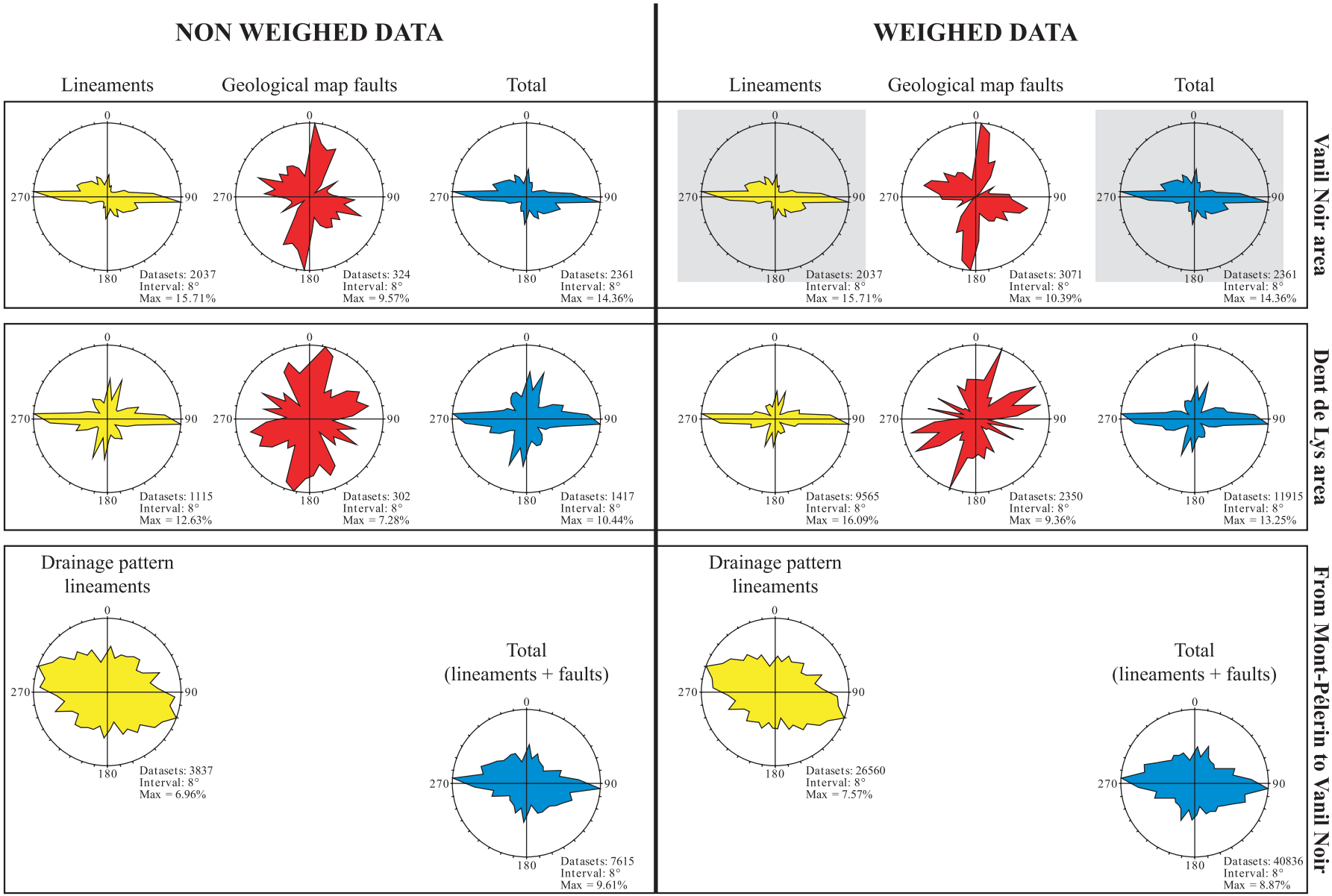
NON WEIGHED DATA
WEIGHED DATA
Lineaments
Geological map faults
Total
Lineaments
Geological map faults
Total
Vanil Noir area
Datasets: 2037
Interval: 8°
Max = 15.71%
Datasets: 324
Interval: 8°
Max = 9.57%
Datasets: 2361
Interval: 8°
Max = 14.36%
Datasets: 2037
Interval: 8°
Max = 15.71%
Datasets: 3071
Interval: 8°
Max = 10.39%
Datasets: 2361
Interval: 8°
Max = 14.36%
Dent de Lys area
Datasets: 1115
Interval: 8°
Max = 12.63%
Datasets: 302
Interval: 8°
Max = 7.28%
Datasets: 1417
Interval: 8°
Max = 10.44%
Datasets: 9565
Interval: 8°
Max = 16.09%
Datasets: 2350
Interval: 8°
Max = 9.36%
Datasets: 11915
Interval: 8°
Max = 13.25%
From Mont-Pélerin to Vanil Noir
Drainage pattern lineaments
Datasets: 3837
Interval: 8°
Max = 6.96%
Total (lineaments + faults)
Datasets: 7615
Interval: 8°
Max = 9.61%
Drainage pattern lineaments
Datasets: 26560
Interval: 8°
Max = 7.57%
Total (lineaments + faults)
Datasets: 40836
Interval: 8°
Max = 8.87%

Fig. 5.19 *Analysis of the fault and lineament orientations in the Western Prealpes Romandes. Bipolar rose diagrams with class centre representation and orientation interval of 8°. For each diagram the datasets, the interval and the maximal value expressed as percent are indicated. Diagrams are yellow for lineaments, red for faults and blue for the sum. Data are at the top for the Vanil Noir area, in the middle for the Dent de Lys area and at the bottom for the large surrounding area. Non weighed data are presented on the left and weighed diagrams on the right, but darker rose diagrams remain non weighed. The main orientation is N-S for the geologic faults, E-W for the lineaments and WNW-ESE for the "morphologic lineaments" (drainage pattern). The sum of all the datasets shows a main E-W orientation that represents the fracture trend in the Western Prealpes Romandes and adjacent Molasse Plateau.*

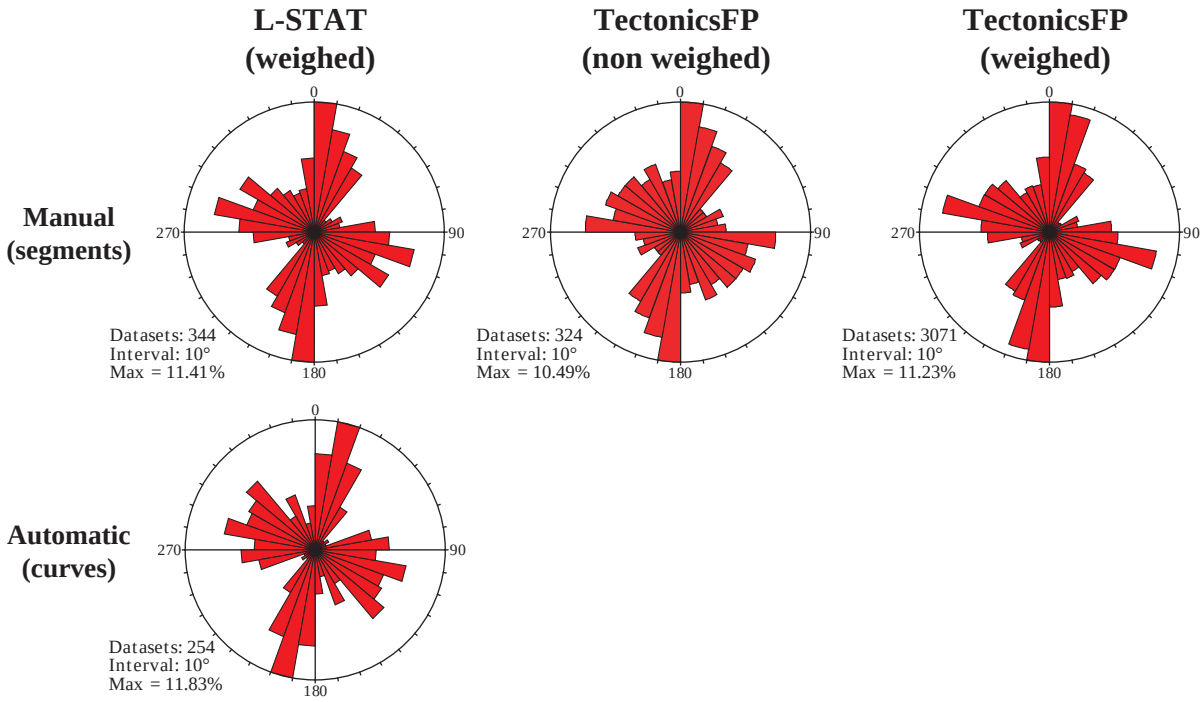

Fig. 5.20 *Inter- and intra-comparisons between two methods/analyses (TectonicsFP and L-STAT (Kim 2004) on ArcView 3.2) used on the Vanil Noir area faults. The bipolar rose diagrams present class boundaries of 10° and the datasets and maximal value expressed as percent are indicated for each diagram. The bottom diagram presents the orientations of the drawn geologic faults (curves), while the three top diagrams concern the same faults manually cut out as segments. The comparison of the two left diagrams proves that the transformation of the curved features as a succession of segments is a valid assumption. The procedure using TectonicsFP (top right diagram) and the script L-STAT (top left diagram) provide similar results but the latter is a fast automatic method. Peaks of orientation are better constrained when the data are weighed (comparison between the two top right diagrams).*

cut out (the two left diagrams Fig. 5.20). While the peaks are not exactly similar on both diagrams, they indicate the same main orientation trends: NNE-SSW and ESE-WNW. The major difference between the diagram of curve analysis (bottom diagram Fig. 5.20) and the diagrams of segment analysis (three top diagrams Fig. 5.20) is that from a N010°-N020° trend, the major peak goes to a more longitudinal orientation N000°-N010°. We consider consequently the simplification valid. The intra-comparison of the results from TectonicsFP shows that weighing provides a better definition of the peaks. The Vanil Noir example illustrates clearly this observation since on the weighed rose diagram (right diagram Fig. 5.20) a major peak appears striking N110°-N120°, while it is lost among the other peaks on the non weighed diagram (central diagram Fig. 5.20).

5.3.2.4 Stress analysis

(Jon Mosar and Cécile Bonnet)

Similarly to an investigation in the Chablais Prealpes (Chapter 5.4.2.2, and Saudan & Mosar 2006), we have carried out an analysis of paleostress based on measurements of faults and slickenlines. Similar studies (Mosar & Borel 1992) have shown that in the Prealpes Medianes, the paleostress field can be associated with local tectonic structures. Links to neo-tectonics and the present-day stress field, however, remain elusive. In order to investigate in more detail the stress field associated with the late to recent tectonics in the Western Prealpes Medianes Plastiques Romandes, we selected three areas (Fig. 5.21) with

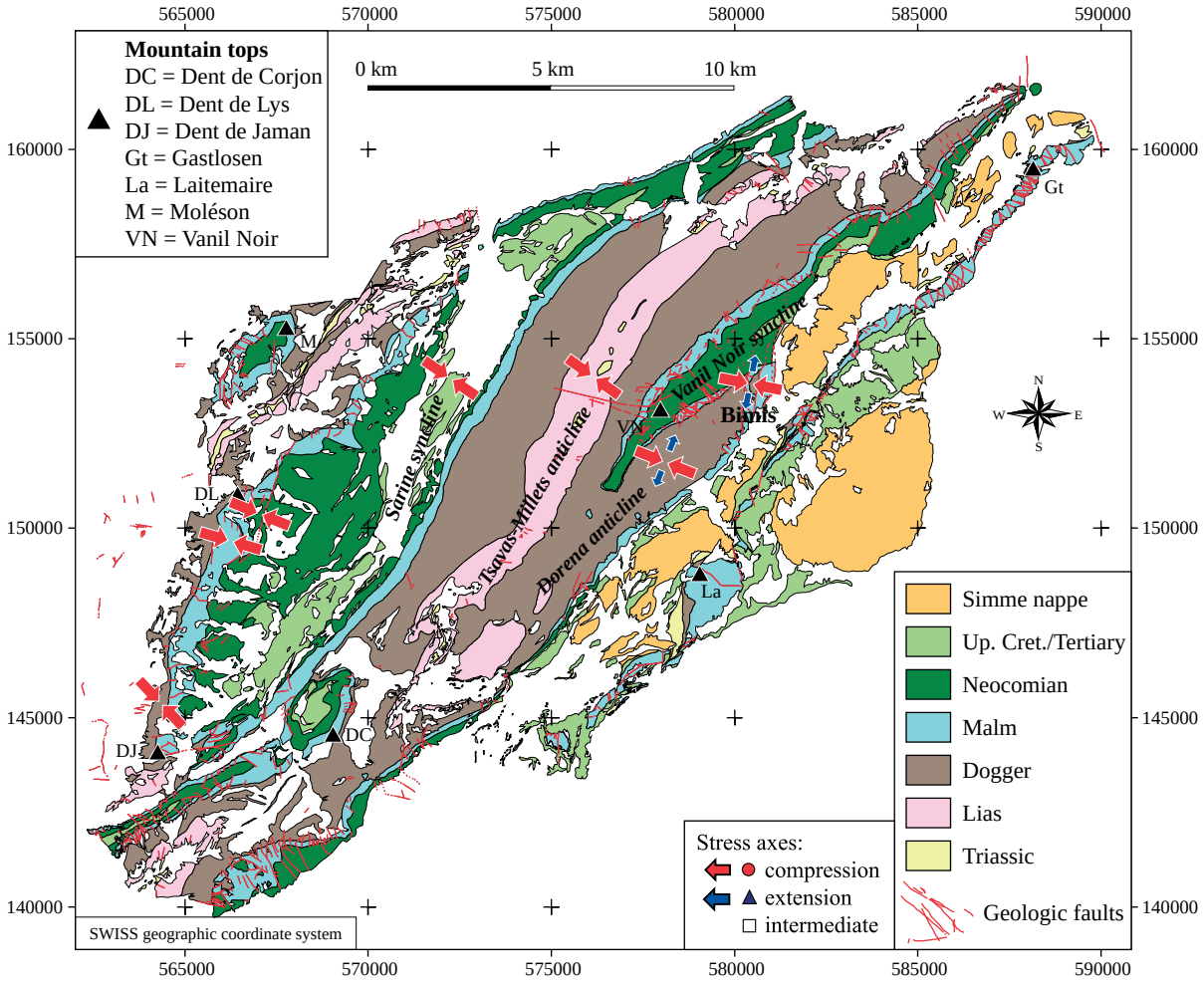

Fig. 5.21 *Geological map of the Western Prealpes Medianes in the Sarine area. Shown on the map are the main stress orientations (red arrows) from the fault kinematic analysis. A cross section through the Vanil Noir – Moléson area is shown in Fig. 5.10A.*

quite different tectonic settings (MOSAR 1994, 1997):

1) The region of the Dorena anticline, Vanil Noir syncline, and Tsavas-Millets anticline. This area of high topographic relief is formed by a succession of large fault-related folds trending NE-SW.

2) The Sarine (Intyamon) syncline. The broad valley of the Sarine forms a topographic low also reflecting a structural low formed by a large syncline with a steep eastern limb and a monoclinal western limb. The core of the structure is filled with the series of the Couches Rouges Group of Late Cretaceous to Tertiary age. These well bedded layers easily record faulting, and calcite slickenfibres are frequent.

3) The Dent de Lys - Jaman monoclinal area. This zone forms a large 45-60° east-dipping monocline which corresponds to the western limb of the Sarine syncline. The very regular bedding inclination allows us to investigate the fault pattern in relation with bedding and changing rheologies since series three different types are out-cropping: Dogger, Malm and Neocomian.

The analysis of the fault-slickenline data was performed using Tectonics FP (ORTNER 2002). Interpretation of the data is done based on the right dihedra method and distribution of the P,T axes for each dataset. The results are discussed in light of the distribution of fractures, fold geometry and orientation of vein sets.

1) The general fold axial direction in the area between the Sarine valley and the Dorena anticline is N30-40° (Fig. 5.21 and 5.22). Paleostress settings were expected to reflect folding processes or post-date them. The northern periclinal termination of the Dorena anticline is cut by a morphologically well expressed fault which shows a clear offset of the Malm cliff. This zone

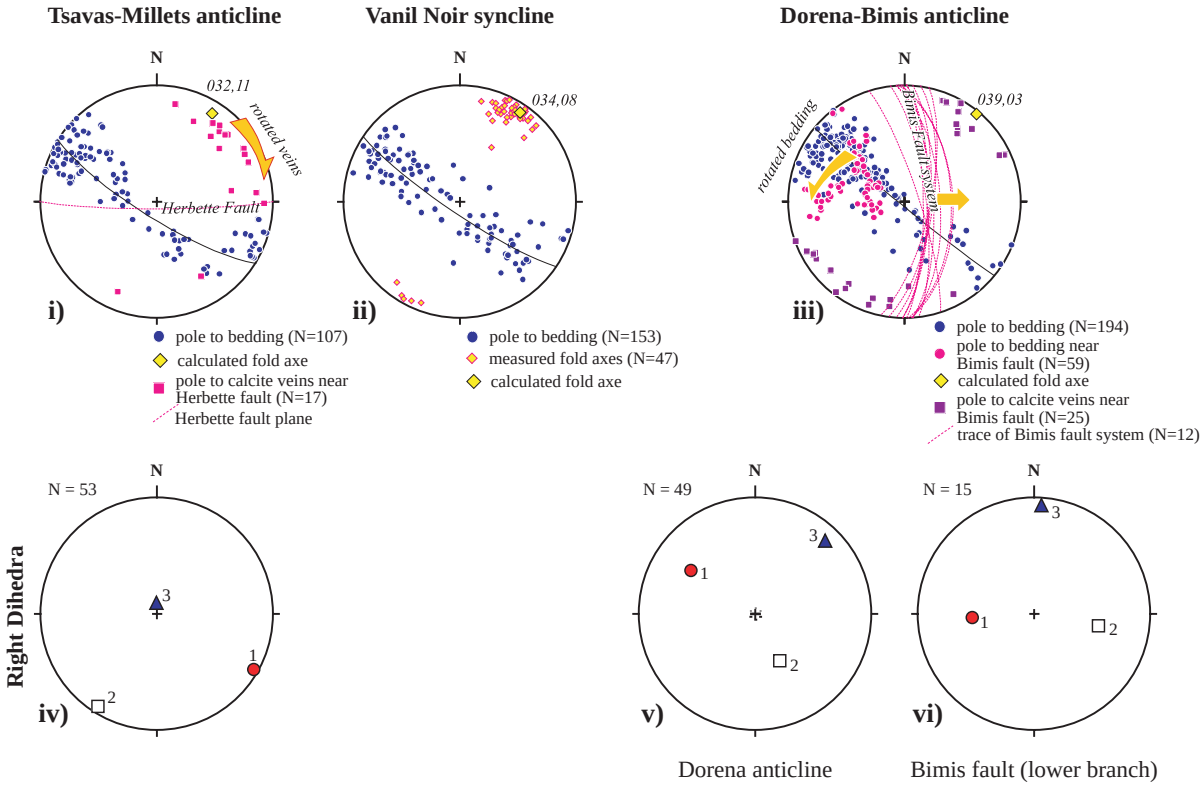

Fig. 5.22 *Stereographic projections (lower hemisphere Wulff) showing the structural elements and the results from the fault kinematic analysis in the Tsavas-Millets and Dorena area (see Fig. 5.21 for location).*

is made of a string of subvertical to steeply east-dipping faults (Fig. 5.22-iii, and Appendix 5.I - pictures E) with E compartment moving down. Rotated beds in the fault vicinity indicate an anticlockwise rotational component. The orientation of the stress axes obtained from the kinematic analysis of data in the fault vicinity shows a subhorizontal N-S extension and a 46° west dipping compression (Fig. 5.22-vi). This corroborates the dominant normal component of this fault system. Elsewhere in the anticline, the fault-striae analysis shows a NE-SW extension with compression gently dipping to the NW and which is related here to fault-related folding (Fig. 5.22-v and Fig. 5.21).

In the topographically elevated portions of the SE limb of the Tsavas anticline near the summit of Herbette, it was possible to observe an important subvertical E-W oriented fracture with vein sets (Fig. 5.22-i). Away from the fracture, the veins show extension parallel to the fold axes and are linked to the process of axial parallel stretching during folding (Appendix 5.I – pictures F). In the close vicinity and inside the fracture, these veins appear rotated clockwise hinting to a post-folding event associated with this E-W fault (Fig. 5.22-i). The stress analysis shows a NW-SE oriented compression with a vertical extension and a NE-SW oriented intermediate axis (Fig. 5.22-iv). A complementary analysis based on inversion techniques shows that extension and intermediate axis are close and may be interchangeable. The stress field is linked, here too, to folding.

2) In the central-western part of the Sarine syncline, rocks of the Late Cretaceous Couches Rouges Group are exposed (Fig. 5.21). These well layered limestones form numerous second-order folds and constitute locally two small anticlines. The general fold trend is NE-SW with a predominance of east-dipping beds. The intense fracturation and the ubiquitous calcite striation offered the possibility to explore the tectonic regime in this area and possibly discriminate between successive structural events. Some authors interpret this structure as related to an important NNE-SSW oriented left-lateral strike-slip zone (Plancherel 1979), while a more classic view links the valley and its tectonic geomorphology to a deepening of the basal décollement level and fault-related folding (Mosar 1994, 1997).

The fractures analysed are predominantly axial-parallel, oriented N20°-60° with dips between 10° and vertical (Fig. 5.23B-iv and 5.23B-v). Superposed and

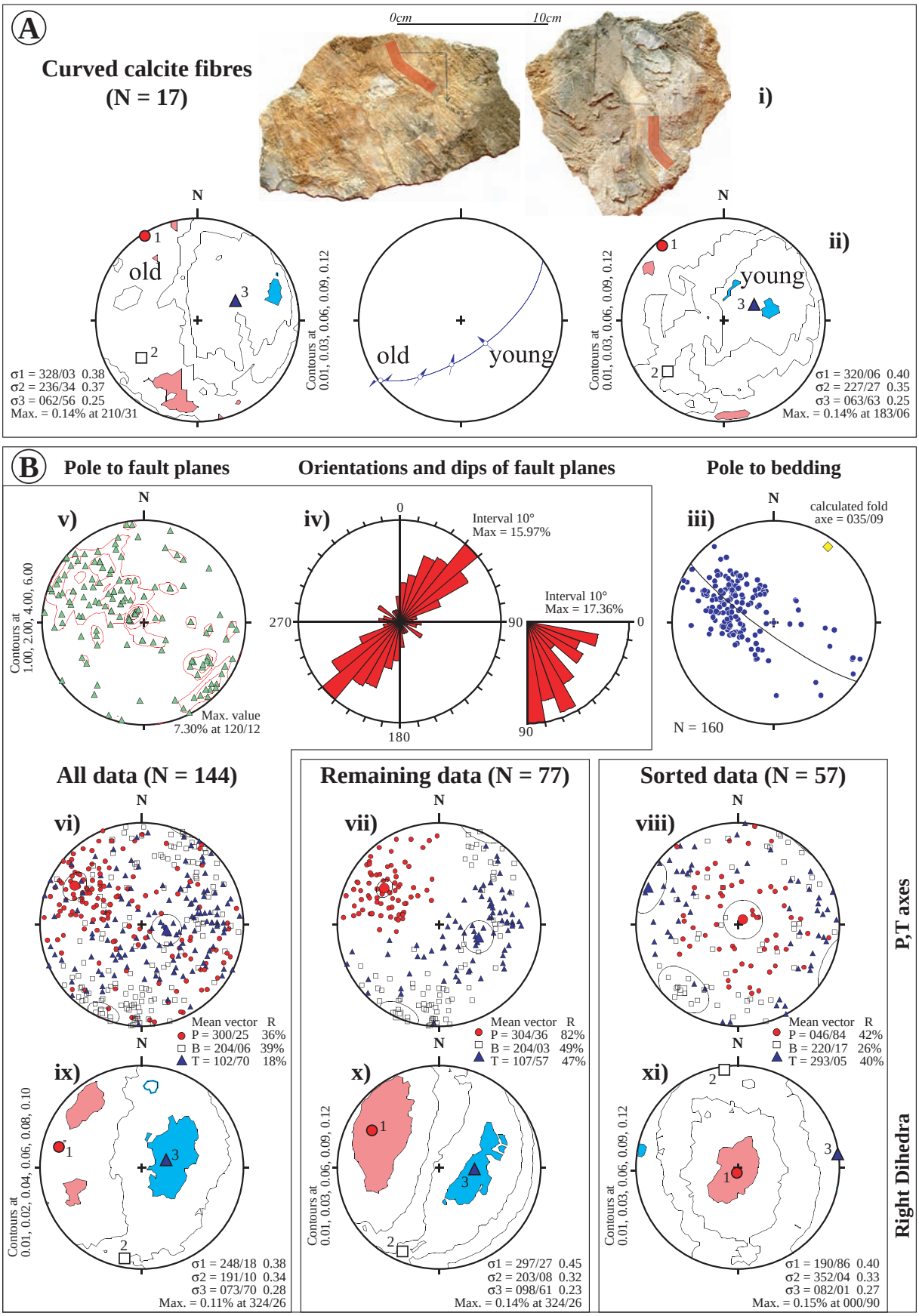
A
Curved calcite fibres
(N = 17)
0cm
10cm
i)
N
1
old
3
2
σ1 = 328/03 0.38
σ2 = 236/34 0.37
σ3 = 062/56 0.25
Max. = 0.14% at 210/31
Contours at
0.01, 0.03, 0.06, 0.09, 0.12
old
young
N
1
young
3
2
ii)
Contours at
0.01, 0.03, 0.06, 0.09, 0.12
σ1 = 320/06 0.40
σ2 = 227/27 0.35
σ3 = 063/63 0.25
Max. = 0.14% at 183/06
B
Pole to fault planes
Orientations and dips of fault planes
Pole to bedding
v)
N
Contours at
1.00, 2.00, 4.00, 6.00
Max. value
7.30% at 120/12
iv)
0
Interval 10°
Max = 15.97%
270
90
Interval 10°
Max = 17.36%
0
180
90
iii)
N
calculated fold
axe = 035/09
N = 160
All data (N = 144)
Remaining data (N = 77)
Sorted data (N = 57)
vi)
N
Mean vector R
P = 300/25 36%
B = 204/06 39%
T = 102/70 18%
vii)
N
Mean vector R
P = 304/36 82%
B = 204/03 49%
T = 107/57 47%
viii)
N
Mean vector R
P = 046/84 42%
B = 220/17 26%
T = 293/05 40%
P,T axes
ix)
N
1
3
2
Contours at
0.01, 0.02, 0.04, 0.06, 0.08, 0.10
σ1 = 248/18 0.38
σ2 = 191/10 0.34
σ3 = 073/70 0.28
Max. = 0.11% at 324/26
x)
N
1
3
2
Contours at
0.01, 0.03, 0.06, 0.09, 0.12
σ1 = 297/27 0.45
σ2 = 203/08 0.32
σ3 = 098/61 0.23
Max. = 0.14% at 324/26
xi)
N
2
3
1
Contours at
0.01, 0.03, 0.06, 0.09, 0.12
σ1 = 190/86 0.40
σ2 = 352/04 0.33
σ3 = 082/01 0.27
Max. = 0.15% at 000/90
Right Dihedra

Fig. 5.23 *A) Curved fibres (i) and stress analysis on the older and younger populations (ii). Note that the results from the analysis show a strikingly similar result despite considerable differences in orientation of striations. B) Orientation of bedding (iii), faults (iv, v) and fault kinematic analysis (vi – xi). Orientation of main stress axes from P,T analysis (vi – viii) and based on the right dihedra method (ix – xi).*

curved striation could be observed occasionally, and in one instance (quarry near Ennay) we found numerous populations of curved striae (Fig. 5.23A-i) and it was possible to make relative age attributions. In a general way the older striations are horizontal, oriented NE-SW with a left-lateral movement, whereas the younger striations are dipping to the SE and show an up-dip inverse movement (Fig. 5.23A-ii). The stress analysis shows that the older and younger striations yield the same orientation of σ_1, σ_2, and σ_3. It is thus impossible, based on stress orientation only, to discriminate between the two successive events. This is similar to findings from calcite twinning experiments that use the same methods of stress inversion/determination. Indeed, experiments with superposed stress at different orientations were analysed after deformation, and it was possible to discriminate between the original orientations only if the direction of compression differed by more than 45° and ideally were at 90° (Teufel 1980). In addition the experiments show that a high percentage of up to 45% of NEV (negative expected values – twins that do not fit the proposed strain/stress orientations) are to be expected. This was also observed in our dataset on faults in the Sarine syncline. When performing stress analyses on the bulk dataset we observe an important mix of the P and T axis (Fig. 5.23B-vi and 5.23B-ix). Some 45% of NEV (Fig. 5.23B-viii) can be sorted out. The stress analysis on the remaining data (Fig. 5.23B-vii) shows a very homogeneous pattern with a NW dipping compression, a horizontal NE-SW oriented intermediate stress axis and a SE-dipping extension. This result is very similar to the bulk data analysis (Fig. 5.23B-vi). The orientation of the stress axes is consistent with thrusting and folding. This is also consistent with the mostly SE dipping fault surface – given that the general thrust direction is to the NW (Mosar 1997). The analysis of the NEV shows a vertical compression, horizontal N-S oriented σ_2 as in the two other datasets, and a horizontal E-W directed extension (Fig. 5.23B-xi). The interpretation is more difficult, however the same orientation of the intermediate stress axes in the two datasets, leaves the possibility that σ_1 and σ_3 are close in magnitude and interchangeable. Alternatively a NW-SE oriented extensional event in this area would be undocumented to date. The analyses are corroborated by the right dihedra method on the same datasets (Fig. 5.23B-ix to xi).

3) In the Jaman – Dent de Lys area (Fig. 5.4, 5.9B, 5.18 and 5.21) the rather constant monoclinal dip (50-60° to the SE) of the large western limb of the Sarine syncline opens the prospect of fracturing related to layer parallel shortening, reflecting the initial stages of folding.

Results from all three lithologies investigated - Middle and Late Jurassic, and Early Cretaceous - show that some fractures are parallel to the fold axis, some perpendicular and that some are possibly diagonal fracture sets. The results from the fault kinematic analysis show that the intermediate σ_2 axis is parallel to the pole of bedding in each lithology (Fig. 5.24) that is perpendicular to bedding. Consequently, σ_1 and σ_3 (compression and extension) are in the bedding plane and the P,T axes are distributed on a girdle corresponding to the average pole to bedding. σ_1 is dipping to the E-SSE and σ_3 is more or less oriented NNE to ENE, but P and T axes appear to be interchangeable (Fig. 5.24). Sorting does not “improve” the results but may help discriminate between the different sets of fractures. This configuration with shortening parallel to bedding and sub-perpendicular to the regional fold axial trend, is similar to observations based on internal deformation of rocks in the Prealpes Medianes Plastiques (calcite twinning, deformed objects analysis, see Mosar 1989) which show that strain records the initial layer parallel shortening preceding folding and thrusting.

The interpretation of the results from the structural analysis shows different tectonic regimes in the investigated areas. The major results are summarized in the following:

- in the long dip slope area of the western Sarine valley, we observe the existence of faulting and fracturing associated with layer parallel shortening related to the initial stages of folding and thrusting, probably;
- stress and fault orientations in the core of the Sarine syncline and in the Tsavas and Dorena anticlines are compatible with fault-related folding;
- small components of local strike-slip movements are observable in local faults such as the Bimis fault at the NE periclinal termination of the Dorena anticline. This faulting is probably synchronous with folding or may postdate it;
- extensional veins perpendicular to fold axis indicate synfolding axial parallel extension;

- fracturing reorienting vein sets such as in the E-W Herbette strike-slip fault postdates folding.

The general pattern of stress related to the fold-and-thrust development (see also discussion in MOSAR & BOREL 1992) is the dominant regime in the Western Prealpes Medianes Plastiques. Strike-slip faulting is only a minor component of the recorded paleostress fields, especially an important strike-slip fault could not be documented in the Sarine valley, unlike structures like the Taney fault in the Chablais Prealpes, or the Weissenburgbad fault, and the fault near the Rhone valley in the Prealpes Romandes (MOSAR & BOREL 1992).

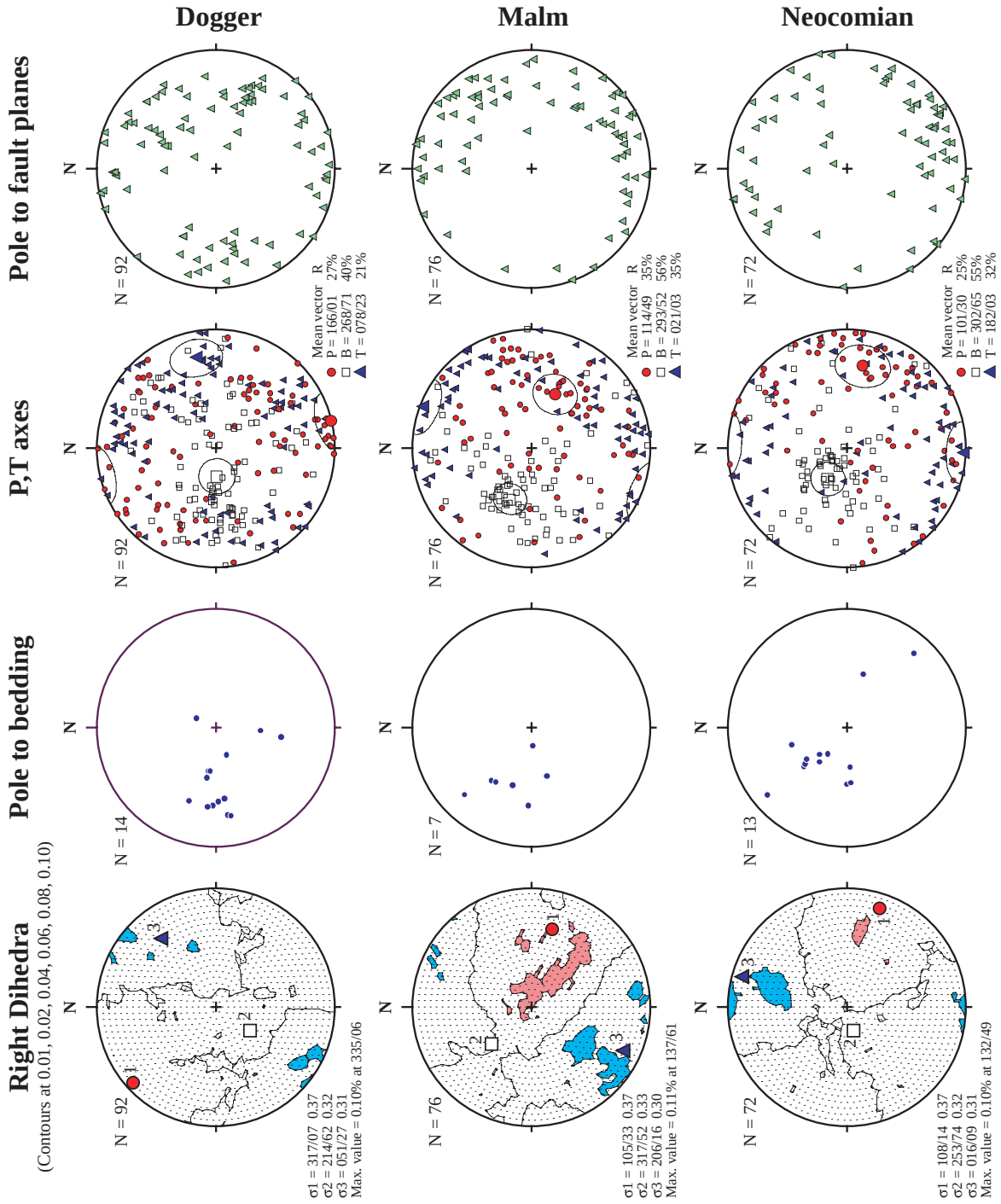

Fig. 5.24 *Paleostress analysis of monoclinal stratification in the Jaman – Dent de Lys area for three stratigraphic horizons with different lithological properties. Dip of bedding and distribution of fractures are shown as well as result of stress analysis based on the P,T and the right dihedra methods. Note that fracture sets are not only parallel to the general fold axial direction (NE-SW) but are also distributed in a way to reflect longitudinal, axial perpendicular and diagonal fault sets (see VIALON 1976).*

5.4 Chablais Prealpes

(Corinne Saudan and Cécile Bonnet)

5.4.1 Presentation of the study area

The study area is located in the Swiss part of the Chablais Prealpes Medianes (south of Leman Lake), with a little incursion in the French part (south of Memises-Novel-Mont de Chillon). The major summits of the area are the Cornettes de Bise (2432.3m), Chambairy (2206m), Grammont (2171.8m) and Blanchard (France). The fracture and lineament analyses cover a zone situated between 545'500 and 558'000 of longitude and 128'000 and 138'000 of latitude (Swiss geographic coordinate system). The stress analysis will focus on the Taney region.

5.4.1.1 Structural and tectonic features

The Chablais Prealpes, on the left bank of the Rhone, are divided into two parts. South of the village of Vionnaz, we distinguish a complex zone constituted of the Ultrahelvetics, Prealpes Medianes Rigides and Breccia nappe. In the North, are the regular folds of the Medianes Plastiques nappe (Fig. 5.25).

In the Chablais area, the Prealpes Medianes Plastiques are composed of a succession of inclined and overturned folds (Fig. 5.26). The successive anticlines and synclines are inclined to the North. Their axes plunge into the Rhone valley with mean values of 10° to 12°. A multitude of large-scale strike-slip faults cross-cut the fold axes.

The Cornettes de Bise syncline extends from the French border to the village of Vésenand. This asymmetric fold has a southern side reversed to 60° and a northern side inclined from 30° to 45°. When the syncline reaches the Taney pass, it undergoes a dextral displacement due to the prolongation of the Jumelles strike-slip fault (Badoux 1962). The Bise anticline is 1 km large with a double lobed core. The south flank is inclined at 45°, the north flank is vertical. The anticline width decreases strongly to the East. In the slope above Vésenand, the north side totally disappears and the anticline changes in a broken fold (Badoux 1962). The complex Taney syncline is constituted by two synclines put side by side east of the lake. The first one follows the axis of the Taney small valley, while the second cuts the side of the Grammont anticline. The Grammont anticline is 1 km large west of Lovenex Lake and measures 3 km along the Rhone valley. The central part of the anticline thrust the Chaumény syn-

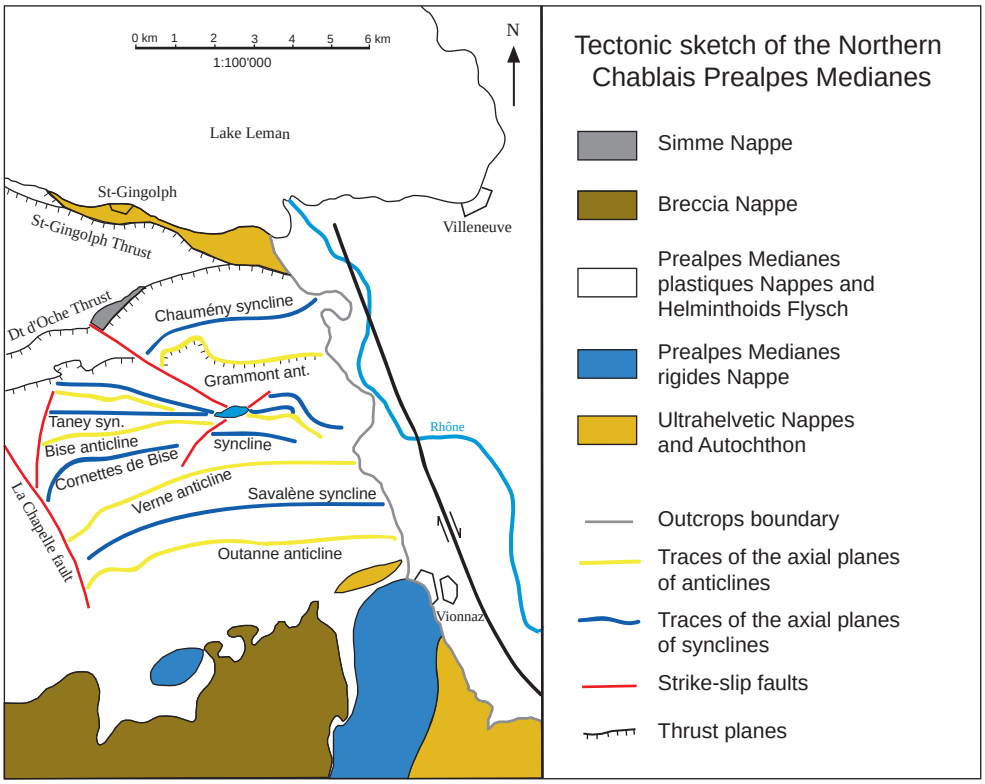

Fig. 5.25 *Tectonic sketch of the northern Chablais Prealpes Medianes with the main anticlines and synclines as well as the major thrusts (modified after Badoux & Mercanton 1962).*

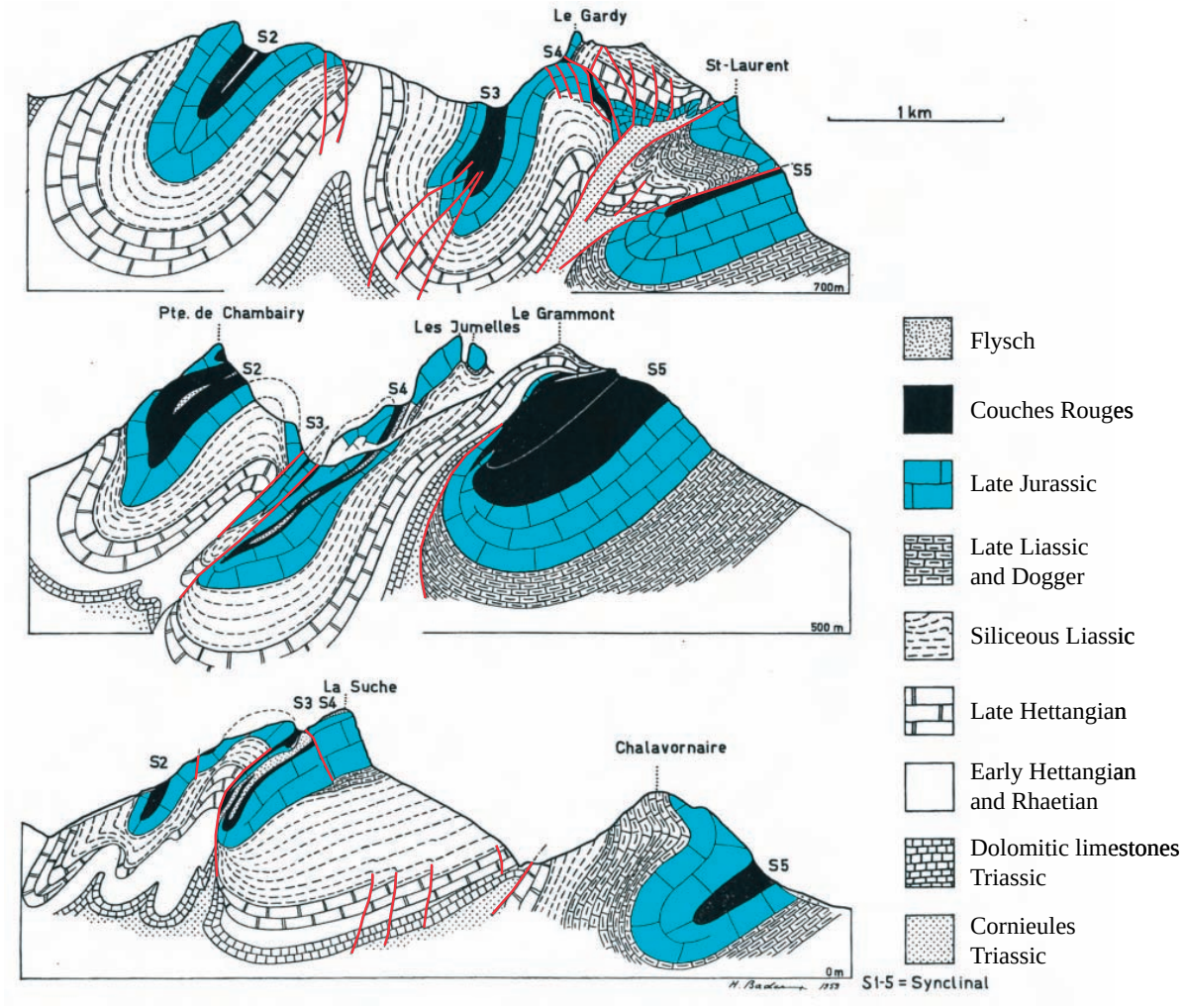

Fig. 5.26 *Cross sections of the frontal Chablais Prealpes Medianes with S2=Cornettes de Bise syncline, S3-S4=Taney complex syncline and S5=Chaumény syncline (*Badoux *1962).*

cline towards the North. Erosion is at the origin of the separation between the two summits called Jumelles.

5.4.1.2 Stratigraphy and sedimentology

The successive sedimentary deposits observed in the study area are from Late Triassic to Eocene in age. The description of the varying formations presented in ascending chronology is compiled from bibliography. For more details on the macroscopic and microscopic natures of rocks as well as their fossil content, see Favre & Schardt (1887), Jeannet (1912-1913), Peterhans (1926), Chamot (1961), Badoux & Mercanton (1962), Badoux (1965a), Baud (1972), Baud & Septfontaine (1980), Heinz (1985), Guillaume (1986), Mettraux (1989), Septfontaine (1995), Hable (1997), Borel (1998).

The "Dolomies Blondes" formation appears in the core of the Verne and Bise anticlines. It is represented by 20 to 100 cm bars of light dolomite with white patina, separated by thin marl intercalations. These rocks have a characteristic yellow-beige patina. The thickness of the formation waves between 80 and 150 m (Baud 1972). Cornieules with dolomitic fragments are often found at the base of the formation (Girod 1995) and are characteristic of the thrust planes in the Prealpes Medianes Plastiques (Baud 1972). The "Dolomies Blondes" constitute the last formation of the Late Triassic or Keuper (Norian). A progressive increase of the clay-marly layers indicates the gradual transition to the upper formation (Martini et al. 1998).

The "Plan Falcon" layers are dark marls with intercalation of bioclastic limestone banks with ochre patina, on about 20 m thick (Mettraux 1989). They are located in the Grammont anticline, at the Murailles

pass between the summits Jumelles and Grammont. The presence of the benthic foraminifera *Hoyenella inconstans* indicates an age Norian to Rhaetian. The gradual transition to the next formation is stratigraphic (Martini et al. 1998).

The "Col de Tompey" layers are constituted of beige dolomitic marls and thin sandstone bars, with a maximal thickness of 20 m. The partial or total lack of these layers is because of erosion and gap observation due to the tectonic activity (Mettraux 1989). Palynologic dating of this facies indicates a heterochronous age Late Rhaetian to Early Hettangian (Mettraux & Mohr 1989).

The "Bois de Luan" layers are light grey biomicritic limestones (wackestones) with spicules of Spongiae. Nodules of flint appear at the top of the series. A breccia forming a Neptunian ledge has been found cross-cutting the series (Girod 1995). The formation outcrops at the Murailles pass in the Grammont anticline and its total thickness varies from 200 to 250 m (Mettraux 1989). The cross section is described by Peterhans (1926). No dating criterion was made possible. The "Bois de Luan" layers belong to the Hettangian stage according to Jeannet (1912-1913) and Mettraux (1989). As the contact with the upper formation is continuous, the limit is arbitrary fixed to the appearance of the first beds rich in spongolitic nodules (Girod 1995).

The "Heiti" layers start with biomicritic limestones (wackestones) rich in spicules of Spongiae. In the upper part, the limestones contain few spicules, ossiles, Ostracods as well as a few benthic foraminifera. The banks are often separated by thin marls intercalations strongly increasing at the top of the series (Girod 1995). Important thickness variations (200 to 400 m) are observed in this unit (Mettraux 1989). The deposits outcrop on the southern flank of the Grammont anticline between Les Crosses and Alamon. In the northern flank of the Bise anticline, they appear at the base of the cliffs along the path from Taney to the Cornettes de Bise. The age of the layers is between Sinemurian and Pliensbachian (Septfontaine 1983).

The "Rossinière" formation is composed of echinodermic limestones in decimetre bars without marl intercalations. This bioclastic grainstone contains foraminifera: *Nodosaria* sp., *Planiinvoluta* sp., *Lenticulina* sp. and *Valvulina* sp. The thickness varies from 0 to 150 m (Borel 1998). This unit forms the Alamon summit. The formation has not been directly dated, but Mettraux (1989) and Borel (1998) suggest a Late Toarcian age. The upper limit is erosive and in contact with the Late Jurassic "Calcaires Massifs". In the Mont Gardy, the contact is clean and sharp, while in En l'Au, the "Rossinière" formation is progressively reduced by erosion (Borel 1998).

The base of the "Couches à Mytilus" formation is characterized by a conglomerate of one meter thick, containing siliceous elements and a few coal lenses in a sandy matrix (Girod 1995). In a typical cross section, the series continues with banks of sandy, lumachellic limestones alternating with sandy calcareous schists; blue grey limestones rich in bioclastic elements, coarse gravelly microconglomeratic limestones with flint nodules. The formation can strongly change from few meters to 130 m thick (Septfontaine 1983). Northern of the Verne anticline, the "Couches à Mytilus" formation does not exist. In the area covering the Bise and the Grammont anticlines, the Late Jurassic directly lies on the Early Jurassic (Badoux 1962). The age stretches from Early Bajocian to Callovian (Septfontaine 1983).

The "Calcaires Massif" Unit (Malm) is composed of thick calcareous bars forming most of the crests and cliffs in the Prealpes Medianes. It is constituted of light grey micritic limestones (mudstones) containing at the top a lot of biogenic elements: Calpionellidae, algal spores, corals fragments, Echinoderm plates, Bivalvia shells and small Ammonites (Girod 1995). The thickness is constant in the Bise and Grammont anticlines from 100 to 160 m with a mean value of 125 m (Badoux 1962). In the study area, this lithology represents the biggest surface. The Mont Gardy and both Jumelles are constituted of "Calcaires Massifs". The Upper Malm groups the Oxfordian stage to the Tithonian (Heinz & Isenschmid 1988).

The "Calcaires Plaquetés" formation is composed of quite soft grey whitish micritic limestones with flint concretions. The banks are not very thick (more or less 10 cm) and separated by slaty limestone intercalations. The total thickness is hard to determine because this lithology is often folded, especially its upper part but it is estimated to 100 m (Spicher 1966, Hable 1997). The transgression of the "Couches Rouges" is partially responsible for the disappearance of the formation to the South (Badoux & Mercanton 1962). The "Calcaires Plaquetés" formation is from Early Berriasian to Barremian in age (Hable 1997).

The "Couches Rouges" Group is characterized by

clayey platy limestones and marls. The planktonic fauna is abundant (*Globogerinidae*, *Globorotalidae*, *Heterohelicidae*) as well as the Radiolaria (BADOUX & MERCANTON 1962). The determination of Foraminifera allows to subdivide the unit: Rote Platte fm. (end of Middle Turonian-beginning of Late Turonian), Forclettes fm. (Late Maastrichtian) and Chenaux Rouges fm. (Ypresian-Lutetian) (GUILLAUME 1986, GIROD 1995). These units can be found in the Taney syncline and on the Flon-Taney pass track.

The "Prealpes Medianes Flysch" is composed of red to green argillites and a few sandy bars of 20 to 100 cm thick, with cross-bedding sedimentary structures. While the total thickness is hard to estimate, the minimal thickness seems to be around 7-8 m (GIROD 1995). This lithology appears in the core of the synclines under the Chambairy summit. The microfauna being reworked, no dating is possible. According to GUILLAUME (1986), the "Prealpes Medianes Flysch" is of Middle Eocene.

5.4.2 Results of the feature analyses

5.4.2.1 Lineament and fracture analysis

In the Taney area, the results of the analysis of faults (taken from existing geological maps), lineaments and fault planes measured in the field are represented together with the sampling localities for fault/striae analysis (Fig. 5.27). Faults indicated on the geological maps generally show the regional offsets of the major cliffs constituted predominantly by the "Calcaires Massifs" Fm. of Late Jurassic. Resistant to alteration, they form the structural morphology of the area, constituted by a succession of anticlines and synclines. Many lineaments correlate well with fractures observed in the field.

From a total of 737 faults, 4 families can be discriminated in the directional analysis (Fig. 5.27A). The main orientations are: (1) NE-SW (from N030° to N040°), (2) NW-SE stands out from a group of faults (from N140° to N150°), (3) ENE-WSW (from N050° to N060°) and possibly a last fourth set with a broader distribution around NNE-SSW (from N000° to N030°).

From a total of 1946 lineaments, 3 families can be highlighted in the rose diagram (Fig. 5.27B). The main peak shows the orientation (1) NNE-SSW (from N020° to N030°). A second direction (2), composed of a somewhat broader peak, stands out in a general way NW-SE (from N120° to N140°) and the last main orientation is (3) ENE-WSW.

The added values of the faults from geological maps and the lineaments are represented in the diagram (Fig. 5.27C). Again, three main families appear. The major direction (1) NNE-SSW is composed of two peaks of orientation from N020° to N040°. The second direction (2) has a NW-SE general tendency and the last orientation (3) is ENE-WSW (from N060° to N070°).

The orientation of measured fault planes bearing striae shows a somewhat different pattern (Fig. 5.27D). From a total of 133 values, four families can be highlighted. The most important peak (3) points out an ENE-WSW direction (from N060° to N070°). A peak (1) NE-SW (from N030° to N040°) is also present. A family containing two peaks of the same intensity (from N110° to N130°) constitutes the direction (2) WNW-ESE. Finally the direction (4) NNW-SSE is symbolised by a group of three little peaks (from N150° to N180°).

5.4.2.2 Stress analysis

In the Flon-Taney-Tombeau des Allemands area, the stress analysis is based on 133 measures of fault planes on which offsets have been determined. Four fami-

Fig. 5.27 *Map of the study area showing the faults (red) taken from existing geological maps and the lineaments (light brown) seen on orthophotographs. The faults generally show the regional offsets of the major cliffs constituted predominantly by the Late Jurassic limestone formation. Resistant to alteration, the Malm lithology shows the structural morphology of the area, and highlights the fold-and-thrust structure. The inbox represents the sampling localities where the measurement of fault planes with striae was done. The results of the fracturation analysis are shown in four rose diagrams of orientation below the map. The rose diagrams are in class boundaries with an azimuth interval of 10°. N is the total number of datasets and Max represents the maximum counting value. A) Rose diagram showing the orientation of faults from geological maps. The main orientations are (1) NE-SW, (2) NW-SE, (3) ENE-WSW and (4) NNE-SSW. B) Rose diagram showing the orientation of lineaments. The main orientations are (1) NNE-SSW, (2) NW-SE and (3) ENE-WSW. C) Rose diagram showing the orientation of both faults from geological maps and the lineaments. The main orientations are (1) NNE-SSW, (2) NW-SE and (3) ENE-WSW. D) Rose diagram showing the orientation of fault planes bearing striae. The main orientations are (1) NE-SW, (2) WNW-ESE, (3) ENE-WSW and (4) NNW-SSE.*

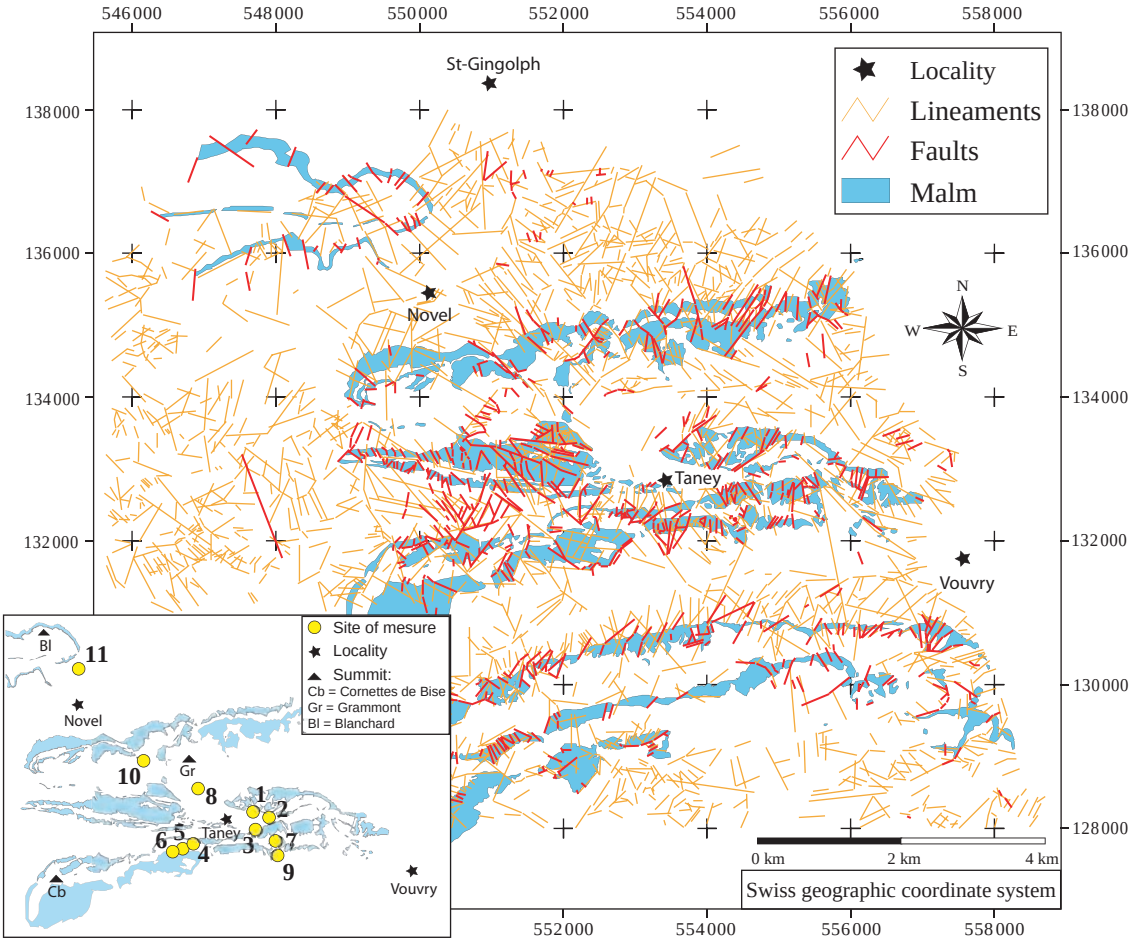
546000
548000
550000
552000
554000
556000
558000
138000
136000
134000
132000
130000
128000
St-Gingolph
Novel
Taney
Vouvry
Locality
Lineaments
Faults
Malm
N
W
E
S
0 km
2 km
4 km
Swiss geographic coordinate system
Site of mesure
Locality
Summit:
Cb = Cornettes de Bise
Gr = Grammont
Bl = Blanchard
Bl
11
Novel
10
Gr
8
1
2
Taney
6
5
4
3
7
9
Cb
Vouvry

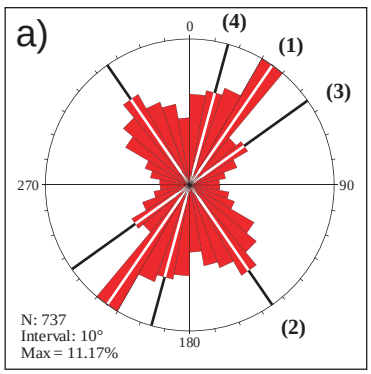
a)
(4)
(1)
(3)
(2)
0
90
180
270
N: 737
Interval: 10°
Max = 11.17%

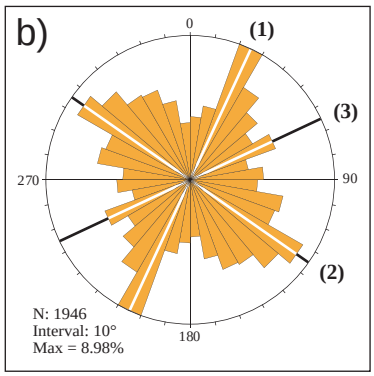
b)
(1)
(3)
(2)
0
90
180
270
N: 1946
Interval: 10°
Max = 8.98%

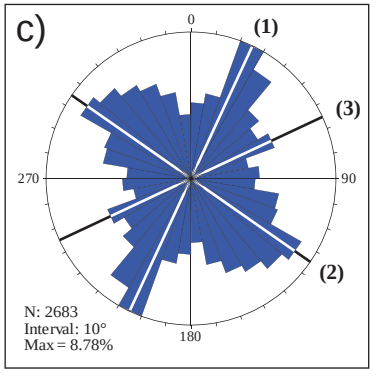
c)
(1)
(3)
(2)
0
90
180
270
N: 2683
Interval: 10°
Max = 8.78%

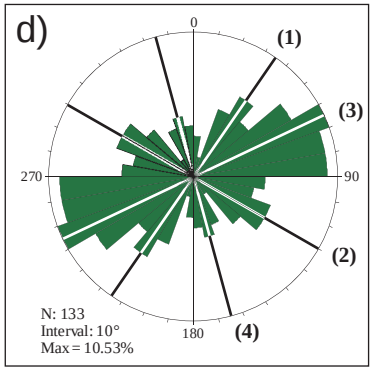
d)
(1)
(3)
(2)
(4)
0
90
180
270
N: 133
Interval: 10°
Max = 10.53%

lies of faults are distinguishable on the rose diagram of orientations (Fig. 5.28A). The four main families are: NE-SW, WNW-ESE, ENE-WSW and NNW-SSE. The faults are subvertical and the striation subhorizontal (Fig. 5.28B). The maximal dip of the fault planes reaches 85° and the plunge of the lineation correspond to a maximum of 20°. This suggests a transcurrent tectonic setting with a dominant strike-slip component. From the 133 slickenfibre lineations collected in the area, a stress analysis was done using the right dihedra method. This analysis shows a N-S oriented compression around a subvertical strike-slip system (Fig. 5.28C). This confirms that the main strike-slip fault plane corresponds to the NW-SE oriented principal plane. This NW-SE oriented major fault plane can be correlated to the Flon-Taney-Tombeau des Allemands fault (Appendix 5.VI). The sense of slip along this fault is dextral, as suggested also by field evidence of fold/fault offsets. The fluctuation histogram shows the good quality of the tensor, since from a maximum of 22% the error has a general decreasing trend and reaches a very weak rate at 90° (Fig. 5.28D). Thus the dataset is homogeneous and suggests that the analysed fault sets pertain to the same tectonic event.

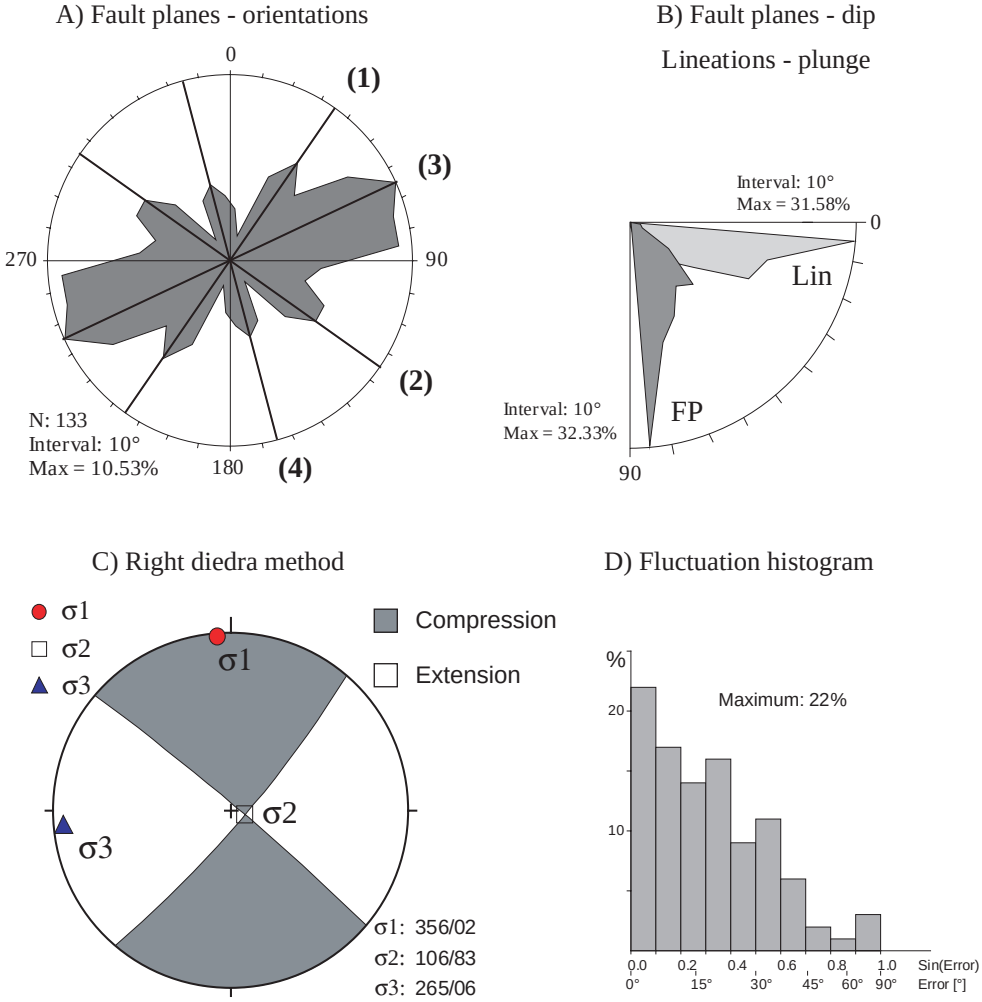

Fig. 5.28 *Kinematic analysis of fault planes measured in the Flon-Taney-Tombeau des Allemands area. A) Four families of orientation are noticeable on the rose diagram of orientation. N is the total number of datasets. Max is the maximum counting value, related to the total number of values. B) The analysis shows that the faults are subvertical and the striations subhorizontal. The maximum dip of the fault planes reaches 85° and the maximum plunge of the lineations is 20°. This suggests a transcurrent tectonic setting with a dominant strike-slip component. C) The right dihedra method shows a N-S oriented compression around a subvertical strike-slip system with a dextral movement. The main strike-slip fault plane corresponds to the NW-SE oriented principal plane. The dihedra is calculated in the lower hemisphere with an equal-area projection (Lambert-projection).* σ_1, σ_2 *and* σ_3 *represent the principal stress axes with their respective azimuth/plunge value. D) In the fluctuation histogram, the angular deviation of the calculated maximum shear stress in the fault plane from the measured striae is plotted in a histogram. The maximum of the deviation in the far left and a steep slope towards the right of the graph indicate a homogeneous dataset. The dataset of the Flon-Taney-Tombeau des Allemands area shows that the quality of the tensors is acceptable, since from a maximum of 20% the error is always decreasing. It also suggests that the collected fault planes belong to the same tectonic event.*

5.5 Interpretation in terms of deformation model

5.5.1 Theoretical models

In laboratory experiments with rocks and model materials, it is found that a conjugate fracture system develops by a three-step sequential movement along the fault planes (Fig. 5.29) (Ramsay 1987). It is nevertheless evident that, for mechanical reasons, pre-existing planar weak zones oriented in the correct position are more likely reactivated than new developing faults might be formed. In such a sequential fault activity, large overall displacements may be developed without any tendency for the fault blocks to separate and open up (Ramsay 1987). The grey zone (Fig. 5.29) that corresponds to the half of the original area is actually not really deformed but rather complexly fractured and cut in a great number of pieces. Fracture mechanics (Coulomb and Byerlee laws) govern the precise orientation of faults with respect to the stress axes.

A classic model used to simulate the formation and development of shear zone structures is the Riedel experiment (Fig. 5.30A). Both clay (Riedel 1929, Tchalenko 1970, Wilcox 1973) and sand models (Naylor 1986) have been used in now classic experiments. While clay models are more applicable for the ductile lower crust, sand models are more appropriate to faulting in sedimentary rocks of the brittle upper crust. Naylor (1986) described the sandbox used for modelling as a table divided into two halves; one half

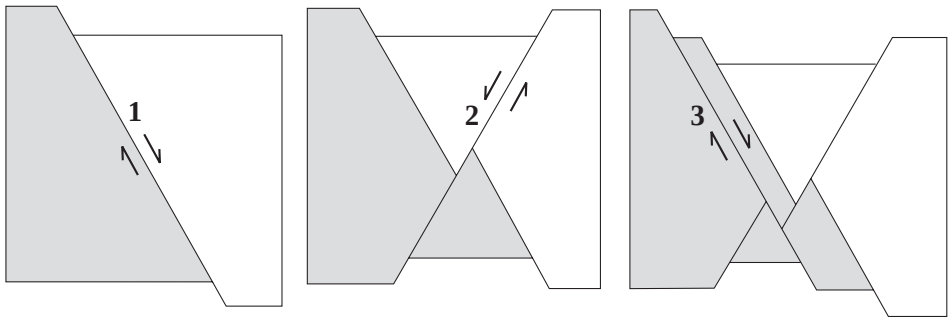

Fig. 5.29 *Individual inclined fault planes show a three-step sequential development in conjugate fault systems (modified after Ramsay 1987). The movement of the active normal fault is indicated by arrows. When fault 1 becomes stabilized, conjugate fault 2 truncates it. Fault 2 then becomes inactive and fault 3, parallel to fault 1, displaces the earlier fault plane.*

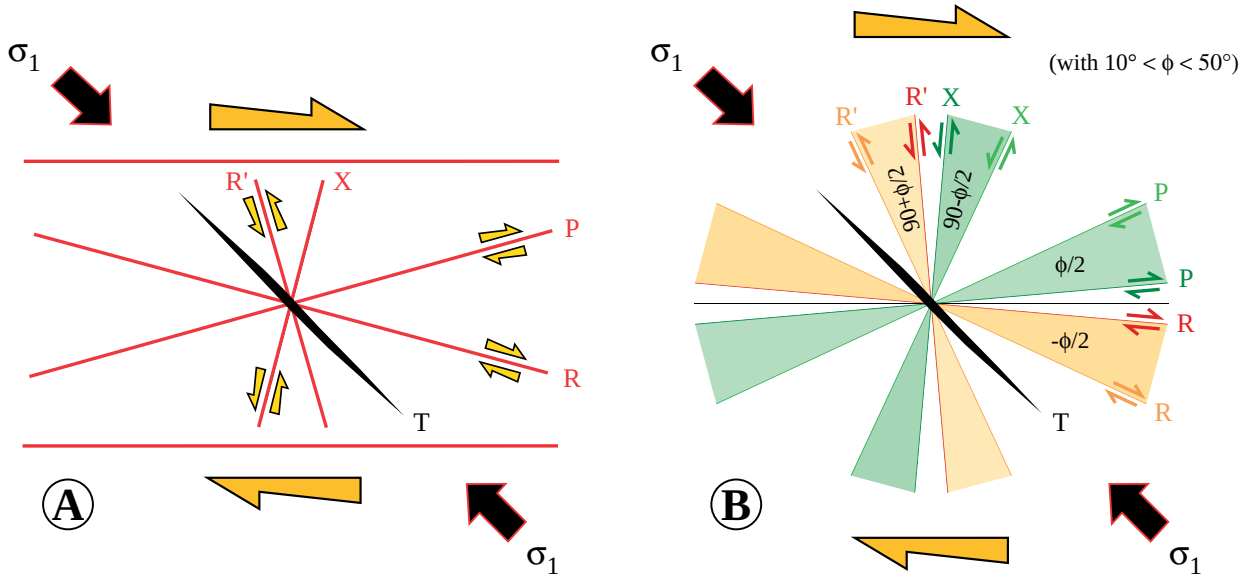

Fig. 5.30 *A) Dextral Riedel shear system with orientation of major fault subsets, stress orientation and veins (modified after Nicolas 1984). Chronology generally observed is growth of tension gashes T, propagation of 2nd order faults R and R' and then of P and X, respectively symmetrics of R and R' and B) Range of possible orientations of fault subsets according to endmember coefficients of friction (Φ).*

of the table can be displaced laterally past the other by a motor drive, imitating movement on a single basement wrench fault. The characteristic en echelon shears (parallel to one another and arranged along a common line of bearing) formed at an angle to the board's interface during the early stages of the deformation were first investigated in detail notably by RIEDEL (1929). The synthetic strike-slip faults are Riedel shears (R; Fig. 5.30A), and they are typically oriented at a small, acute angle to the trace of the main fault zone. The antithetic strike-slip faults are conjugate Riedel shears (R'; Fig. 5.30A), and they are oriented at a very high angle to the main zone (WILCOX 1973). The direction of the greatest principal stress (σ_1) bisects the angle between R and R' (DAVIS 1996).

Riedel shears (R) form during early stages in experimental models and conjugate Riedel shears (R') do not develop systematically (RINGENBACH 1992). Both structures appear oriented respectively at $\Phi/2$ and $-\Phi/2$ to the general direction of movement, according to the Coulomb-Mohr slip concept (JAEGER 1976), with Φ the angle of internal friction (TCHALENKO 1970, NAYLOR 1986). As a result of varying Φ (10-50°), the orientation of R to the imposed dextral shear direction varies between -5° and -25° and the orientation of R' between 95° and 115° (Fig. 5.30B). Common values, as for instance observed in sand, are -15° and 105°. Tension gashes T are approximately oriented at -45° to the principal displacement zone/fault (NICOLAS 1984).

R' shears are almost perpendicular to the general direction of movement and are subjected to distortion and rotation that make them "regress" (Fig. 5.31A) (MERCIER 1992). If they cannot accommodate the whole displacement, P shears are occasionally formed to connect the discontinuous Riedel shears (Fig. 5.31B). They have the same sense of shear displacement as the Riedel shears R but cross the principal displacement zone/fault in the opposite direction, ideally at 15° to the basement fault in a dextral Riedel shear system (Fig. 5.30A) (NAYLOR 1986). The orientation of P shears at $-\Phi/2$ to the principal displacement zone/fault is explained by deviation of the stress field among the en echelon Riedel shear. P shears are the second order faults symmetric of R and their conjugated X shears are symmetric of R' (NICOLAS 1984). The final fault pattern is thus an anastomosing zone of faults defining shear lenses. The displacement may be concentrated on a central, throughgoing fault (NAYLOR 1986).

The different fractures are not active simultaneously. When external conditions allow dilatation of the fault zone, the P, X, T system is preferentially activated. When there is no dilatation because faults are deep and dry or because fault planes are orientated at a high angle to σ_1, the R, R' system dominates (NICOLAS 1984).

Each elementary shear (R, R', P and X) may itself represent a principal displacement zone/fault within which one can find smaller subsets of faults organised in the same Riedel pattern. Such subsystems define different orders of faults organised in a complex pattern

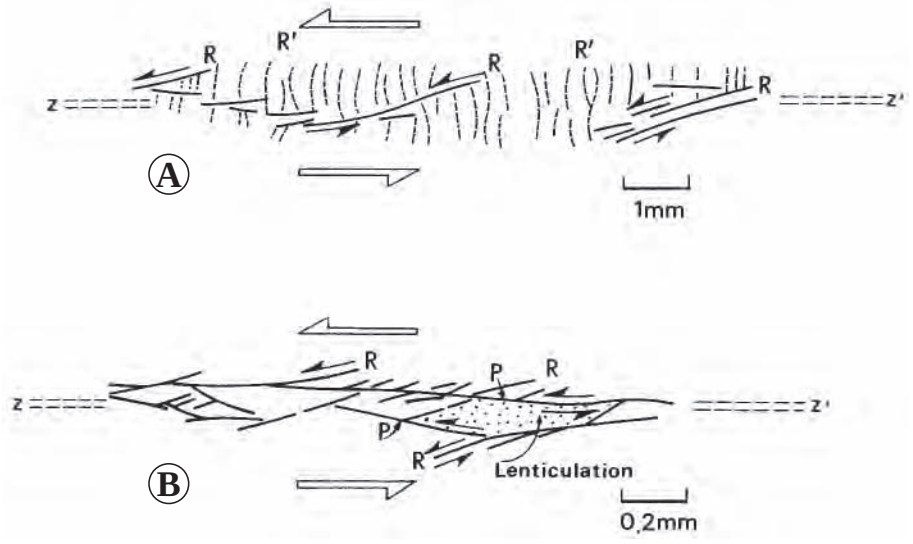

Fig. 5.31 *Evolution of Riedel shears (modified after TCHALENKO 1970, MERCIER 1992). A) R' shears are subjected to distortion and rotation that make them "regress" and B) Due to the deviation of the stress field among the en echelon Riedel shear, R' shears cannot accommodate the whole displacement and P shears may form to connect the discontinuous Riedel shears. They have the same sense of shear displacement as the Riedel shears R but cross the principal displacement zone/fault in the opposite direction.*

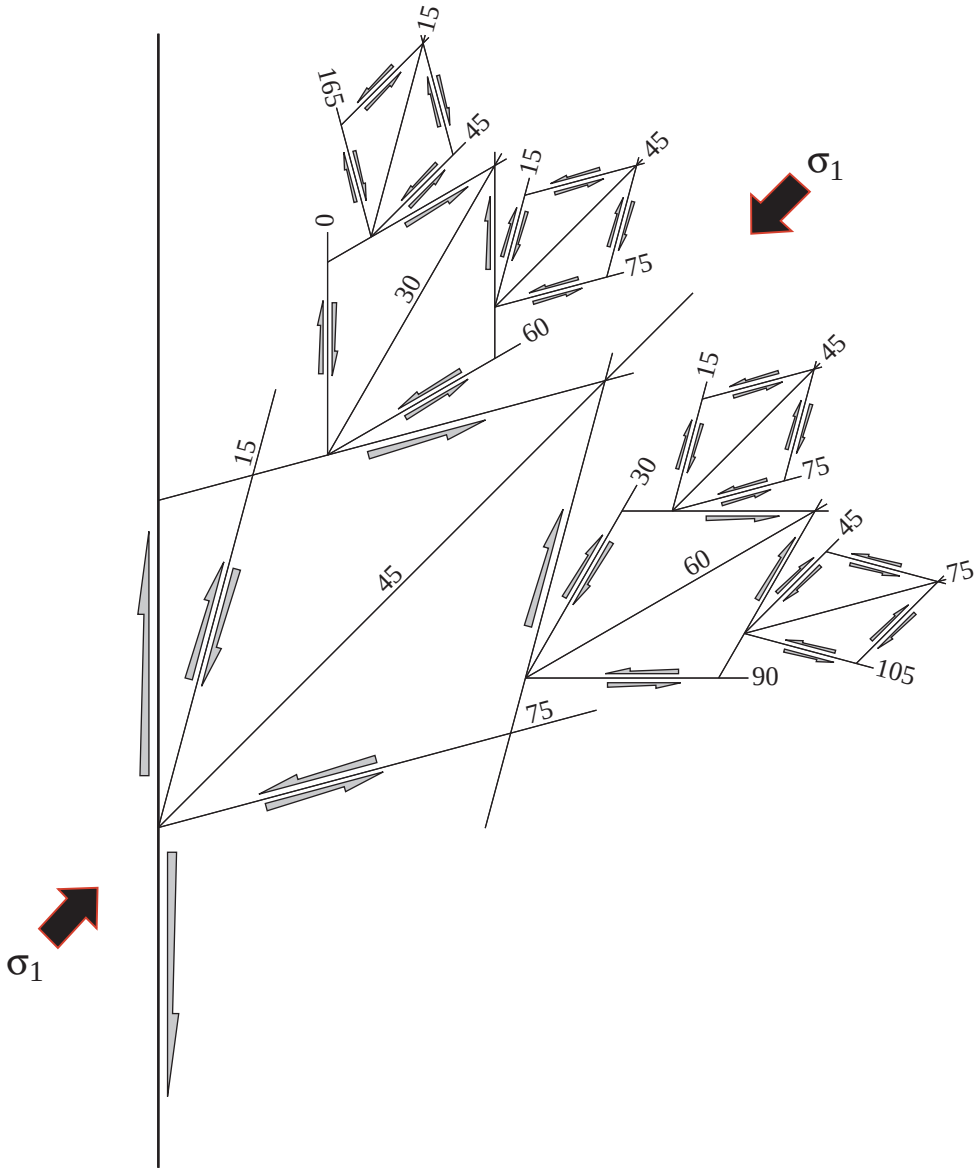

Fig. 5.32 *Four successive orders of shear zones linked to a N-S dextral strike-slip considered as first order (modified after* VIALON *1976). The general direction of movement is NE-SW (σ_1) and the angular relations between R, R' and T shears are indicated for each order.*

(Fig. 5.32) (VIALON 1976). Conversely careful analyses of such complex systems will also make it possible to determine higher order regional principal displacement zones/faults. Thus smaller Riedel systems may cluster in more or less broad corridors. They present a general direction and a general sense of displacement, but strike-slip faults may also be associated as conjugated networks (VIALON 1976).

A transcurrent fault is a major wrench fault, or strike-slip fault, i.e. a major fault with strike-slip component and subvertical orientation (SYLVESTER 1988, PRICE & COSGROVE 1990). The more general term of transcurrent fault is used in a descriptive way. Although many of the experiments on Riedel faults show that the fault pattern develops above a "basement" fault, our use of the terms Riedel shear zone or transcurrent fault is not restrictive in the sense that a basement fault must be involved. Riedel structures of different scales form together a transcurrent system. In a transcurrent shear zone, the particular structures that develop (Fig. 5.33) depend on the rheology of the sheared rocks and the presence of pre-existing mechanical heterogeneities. The orientation of the structures presented here is the one the structures acquired during the first increment of deformation. During shearing, the structures progressively rotate (REY 2003).

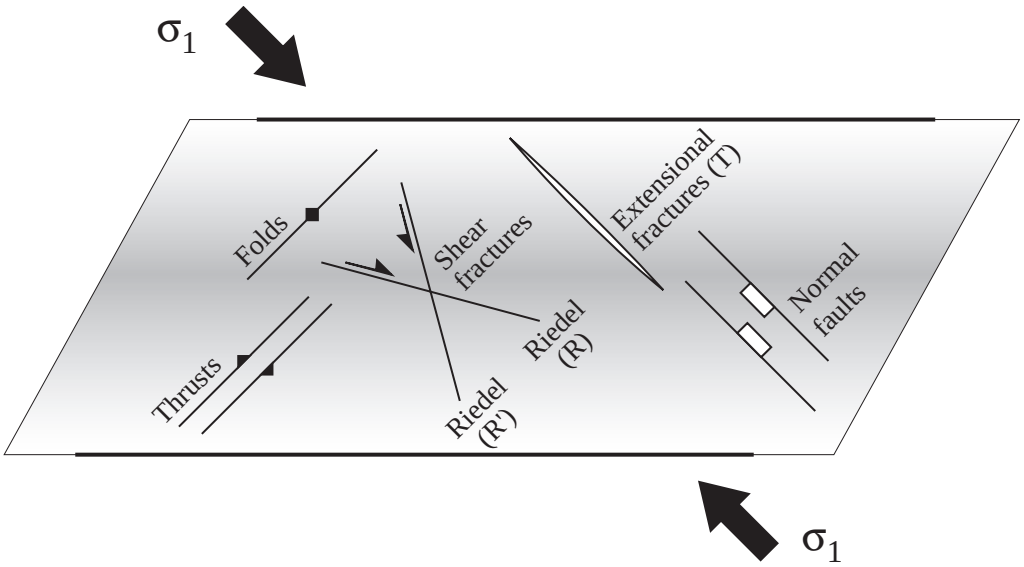

Fig. 5.33 *Map view of the associated structures developed in a transcurrent shear zone (modified after Rey 2003). The normal faults and extensional fractures (T) grow parallel to the general direction of movement (σ_1), while the folds and thrusts are perpendicular. The Riedel shear fractures (R and R') appear oriented respectively at Φ/2 and - Φ/2 to the direction of movement (σ_1), with Φ varying from 10° to 50°.*

5.5.2 Local interpretation

5.5.2.1 Prealpes Romandes

In the Western Prealpes Romandes, the orientation rose diagram of the "morphologic lineaments" (Fig. .34A) on the one hand and the diagram of the lineaments and geologic faults (Fig. 5.34B) on the other hand, may be interpreted in a unique Riedel shear system striking WNW-ESE, with a dextral sense of movement. The NNW-SSE orientation of the principal shear stress σ_1 in such a Riedel shear system (Fig. 5.34) is in a good agreement with the regional compression in the Western Prealpes Romandes. The different directions of faults are not expressed with the

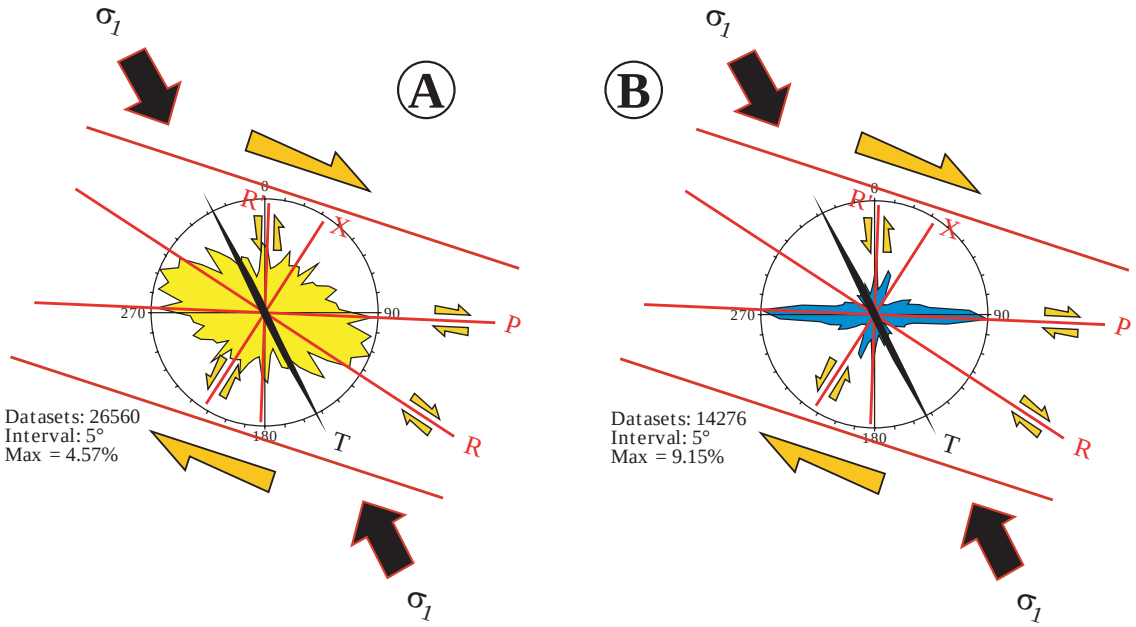

Fig. 5.34 *In the Western Prealpes Romandes, we may interpret in a unique Riedel shear system striking WNW-ESE, with a dextral sense of movement A) The morphologic lineament orientations (weighed data) and B) The map fault and lineament orientations (weighed data). The principal shear stress σ_1 is orientated NNW-SSE similarly as the regional compression in the Western Prealpes Romandes. The dextral faults R and P are more represented than their conjugate R' and X shear faults.*

same frequency since the dextral R and P are more represented than the R' and X shear faults. This is easily explained by the fact that conjugate shears (R' and X) do not develop systematically.

On the geologic map of the Western Prealpes Romandes (Fig. 5.35), we attempted to determine the sense of movement (on map view) of the 995 represented faults. As a result, we found 136 dextral faults and 176 sinistral faults (Fig. 5.35). We analysed fault orientation for both dextral and sinistral faults with the script L-STAT (KIM 2004) on ArcView 3.2. The sinistral fault orientation rose diagram (Fig. 5.36A) shows two main orientation trends that are N000°-N010° and N150°-N160°. The latter is also present on the dextral fault orientation rose diagram (Fig. 5.36B) in addition to a major peak striking N120°-N130°. The WNW-ESE dextral Riedel shear system proposed to interpret the fault and lineament orientation distribution in the Western Prealpes Romandes, correlates very well with the fault senses of movement. The major trend (N150°-N160°) observed for both sinistral and dextral

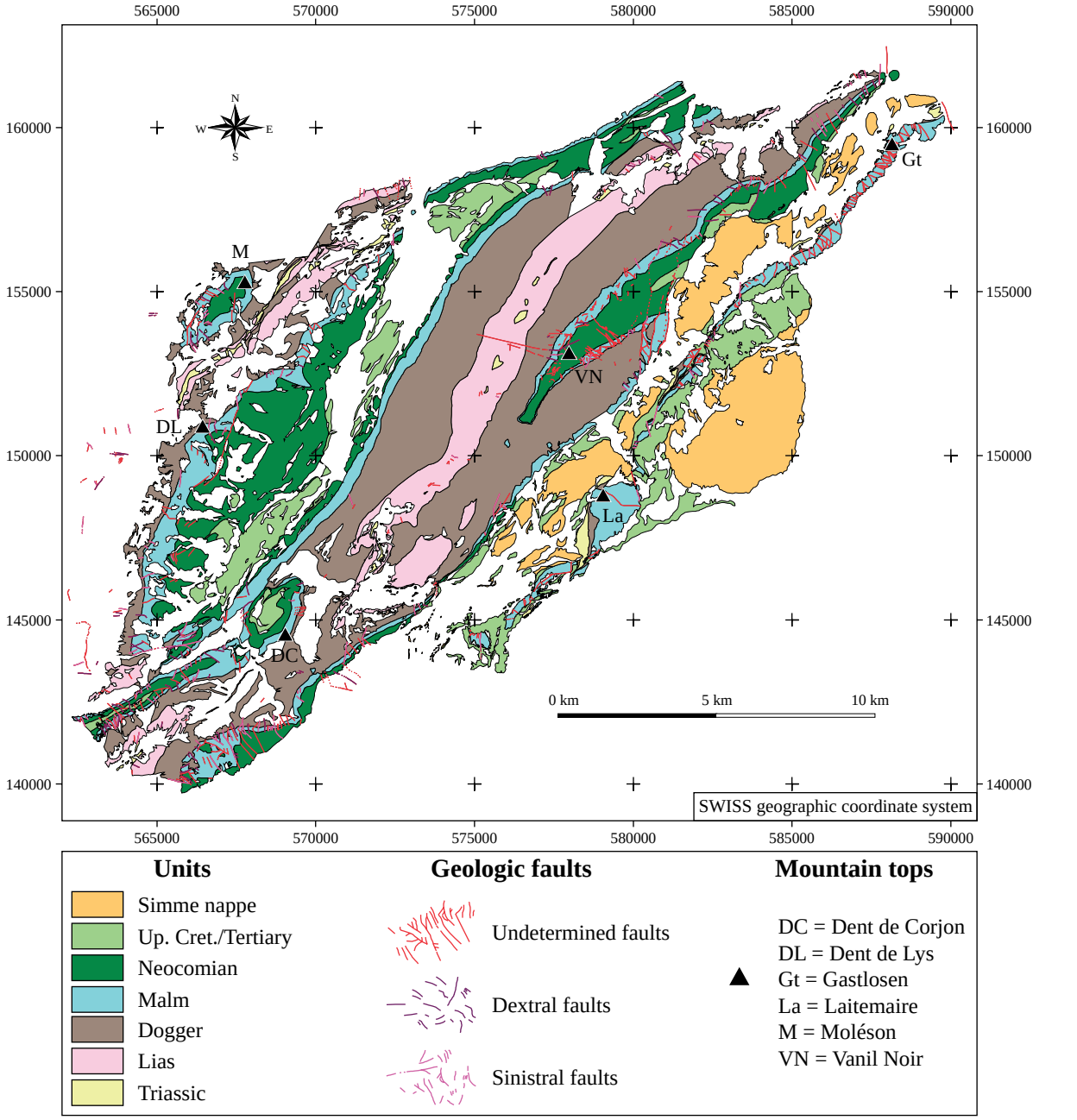

Fig. 5.35 *Simplified geologic map of the Dent de Lys/Vanil Noir area with the geologic faults indicated. When possible, the cartographic interpretation of fault sense of movement (dextral or sinistral) was determined. As a result, on the 995 represented faults, 136 appeared dextral and 176 sinistral.*

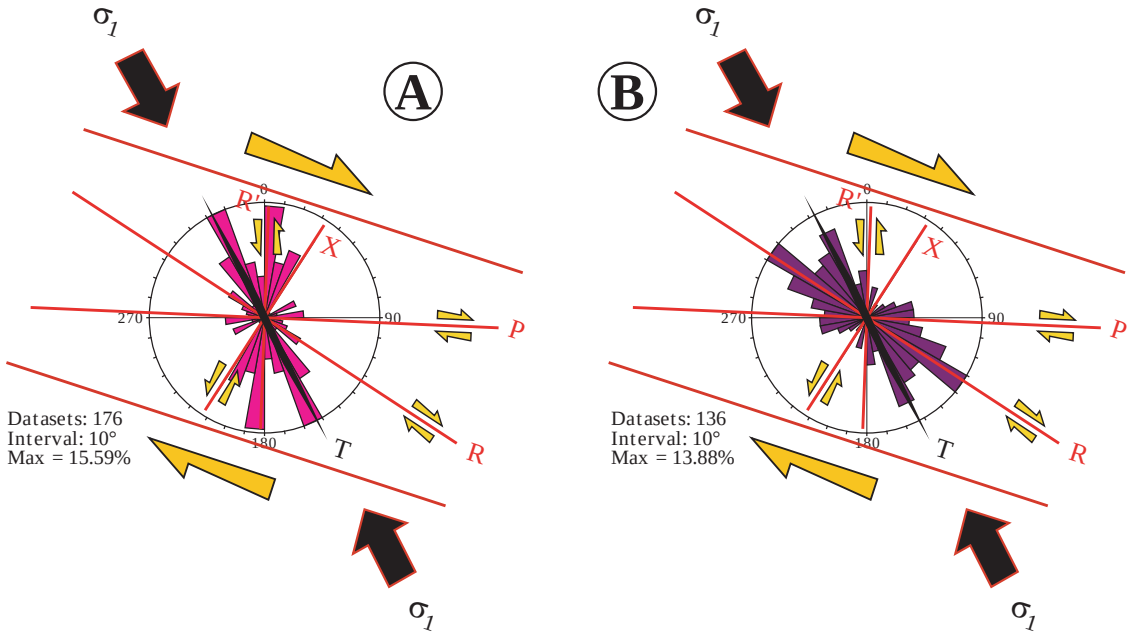

Fig. 5.36 *The WNW-ESE dextral Riedel shear system applied on the fault and lineament patterns of the Western Prealpes Romandes fits also with A) The cartographic sinistral fault orientations and B) The cartographic dextral fault orientations in the Dent de Lys/Vanil Noir area. The trend N150°-N160°, well expressed in both dextral and sinistral fault diagrams, fits the orientation of the extensional fractures T. The sinistral fault orientation striking N000°-N010° corresponds to the sinistral conjugate Riedel shears R' and the orientation N020°-N030° to the second order sinistral X shears. The dextral fault orientation striking N120°-N130° follows the dextral Riedel shears R and the orientation E-W fits with the second order dextral P shears.*

faults, corresponds to the orientation of extensional fractures T (Fig. 5.36A and 5.36B). The second main sinistral fault orientation striking N000°-N010° fits perfectly with the sinistral conjugate Riedel shears R' (Fig. 5.36A). In the same way, the dextral fault orientation striking N120°-N130° follows the dextral Riedel shears R (Fig. 5.36B). Finally, the third peak on the sinistral fault orientation rose diagram (N020°-N030°) corresponds roughly to the second order sinistral X shears (Fig. 5.36A), while on the dextral fault orientation diagram, the third peak (approximately E-W) fits with the second order dextral P shears (Fig. 5.36B).

The analysis of fault orientation and sense of movement in the Dent de Lys/Vanil Noir area corroborates the dextral Riedel shear model purposed to interpret the fracturation system in the Western Prealpes Romandes. Faults were thus generated by a dextral movement of a WNW-ESE general direction where the R, R' system dominates and also extensional fractures T. The second order P, X system, symmetric of R, R', is also present. This dextral Riedel shear system corresponds to a major fault corridor/zone with strike-slip component and subvertical orientation, also called transcurrent fault system.

5.5.2.2 Chablais

(Corinne Saudan and Cécile Bonnet)

In the Taney area, field data and results from the orientation analysis were confronted with the Riedel shear model by superposing the rose diagrams of fault orientations with the theoretical model (Fig. 5.37 bottom). The model is adjusted so that the major peaks of rose diagrams best correlate with the different Riedel shear directions. In the Taney area of the Swiss Chablais, the main orientation of the Riedel shear zone is NW-SE with a dextral movement. This direction matches perfectly the Flon-Taney-Tombeau des Allemands strike-slip zone, also with a right-lateral movement. In the investigated area not all possible Riedel shear orientations are equally well represented. Orientation distribution obtained from fault planes bearing striae (Fig. 5.37 bottom left) shows a predominance of the left lateral shear faults X and R', as well as the dextral shear faults P. The Riedel shears R are the less well represented. The rose diagram representing the sum of the faults from geological maps and the lineaments seen on aerial photographies (Fig. 5.37 bottom right), shows that the most representative faults are the sinis-

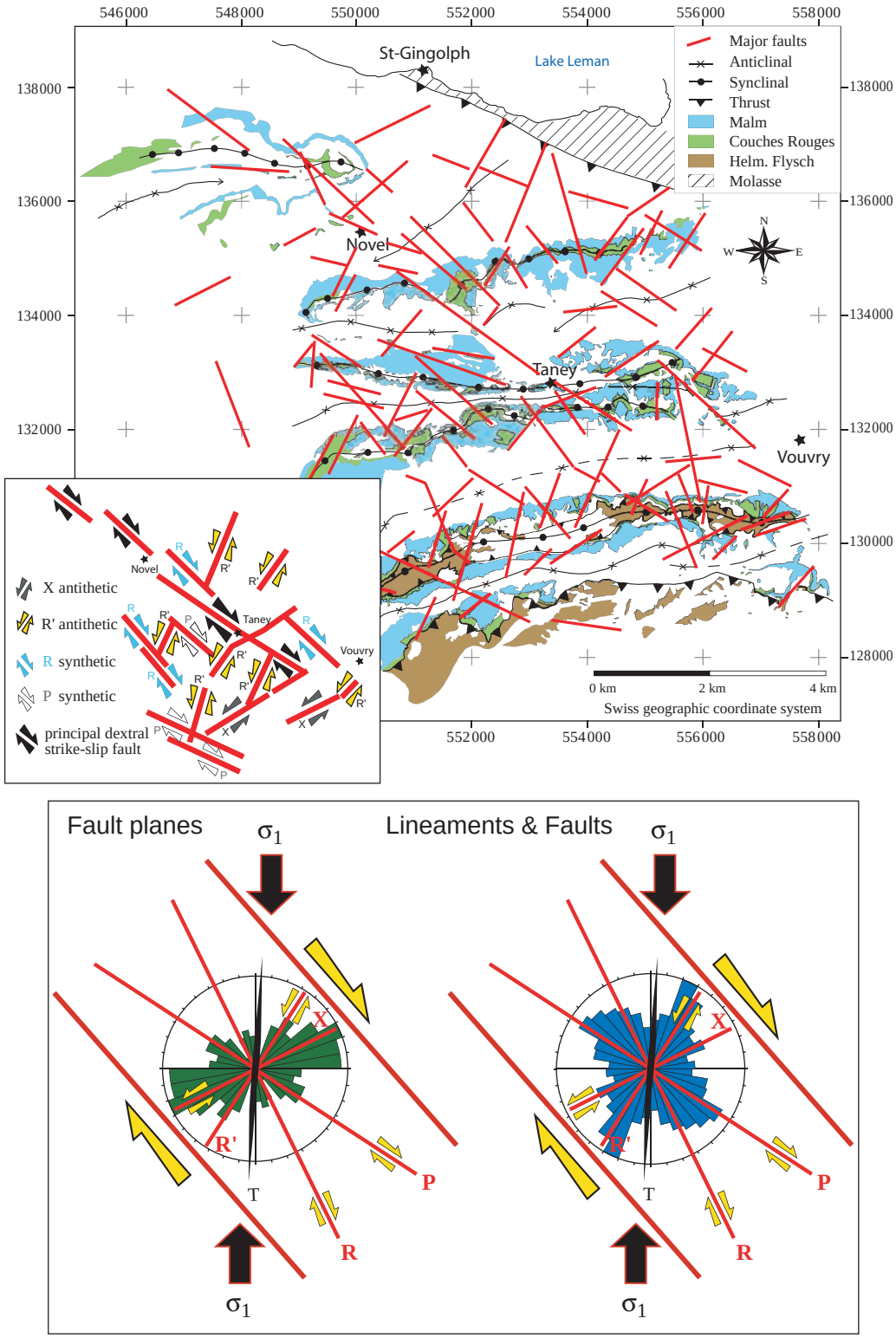

Fig. 5.37 *Simplified tectonic map of the Chablais Prealpes showing the major faults compiled from geological maps and interpretation of the lineaments map. Below, the results from our analyses were confronted with the Riedel shear model by superposing it with the rose diagrams. The model is adjusted so that the major peaks of rose diagrams best correlate with the different shear directions. The main orientation of the Riedel shear zone is NW-SE with a dextral movement. This direction matches perfectly the Flon-Taney-Tombeau des Allemands strike-slip fault. The direction of the principal stress axis corresponds to a N-S oriented compression. The inbox represents a simplified scheme highlighting only the main fault accidents (drawn from the map of major faults) with their sense of movement in order to discriminate between the different Riedel shear faults (R, R', X, P). For each major fault, it is possible to attribute its correspondent Riedel shear. The orientation and sense of displacement (dextral or sinistral) match up quite well. The good correspondence of the data and the model proves that the interpretation in term of Riedel shear system is fully justified.*

tral faults R' with however a well marked presence of dextral shears P and sinistral faults X.

Both the results from the kinematic and fracture orientation analyses converge to indicate that the main structure is a NW-SE oriented Riedel shear system with a subhorizontal N-S compression (principal stress axis σ_1) and E-W extension. This is in apparent conflict with the regional NW-SE oriented compression (σ_1) of the alpine arc and foreland, also observed in the Western Prealpes Romandes (see Chapter 5.5.2.1). However, if the Taney transcurrent fault is considered a subsidiary of a larger transcurrent system, the apparent contradiction in stress orientation can be resolved. Thus the Eastern Chablais area belongs to a third order subsidiary fault system (N-S compression and dextral movement), which explains the deviation in stress orientation from the general direction.

Based on the map of major faults (Fig. 5.37 top), we drew a simplified scheme highlighting only the main accidents with the indication of their senses of movement in order to discriminate between the different Riedel shear faults (R, R' X, P and T). For each major fault system, it is than possible to attribute the correspondent Riedel shear. The principal strike-slip fault of the Flon-Taney-Tombeau des Allemands corresponds well with the principal shear plane of the Riedel shear system. We suggest also that this strike-slip persists to the NW beyond the village of Novel and may possibly extend into Geneva Lake thus linking to the fault systems described on the northern shores of Leman Lake (Scheidhauer et al. 2005). All sinistral faults can be compared to the Riedel shears R' or X, with a proportion of R' definitely more accentuated. For the dextral faults, the occurrence factor between Riedel shears R and P is noticeably identical. According to the degree of orientation, it is sometimes difficult to decide between faults from an R or P type.

5.6 Conclusions

In order to investigate the recent tectonics (post-nappe emplacement), we studied the fracture patterns in the Western Prealpes Romandes and in the Chablais Prealpes. The results obtained in our morphostructural study are based on morphologic, fault and lineament orientation and paleostress analyses.

5.6.1 Morphologic analysis

The morphologic analysis and study of the hydrographic network at the transition between the Prealpes klippen and the Molasse Plateau suggests that the location and orientation of the major morphologic features (hydrographic and/or glacial) are determined by the structural trends from the fracture pattern and the fold/thrust system, in addition to the glacial morphology in the Molasse.

5.6.2 Fault and lineament analysis

The data sets were collected from geological maps and orthophotographs of the study area. To investigate the orientations of analysed structures, two methods were used to determine the structure orientations: the script L-STAT (Kim 2004) on ArcView 3.2 and a procedure using TectonicsFP. The comparison of these methods showed that they provide very similar results, but L-STAT is a user-friendly fast automatic method. The transformation of curved features into successive linear segments appears to be a valid simplification for the orientation analysis. In order to compare long and short fractures, we weighed the orientation measures for length.

Both in the Vanil Noir area and the Dent de Lys zone (Western Prealpes Romandes), the orientation analysis of lineaments and geologic faults provides the five following subsidiary fault families: (1) E-W, (2) ESE-WNW, (3) N-S, (4) SSE-NNW and (5) NNE-SSW. In a larger area extending from the Mont-Pélerin (West) to the East of the Vanil Noir, a similar orientation analysis also shows a dominant E-W orientation. In the Chablais Prealpes area, three different subsidiary fault families have been highlighted thanks to the study of fault and lineament orientations: (1) NE-SW, (2) NW-SE and (3) ENE-WSW.

After a thorough analysis of the fault patterns and orientations, we confronted our observation with different deformational models applicable to fault systems. Several models were considered: 1) pure fractures, 2) a conjugate fracture system, and 3) Riedel shear system. It appears that the Riedel system is the most adapted model to explain a variety of fault directions otherwise difficult to interpret.

In the Western Prealpes Romandes, the lineaments and geologic faults are interpreted in a unique Riedel

shear system striking WNW-ESE, with a dextral sense of movement. The NNW-SSE orientation of the principal stress σ_1 in such a Riedel shear system is in agreement with the regional present-day stress field. Faults were generated by a dextral movement of a general WNW-ESE oriented shear zone, where the extensional fractures T (SSE-NNW) and the R, R' system (ESE-WNW and N-S) dominate, although the second order P, X system (E-W and NNE-SSW), symmetric of R, R', is also present. This dextral Riedel shear system corresponds to a major fault zone with strike-slip component and subvertical orientation. In the Chablais Prealpes, in the vicinity of the Taney area, the conclusion based on the orientation analysis of the fracturation is that the whole zone is governed by a dextral Riedel shear system with a general NW-SE orientation. The results suggest that the principal N-S compressional stress based on the orientation of Riedel model interpretation corresponds to a local stress field.

5.6.3 Stress analysis

Faults with striation are found readily on small fault surfaces in limestone and marls throughout the Prealpes Medianes, both in the Chablais and the Romandes area. It was thus possible to conduct a survey of fault movement and paleostress orientations based on these observations.

The paleostress analysis performed in the Western Prealpes Medianes Plastiques showed that the general pattern of stress is related to the fold-and-thrust development that dominates in the area. From west to east of the study area, the orientation of the structures rotates. Their trend is N-S to N020° in the Dent de Lys – Jaman monoclinal area. In the Sarine (Intyamon) syncline their orientation is NNE-SSW and in the region of the Dorena anticline, Vanil Noir syncline and Tsavas-Millets anticline, the large fault-related folds are oriented NE-SW. In contrast to the Chablais Prealpes, strike-slip faulting is only a minor component of the recorded paleostress fields. Different tectonic regimes are represented in the investigated areas of the Western Prealpes Romandes. In the long dip slope area of the western Sarine valley, we observe the existence of faulting and fracturing associated with layer parallel shortening, probably related to the initial stages of folding and thrusting. Here in this western limb of the Sarine syncline, σ_1 (dipping to the E-SSE) and σ_3 (dipping to NNE-ENE) are parallel to bedding and σ_2 perpendicular. In the core of the Sarine syncline and in the Tsavas and Dorena anticlines, stress and fault orientations are compatible with fault-related folding. In the Tsavas anticline, compression is oriented NW-SE, extension is vertical and the intermediate axis is oriented NE-SW. In the Dorena anticline, extension is oriented NE-SW with compression gently dipping to the NW. In the Sarine syncline, compression dips to the NW, extension to the SE and the horizontal intermediate axis is oriented NE-SW. In local faults, small components of strike-slip movements are observable (probably synchronous with folding or postdating it). We also found extensional veins perpendicular to fold axis, indicating synfolding axial parallel extension. Along some faults it is possible to observe that strike-slip movement on the faults is reorienting vein sets and thus that this movement postdates folding.

In the Chablais Prealpes, the overwhelming majority of faults and fractures studied are subvertical and show subhorizontal strike-slip movements. Four main families are identifiable: NE-SW, WNW-ESE, ENE-WSW and NNW-SSE. The stress analysis using the right dihedral method indicates that the faults constitute a subvertical strike-slip system (NW-SE and NE-SW) with a N-S compression. The main strike-slip fault plane corresponds to the NW-SE oriented principal plane that can be correlated to the Flon-Taney-Tombeau des Allemands fault. Field evidence of fold/fault offsets indicates a dextral sense of slip along this fault. As the fault dataset is very homogeneous, it suggests that the analysed fault sets pertain to the same tectonic event.

To sum up, the following chronology may be suggested to explain the different deformational structures observed in the Chablais and Western Romandes Prealpes. Initial layer parallel shortening, is followed by folding and thrusting with synfolding axial parallel extension generating extensional veins perpendicular to fold axis. Post-folding, local strike-slip components of faults may be observed as well as strike-slip movement reorienting the previously formed vein sets. Finally, during the last stage of deformation, large-scale faults develop, cross-cutting the existing fold-and-thrust structures.

5.6.4 Regional fracture model: transcurrent faulting

In an effort to interpret the local stress fields and to integrate the results from the different datasets, we propose a more regional deformational model exten-

ding from the Prealpes to the Jura. The Riedel shear model has proven to be the most adapted model and local/regional Riedel shear zones are combined in a general transcurrent model for the Alpine foreland, including the Prealpes klippen, the foreland Molasse basin and the Jura fold-and-thrust belt (Fig. 5.38). The drainage and fracture patterns in the Prealpes correlate well with those in the underlying Molasse s.l. (Fig. 5.39). This suggests that the transcurrent tectonic fault system of the Prealpes is coincident with the transcurrent fault system in the Molasse and possibly the Jura foreland. Stress orientations were obtained, both from the Riedel model analyses and from fault kinematics. In both cases they show regional variations and a series of superposed events:

- Layer parallel shortening is associated with early fracturing of layers possibly during initial stages of compression and shortening.

- Subsequent folding and thrusting is coeval with fracturing of the layers and extension parallel to the fold axis. This event generates fractures and veins.

Following folding, cross-cutting faults develop that re-orient existing vein/fracture sets and bedding. They are mainly strike-slip faults, but no dominant direction could be determined.

- Finally, in the last stages ubiquitous fracturing develops throughout the Prealpes Medianes. This fracturing is tied to Riedel shear zones either dextral

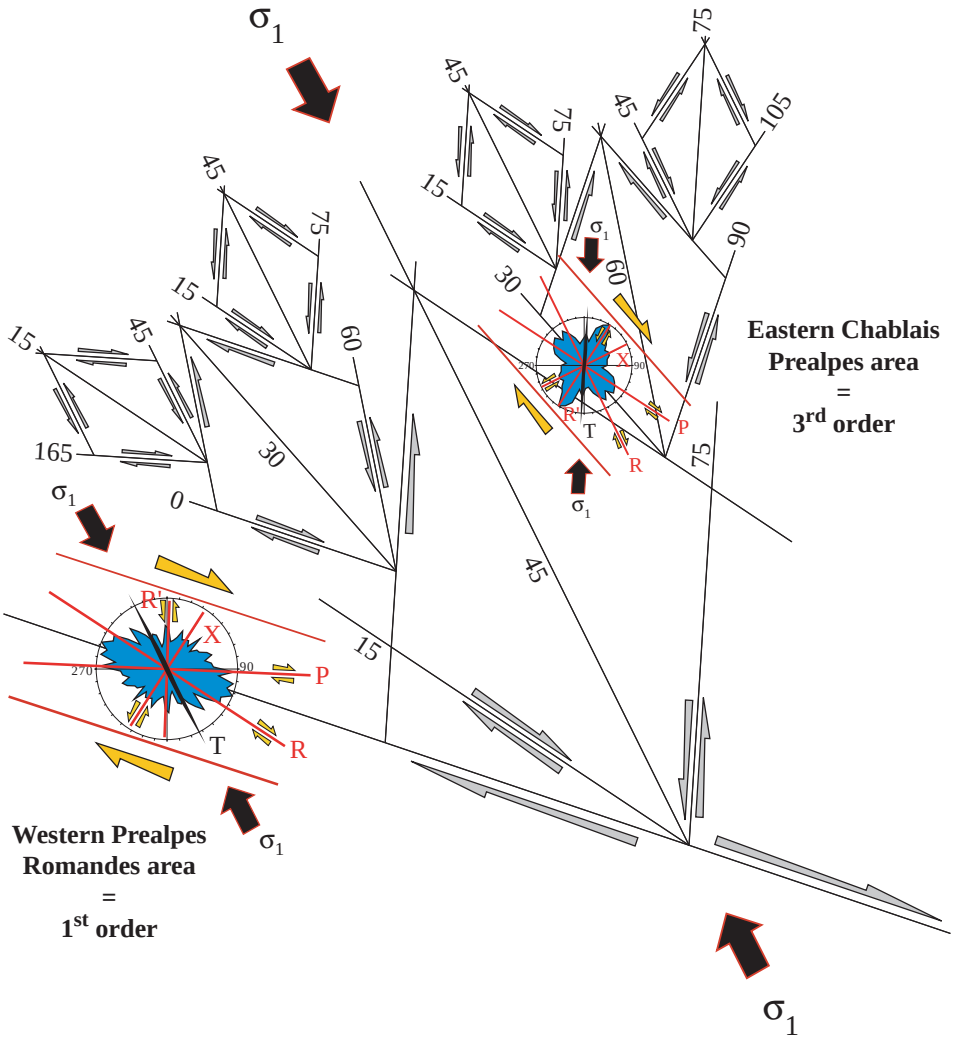

Fig. 5.38 *On a more regional scale it is proposed that the two dextral Riedel shear systems, which have been used as deformation model in the Chablais Prealpes and Western Prealpes Romandes, belong to two different orders of Riedel zones in a broader dextral transcurrent system. This regional system is orientated WNW-ESE with a NW-SE regional direction of shortening (σ_1). This paleostress direction corresponds to the orientation of the present day compressional stresses measured in the Alpine arc. The fault pattern in the Western Prealpes Romandes area fits a WNW-ESE dextral zone, and is considered to be a first order system in the regional transcurrent system. In contrast, the deviation in stress orientation of the Chablais area (N-S compression and dextral movement) from the general transcurrent direction is explained because of the third order nature of the Riedel shear system.*

or sinistral depending on the orientation of the first-order shear zone. This is corroborated by the observation that many of the investigated faults and fractures cross-cut the existing fold-and-thrust structures in the study area. Most visible are the large-scale structures such as the Tombeau des Allemands fault that dextrally offset the Grammont anticlinal ramp-related fold (MOSAR 1999).

The Prealpes Romandes area thus fits a WNW-ESE oriented dextral Riedel shear zone with NW-SE shortening (Fig. 5.38), and the eastern Chablais area fits a N-S shortening and dextral movement along a NNW-SSE oriented shear zone (Fig. 5.38). The apparent contradiction between these two fault systems (believed to be coeval in time) and the orientation of the stress field, can be resolved if we consider organizing into a hierarchy the shear zones, in a regional Riedel shear system with fault subsets of several degrees. The Western Prealpes Romandes are thus first order, but the Taney fault system in the Chablais is considered a third order Riedel shear system. On a more regional scale, this system is part of a larger first order transcurrent system. Subsidiary order fault systems explain the

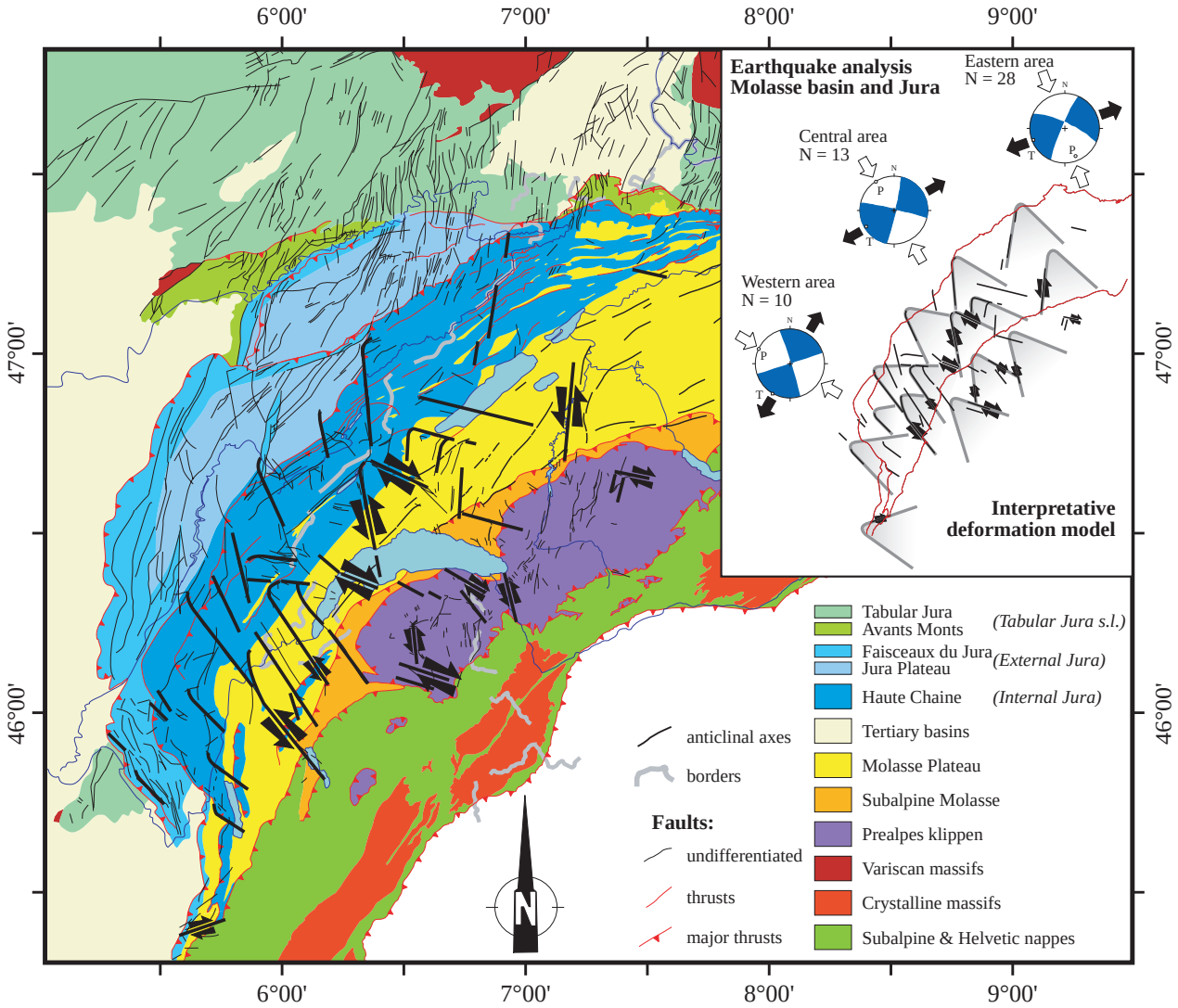

Fig. 5.39 *Simplified tectonic map of the Western Alpine foreland, including the Jura mountains, the Molasse basin and the Prealpes. Anticlinal axes are indicated in the Molasse Plateau. The major strike-slip faults and fault systems of the Prealpes, Molasse Plateau and Jura are highlighted (thick black lines), including the newly described systems in the Prealpes. Sense of movement along these major zones is given if known. From this, a pattern of conjugate faults emerges. This fault system is consistent across the Prealpes klippen resting on Molasse, the Molasse Basin, and the Jura mountains. Along strike of the Jura arc the individual conjugate systems rotates suggesting a rotation of the paleostress direction from a NNW-SSE directed shortening in the East to an almost W-E direction in the West. The whole fault system may be interpreted as belonging to a regional transcurrent system (top right scheme). This system is considered to be relatively young since in many instances it cross-cuts fold and thrust-related structures and is conspicuously similar to the present-day stress field indicated by the focal mechanism of earthquakes (MOSAR & BOREL 1992).*

deviation in stress orientation from the general direction. The broader, dextral NW-SE oriented zone may be seen as a first order system, while the narrower Taney fault system with its NNW-SSE orientation and sinistral motion is a lesser order. In addition, along strike of the Jura arc, the orientation of the conjugate fault system rotates and the shortening direction bisecting the conjugate fault sets changes from NNW-SSE in the East to almost W-E in the West. This is similar to the present day general stress field (MOSAR & BOREL 1992, KASTRUP 2002). Given the coherence of the whole fault system investigated, we suggest that the bulk of the brittle deformation in the transcurrent regime is recent and possibly has developed in a tectonic regime coincident with the present day stress field. The fault systems both in the Chablais and Western Prealpes Romandes are most likely recent and postdate the nappe emplacement.

APPENDICES TRANSCURRENT FAULTING

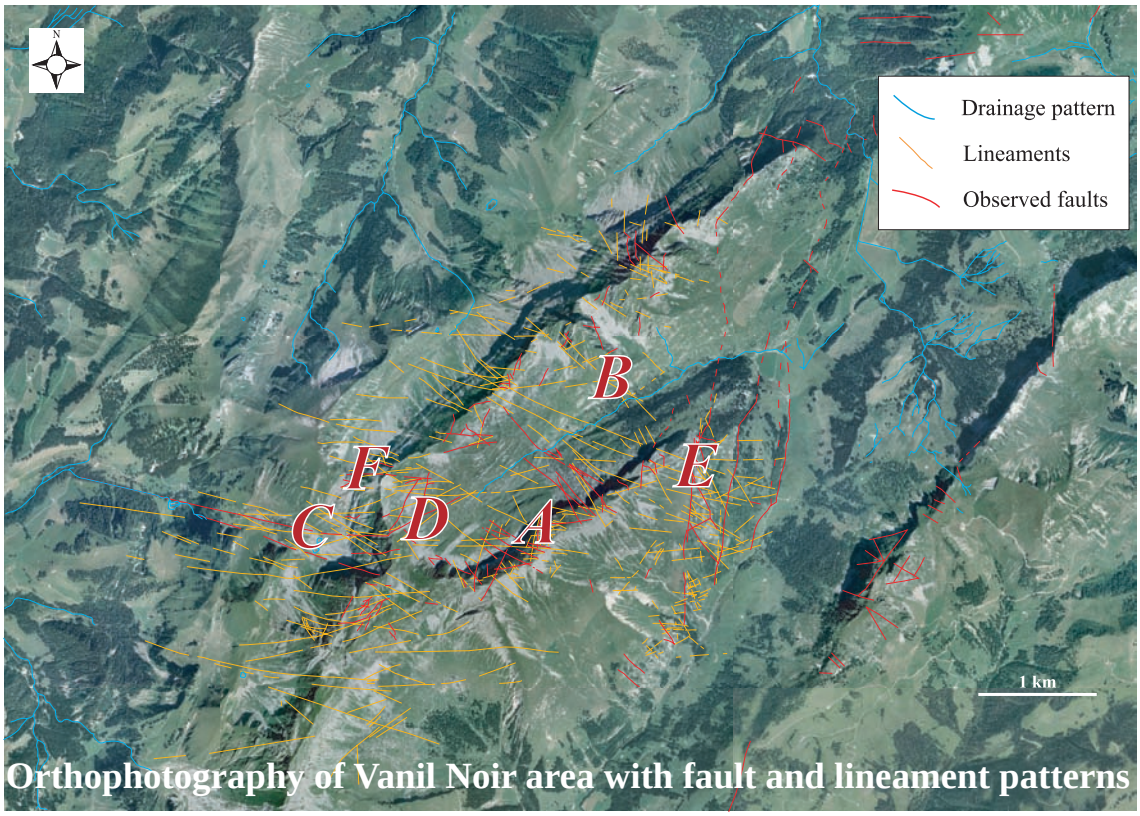

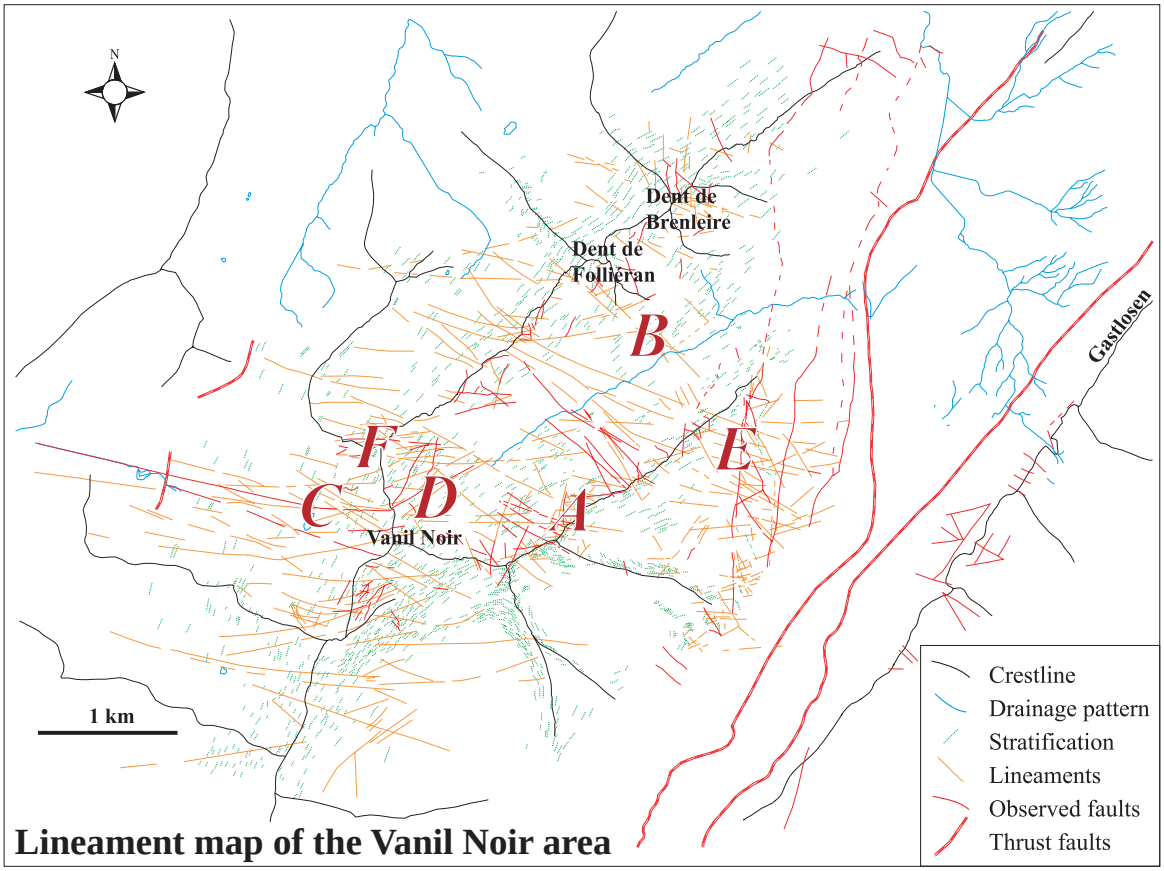

Appendix 5.I *The lineaments have been identified and reported on the orthophotography of the Vanil Noir area (Western Prealpes Romandes) as well as the faults taken from a set of geologic maps. On the lineament map of the Vanil Noir area are indicated the crest lines, drainage pattern, stratification, faults and some major nappe boundaries. The big letters A to F indicate the location of the different photographies.*

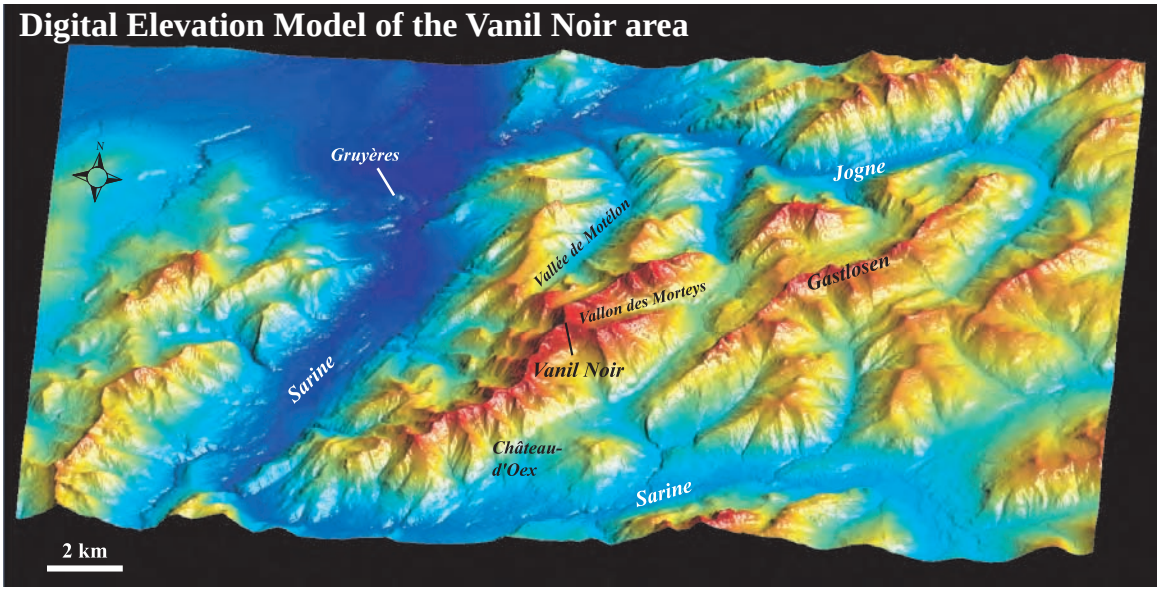

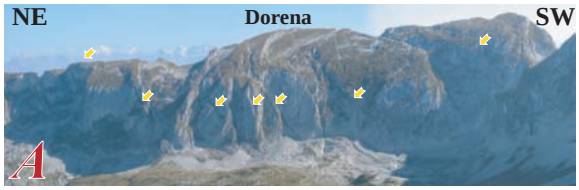

Anticlinal Dorena-Bimis

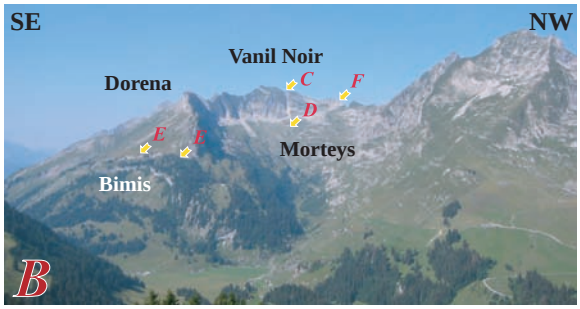

View on Dorena-Morteys-Vanil Noir

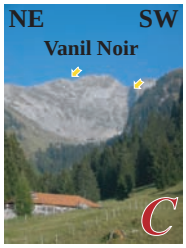

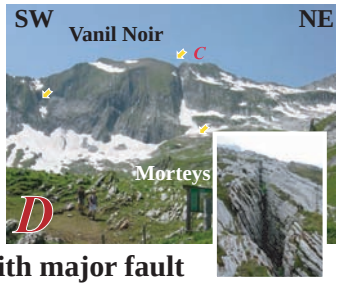

Vanil Noir with major fault

Dent de Bimis fault

Veins near fault **Cataclasites**

Herbette fault zone

The Digital Elevation Model (MNT25) of the investigated area shows the main geomorphological features. The photographs present different localities where some of the brittle faults detected from orthophotography were observed and investigated in the field. A) In the large East-plunging anticline the important set of cross faults is highlighted. B) A view from the Dent de Savigny into the Vanil Noir syncline indicates the location of some of the major faults present in the study zone. C) The Pas de la Borière fault (observed from the W) cuts the Vanil Noir syncline in the vicinity of the summit. D) The same fault (observed from the E) extends into the vallon des Morteys as a succession of sink holes ("dolines"). E) The Bimis strike-slip fault cuts the NE tip of the plunging Dorena anticline on a long distance. This fault system is made of two major faults overprinted by an important karst depression. F) Along the same ridge as the Vanil Noir summit, a large brittle fault shows extensive cataclasites and a higher than average density of calcite veins. The veins near the fault are rotated when compared with the more regional orientation of veins.

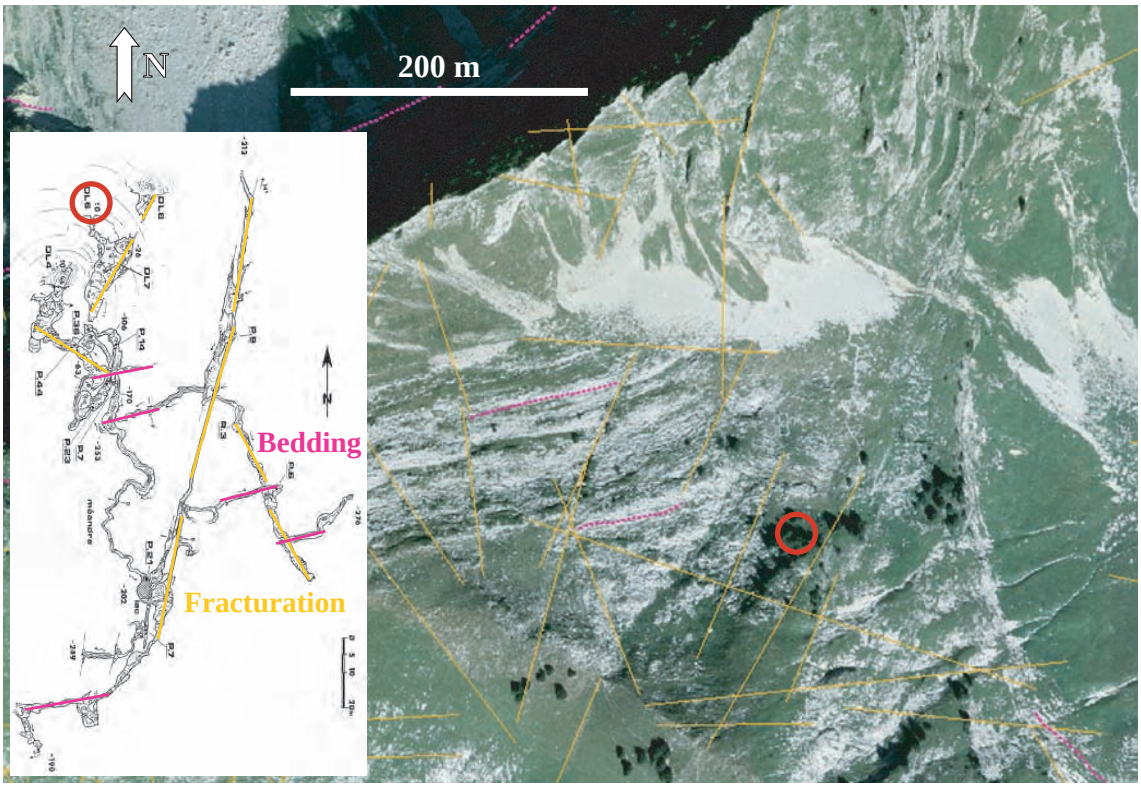

Appendix 5.II *Structural analysis of the karst area located East of the Dent de Lys summit in the Western Prealpes Romandes. The lineaments appear as yellow lines and the bedding is underlined by pink ones. A map view of the karst system (*Wenger *1984) shows that the galleries follow both the stratification and the fracturation orientations. A pit entrance into the system of caverns (DL6) is located by a red circle both on the karst map and the orthophotography.*

Appendix 5.III *(Right) Geologic map of the Vanil Noir area (Western Prealpes Romandes) with axes of the successive synclines and anticlines. The serial sections across the Vanil Noir syncline and the Dorena anticline (modified after* Brasey *1989) are located on the map. The Late Jurassic formation constitutes the cliffs resistant to erosion bordering the Early Cretaceous unit located in the core of the syncline. This unit has been largely eroded by the glacial activity as for instance in the vallon des Morteys, but also forms singularly the highest summit of the area (Vanil Noir and Vanil de l'Ecri).*

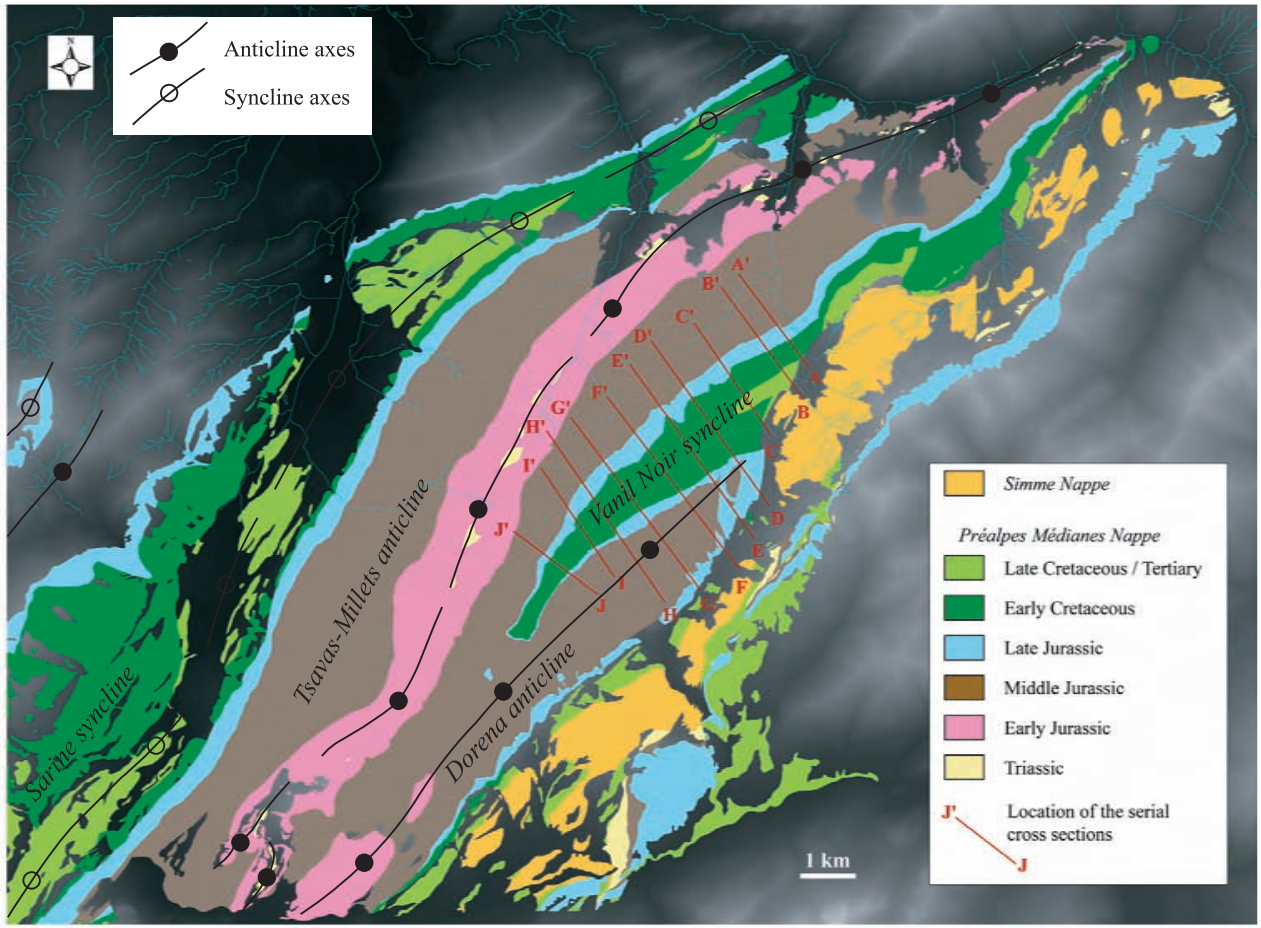

Geologic map of the Vanil Noir area

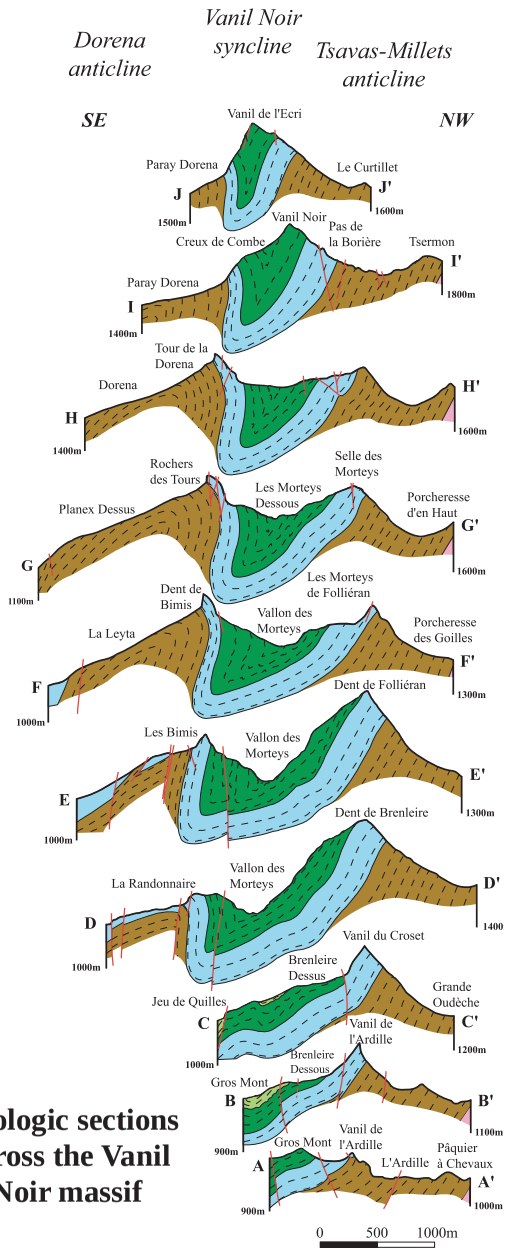

Geologic sections across the Vanil Noir massif

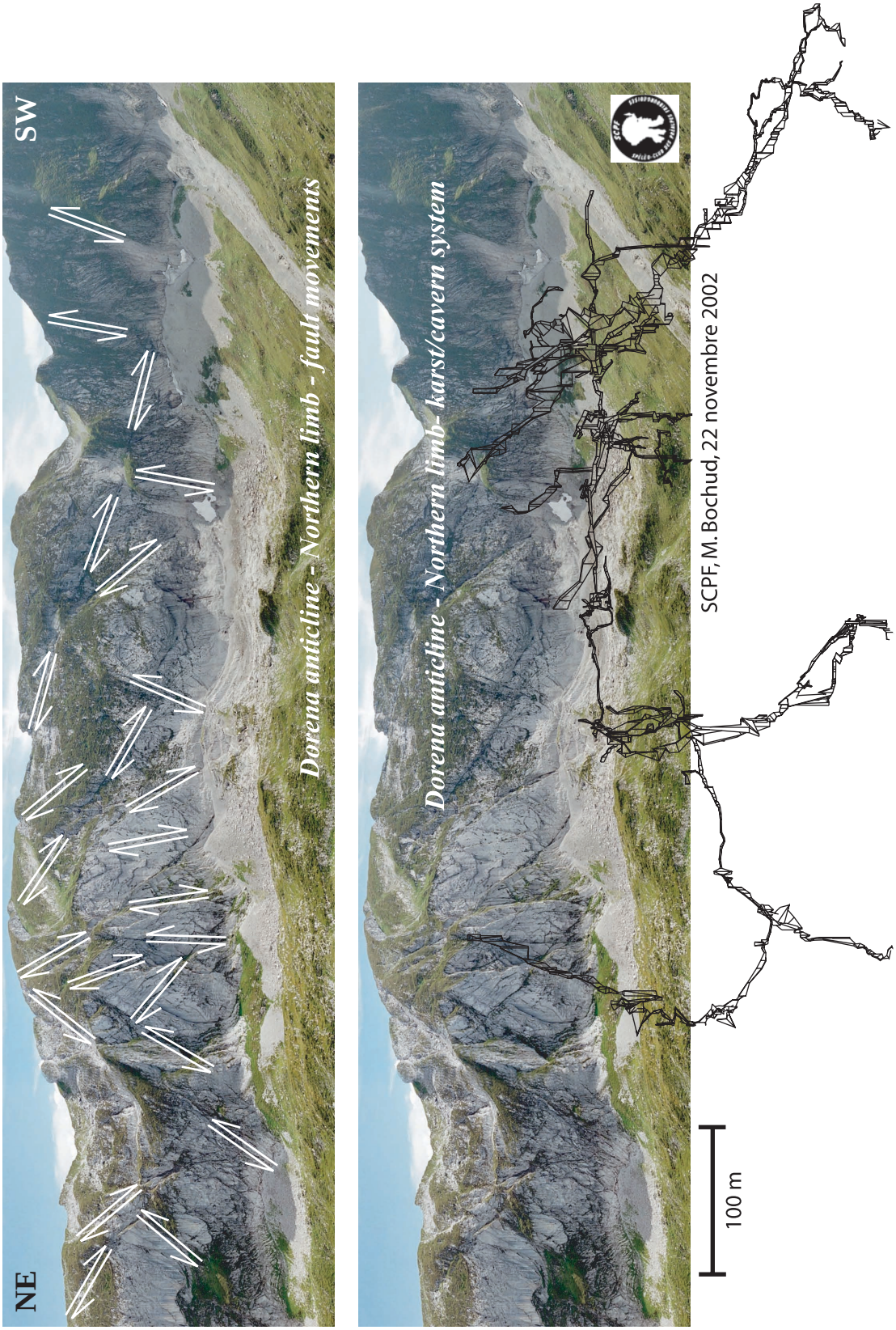

Appendix 5.IV *Northern limb of the Dorena anticline (Vanil Noir area in the Western Prealpes Romandes) affected by an important set of cross faults, whose supposed senses of movement are indicated (M. Bochud, personal communication). A system of karst caverns is overprinted on this fault system as illustrated by a part of the cave survey (Spéléo-club des Préalpes Fribourgeoises, M. Bochud, personal communication).*

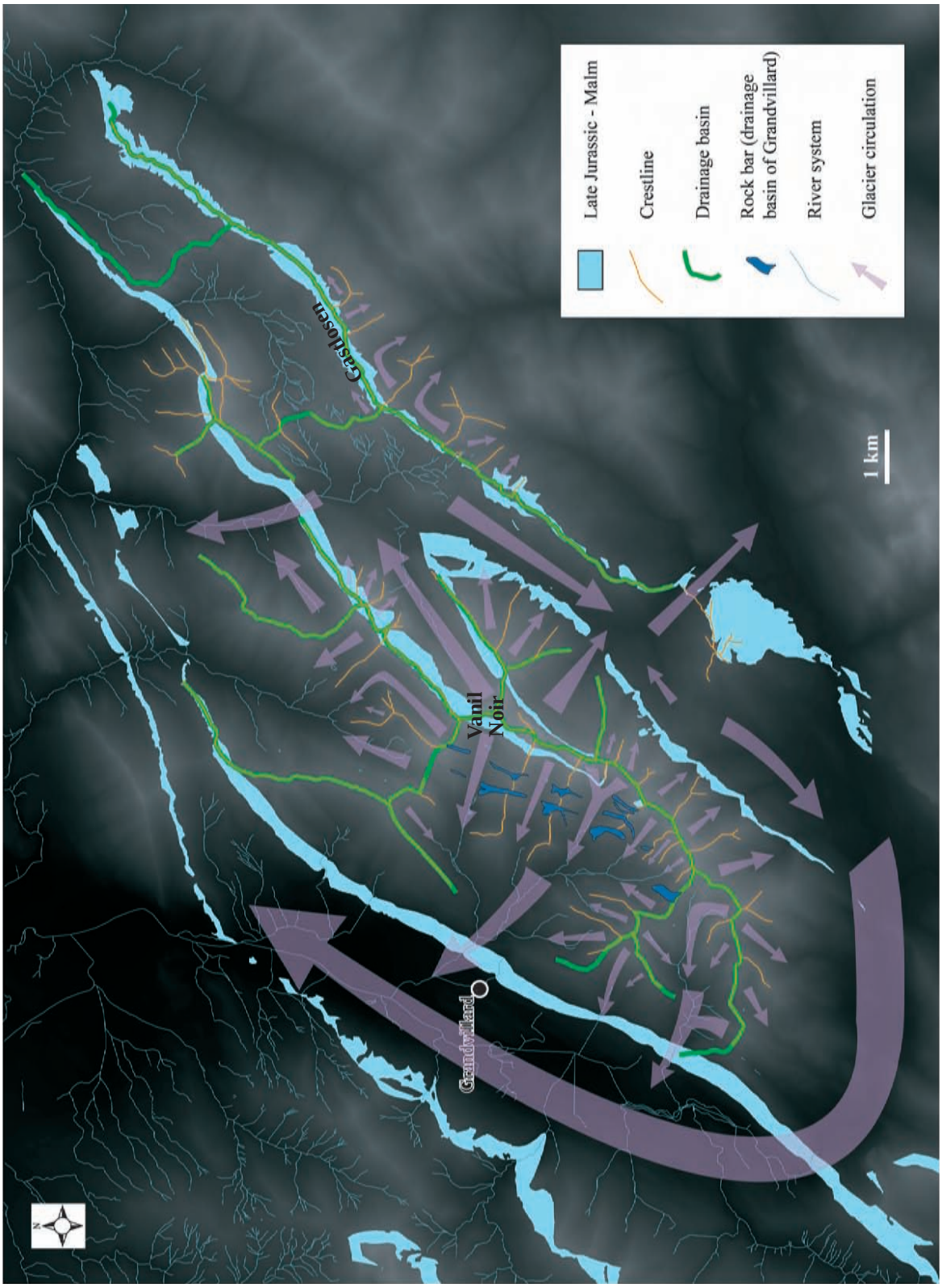

Appendix 5.V *Morphological map draped on the 2-dimensional Digital Elevation Model of the Vanil Noir area (Western Prealpes Romandes) indicating the more recent glacial trajectories. The main glacier of the area was located in the Sarine valley and was alimented by a number of small glaciers leading to the actual morphology of the landscape. The glacial valleys follow a combination of structural trends from faults and folds.*

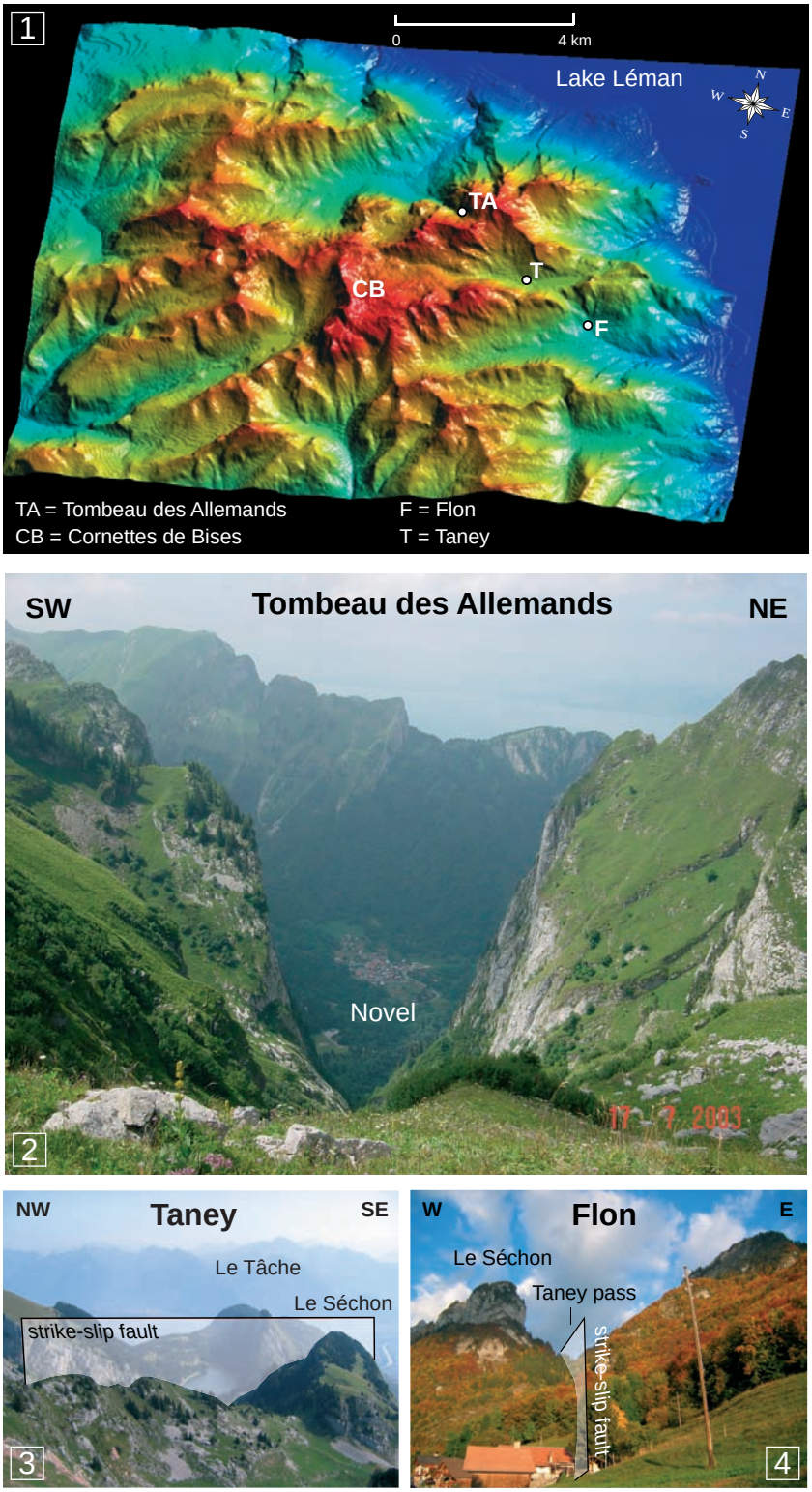

Appendix 5.VI *Views of the Flon-Taney-Tombeau des Allemands strike-slip fault. 1) Digital elevation model (©swisstopo) of the studied area with the topographic alignment of the localities of Le Flon, Taney (1415m) and Tombeau des Allemands. View on the NNW with the maximum elevation in dark. 2) View of the strike-slip fault in the Tombeau des Allemands area. The distance between the two cliffs is around 150m. The village of Novel is visible in the background. 3) View of the strike-slip fault in the Taney area from the summit of Chambairy (2206m). The difference of alignment between Le Tâche and Le Séchon is clearly visible. 4) View from the locality of Le Flon. The strike-slip fault crosses the Taney pass.*

*****

REFERENCES

ACKERMANN A. 1986. Le flysch de la nappe du Niesen. Eclogae geologicae Helvetiae 79, 641-684.

ALLEN P.A. & ALLEN J.R. 2005. Basin Analysis: Principles and Applications. Oxford, 549 pp.

ANGELIER J. & MECHLER P. 1977. Sur une méthode graphique de recherche des contraintes principales également utilisable en tectonique et en séismologie: la méthode des dièdres droits. Bulletin de la Société géologique de France 7, 1309-1318.

AUBERT D. 1945. Le Jura et la tectonique d'écoulement. Mémoire de la société vaudoise des sciences naturelles 8, 217-236.

AVOUAC J.-P. 2003. Mountain building, erosion, and the seismic cycle in the Nepal Himalaya. Advances in Geophysics 46, 1-80.

BADOUX H. & MERCANTON C.H. 1962. Essai sur l'évolution tectonique des Préalpes médianes du Chablais. Eclogae geologicae Helvetiae 55, 135-188.

BADOUX H. 1962. Géologie des Préalpes valaisannes. Matériaux pour la Carte Géologique de la Suisse n.s. 113, 1-86.

BADOUX H. 1963. Les unités ultrahelvétiques de la Zone des Cols. Eclogae geologicae Helvetiae 56, 1-13.

BADOUX H. 1965a. Les relations de l'Ultrahelvétique et des Préalpes médianes dans la vallée de la Grande Eau. Eclogae geologicae Helvetiae 58, 11-16.

BALLY A.W., GORDY P.L. & STEWART G.A. 1966. Structure, seismic data and orogenic evolution of southern Canadian Rocky Mountains. Bulletin of Canadian Petroleum Geology 14, 337-381.

BALLY A.W. 1989. Phanerozoic basins of North America. In: The geology of North America-An overview, Geological Society of America, Boulder, Colorado, 397-446.

BALMAT B. 1982. Processus et formations de versant dans le bassin du Rio des Marais (Région du Vanil Noir) et établissement d'une carte géomorphologique au 1:5000. Travail de séminaire, Fribourg.

BAUD A. 1972. Observations et hypothèses sur la géologie de la partie radicale des Préalpes médianes. Eclogae geologicae Helvetiae 65, 43-55.

BAUD A. & SEPTFONTAINE M. 1980. Présentation d'un profil palinspastique de la nappe des Préalpes médianes en Suisse occidentale. Eclogae geologicae Helvetiae 73, 651-660.

BAUD A., HEINZ R. & SEPTFONTAINE M. 1989. Compte rendu de l'excursion de la Société Géologique Suisse dans les Préalpes, du 2 au 4 octobre 1988. Eclogae Geologicae Helvetiae 82, 359-377.

BAUDRAZ G. 1997. Etude géomorphologique de la région Vanil Noir - Gastlosen. Travail de séminaire, Fribourg.

BEAUMONT C., ELLIS S., HAMILTON J. & PH. F. 1996. Mechanical model for subduction-collision tectonics of Alpine-type compressional orogens. Geology 24, 675-678.

BEAUMONT C., KOOI H. & WILLETT S. 2000. Coupled tectonic-surface process models with applications to rifted margins and collisional orogens. In: Geomorphology and global tectonics, J. Wiley and sons, New York, 29-55.

BECK C., DEVILLE E., BLANC E., PHILIPPE Y. & TARDY M. 1998. Horizontal shortening control of middle Miocene marine siliciclastic accumulation (Upper Marine Molasse) in the southern termination of the Savoy Molasse Basin (northwestern Alps/southern Jura). Geological Society of London, Special Publication 134, 263-278.

BERGER J.-P., REICHENBACHER B., BECKER D., GRIMM M., GRIMM K., PICOT L., STORNI A., PIRKENSEER C., DERER C. & SCHAEFER A. 2005. Paleogeography of the Upper Rhine Graben (URG) and the Swiss Molasse Basin (SMB) from Eocene to Pliocene. International Journal of Earth Sciences 94, 697-710.

BERNOULLI D., CARON C., HOMEWOOD P., KÄLIN O. & STUIJVENBERG V.J. 1979. Evolution of continental margins of the Alps. Schweizerische Mineralogische und Petrographische Mitteilungen 59, 165-170.

BOILLOT G., MONTADERT L., LEMOINE M. & BIJU-DUVAL B. 1984. Les marges continentales actuelles et fossiles autour de la France. Masson, Paris, pp.

BOLLIGER T. 1999. Geologie des Kantons Zürich. Ott Verlag Thun, Thun, 163 pp.

Bonnet C., Malavieille J. & Mosar J. 2006. Interactions between Tectonics, erosion and sedimentation during the recent evolution of the Alpine orogen - Analogue modeling insights. Tectonics Submitted.

Bonnet C., Malavieille J. & Mosar J. 2007. Surface processes versus kinematics of thrust belts: rates of erosion, sedimentation and exhumation - Insights from analogue modelling. Bulletin de la Société Géologique de France Submitted.

Borel G. 1995. Préalpes médianes: courbes de subsidence et implications géodynamiques. Bulletin de la Société Vaudoise des Sciences naturelles 83, 293-315.

Borel G. 1998. Dynamique de l'extension mésozoique du domaine briançonnais: les Préalpes médianes au Lias. Mémoires Géologie (Lausanne), 157.

Boyer S.E. & Elliott D. 1982. The geometry of thrust systems. American Association of Petroleum Geologists Bulletin 66, 1196-1230.

Brasey J. 1989. Etude géologique du Vanil Noir et du vallon des Morteys. Diplôme, Fribourg.

Burkhard M. 1988. L'Helvétique de la bordure occidentale du massif de l'Aar (évolution tectonique et métamorphique). Eclogae geologicae Helvetiae 81, 63-114.

Burkhard M. 1990. Aspects of large-scale Miocene deformation in the most external part of the Swiss Alps (Subalpine Molasse to Jura fold belt). Eclogae geologicae Helvetiae 83, 559-584.

Burkhard M. & Sommaruga A. 1998. Evolution of the Swiss Molasse basin: structural relations with the Alps and the Jura belt. Geological Society of London, Special Publication 134, 279-298.

Burkhard M., Ateia O., Sommaruga A., Gogniat S. & Evard D. 1998. Tectonique et hydrogeologie dans le Jura Neuchâtelois. Eclogae geologicae Helvetiae 91, 177-183.

Burri M. 1987. Les Roches. Editions Pillet, Martigny, 159 pp.

Byrne D., Davis D. & Sykes L. 1988. Loci and maximum size of thrust earthquakes and the mechanics of the shallow region of subduction zones. Tectonics 7, 833-857.

Calais E., Nocquet J.-M., Jouanne F. & Tardy M. 2002. Current strain regime in the Western Alps from continuous GPS measurements, 1996-2001. Geology 30, 651-654.

Campana B. 1941. Faciès et extension de la nappe de la Simme au nord-est de Château d'Oex. Eclogae geologicae Helvetiae 34, 221-227.

Caron C. 1972. La nappe supérieure des Préalpes: subdivisions et principaux caractères du sommet de l'édifice préalpin. Eclogae geologicae Helvetiae 65, 47-73.

Caron C. 1973. Survol géologique des Alpes occidentales. Bulletin de la Société Fribourgeoise des Sciences Naturelles 62, 73-81.

Caron C. 1976. La nappe du Gurnigel dans les Préalpes. Eclogae geologicae Helvetiae 69, 297-308.

Caron M. & Dupasquier C. 1989. Litho- et biostratigraphie des dépôts du "Crétacé moyen" dans les Préalpes Médianes. Geobios, mémoire spécial 11, 49-58.

Cederbom C.E., Sinclair H.D., Schlunegger F. & Rahn M.K. 2004. Climate-induced rebound and exhumation of the European Alps. Geology 32, 709-712.

Chamot G. 1961. La Nappe des Préalpes médianes entre les Cornettes de Bise et le col du Corbier (Chablais français). Bulletin des laboratoires de géologie, minéralogie, géophysique et du Musée géologique de l'Université de Lausanne 131, 1-86.

Chatton M. 1974. Géologie des Préalpes médianes entre Gruyères et Charmey. Mémoires de la Société Fribourgeoise des Sciences Naturelles 13, 1-128.

Chenevart C. 1945. Les nappes des Préalpes Médianes et de la Simme dans la région de la Hochmatt. Mémoire Société des Sciences naturelles, Fribourg 12, 1-213.

Cobbold P.R., Durand S. & Mourgues R. 2001. Sandbox modelling of thrust wedges with fluid-assisted detachments. Tectonophysics 334, 245-258.

Dahlen F.A., Suppe J. & Davis D.M. 1984. Mechanics of fold and thrust belts and accretionary wedges: Cohesive Coulomb theory. Journal of Geophysical Research B, solid earth and planets 89, 10087-10101.

Dahlen F.A. 1984. Noncohesive critical Coulomb wedges: an exact solution. Journal of Geophysical Research B, solid earth and planets 89, 10,125-10,133.

Dal Piaz G.V., Hunziker J.C. & Martinotti G. 1972. La zona Sesia-Lanzo e l'evolutione tettonico-metamorfica delle Alpi nordoccidentali interne. Mem. Soc. Geol. Padova 32, 1-16.

Davies J.H. & von Blanckenburg F. 1995. Slab breakoff: a model of lithosphere detachment and its test in the magmatism and deformation of collisional orogens. Earth and planetary Science Letters 129, 85-102.

Davis D.M., Suppe J. & Dahlen F.A. 1983. Mechanics of Fold-and-Thrust Belts and Accretionary Wedges. Journal of Geophysical Research B, Solid earth and planets 88, 1153-1172.

Davis G.H., Reynolds, S. J. 1996. Structural geology of rocks and regions. John Wiley & Sons, inc., New York, 776 pp.

Dickinson W.R. 1974. Plate tectonics and sedimentation. In: Tectonics and Sedimentation, Special Publication of the Society of economic Paleontologists and Mineralogists, Tulsa, 1-27.

Doerfliger N. 1989. Etude géologique de la région Gros-Mont (entre Hochmatt et Dent de Ruth). Diplôme, Fribourg.

Dousse B. 1965. Géologie des Rochers de Château d'Oex. Matériaux pour la Carte Géologique de la Suisse, [n.s.] 119, 1-77.

England P. & Molnar P. 1990. Surface uplift, uplift of rocks, and exhumation of rocks. Geology 18, 1173-1177.

Escher A., Masson H. & Steck A. 1988. Coupe géologique des Alpes occidentales suisses. Rapp. géol. Serv. hydrol. géol. natl. Suisse 2, 11.

Escher A., Masson H. & Steck A. 1993. Nappe geometry in the Western Swiss Alps. Journal of Structural Geology 15, 501-509.

Escher A. & Beaumont C. 1997. Formation, burial and exhumation of basement nappes at crustal scale: a geometric model based on the Western Swiss-Italian Alps. Journal of Structural Geology 19, 955-974.

Escher A., Hunziker J., Masson H., Sartori M. & Steck A. 1997. Geologic framework and structural evolution of the western Swiss-Italian Alps. In: Deep structure of the Swiss Alps - Results from NRP 20, Birkhäuser AG., Basel, 205-222.

Favre E. & Schardt H. 1887. Description géologique des Préalpes du canton de Vaud et du Chablais jusqu'à la Dranse et de la chaîne des Dents du Midi formant la partie NW de la feuille XVII. Matériaux pour la Carte Géologique de la Suisse 22, 1-636.

Fierz S. 1994. Evaluation des ressources en eau de l'Intyamon. Diplôme, Fribourg.

Foster D.A. & John B.E. 1999. Quantifying tectonic exhumation in an extensional orogen with thermochronology: examples from the southern Basin and Range Province. Geological Society of London Special Publication 154, 343-364.

Frasson B.A. 1947. Geologie der Umgebung von Schwarzenburg. Matériaux pour la Carte Géologique de la Suisse n.s. 88, 1-62.

Funk H. & Loup B. 1992. Mesozoic subsidence analysis from the Jura to the Helvetic realm. Eclogae geologicae Helvetiae 85, 774-775.

Girod F. 1995. Géologie de la région des Cornettes de Bise (Préalpes du Chablais franco-suisse). Bulletin de la Société Vaudoise des Sciences naturelles 83, 317-334.

Gorin G.E., Signer C. & Amberger G. 1993. Structural configuration of the western Swiss Molasse Basin as defined by reflection seismic data. Eclogae geologicae Helvetiae 86, 693-716.

Guellec S., Tardy M., Roure F. & Mugnier J.L. 1989. Une interprétation tectonique nouvelle du massif subalpin des Bornes (Alpes occidentales): apports des données de la géologie et de la géophysique profondes. Comptes Rendus de l'Académie des Sciences de Paris, Série 2 309, 913-920.

Guellec S., Mugnier J.L., Tardy M. & Roure F. 1990. Neogene evolution of the western Alpine foreland in the light of ECORS data and balanced cross sections. In: Deep structure of the Alps, Mém. Soc. géol. suisse, Zürich, 165-184.

Guillaume M. 1986. Révision stratigraphique des Couches Rouges de la nappe des Préalpes Médianes Romandes. PhD, n° 910, Fribourg.

Gutscher M.-A., Kukowski N., Malavieille J. & S. L. 1996. Cyclical behavior of thrust wedges: Insights from high basal friction sandbox experiments. Geology 24, 135-138.

Gutscher M.-A., Kukowski N., Malavieille J. & Lallemand S. 1998a. Episodic imbricate thrusting and underthrusting: Analog experiments and mechanical analysis applied to the Alaskan Accretionary Wedge. Journal of Geophysical Research 103, 10,161-10,176.

Gutscher M.-A., Kukowski N., Malavieille J. & Lallemand S. 1998b. Materiel transfer in accretionary wedges from analysis of a systematic series of analog experiments. Journal of Structural Geology 20, 407-416.

Hable R. 1997. Biostratigraphie, Sedimentologie und paläogeographische Entwicklung der Préalpes Médianes des Chablais (Haute Savoie) von Apt bis Unter-Eozän. Ph.D, Fribourg.

Hay W.W., Soeding E., DeConto R.M. & Wold C.N. 2002. The late Cenozoic uplift - climate change paradox. International Journal of Earth Sciences 91, 746-774.

Heinz R. & Isenschmid C. 1988. Mikrofazielle und stratigrafische Untersuchungen im Massifkalk (Malm) der Préalpes Médianes. Eclogae geologicae Helvetiae 81, 1-62.

Heinz R.A. 1985. Mikrofazielle Untersuchungen des Massifkalks (Malm) der Préalpes Médianes im Querschnitt Moléson Ruebli/Gummfluh. PhD, n° 209, Bern.

Herb R. 1988. Eocaecene Palägeographie und Paläotektonik des Helvetikums. Eclogae geologicae Helvetiae 81, 611-657.

Hobbs W.H. 1904. Lineaments of the Atlantic border region. Geological Society of America Bulletin 15, 483-506.

Homewood P. 1977. Ultrahelvetic and North-Penninic flysch of the Prealps: a general account. Eclogae geologicae Helvetiae 70, 627-641.

Homewood P. & Caron C. 1982. Flysch of the Western Alps. In: Mountain building processes, Academic Press, 157-168.

Homewood P., Allen P.A. & Williams G.D. 1986. Dynamics of the Molasse Basin of western Switzerland. Special Publication of the international Association of sedimentologists 8, 199-217.

Homewood P. 1986. Geodynamics and paleogeography of the western Molasse basin: a review. Giornale di Geologia, ser. 3a 48, 275-284.

Homewood P. & Lateltin O. 1988. Classic Swiss clastics. Flysch and Molasse. The Alpine connection. Acta Geodynamica 2, 1-11.

Homewood P., Rigassi D. & Weidmann M. 1989. Le bassin molassique Suisse. In: Dynamique et méthodes d'étude des bassins sédimentaires, Technip, Paris, 299-314.

Horton B.K. 1999. Erosional control on the geometry and kinematics of thrust belt development in the central Andes. Tectonics 18, 1292-1304.

Hoth S., Kukowski N., Oncken O. & Pfeifer J. 2004. The flysch to molasse transition - Insight from scaled sandbox simulations. Proceedings of the GeoMod2004, Emmetten - Lake Lucerne, 225-229.

HOWARD A.D. 1967. Drainage analysis in geologic interpretation: a summary. American Association of Petroleum Geologists 51, 2246-2259.

HUNZIKER J.C., DESMONS J. & MARTINOTTI G. 1989. Apine thermal evolution in the central and western Alps. COWARD et al, ed., Alpine tectonics Geol. Soc. Spec. Publ., 45, 353-367.

HUNZIKER J.C., DESMONS J. & HURFORD A.J. 1992. Thirty-two years of geochronological work in the Central and Western Alps: a review on seven maps. Mémories de Géologie (Lausanne) 13, 1-52.

HUNZIKER J.C., HURFORD A.J. & CALMBACH L. 1997. Alpine cooling and uplift. In: Deep structure of the Swiss Alps - Results from NRP 20, Birkhäuser AG., Basel, 260-263.

HURFORD A.J. 1986. Cooling and uplift patterns in the Lepontine Alps South Central Switzerland and an age of vertical movement on the Insubric fault line. Contributions to Mineralogy and Petrology 92, 413-427.

JAEGER J.C., COOK, N. G. W. 1976. Fundamentals of Rock Mechanics. John Wiley, New York, pp.

JEANBOURQUIN P. 1988. Nouvelles observations sur les cornieules en Suisse occidentale. Eclogae geologicae Helvetiae 81, 511-538.

JEANBOURQUIN P. & GOY-EGGENBERGER D. 1991. Mélanges suprahelvétiques: sédimentation et tectonique au front de la nappe de Morcles (Vaud, Suisse). Géologie Alpine 67, 43-62.

JEANBOURQUIN P. 1991. Ultrahelvétique et mélanges sur le dos des nappes helvétiques des Diablerets et du Wildhorn. Bulletin de la Société Fribourgeoise des Sciences Naturelles 80, 76-104.

JEANBOURQUIN P., KINDLER P. & DALL'AGNOLO S. 1992. Les mélanges des Préalpes internes entre Arve et Rhône (Alpes occidentales franco-suisses). Eclogae geologicae Helvetiae 85, 59-83.

JEANBOURQUIN P. 1992. Les mélanges suprahelvétiques dans le synclinal de Thônes (Massifs subalpins, Haute-Savoie, France): une nouvelle hypothèse de travail. Archives de physique et des sciences naturelles de Genève 45, 109-126.

JEANBOURQUIN P. 1994. Early deformation of Ultrahelvetic mélanges in the Helvetic nappes (Western Swiss Alps). J. Struct. Geol. 16, 1367-1383.

JEANNET A. 1912-1913. Monographie géologique des Tours d'Aï. 1. Stratigraphie de la nappe rhétique, du Trias et du Lias des Préalpes médianes et de la zone interne. Matériaux pour la Carte Géologique de la Suisse n.s. 32, 1-466.

JEANNET A. 1922. Das romanische Deckengebirge, Préalpes und Klippen. In: Geologie der Schweiz, Tauschniz, Leibzig, 589-676.

JORDAN P. & NÜESCH R. 1989. Deformational behavior of shale interlayers in evaporite detachment horizons, Jura overthrust, Switzerland. Journal of Structural Geology 11, 859-871.

JORDAN P. 1992. Evidence for large scale decoupling in the Triassic evaporites of Northern Switzerland: an overview. Eclogae geologicae Helvetiae 85, 677-69.

JORDI H.A. 1990. Tektonisch-strukturelle Übersicht Westschweizerisches Molassebecken. Bulletin der Vereinigung Schweizerischen Petroleum-Geologen und -Ingenieure 56, 1-11.

JORDI H.A. 1993. Tectonique du bassin molassique et de son substratum jurassique-crétacé dans la région Orbe-Yverdon-Grandson. Bulletin de la Société Vaudoise des Sciences naturelles 82, 279-299.

JOUANNE F., MÉNARD G. & DARMENDRAIL X. 1995. Present-day vertical displacements in the north-western Alps and southern Jura Mountains: Data from leveling comparisons. Tectonics 14, 606-616.

JOUANNE F., GENAUDEAU N., MÉNARD G. & DARMENDRAIL X. 1998. Estimating present-day displacement fields and tectonic deformation in active mountain belts: an example from the Chartreuse Massif and the southern Jura Mountains, western Alps. Tectonophysics 296, 403-419.

KAELIN D. 1997. Litho- und Biostratigraphie der mittel- bis obermiozänen Bois de Raube-Formation (Nordwestschweiz). Eclogae geologicae Helvetiae 90, 97-114.

KASTRUP U. 2002. Seismotectonics and stress field variations in Switzerland. Swiss Federal Institute of Technology Zurich, Zurich.

KEMPF O. & PFIFFNER O.A. 2004. Early Tertiary evolution of the north Alpine Foreland Basin of the Swiss Alps and adjoining areas. Basin Research 16, 549-567.

KIM G.-B., LEE, J.-Y. & LEE K.-K. 2004. Construction of lineament maps related to groundwater occurence with ArcView and AvenueTM scripts. Computers & Geosciences 30, 1117-1126.

KONSTANTINOVSKAIA E. & MALAVIEILLE J. 2005. Erosion and exhumation in accretionary orogens: Experimental and geological approaches. Geochemistry, Geophysics, Geosystems 6, 1-25.

KOOI H. & BEAUMONT C. 1996. Large-scale geomorphology: Classical concepts reconciled and integrated with contemporary ideas via a surface process model. Journal of Geophysical Research B, solid earth and planets 101, 3361-3386.

KUHLEMANN J. 2000. Post-collisional sediment budget of circum-Alpine basins (Central Europe). Mem. Soc. Geol. Padova 52, 1-91.

KUHLEMANN J., FRISCH W., DUNKL I. & SZÉKELY B. 2001. Quantifying tectonic versus erosive denudation by the sediment budget: the Miocene core complexes of the Alps. Tectonophysics 330, 1-23.

KUHLEMANN J., FRISCH W., SZÉKELY B. & DUNKL I. 2002. Post-collisional sediment budget history of the Alps: tectonic versus climatic control. International Journal of Earth Sciences 91, 818-837.

KUHLEMANN J. & KEMPF O. 2002. Post-Eocene evolution of the north Alpine Foreland Basin and its response to

Alpine tectonics. Sedimentary Geology 152, 45-78.

Kühni A. & Pfiffner O.A. 2001. Drainage patterns and tectonic forcing: a model study for the Swiss Alps. Basin Research 13, 169-197.

Kukowski N., Lallemand S., Malavieille J., Gutscher M.-A. & Reston T.J. 2002. Mechanical decoupling and basal duplex formation observed in sandbox experiments with application to the Mediterranean Ridge accretionary complex. Marine Geology 186, 29-42.

Lacombe O. & Mouthereau F. 2002. Basement-involved shortening and deep detachment tectonics in forelands of orogens: Insights from recent collision belts (Taiwan, Western Alps, Pyrenees). Tectonics 21, 1-22.

Lallemand S., Schnurle P. & Malavieille J. 1994. Coulomb theory applied to accretionary and non-accretionary wedges - Possible causes for tectonic erosion and/or frontal accretion. Journal of Geophysical Research 99, 12033-12055.

Laubscher H.P. 1973. Jura Mountains. In: Gravity and Tectonics, Wiley, New York, 217-227.

Laubscher H.P. 1987. Die tektonische Entwicklung der Nordschweiz. Eclogae geologicae Helvetiae 80, 287-303.

Laubscher H.P. 1992. Jura kinematics and the Molasse basin. Eclogae geologicae Helvetiae 85, 653-676.

Lemoine M. 1984. La marge occidentale de la Téthys ligure et les Alpes occidentales. In: Les marges continentales actuelles et fossiles autour de la France, Masson, Paris, 155-248.

Lempicka Münch A. & Masson H. 1993. Dépôts d'âge tertiaire de la nappe ultrahelvétique du Sex Mort entre la Simme et Adelboden (Préalpes). Bulletin de la Société Vaudoise des Sciences Naturelles 82, 369-389.

Lihou J.C. & Allen P.A. 1996. Importance of inherited rift margin structures in the early north Alpine foreland basin, Switzerland. Basin research 8, 425-442.

Lihou J.C. 1996. Stratigraphy and sedimentology of the Sardona unit, Glarus Alps: Upper Crteaceous/middle Eocene deep marine flysch sediments from the Ultrahelvetic realm. Eclogae geologicae Helvetiae 89, 721-752.

Liu H., McClay K.R. & Powell D. 1992. Physical models of thrust wedges. In: Thrust Tectonics, Chapman & Hall, 71-81.

Lohrmann J., Kukowski N., Adam J. & Oncken O. 2003. The impact of analogue material properties on the geometry, kinematics and dynamics of convergent sand wedges. Journal of Structural Geology 25, 1691-1711.

Loup B. 1992. Evolution de la partie septentrionale du domaine helvétique en Suisse occidentale au Trias et au Lias: contrôle par subsidence thermique et variations du niveau marin. PhD. Thesis. Publ. Dept. Géol. Paléont. (Genève) 12.

Lugeon M. & Gagnebin E. 1941. Observations et vues nouvelles sur la géologie des Préalpes romandes. Bulletin du Laboratoire de Géologie de l'Université de Lausanne 72, 1-90.

Malavieille J. 1984. Modélisation expérimentale des chevauchements imbriqués: application aux chaînes de montagnes. Bulletin de la Société géologique de France 26, 129-138.

Marescot L. 2000. La Molasse de la région de la Sense. Diploma, Fribourg.

Martini R., Girod F. & Zaninetti L. 1998. Découverte de foraminifères et confirmation de l'âge Norien et Rhétien du Trias des Préalpes Médianes Plastiques (Massif des Cornettes de Bise, Préalpes du Chablais, Suisse et France). Eclogae geologicae Helvetiae 91, 69-74.

Masson H. 1972. Sur l'origine de la cornieule par fracturation hydraulique. Eclogae geologicae Helvetiae 65, 27-41.

Masson H. 1976. Un siècle de géologie dans des Préalpes: de la découverte des nappes à la recherche de leur dynamique. Eclogae geologicae Helvetiae 69, 527-575.

Mattauer M. 1986. Intracontinental subduction, crust-mantle décollement and crustal-stacking wedge in the Himalayas and other collision belts. Geological Society of London, Special Publication 19, 37-50.

Matter A., Homewood P., Caron C., Rigassi D., van Stuijvenberg J., Weidmann M. & Winkler W. 1980. Flysch and Molasse of Western and Central Switzerland. In: Geology of Switzerland, Wepf, Basel, 261-293.

Mercier J., Vergely, P. 1992. Tectonique. Dunod, Paris, 214 pp.

Mettraux M. 1989. Sédimentologie, paléotectonique et paléoocéanographie des Préalpes Médianes (Suisse Romande) du Rhétien au Toarcien. PhD, n° 947, Fribourg.

Mettraux M. & Mohr B. 1989. Stratigraphy of Triassic/Jurassic boundary in the Préalpes médianes nappe: facies and palynology. Eclogae geologicae Helvetiae 82, 743-763.

Mettraux M. & Mosar J. 1989. Tectonique alpine et paléotectonique liasique dans les Préalpes Médianes en rive gauche du Rhône. Eclogae geologicae Helvetiae 82, 517-540.

Molnar P. & Lyon-Caen H. 1988. Some simple physical aspects of the support, structure, and evolution of mountain belts. Geological Society of America Special Paper 179-207.

Mosar J. 1988a. Métamorphisme transporté dans les Préalpes. Schweizerische Mineralogische und Petrographische Mitteilungen 68, 77-94.

Mosar J. 1988b. Structures, déformation et métamorphisme dans les Préalpes Romandes (Suisse). PhD, Neuchâtel.

Mosar J. 1989. Déformation interne dans les Préalpes Médianes (Suisse). Eclogae geologicae Helvetiae 82, 765-793.

MOSAR J. 1991. Géologie structurale dans les Préalpes médianes (Suisse). Eclogae geologicae Helvetiae 84, 689-725.

MOSAR J. & BOREL G. 1992. Paleostress from the Préalpes Médianes (Switzerland). Annales Tectonicae 6, 115-133.

MOSAR J. & BOREL G. 1993. Le pli de Malatraix: fiction ou réalité. Bulletin de la Société Vaudoise des Sciences Naturelles 82, 319-343.

MOSAR J. 1994. Géologie structurale à l'est de Montreux (Préalpes médianes plastiques, Suisse). Eclogae geologicae Helvetiae 87, 11-32.

MOSAR J., STAMPFLI G.M. & GIROD F. 1996. Western Préalpes médianes: timing and structure. A review. Eclogae geologica Helvetiae 89, 389-425.

MOSAR J. 1997. Folds and thrust in the Préalpes Médianes plastiques romandes. Bulletin de la Société Vaudoise des Sciences naturelles 84, 347-384.

MOSAR J. 1999. Present-day and future tectonic underplating in the Western SwissAlps: reconciliation of basement/ wrench-faulting and décollement folding of the Jura and Molasse Basin in the Alpine foreland. Earth and planetary Science Letters 173, 143-145.

MUGNIER J.-L., GUELLEC S., MÉNARD G., ROURE F., TARDY M. & VIALON P. 1990. Crustal balanced cross-sections through the external Alps deduced from the Ecors profile. In: Deep structure of the Alps, 203-216.

MÜLLER I. & PLANCHEREL R. 1982. Contribution à l'étude de l'hydrogéologie karstique du massif du Vanil Noir et de la chaîne des Gastlosen (Préalpes fribourgeoises, Suisse). Bulletin de la Société Fribourgeoise des Sciences Naturelles 71, 102-132.

MÜLLER M., NIEBERDING F. & WANNINGER A. 1988. Tectonic style and pressure distribution at the northern margin of the Alps between Lake Constance and the River Inn. Geologische Rundschau 77, 787-796.

MULUGETA G. 1988. Modelling the geometry of Coulomb thrust wedges. Journal of Structural Geology 10, 847-859.

MURALT R., VUATAZ F.D., SCHÖNBORN G., SOMMARUGA A. & JENNY J. 1997. Intégration des méthodes hydrochimiques, géologiques et géophysiques pour la prospection d'une nouvelle ressource en eau thermale. Cas d'Yverdon les Bains, pied du Jura. Eclogae geologicae Helvetiae 90, 179-197.

NAEF H., DIEBOLD P. & SCHLANKE S. 1985. Sedimentation und Tektonik im Tertiär der Nordschweiz.

NAYLOR M.A., MANDL, G., SIJPESTEIJN, C. H. K. 1986. Fault geometries in basement-induced wrench faulting under different initial stress states. Journal of Structural Geology 8, 737-752.

NICOLAS A. 1984. Principes de Tectonique. Masson éd., Paris, 196 pp.

ORTNER H., REITER F. & ACS P. 2002. Easy handling of tectonic data: the programs TectonicsVB for Mac and TectonicsFP for Windows. Computers & Geosciences 28, 1193-1200.

ORTNER H., REITER, F., ACS, P. 2002. Easy handling of tectonic data: the programs TectonicVB for Mac and TectonicsFP for Windows. Computers & Geosciences 28, 1193-1200.

PAVONI N. 1961. Faltung durch Horizontalverschiebung. Eclogae geologicae Helvetiae 54, 515-534.

PERESSON H. 1992. Computer aided kinematic analysis of fault sets. Mitteilungen der Gesellschaft für Geologie und Bergbaustudien 38, 107-119.

PERSSON K.S. & SOKOUTIS D. 2002. Analogue models of orogenic wedges controlled by erosion. Tectonophysics 356, 323-336.

PETERHANS E. 1926. Etude du Lias et des géanticlinaux des Préalpes médianes entre la vallée du Rhône et le lac d'Annecy. Mémoires de la Société Helvétique des Sciences Naturelles 69, 191-344.

PFIFFNER O.A. 1986. Evolution of the north Alpine foreland basin in the Central Alps. Special Publication of the international Association of sedimentologists 8, 219-228.

PFIFFNER O.A., FREI W., VALASEK P., STÄUBLE M., LEVATO L., DUBOIS L., SCHMID S.M. & SMITHON S.B. 1990. Crustal shortening in the alpine orogen: results from deep seismic reflection profiling in the eastern swiss Alps line NFP 20-east. Tectonics 9, 1327-1355.

PFIFFNER O.A. 1994. Structure and evolution of the Swiss Molasse Basin in the transect Aar Massif-Bern-Central Jura. Géologie Alpine 4, 85.

PFIFFNER O.A., HEITZMANN P., LEHNER P., FREI W., PUGIN A. & FELBER M. 1997b. Incision and backfilling of Alpine valleys: Pliocene, Pleistocene and Holocene processes. In: Deep structure of the Swiss Alps - Results from NRP 20, Birkhäuser AG., Basel, 265-288.

PFIFFNER O.A., ERARD P.-F. & STÄUBLE M. 1997c. Two cross-sections through the Swiss Molasse Basin (lines E4-E6, W1, W7-W10). In: Deep structure of the Swiss Alps - Results from NRP 20, Birkhäuser AG., Basel, 64-72.

PFIFFNER O.A., ERARD P.-F. & STÄUBLE M. 1997d. Two cross sections through the Swiss Molasse basin (lines E4-E6, W1, W7-W10). In: Deep structure of the Swiss Alps - Results from NRP 20, Birkhäuser AG., Basel, 64-72.

PFIFFNER O.A., ELLIS S. & BEAUMONT C. 2000. Collision tectonics in the Swiss Alps: Insight from geodynamic modeling. Tectonics 19, 1065-1094.

PFIFFNER O.A., SCHLUNEGGER F. & BUITER S.J.H. 2002. The Swiss Alps and their peripheral foreland basin: Stratigraphic response to deep crustal processes. Tectonics 21, 1-15.

PHILIPPE Y., COLETTA B., DEVILLE E. & MASCLE A. 1996. The Jura fold-and-thrust belt: a kinematic model based on map-balancing. In: Peri-Tethys Memoir 2: Structure and Prospects of Alpine Basins and Forelands, Mémoire du Muséum national d'Histoire naturelle, Paris, 235-261.

Plancherel R. 1979. Aspects de la déformation en grand dans les Préalpes médianes plastiques entre Rhône et Aar. Eclogae geologicae Helvetiae 72, 145-214.

Plancherel R. 1990. Les Préalpes du Chablais - Présentation générale. In: Suisse Lémanique pays de Genève et Chablais. Guides Géologiques Régionaux, Masson, 183-190.

Platt J.P. 1986. Dynamics of orogenic wedges and the uplift of high-pressure metamorphic rocks. Geological Society of America Bulletin 97, 1037-1053.

Price N.J. & Cosgrove J.W. 1990. Analysis of geological structures. Cambridge University Press, Cambridge, 502 pp.

Price R.A. 1973. Large-scale gravitational flow of supracrustal rocks, southern Canadian Rockies. In: Gravity and tectonics, Wiley and Sons, New York, 491-502.

Ramsay J.G., Huber, I.M. 1987. The techniques of modern structural geology. Academic Press, pp.

Ramsay J.G., Lisle, R. J. 2000. The techniques of modern structural geology. Academic Press, 1061 pp.

Riedel W. 1929. Zur Mechanik geologischer Brucherscheinungen. Centralblatt für Mineralogie, Geologie und Paläontologie 1929B, 354-368.

Rigassi D.A. 1962. A propos de la tectonique du Risoux (Jura vaudois et franc-comtois). Bulletin der Vereinigung Schweizerischen Petroleum-Geologen und -Ingenieure 29, 39-50.

Ringenbach J.-C., Pinet, N., Delteil, J. & Stephan, J.-F. 1992. Analyse des structures engendrées en régime décrochant par le séisme de Nueva Ecija du 16 juillet 1990, Luzon, Philippines. Bulletin de la Société géologique de France 163, 109-123.

Sartori M. 1987. Blocs basculés briançonnais en relation avec leur socle originel dans la nappe de Siviez-Mischabel (Valais, Suisse). Comptes Rendus de l'Académie des Sciences de Paris, Série II 305, 999-1005.

Saudan C. & Mosar J. 2006. Fractures and tectonics in the Prealpes Medianes: Chablais, Switzerland. Eclogae geologicae Helvetiae Submitted.

Schaer J.P., Reimer G.M. & Wagner G.A. 1975. Actual and ancient uplift rate in the Gotthard region, Swiss Alps: a comparison between precise levelling and fission track apatite age. Tectonophysics 29, 293-300.

Schardt H. 1893. Coup d'oeil sur la structure géologique des environs de Montreux. Bulletin de la Société Vaudoise des Sciences Naturelles 29, 241-255.

Schegg R. 1994. The Coalification Profile of the Well Weggis (Subalpine Molasse, Central Switzerland): Implications for Erosion Estimates and the Paleogeothermal Regime in the External Part of the Alps. Bulletin der Vereinigung schweizer Petroleum-Geologen und -Ingenieure 61, 57-67.

Schegg R., Leu W., Cornford C. & Allen P.A. 1997. New coalification profiles in the Molasse Basin of Western Switzerland: Implications for the thermal and geodynamic evolution of the Alpine Foreland. Eclogae geologicae Helvetiae 90, 79-96.

Schegg R. & Leu W. 1998. Analysis of erosion events and palaeogeothermal gradients in the North Alpine Foreland Basin of Switzerland. Geological Society of London, Special Publication 141, 137-155.

Scheidhauer M., Marillier F. & Thierry P. 2005. Detailed 3D seismic imaging of a fault zone beneath Lake Geneva, Switzerland. Basin Research 17, 155-169.

Schlunegger F., Jordan T.E. & Klaper E. 1997a. Controls of erosional denudation in the orogen on foreland basin evolution: the Oligocene central Swiss Molasse Basin as an example. Tectonics 16, 823-840.

Schlunegger F., Matter A., Burbank D.W. & Klaper E.M. 1997b. Magnetostratigraphic contraints on relationships between evolution of the central Swiss Molasse basin and Alpine orogenic events. Geological Society of America Bulletin 109, 225-241.

Schlunegger F., Leu W. & Matter A. 1997c. Sedimentary sequences, seismic facies, subsidence analysis, and evolution of the Burdigalian Upper Marine Molasse group, Central Switzerland. Bulletin of American Association of Petrol. Geol. 81, 1185-1207.

Schlunegger F., Slingerland R. & Matter A. 1998. Crustal thickening and crustal extension as controls on the evolution of the drainage network of the central Swiss Alps between 30 Ma and the present: constraints from the stratigraphy of the North Alpine Foreland Basin and the structural evolution of the Alps. Basin Research 10, 197-212.

Schlunegger F. 1999. Controls of surface erosion on the evolution of the Alps: constraints from the stratigraphies of the adjacent foreland basins. International Journal of Earth Sciences 88, 285-304.

Schlunegger F., Melzer J. & Tucker G. 2001. Climate, exposed source rock lithologies, crustal uplift and surface erosion-a theoretical analysis calibrated with data from the Alps/North Alpine Foreland Basin system. International Journal of Earth Sciences 90, 484-499.

Schlunegger F. & Hinderer M. 2001. Crustal uplift in the Alps: why the drainage pattern matters. Terra Nova 13, 425-432.

Schlunegger F. & Hinderer M. 2003. Pleistocene/Holocene climate change, re-establishment of fluvial drainage network and increase in relief in the Swiss Alps. Terra Nova 15, 88-95.

Schmid S.M., Pfiffner A.O., Froitzheim N., Schönborn G. & Kissling E. 1996. Geophysical-geological transect and tectonic evolution of the Swiss-Italian Alps. Tectonics 15, 1036-1064.

Schmid S.M., Fügenschuh B., Kissling E. & Schuster R. 2004. Tectonic map and overall architecture of the Alpine orogen. Eclogae geologicae Helvetiae 97, 93-117.

Septfontaine M. 1983. Le Dogger des Préalpes médianes suisses et françaises (Stratigraphie, évolution paléogéographique et paléotectonique). Mémoires de la Société Helvétique des Sciences Naturelles 97, 1-121.

Septfontaine M. 1995. Large scale progressive unconformities in Jurassic strata of the Préalpes S of lake Geneva: interpretation as synsedimentary inversion structures, Paleotectonic implications. Eclogae geologicae Helvetiae 88, 553-576.

Signer C. 1992. Interprétation sismique structurale et sismostratigraphique entre Jura et front alpin dans la région genevoise. Diplôme, Genève.

Signer C. & Gorin G.E. 1995. New geological observations between the Jura and the Alps in the Geneva area, as derived from reflection seismic data. Eclogae geologicae Helvetiae 88, 235-265.

Simoes M., Avouac J.-P., Beyssac O., Goffé B., Farley K. & Chen Y.-G. 2006. Mountain-building in Taiwan: a thermo-kinematic model. Journal of Geophysical Research In press.

Simpson G.D.H. 2006. Modelling interactions between fold-thrust belt deformation, foreland flexure and surface mass transport. Basin Research 18, 125-143.

Sinclair H.D., Coakley B.J., Allan P.A. & Watts A.B. 1991. Simulation of foreland basin stratigraphy using a diffusion model of mountain belt uplift and erosion: an example from the Central Alps, Switzerland. Tectonics 10, 599-620.

Sinclair H.D. 1997a. Flysch to molasse transition in peripheral foreland basins: The role of the passive margin versus slab breakoff. Geology 25, 1123-1126.

Sinclair H.D. 1997b. Tectonostratigraphic model for underfilled peripheral foreland basins: an Alpine perpspective. Geological Society of America Bulletin 109, 324-346.

Sissingh W. 1997. Tectonostratigraphy of the North Alpine Foreland Basin: correlation of tertiary depositional cycles and orogenic phases. Tectonophysics 282, 223-256.

Sissingh W. 2006a. Kinematic sequence stratigraphy of the European Cenozoic Rift System and Alpine Foreland Basin: correlation with Mediterranean and Atlantic plate-boundary events. Netherlands Journal of Geosciences 85, 77-129.

Sissingh W. 2006b. Syn-kinematic palaeogeographic evolution of the West European Platform: correlation with Alpine plate collision and foreland deformation. Netherlands Journal of Geosciences 85, 131-180.

Smit J.H.W., Brun J.P. & Sokoutis D. 2003. Deformation of brittle-ductile thrust wedges in experiments and nature. Journal of Geophysical Research 108, 1-17.

Sommaruga A. 1997. Geology of the Central Jura and the Molasse Basin: new insight into an evaporite-based foreland fold and thrust belt. Mémoire de la société neuchâteloise des sciences naturelles 12, 176.

Sommaruga A. 1999. Décollement tectonics in the Jura foreland fold-and-thrust belt. Marine and Petroleum Geology 16, 111-134.

Spicher J.P. 1966. Géologie des Préalpes médianes dans le Massif des Bruns, partie occidentale. Eclogae geologicae Helvetiae 58, 591-742.

Spoorenberg J. 1952. Les Préalpes médianes au NW de Château-d'Oex. PhD, Fribourg.

Stampfli G. & Marthaler M. 1990a. Divergent and convergent margins in the North-Western alps. Confrontation to actualistic models. Geodinamica Acta 4, 159-184.

Stampfli G.M. & Marthaler M. 1990b. Divergent and convergent margins in the North-Western Alps confrontation to actualistic models. Geodinamica Acta 4, 159-184.

Stampfli G.M., Marcoux J. & Baud A. 1991. Tethyan margins in space and time. Palaeogeography, Palaeoecolology, Palaeoclimatology 87, 373-409.

Stampfli G.M., Mosar J., Marquer D. & Marchant R. 1997. Subduction and obduction processes in the Swiss Alps. Proceedings of the 3rd workshop on Alpine Geological Studies, Oropa-Biella, 125.

Stampfli G.M., Marchant R. & Mosar J. 1998a. Obduction and subduction in the Western Alps. Proceedings of the Geological dynamics of Alpine type mountain belts ancient and modern, Bern, 74-75.

Stampfli G.M., Mosar J., Marchant R., Marquer D., Baudin T. & Borel G. 1998b. Subduction and obduction processes in the Swiss Alps. Tectonophysics 296, 159-204.

Stampfli G.M., Mosar J., Marchant R. & Borel G. 2001. The geodynamic framework of the western Alps: The Alpine cycle. Mémoires de Géologie (Lausanne) 36 - Geology of the western Swiss Alps, a guide book, 9-26.

Steck A. & Hunziker J. 1994. The Tertiary structural and thermal evolution of the Central Alps - compressional and extensional structures in an orogenic belt. Tectonophysics 238, 229-254.

Storti F. & MacClay K.R. 1995. Influence of syntectonic sedimentation on thrust wedges in analogue models. Geology 23, 999-1002.

Suppe J. & Medwedeff D.A. 1990. Geometry and kinematics of fault-propagation folding. Eclogae geologicae Helvetiae 83, 409-454.

Sylvester A.G. 1988. Strike-slip faults. Geological Society of America Bulletin 100, 1666-1703.

Tchalenko J.S. 1970. Similarities between Shear Zones of Different Magnitudes. Geological Society of America Bulletin 81, 1625-1640.

Teufel L.W. 1980. Strain analysis of experimenta superposed deformation using calcite twin lamellae. Tectonophysics 65, 291-309.

Trümpy R. 1960. Paleotectonic evolution of the Central and Western Alps. Geological Society of America Bulletin 71, 843-908.

Trümpy R. 1973. The timing of orogenic events in the Central Alps. In: Gravity and Tectonics, London, 229-251.

Trümpy R. 1980. Geology of Switzerland: a guide-book. Wepf. and Co., pp.

Turcotte D.L. & Schubert G. 1982. Geodynamics: Application of continuum mechanics to geological problems.

New York, 450 pp.

VALLEY B., BURKHARD M. & SCHNEGG P.-A. 2004. Dépliage 3-D des anticlinaux bordant le synclinal fermé de la vallée des Ponts, Jura central, Suisse. Eclogae geologicae Helvetiae 97, 279-291.

VIALON P., RUHLAND, M., GROLIER, J. 1976. Eléments de tectonique analytique. Masson, Paris, 118 pp.

VON BLANCKENBURG F. & DAVIES J.H. 1995. Slab breakoff: a model for syncollisional magmatism and tectonics in the Alps. Tectonics 14, 120-131.

WEGMANN E. 1963. Le Jura plissé dans la perspective des études sur le comportement des socles. In: Livre Mém. Prof. P. Fallot, Paris, 99-104.

WEIDMANN M., HOMEWOOD P., CARON C. & BAUD A. 1976. Réhabilitation de la "Zone Submédiane" des Préalpes. Eclogae geologicae Helvetiae 69, 265-277.

WENGER R. 1984. Synthèse sur les cavités de la Dent de Ly, FR. Stalactite 34, 8-28.

WILCOX R.E., HARDING, T.P., SEELY, D.R. 1973. Basic Wrench Tectonics. American Association of Petroleum Geologists Bulletin 57, 74-96.

WILDI W., FUNK H.P., LOUP B., AMATO E. & HUGGENBERGER P. 1989a. Mesozoic subsidence history of the European marginal shelves of alpine Tethys (Helvetic realm, Swiss Plateau and Jura). Eclogae geologicae Helvetiae 82, 817-840.

WILDI W., FUNK H., LOUP B., AMATO E. & HUGGENBERGER P. 1989b. Mesozoic subsidence history of the European marginal shelves of the Alpine Tethys (Helvetic realm, Swiss Plateau and Jura). Eclogae geologicae Helvetiae 82, 817-840.

WILDI W., BLONDEL T., CHAROLLAIS J., JAQUET J. & WERNLI R. 1991. Tectonique en rampe latérale à la terminaison occidentale de la Haute Chaîne du Jura. Eclogae geologicae Helvetiae 84, 265-277.

WILDI W. & HUGGENBERGER P. 1993. Reconstitution de la plate-forme européenne anté-orogénique de la Bresse aux Chaînes subalpines: éléments de cinématique alpine (France et Suisse occidentale). Eclogae geologicae Helvetiae 86, 47-64.

WILLETT S.D. 1992. Dynamic growth and change of a Coulomb wedge. In: Thrust Tectonics, Chapman & Hall, 19-31.

WILLETT S.D., BEAUMONT C. & FULLSACK P. 1993. Mechanical model for the tectonics of doubly-vergent compressional orogens. Geology 21, 371-374.

WILLETT S.D. & BRANDON M.T. 2002. On steady states in mountain belts. Geology 2, 175-178.

WISSING S.B. & PFIFFNER O.A. 2002. Structure of the eastern Klippen nappe (BE, FR): Implications for its Alpine tectonic evolution. Eclogae geologicae Helvetiae 95, 381-398.

ZIEGLER P.A. 1982. Geological Atlas of Western and Central Europe. Shell Internationale Petroleum Maatschappij B.V., The Hague, 130 pp.

*****

APPENDICES

APPENDIX 1

The three pictures illustrate the sandbox device and the experimental procedure. Erosion is performed manually with a vacuum cleaner and sedimentation consists in the deposit of sprinkled sand as successive layers.

SANDBOX DEVICE

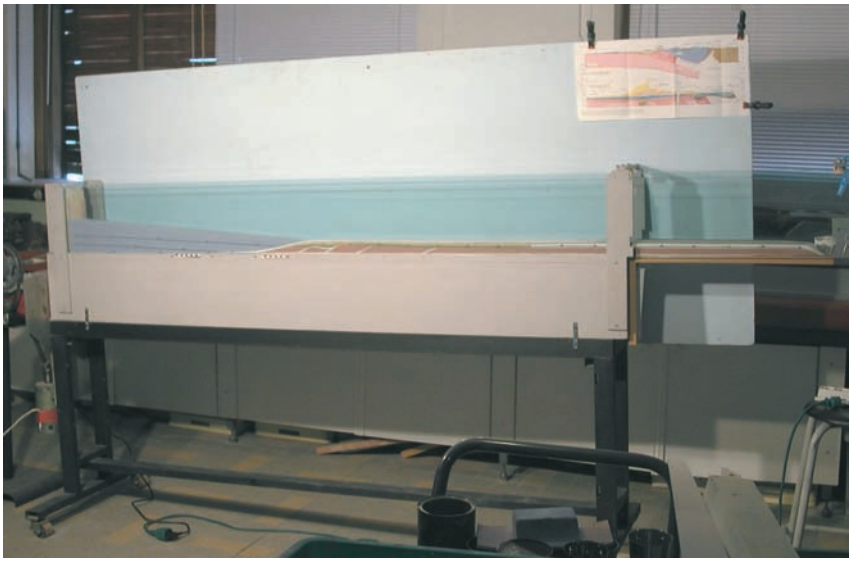

EROSION

SEDIMENTATION

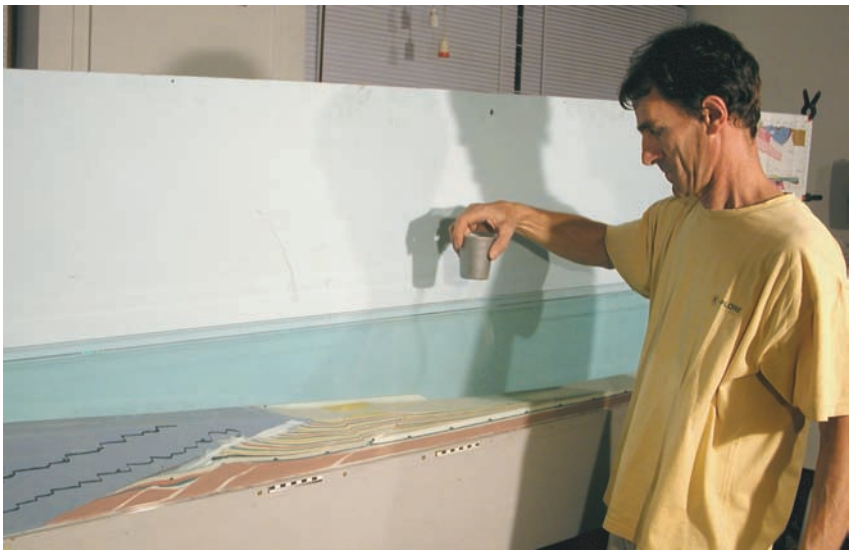

APPENDIX 2

Descriptive plates of the 17 experiments performed in the framework of the analogue modelling study (labelled experiments 31 to 47): technical characteristics, initial and final stages pictures are given and when available, initial stage setup schemes and intermediate stages of development.

EXPERIMENT 31

Subduction window	0.5 cm
Machine length	200 cm
Wedge surface slope α	4°
Wedge basal slope β	2°
Total shortening	no measure
Erosion	no
Sedimentation	no
Others	Same material for the basement units and the orogenic wedge

Initial stage picture

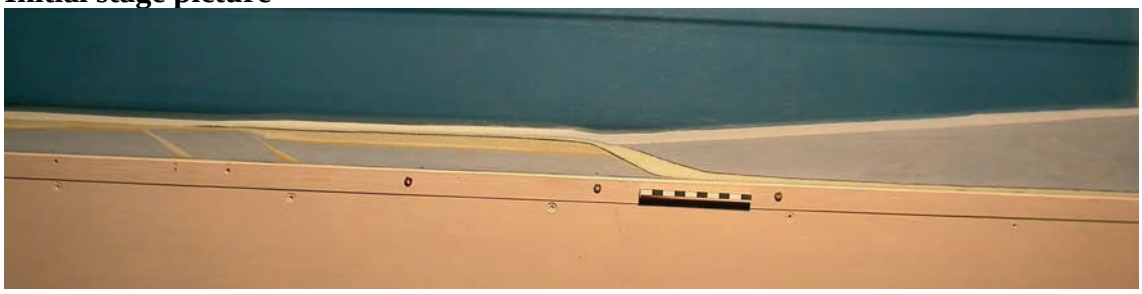

Final stage picture

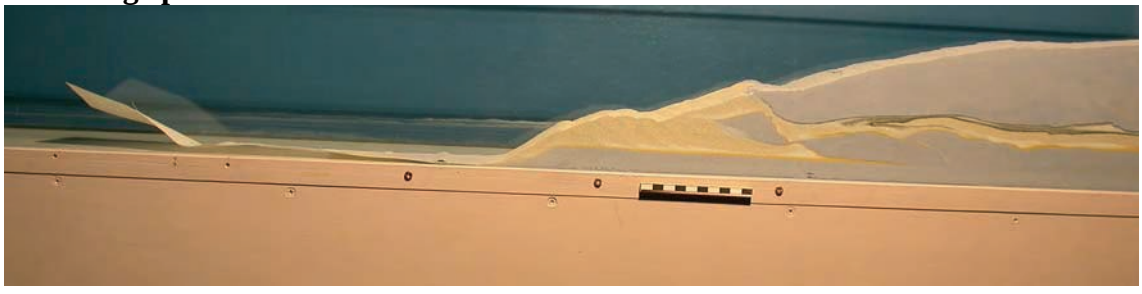

EXPERIMENT 32

Subduction window	0.5 cm
Machine length	200 cm
Wedge surface slope α	5°
Wedge basal slope β	1°
Total shortening	105 cm
Erosion	very low
Sedimentation	low
Others	Same material for the basement units and the orogenic wedge

Initial stage picture

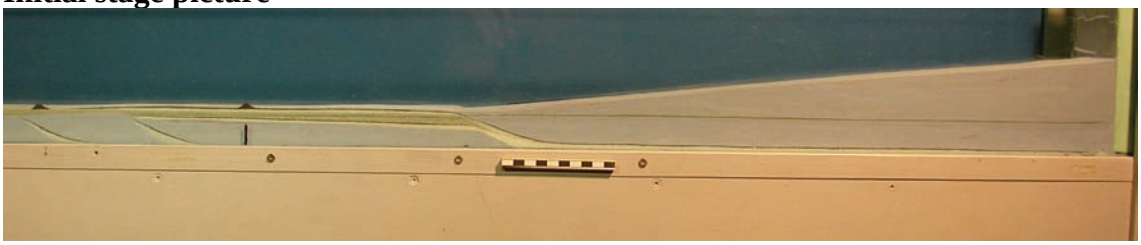

Final stage picture

Stages

	Photographies		
Racc. (cm)	Pas d'action	Erosion	Sédim.
0	0666		
5	0667		
10	0668		
15	0669	0670	0670
20	0671	0672	0672
25	0673	0674	0674
30	0675	0676	0676
35	0677	0678	0678
40	0679	0680	0680
45	0681	0682	0682
50	0683	0684	0684
55	0685	0686	0686
60	0687		
65	0688	0689	0689
70	0690	0691	0691
75	0692	0693	0693
80	0694	0695	0695
85	0696	0697	0697
90	0698 - 0699	0700	0700
95	0701	0702	0702
100	0703	0704	0704
105	0705		

EXPERIMENT 33

Subduction window	no
Machine length	200 cm
Wedge surface slope α	5.5°
Wedge basal slope β	0.5°
Total shortening	120 cm
Erosion	no
Sedimentation	no
Others	Same material for the basement units and the orogenic wedge

Initial stage picture

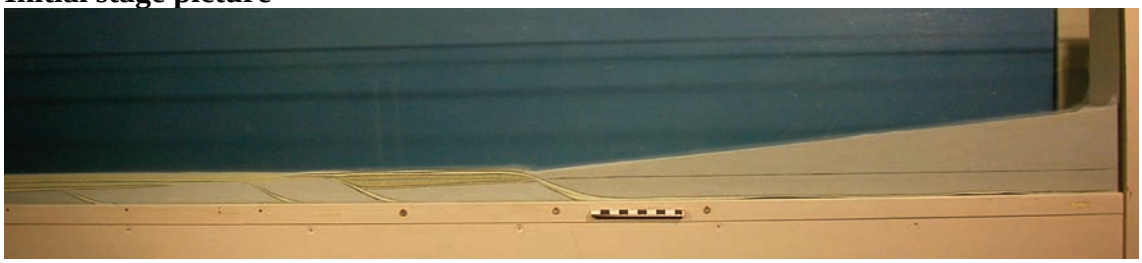

Final stage picture

EXPERIMENT 34

Subduction window	no
Machine length	200 cm
Wedge surface slope α	3°
Wedge basal slope β	5°
Total shortening	94 cm
Erosion	no
Sedimentation	no
Others	Same material for the basement units and the orogenic wedge

Initial stage picture

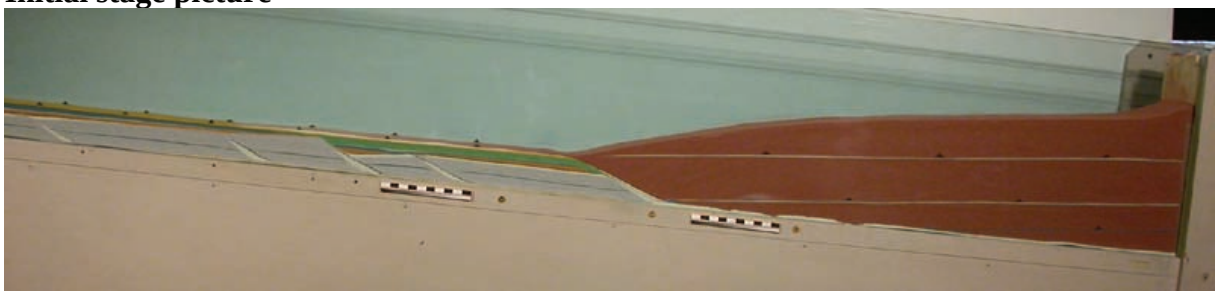

Final stage picture

EXPERIMENT 35

Subduction window	no
Machine length	200 cm
Wedge surface slope α	2°
Wedge basal slope β	3°
Total shortening	88 cm
Erosion	no
Sedimentation	no
Others	Same material for the basement units and the orogenic wedge

Initial stage picture

Final stage picture

EXPERIMENT 36

Subduction window	no
Machine length	200 cm
Wedge surface slope α	2°
Wedge basal slope β	3°
Total shortening	98 cm
Erosion	no
Sedimentation	no
Others	Same material for the basement units and the orogenic wedge

Initial stage picture

Final stage picture

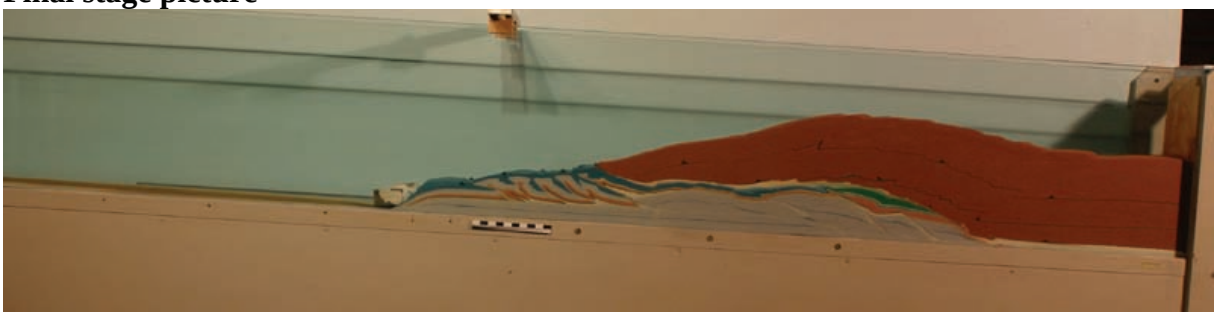

EXPERIMENT 37

Subduction window	no
Machine length	280 cm
Wedge surface slope α	2°
Wedge basal slope β	3°
Total shortening	143.5 cm
Erosion	no
Sedimentation	no
Others	Same material for the basement units and the orogenic wedge

Initial stage picture

Final stage picture

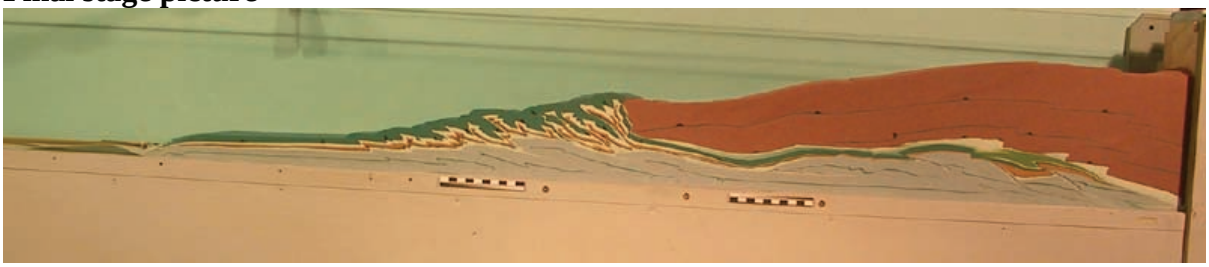

EXPERIMENT 38

Subduction window	no
Machine length	280 cm
Wedge surface slope α	2°
Wedge basal slope β	3°
Total shortening	123 cm
Erosion	no
Sedimentation	no
Others	

Initial stage picture

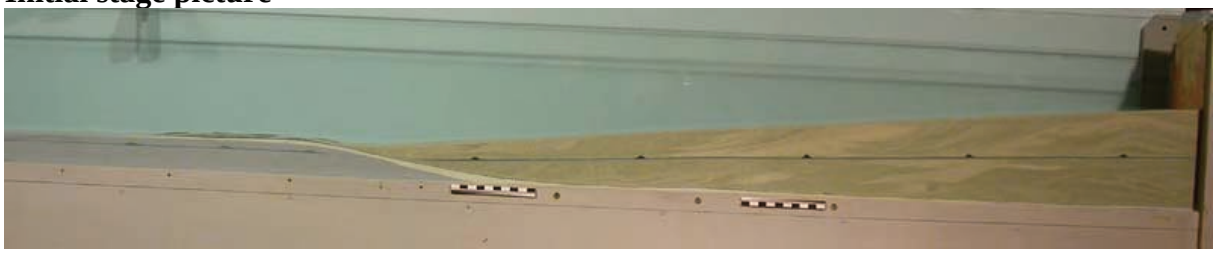

Final stage picture

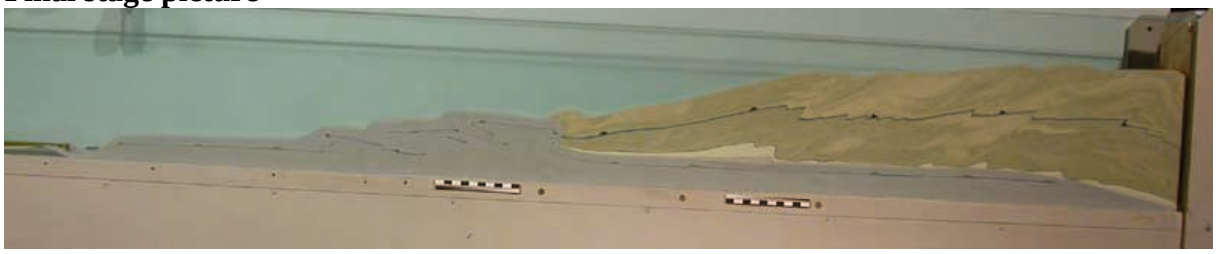

Initial stage scheme

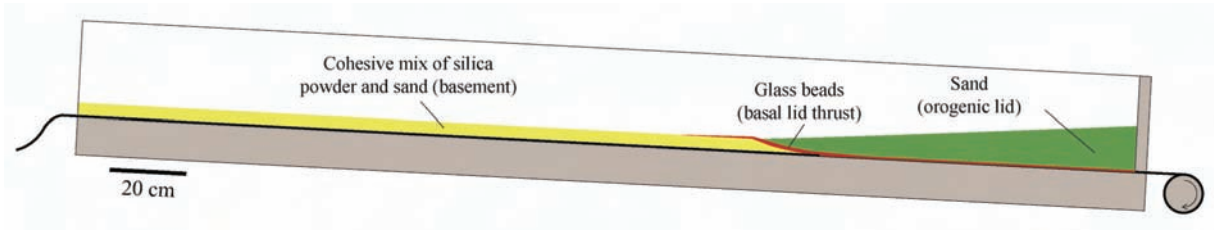

EXPERIMENT 39

Subduction window	no
Machine length	280 cm
Wedge surface slope α	2°
Wedge basal slope β	3°
Total shortening	124 cm
Erosion	no
Sedimentation	no
Others	

Initial stage picture

Final stage picture

Initial stage scheme

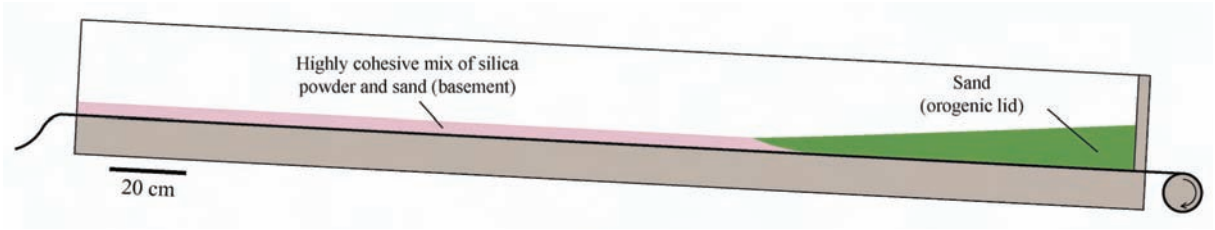

EXPERIMENT 40

Subduction window	no
Machine length	280 cm
Wedge surface slope α	2°
Wedge basal slope β	3°
Total shortening	124 cm
Erosion	no
Sedimentation	no
Others	

Initial stage picture

Final stage picture

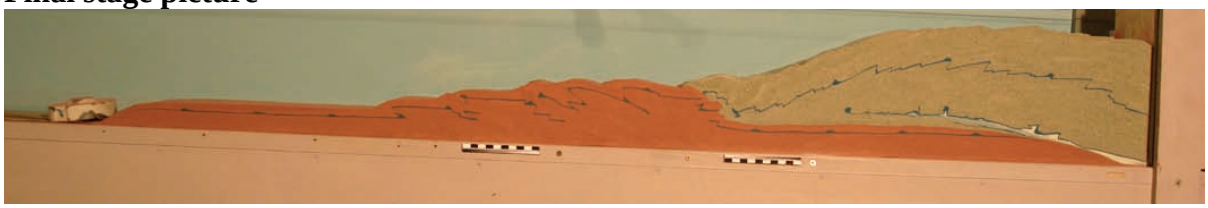

Initial stage scheme

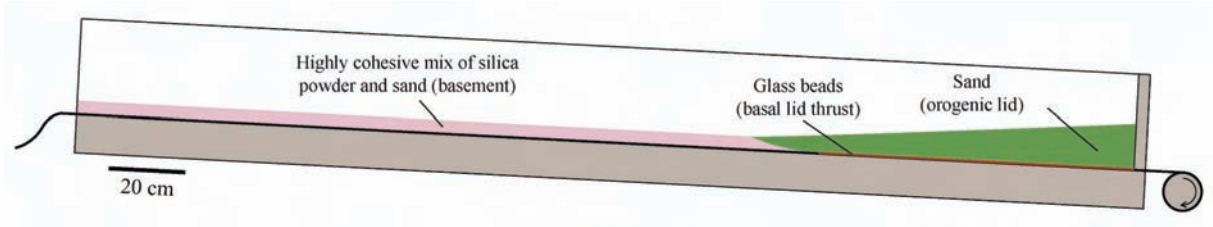

EXPERIMENT 41

Subduction window	no
Machine length	280 cm
Wedge surface slope α	2°
Wedge basal slope β	3°
Total shortening	124 cm
Erosion	no
Sedimentation	no
Others	

Initial stage picture

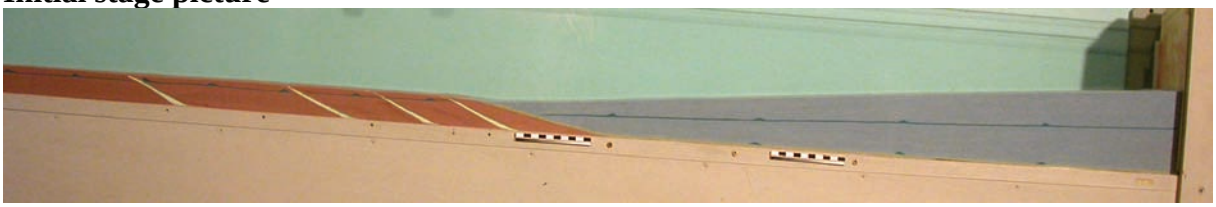

Final stage picture

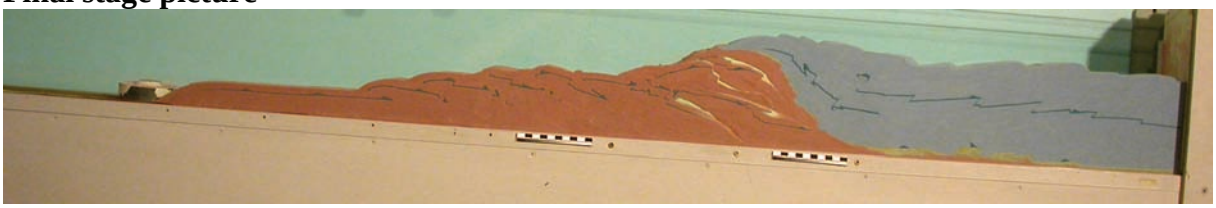

Initial stage scheme

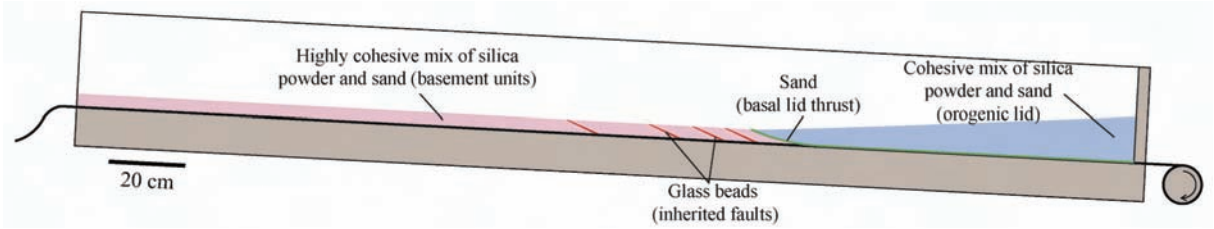

EXPERIMENT 42

Subduction window	no
Machine length	280 cm
Wedge surface slope α	2°
Wedge basal slope β	3°
Total shortening	138 cm
Erosion	no
Sedimentation	no
Others	

Initial stage picture

Final stage picture

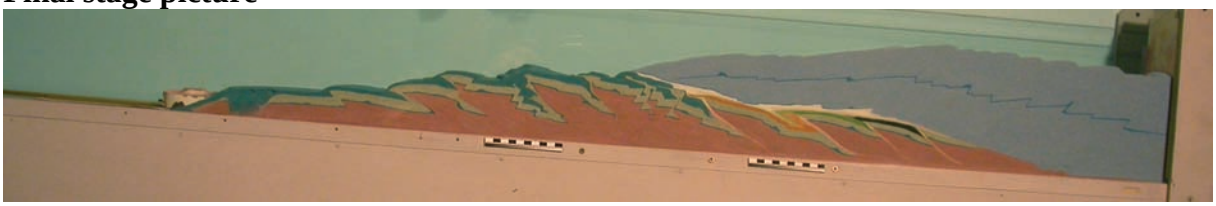

Initial stage scheme

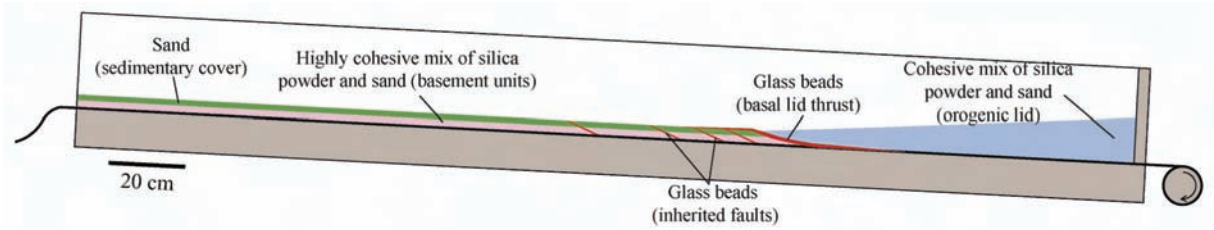

EXPERIMENT 43

Subduction window	no
Machine length	280 cm
Wedge surface slope α	2°
Wedge basal slope β	3°
Total shortening	148 cm
Erosion	high
Sedimentation	very low
Others	

Initial stage picture

Final stage picture

Initial stage scheme

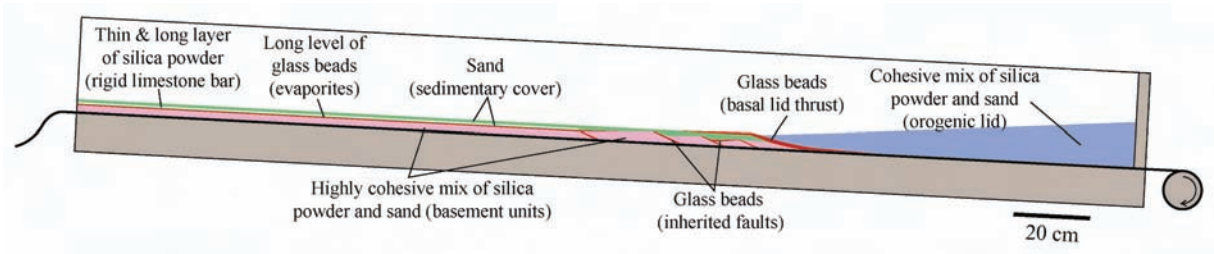

Stages

	Photographies		
Racc. (cm)	Pas d'action	Erosion	Sédim.
0	4180		
2	181		
4	182		
6	183		
8	184		
10	185		
12	186		
14	187		
16	188		
18	189		
20	190	191	191
22	/		
24	192	193	
26	194		
28	195	196	196
30	197		
32	198	199	
34	4200		
36	201	202	202
38	203		
40	204	205	
42	206		
44	207	208	208
46	209		
48	210	211	
50	212		
52	213	214	214
54	215		
56	216	217	
58	218		
60	219	220	220
62	221		
64	222	223	
66	224		
68	225	226	226
70	227		
72	228	229	
74	230		
76	231	232	232
78	233		
80	234	235	
82	236		
84	237	238	238
86	239		
88	240	241	
90	242		
92	243	244	244
94	245		
96	246	247	
98	248		
100	249	250	250
102	251		
104	252	253	
106	254		

	Photographies		
Racc. (cm)	Pas d'action	Erosion	Sédim.
108	255	256	256
110	257		
112	258	259	
114	260		
116	261	262	262
118	263		
120	/	264	
122	265		
124	266	267	267
126	268		
128	269	270	
130	271		
132	272	273	273
134	274		
136	275	276	
138	277		
140	278	279	279
142	280		
144	/	281	
146	282		
148	283		

EXPERIMENT 44

Subduction window	no
Machine length	280 cm
Wedge surface slope α	2°
Wedge basal slope β	3°
Total shortening	138 cm
Erosion	very low
Sedimentation	very high
Others	

Initial stage picture

Final stage picture

Initial stage scheme

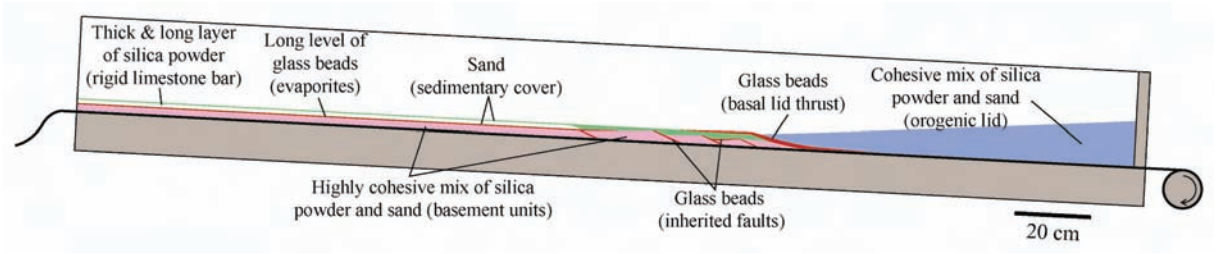

Stages

	Photographies	
Racc. (cm)	Pas d'action	Erosion/Sedimentation
0	1	
2	2	
4	3	
6	4	
8	5	
10	6	
12	7	
14	8	
16	9	
18	10	
20	11	
22	12	13
24	14	
26	15	16
28	17	
30	18	19
32	20	
34	21	22
36	23	
38	24	25
40	26	
42	27	28
44	29	
46	30	31
48	32	
50	33	34
52	35	
54	36	37
56	38	
58	39	40
60	41	
62	42	43
64	44	
66	45	46
68	47	
70	48	49
72	50	
74	51	52
76	53	
78	54	55
80	56	
82	57	58
84	59	
86	60	61
88	62	
90	63	64
92	65	
94	66	67
96	68	
98	69	70
100	71	
102	72	73
104	74	
106	75	76

	Photographies	
Racc. (cm)	Pas d'action	Erosion/Sedimentation
108	77	
110	78	79
112	80	
114	81	82
116	83	
118	84	85
120	86	
122	87	88
124	89	
126	90	91
128	92	
130	93	94
132	95	
134	96	97
136	98	
138	99	

EXPERIMENT 45

Subduction window	no
Machine length	280 cm
Wedge surface slope α	2°
Wedge basal slope β	3°
Total shortening	158 cm
Erosion	low
Sedimentation	high
Others	

Initial stage picture

Final stage picture

Initial stage scheme

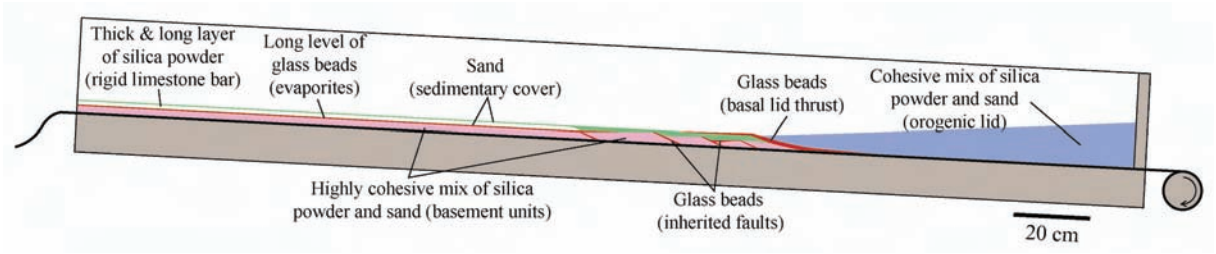

Stages

	Photographies	
Racc. (cm)	Pas d'action	Erosion/Sedimentation
0	1	
2	2	
4	3	
6	4	
8	5	
10	6	
12	7	
14	8	
16	9	
18	10	
20	11	12
22	13	
24	14	15
26	16	
28	17	18
30	19	
32	20	21
34	22	
36	23	24
38	25	
40	26	27
42	28	
44	29	30
46	31	
48	32	33
50	34	
52	35	36
54	37	
56	38	39
58	40	
60	41	42
62	43	
64	44	45
66	46	
68	47	48
70	49	
72	50	51
74	52	
76	53	54
78	55	
80	56	57
82	58	
84	59	60
86	61	
88	62	63
90	64	
92	65	66
94	67	
96	68	69
98	70	
100	71	72
102	73	
104	74	75
106	76	

	Photographies	
Racc. (cm)	Pas d'action	Erosion/Sedimentation
108	77	78
110	79	
112	80	81
114	82	
116	83	84
118	85	
120	86	87
122	88	
124	89	90
126	91	
128	92	93
130	94	
132	95	96
134	97	
136	98	99
138	100	
140	101	102
142	103	
144	104	105
146	106	
148	107	108
150	109	
152	110	111
154	112	
156	113	114
158	115	

EXPERIMENT 46

Subduction window	no
Machine length	280 cm
Wedge surface slope α	2°
Wedge basal slope β	3°
Total shortening	156 cm
Erosion	low
Sedimentation	low
Others	

Initial stage picture

Final stage picture

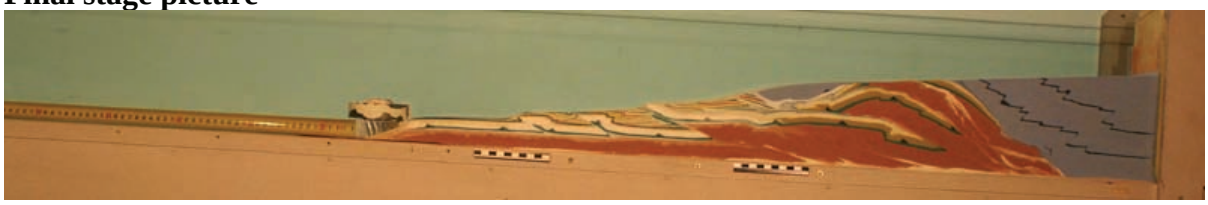

Initial stage scheme

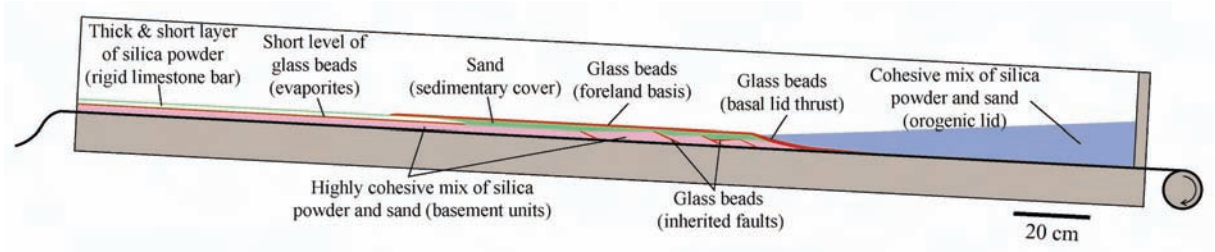

Stages

	Photographies	
Racc. (cm)	Pas d'action	Erosion/Sedimentation
0	1	
2	2	
4	3	
6	4	
8	5	
10	6	
12	7	
14	8	
16	9	
18	10	
20	11	12
22	13	
24	14	15
26	16	
28	17	18
30	19	
32	20	21
34	22	
36	23	24
38	25	
40	26	27
42	28	
44	29	30
46	31	
48	32	33
50	34	
52	35	36
54	37	
56	38	39
58	40	
60	41	42
62	43	
64	44	45
66	46	
68	47	48
70	49	
72	50	51
74	52	
76	53	54
78	55	
80	56	57
82	58	
84	59	60
86	61	
88	62	63
90	64	
92	65	66
94	67	
96	68	69
98	70	
100	71	72
102	73	
104	74	75
106	76	

	Photographies	
Racc. (cm)	Pas d'action	Erosion/Sedimentation
108	77	78
110	79	
112	80	81
114	82	
116	83	84
118	85	
120	86	87
122	88	
124	89	90
126	91	
128	92	93
130	94	
132	95	96
134	97	
136	98	99
138	100	
140	101	102
142	103	
144	104	105
146	106	
148	107	108
150	109	
152	110	111
154	112	
156	113	

EXPERIMENT 47

Subduction window	no
Machine length	280 cm
Wedge surface slope α	2°
Wedge basal slope β	3°
Total shortening	156 cm
Erosion	high
Sedimentation	high
Others	

Initial stage picture

Final stage picture

Initial stage scheme

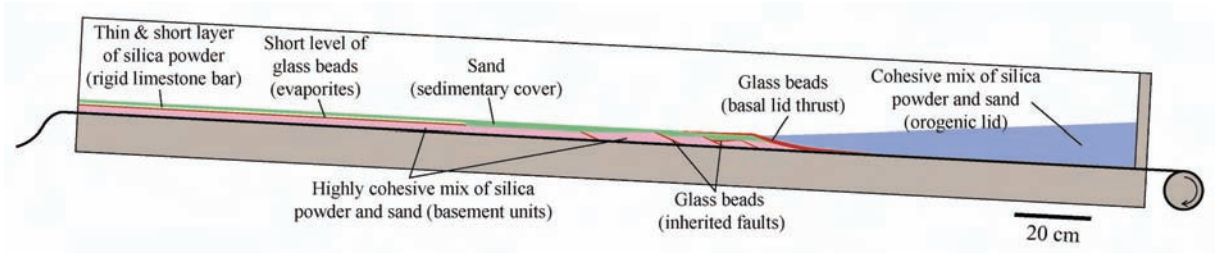

Stages

	Photographies	
Racc. (cm)	Pas d'action	Erosion/Sedimentation
0	1	
2	2	
4	3	
6	4	
8	5	
10	6	
12	7	
14	8	
16	9	
18	10	
20	11	12
22	13	
24	14	15
26	16	
28	17	18
30	19	
32	20	21
34	22	
36	23	24
38	25	
40	26	27
42	28	
44	29	30
46	31	
48	32	33
50	34	
52	35	36
54	37	
56	38	39
58	40	
60	41	42
62	43	
64	44	45
66	46	
68	47	48
70	49	
72	50	51
74	52	
76	53	54
78	55	
80	/	56
82	57	
84	/	58
86	59	
88	60	61
90	62	
92	63	64
94	65	
96	66	67
98	68	
100	69	70
102	71	
104	/	72
106	73	

	Photographies	
Racc. (cm)	Pas d'action	Erosion/Sedimentation
108	74	75
110	76	
112	77	78
114	79	
116	/	80
118	81	
120	82	83
122	84	
124	85	86
126	87	
128	88	89
130	90	
132	91	92
134	93	
136	94	95
138	96	
140	97	98
142	99	
144	100	101
146	102	
148	103	104
150	105	
152	106	107
154	108	
156	109	

APPENDIX 3

List of the movies (Quicktime) showing the evolutionary stages of the 17 experiments of analogue modelling. During the experiments, photographs were taken at each increment of displacement (4 cm of shortening) and then collated as movie illustrating the 2-dimensional development of a wedge section, perpendicular to the orogen axis. In addition for the experiments 35 to 37, a camera located higher on the edge of the sandbox device allows to observe also the surface of the models.

Animation31.mov

Animation32.mov

Animation33.mov

Animation34.mov

Animation35.mov
Animationprofil35.mov
Animationprofil35-model.mov

Animation36.mov
Animationprofil36.mov

Animation37.mov
Animationprofil37.mov

Animation38.mov

Animation39.mov

Animation40.mov

Animation41.mov

Animation42.mov

Animation43.mov

Animation44.mov

Animation45.mov

Animation46.mov

Animation47.mov

APPENDIX 4

Evolutionary plates of the analogue modelling experiments 42 to 47 described in the thesis.

Machine 2D + longue - Forte friction basale
Backstop vertical - sans fenêtre de subduction
base Pennique = 3° - surface Pennique = 2°
Pennique = cohésif bleu, socle = cohésif rouge, couv. = sable
Microbilles sur dernier quart de la base du Pennique et sur rampe
Préstructuration socle + couv. par microbilles

Expérience 42

Mise en place des Alpes sans érosion

Racc. = 0 cm
(photo 4110)
t_0

Racc. = 10 cm
(photo 4115)

Racc. = 20 cm
(photo 4120)

Racc. = 30 cm
(photo 4125)

Racc. = 40 cm
(photo 4130)

Racc. = 50 cm
(photo 4135)

Racc. = 60 cm
(photo 4140)

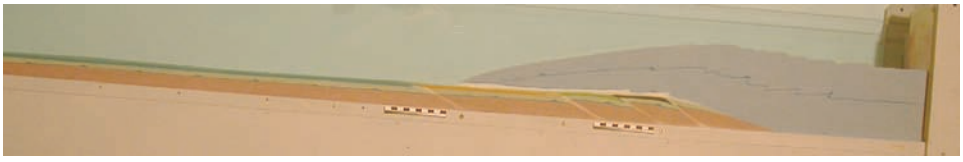

Racc. = 70 cm
(photo 4145)

Machine 2D + longue - Forte friction basale
Backstop vertical - sans fenêtre de subduction
base Pennique = 3° - surface Pennique = 2°
Pennique = cohésif bleu, socle = cohésif rouge, couv. = sable
Microbilles sur dernier quart de la base du Pennique et sur rampe
Préstructuration socle + couv. par microbilles

Expérience 42 (suite)

Mise en place des Alpes sans érosion

Racc. = 80 cm
(photo 4150)

Racc. = 90 cm
(photo 4155)

Racc. = 100 cm
(photo 4160)

Racc. = 110 cm
(photo 4165)

Racc. = 120 cm
(photo 4170)
t_{30}

Racc. = 130 cm
(photo 4175)

Expérience 43

Machine 2D + longue - Forte friction basale
Backstop vertical - sans fenêtre de subduction
base Pennique = 3° - surface Pennique = 2°
Pennique = cohésif bleu, socle = cohésif rouge, couv. = sable et poudre de silice
Microbilles sur dernier quart de la base du Pennique et sur rampe
Préstructuration socle + couv. par microbilles et bassins hérités

Mise en place des Alpes avec érosion

Racc. = 0 cm
(photo 4180)

Racc. = 10 cm
(photo 4185)

Racc. = 20 cm
(photo 4191)

Racc. = 30 cm
(photo 4197)

Racc. = 40 cm
(photo 4205)

Racc. = 50 cm
(photo 4212)

Racc. = 60 cm
(photo 4220)

Racc. = 70 cm
(photo 4227)

Expérience 43 (suite)

Machine 2D + longue - Forte friction basale
Backstop vertical - sans fenêtre de subduction
base Pennique = 3° - surface Pennique = 2°
Pennique = cohésif bleu, socle = cohésif rouge, couv. = sable et poudre de silice
Microbilles sur dernier quart de la base du Pennique et sur rampe
Préstructuration socle + couv. par microbilles et bassins hérités

Mise en place des Alpes avec érosion

Racc. = 80 cm
(photo 4235)

Racc. = 90 cm
(photo 4242)

Racc. = 100 cm
(photo 4250)

Racc. = 110 cm
(photo 4257)

Racc. = 120 cm
(photo 4264)
t_{30}

Racc. = 130 cm
(photo 4271)

Racc. = 140 cm
(photo 4279)

Mise en place des Alpes avec érosion
et forte sédimentation molassique

Expérience 44

Racc. = 0 cm
(photo 001)

Racc. = 22 cm
(photo 013)

Racc. = 74 cm
(photo 051)

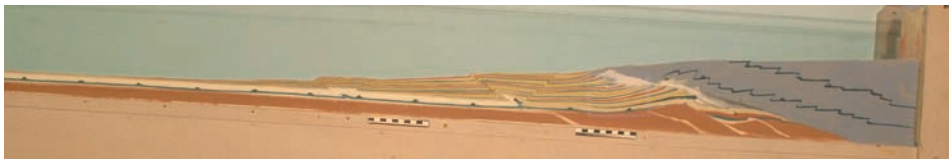

Racc. = 82 cm
(photo 057)

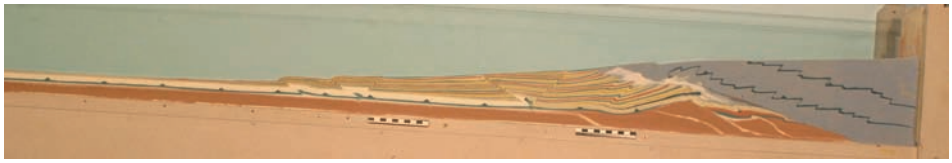

Racc. = 86 cm
(photo 060)

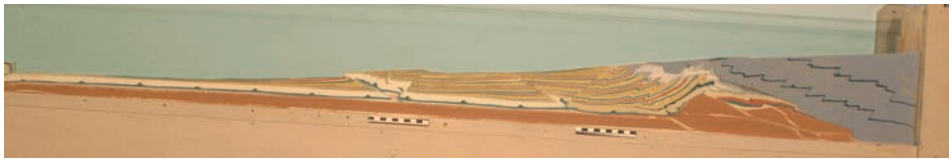

Racc. = 102 cm
(photo 072)

Mise en place des Alpes avec érosion
et forte sédimentation molassique

Expérience 44 (suite)

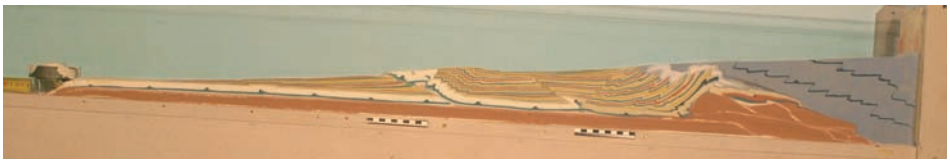

Racc. = 114 cm
(photo 081)

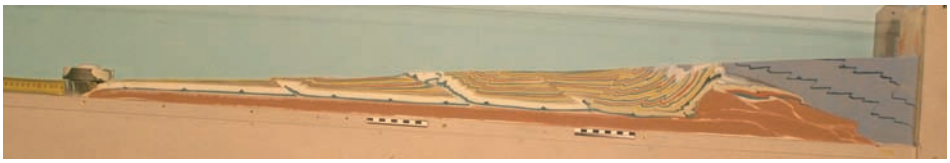

t_{30}

Racc. = 120 cm
(photo 086)

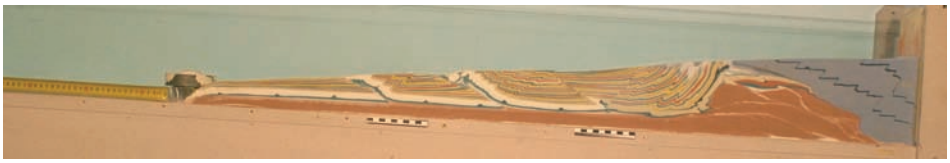

Racc. = 138 cm
(photo 099)

Mise en place des Alpes avec érosion
et moyenne sédimentation molassique

Expérience 45

Racc. = 0 cm
(photo 001)

Racc. = 20 cm
(photo 012)

Racc. = 38 cm
(photo 025)

Racc. = 64 cm
(photo 044)

Racc. = 70 cm
(photo 049)

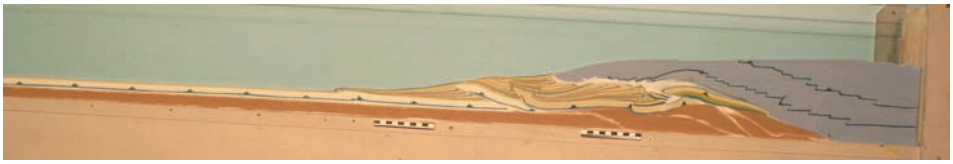

Racc. = 90 cm
(photo 064)

Mise en place des Alpes avec érosion
et moyenne sédimentation molassique

Expérience 45 (suite)

Racc. = 96 cm
(photo 068)

Racc. = 112 cm
(photo 080)

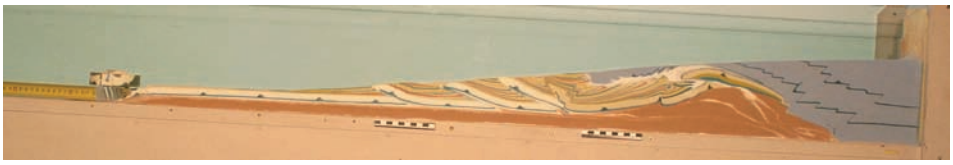

t_{30} Racc. = 122 cm
(photo 088)

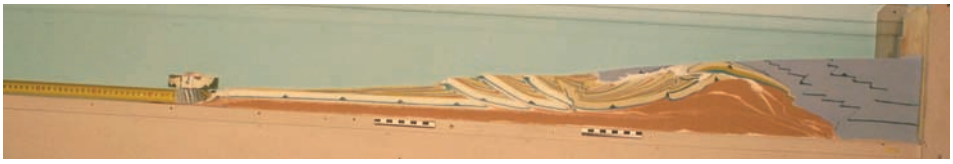

Racc. = 136 cm
(photo 098)

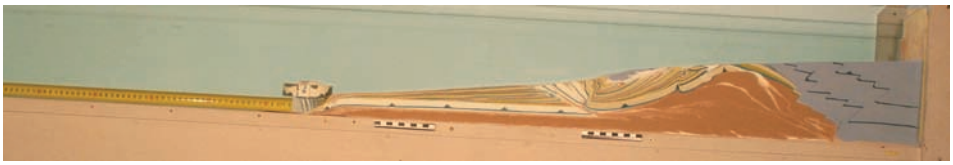

Racc. = 156 cm
(photo 114)

Exp 46

Shortening
0 cm = t_0

20 cm

24 cm

28 cm

32 cm

36 cm

40 cm = t_{10}

44 cm

48 cm

52 cm = t_{13}

Exp 46

Shortening
56 cm

60 cm = t_{15}

64 cm = t_{16}

68 cm

72 cm

76 cm

80 cm

84 cm

88 cm

92 cm = t_{23}

Exp 46

Shortening
96 cm

100 cm

104 cm

108 cm

112 cm = t_{28}

116 cm = t_{29}

120 cm

124 cm

128 cm

132 cm

Exp 46

Shortening
136 cm = t_{34}

140 cm

144 cm

148 cm

152 cm = t_{38}

Mise en place des Alpes avec érosion

Expérience 47

Racc. = 0 cm
(photo 001)

Racc. = 20 cm
(photo 012)

Racc. = 32 cm
(photo 020)

Racc. = 52 cm
(photo 035)

Racc. = 60 cm
(photo 041)

Racc. = 68cm
(photo 047)

Mise en place des Alpes avec érosion

Expérience 47 (suite)

Racc. = 84 cm
(photo 058)

Racc. = 92 cm
(photo 063)

Racc. = 102 cm
(photo 071)

Racc. = 132 cm
(photo 091)

Racc. = 146 cm
(photo 102)

Racc. = 156 cm
(photo 109)

APPENDIX 5

Evolutionary summary plates showing the main stages of structural development for the experiments 42 and 46.

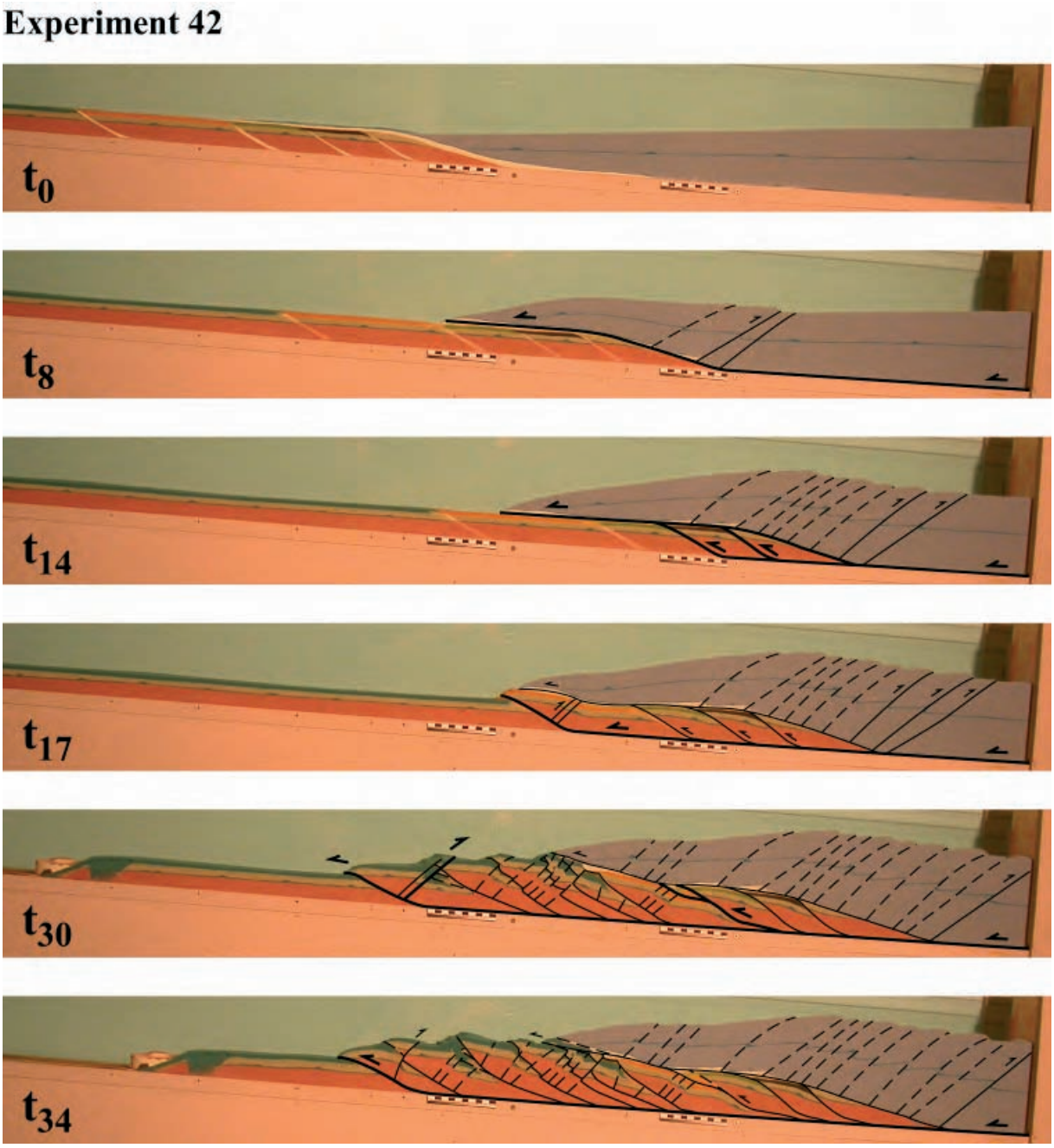

Experiment 46

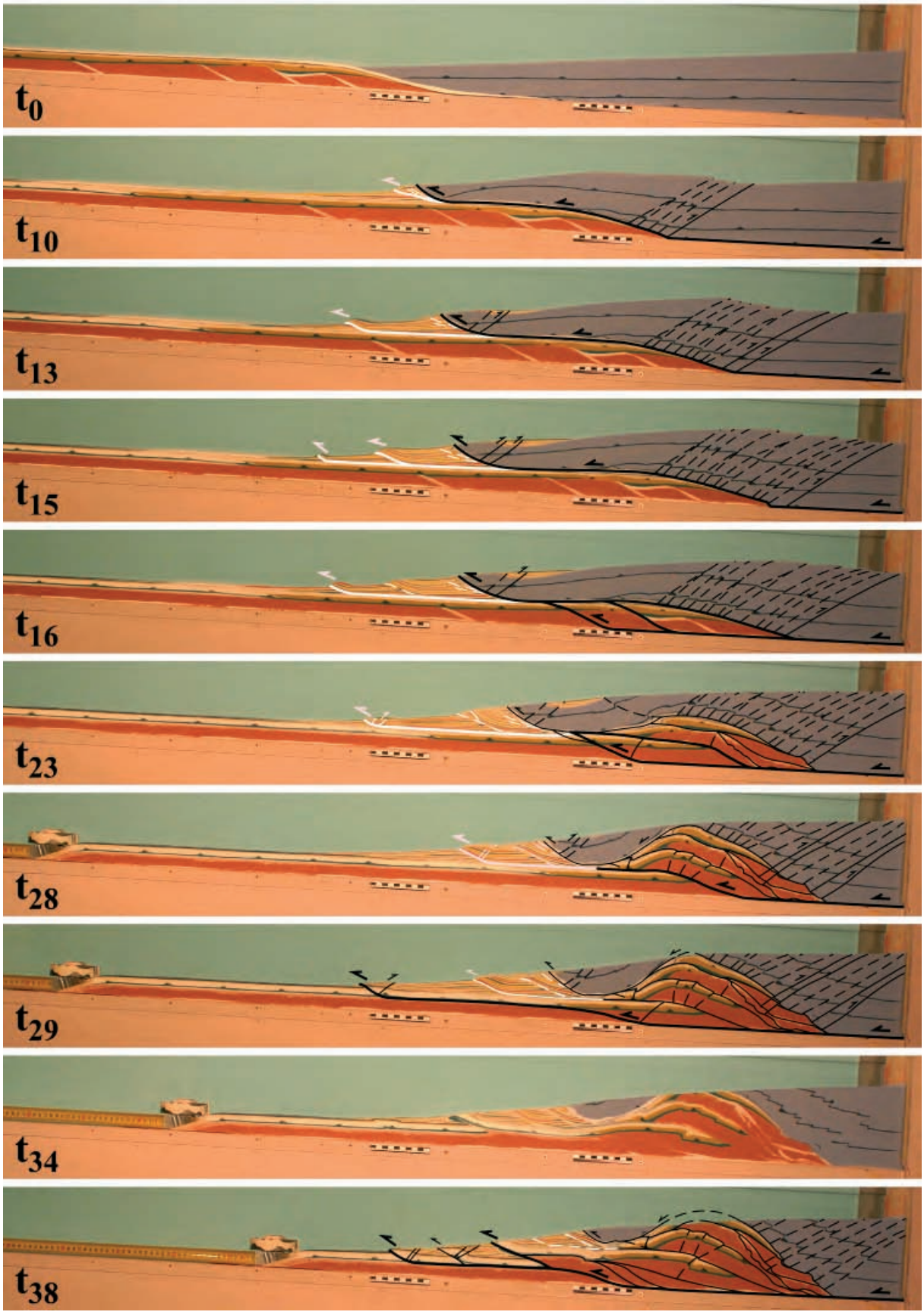

APPENDIX 6

Properties of analogue materials including those used in the series of sandbox experiments presented. The characteristics of the analysed materials (brown corundum, glass beads, pumice powder, silica powder, sand and talcum powder) are described and illustrated by photographs taken with an electron microscope.

FICHES TECHNIQUES DES MATERIAUX UTILISES EN MODELISATION ANALOGIQUE

Matériaux produits par Eyraud S.A. (Lyon, France), Dousselin Geoffray et Jacquet (Couzon au Mont d'Or, France) et SIFRACO (Nemours, France)
Données techniques fournies par Eyraud S.A. et Dousselin Geoffray et Jacquet
Photographies prises au Microscope Electronique à Balayage de l'Université de Fribourg (Suisse), par Christoph Neururer et Cécile Bonnet
Descriptions supplémentaires par Cécile Bonnet

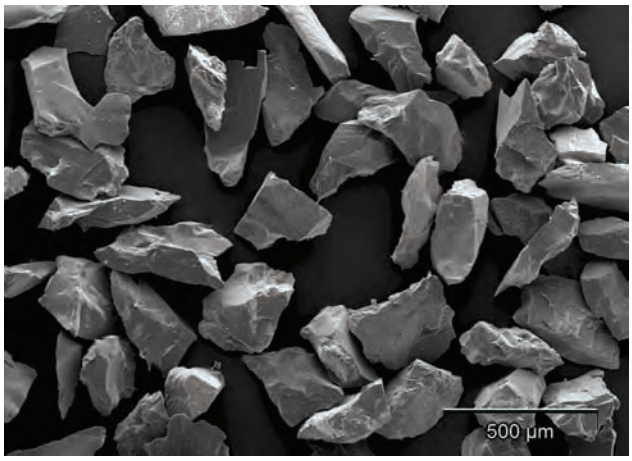

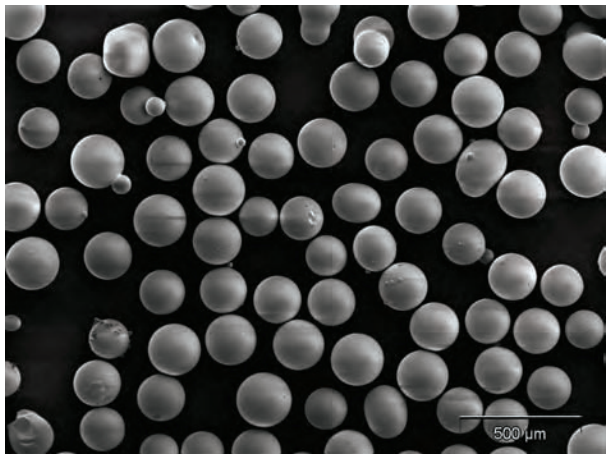

Poudre de corindon brun (149-210 µm) et microbilles de verre (100-200 µm)

Matériaux présentés

- Poudre de corindon brun (44-74 µm)
- Poudre de corindon brun (149-210 µm)
- Microbilles de verre (50-105 µm)
- Microbilles de verre (100-200 µm)
- Poudre de pierre ponce, type XXX (1-40 µm)
- Poudre de pierre ponce (1-210 µm)
- Poudre de pierre ponce (1-250 µm)
- Poudre de silice
- Poudre de verre (1-80 µm)
- Sable (100 à 310 µm)
- Talc

FICHE TECHNIQUE POUDRE DE CORINDON BRUN (44-74µm)

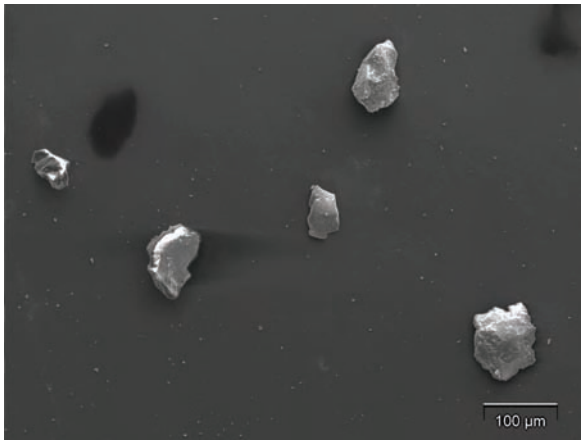

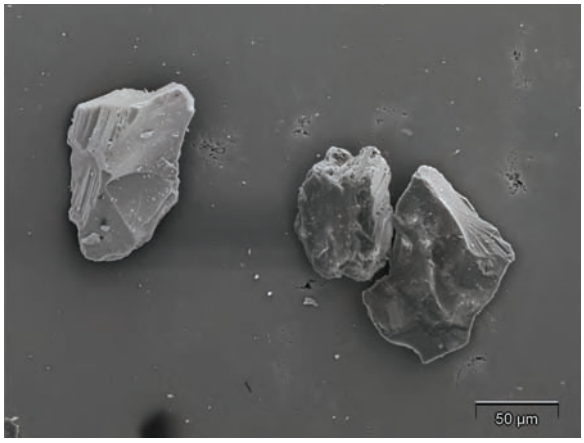

Fournisseur / Références / Emballage	Eyraud S.A. / / Sacs de 25kg sur palettes
Champ d'application	
Procédé de fabrication	
Composition chimique (d'après DIN 8201)	Al_2O_3 95.20 ⁒ Fe_2O_3 0.30 ⁒ TiO_2 2.90 ⁒ MgO+CaO 0.30 ⁒ SiO_2 1.20 ⁒
Propriétés physiques : **- état physique à 20°C** **- couleur**	 - solide - brun
Granulométrie / Répartition de la taille	44 à 74 microns
Forme des grains / Aspect	cube
Poids spécifique	
Densité : à sec, apparente et spécifique **saturation en eau**	1,62 à 1,70 g/cm^3 et 3,94 g/cm^3
Dureté (d'après Mohs)	9
Porosité	
Coefficient de friction interne	
Cohésion	
Température de fusion	1930°C
Précautions en cours de manipulation	

FICHE TECHNIQUE POUDRE DE CORINDON BRUN (149-210µm)

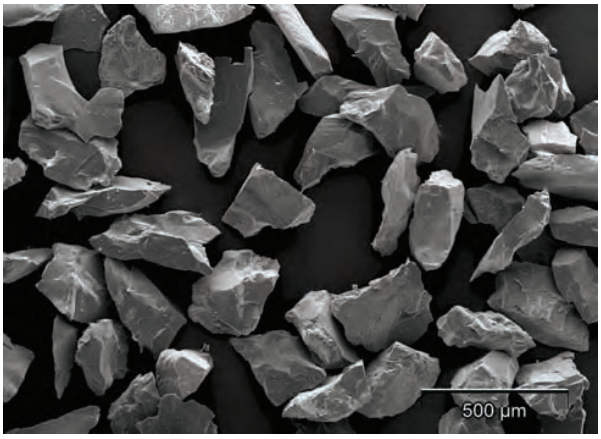

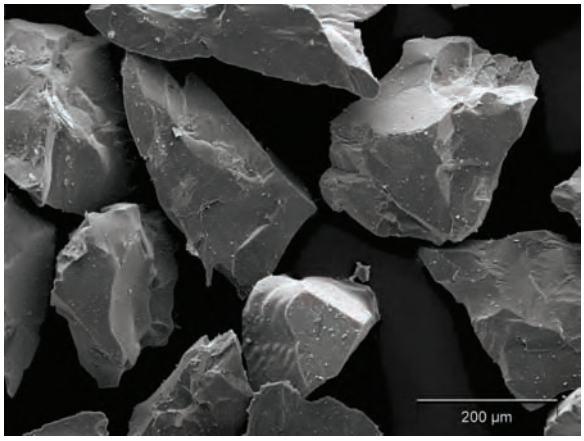

Fournisseur / Références / Emballage	Eyraud S.A. / / Sacs de 25kg sur palettes
Champ d'application	
Procédé de fabrication	
Composition chimique (d'après DIN 8201)	Al_2O_3 95.20 ٪ Fe_2O_3 0.30 ٪ TiO_2 2.90 ٪ MgO+CaO 0.30 ٪ SiO_2 1.20 ٪
Propriétés physiques : **- état physique à 20°C** **- couleur**	 - solide - brun
Granulométrie / Répartition de la taille	149 à 210 microns
Forme des grains / Aspect	cube
Poids spécifique	
Densité : à sec, apparente et spécifique saturation en eau	1,62 à 1,70 g/cm^3 et 3,94 g/cm^3
Dureté (d'après Mohs)	9
Porosité	
Coefficient de friction interne	
Cohésion	
Température de fusion	1930°C
Précautions en cours de manipulation	

FICHE TECHNIQUE MICROBILLES DE VERRE (50-105µm)

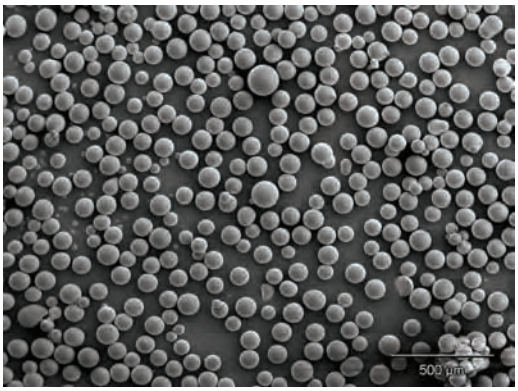

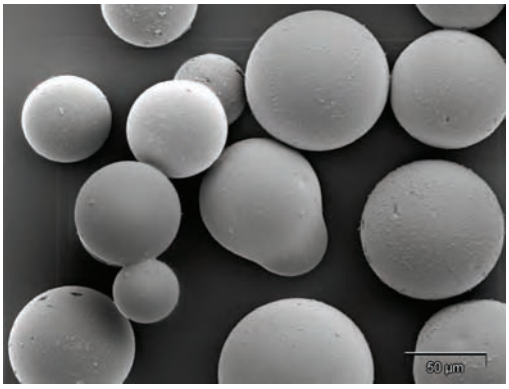

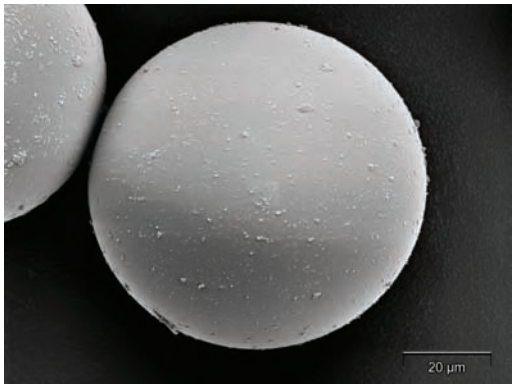

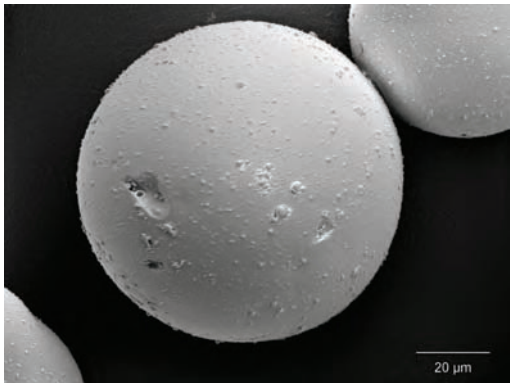

Fournisseur / Références / Emballage	Eyraud S.A./
Champ d'application	Produit de grenaillage de précision pour nettoyage sans dommage, ébavurage, polissage, réduction de la rugosité en profondeur, dépolissage et écrouissage de matériaux métalliques
Procédé de fabrication	Les microbilles sont fondues à partir de silicate de soude broyé. Les impuretés étrangères à l'espèce ne sont tolérées qu'à moins de 0.1 % en poids
Composition chimique (d'après DIN 8201)	$SiO_2 \geq 65.0$ % Al_2O_3 de 0.5 à 2.0 % $Fe_2O_3 \leq 0.15$ % $MgO \geq 2.5$ % $CaO \geq 8.0$ % $Na_2O \geq 14.0$ % Autres ≥ 2.0 %
Propriétés physiques : **- état physique à 20°C** **- couleur**	 - solide - clair
Granulométrie / Répartition de la taille	50 à 105 microns / Assez homogène
Forme des grains / Aspect	Sphérique / Des impuretés parsèment la surface des microbilles, des trous ou des excroissances sont présentes sur certaines et parfois, deux microbilles ont en partie fusionné
Poids spécifique	≈ 2.5
Densité : à sec **saturation en eau**	≈ 1.5 (1.4734) ≈ 2 (1.9505)
Dureté (d'après Mohs)	6-7
Porosité	?
Coefficient de friction interne	0.44
Cohésion	Quasiment négligeable
Température de fusion	670<>800°C
Précautions en cours de manipulation	Comme pour tout produit pulvérulent non toxique, port d'un masque respiratoire protecteur, de gants et de lunettes

FICHE TECHNIQUE MICROBILLES DE VERRE (100-200µm)

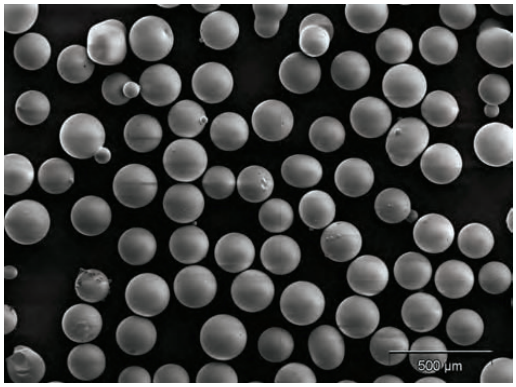

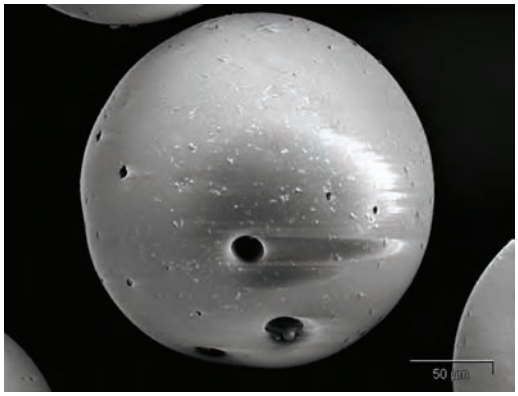

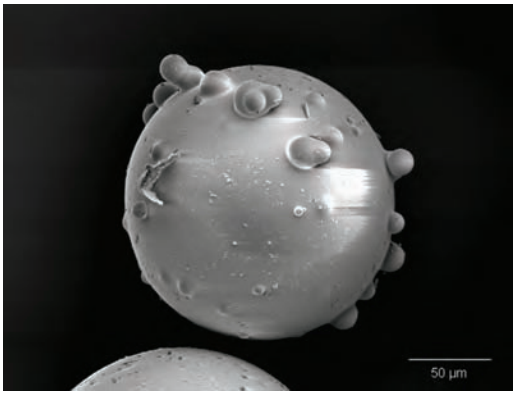

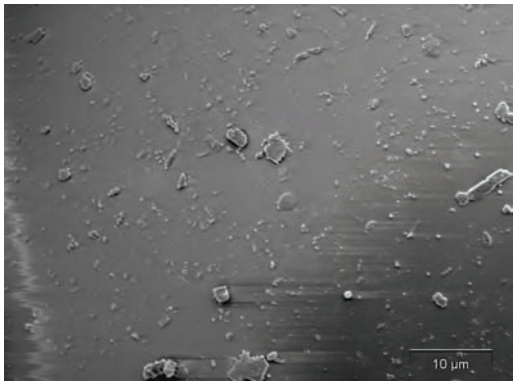

Fournisseur / Références / Emballage	Eyraud S.A./
Champ d'application	Produit de grenaillage de précision pour nettoyage sans dommage, ébavurage, polissage, réduction de la rugosité en profondeur, dépolissage et écrouissage de matériaux métalliques
Procédé de fabrication	Les microbilles sont fondues à partir de silicate de soude broyé. Les impuretés étrangères à l'espèce ne sont tolérées qu'à moins de 0.1 % en poids
Composition chimique (d'après DIN 8201)	$SiO_2 \geq 65.0$ % Al_2O_3 de 0.5 à 2.0 % $Fe_2O_3 \leq 0.15$ % $MgO \geq 2.5$ % $CaO \geq 8.0$ % $Na_2O \geq 14.0$ % Autres ≥ 2.0 %
Propriétés physiques : **- état physique à 20°C** **- couleur**	 - solide - clair
Granulométrie / Répartition de la taille	100 à 200 microns / Assez homogène
Forme des grains / Aspect	Sphérique / Des impuretés parsèment la surface des microbilles, des trous ou des excroissances sont présentes sur certaines et parfois, deux microbilles ont en partie fusionné
Poids spécifique	≈ 2.5
Densité : à sec **saturation en eau**	≈ 1.5 (1.5119) ≈ 1.9 (1.9292)
Dureté (d'après Mohs)	6-7
Porosité	?
Coefficient de friction interne	0.44
Cohésion	Quasiment négligeable
Température de fusion	670<>800°C
Précautions en cours de manipulation	Comme pour tout produit pulvérulent non toxique, port d'un masque respiratoire protecteur, de gants et de lunettes

FICHE TECHNIQUE POUDRE DE PIERRE PONCE TYPE XXX (1-40µm)

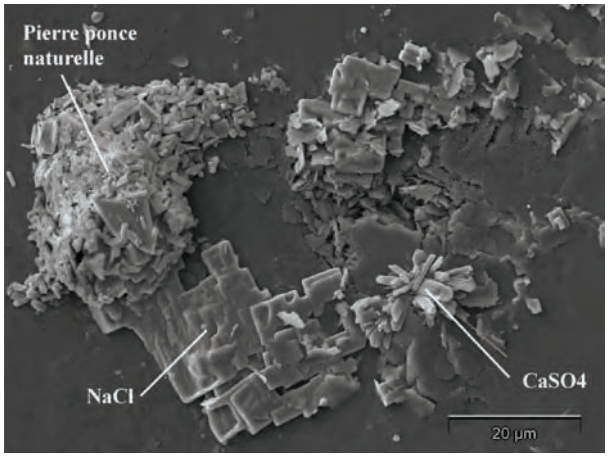

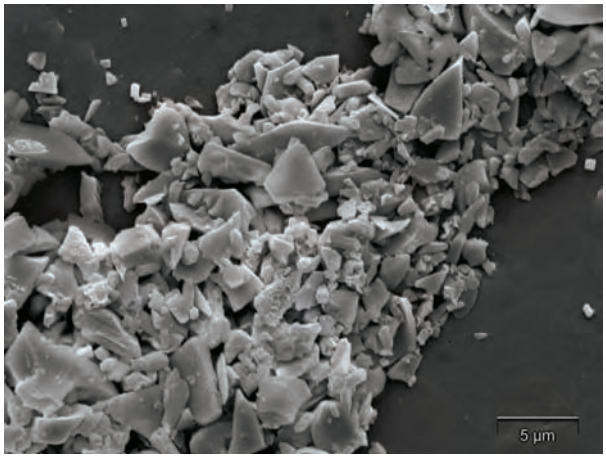

Fournisseur / Références / Emballage	Eyraud S.A. / Type « XXX » / Sacs de 25kg sur palettes
Champ d'application	?
Procédé de fabrication	Lavage et ventilation de la pierre ponce naturelle afin de retirer toute impureté ainsi que l'obsidienne et la magnétite présentes dans le produit volcanique brut
Composition chimique (donnée à titre indicatif puisqu'il s'agit d'un matériau naturel)	SiO_2 71.75% ; Al_2O_3 12.33% ; TiO_2 0.11% ; Fe_2O_3 1.98% ; FeO 0.02% ; MnO 0.07% ; CaO 0.70% ; MgO 0.12% ; Na_2O 3.59% ; K_2O 4.47% ; P_2O_5 0.008% ; CO_2 0.10% ; SO_3 0.18% ; H_2O^+ 3.71%
Propriétés physiques : **- état physique à 20°C** **- couleur**	 - solide - blanc
Granulométrie / Répartition de la taille	1 à 40 microns
Forme des grains / Aspect	Irrégulière, à arêtes vives /
Poids spécifique	
Densité : à sec, réelle et apparente **saturation en eau**	2.31g/cm^3 et 0,400 à 0,470g/cm^3
Dureté (d'après Mohs)	5-6 (valeurs bibliographiques)
Porosité	Jusqu'à 85%
Coefficient de friction interne	
Cohésion	
Température de fusion	La ponce est insensible à la chaleur, seule une légère vitrification apparaît en surface des grains au-delà de 1200°C
Précautions en cours de manipulation	

FICHE TECHNIQUE POUDRE DE PIERRE PONCE TYPE STANDARD (1-210µm)

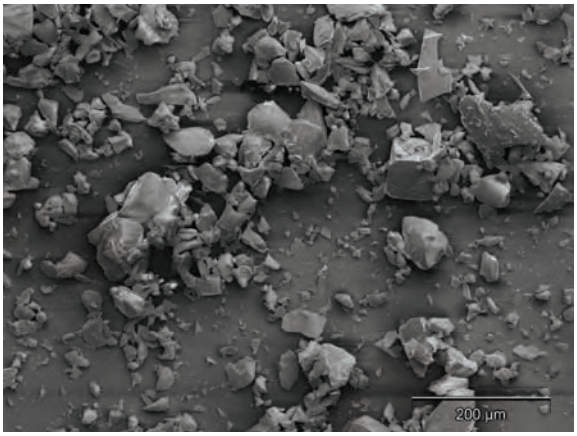

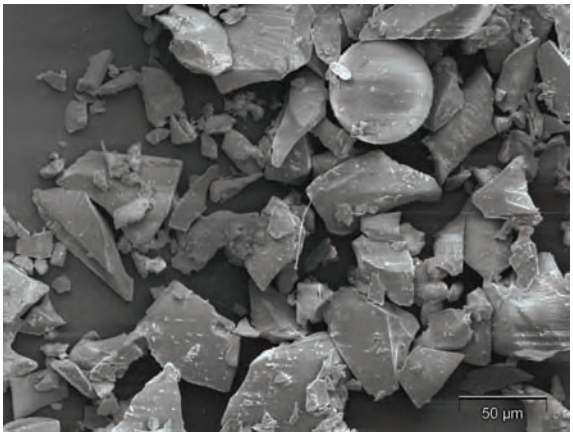

Fournisseur / Références / Emballage	Eyraud S.A. / Type « XXX » / Sacs de 25kg sur palettes
Champ d'application	?
Procédé de fabrication	Lavage et ventilation de la pierre ponce naturelle afin de retirer toute impureté ainsi que l'obsidienne et la magnétite présentes dans le produit volcanique brut
Composition chimique (donnée à titre indicatif puisqu'il s'agit d'un matériau naturel)	SiO_2 71.75% ; Al_2O_3 12.33% ; TiO_2 0.11% ; Fe_2O_3 1.98% ; FeO 0.02% ; MnO 0.07% ; CaO 0.70% ; MgO 0.12% ; Na_2O 3.59% ; K_2O 4.47% ; P_2O_5 0.008% ; CO_2 0.10% ; SO_3 0.18% ; H_2O^+ 3.71%
Propriétés physiques : **- état physique à 20°C** **- couleur**	 - solide - blanc
Granulométrie / Répartition de la taille	1 à 210 microns
Forme des grains / Aspect	Irrégulière, à arêtes vives /
Poids spécifique	
Densité : à sec, réelle et apparente **saturation en eau**	2.31g/cm^3 et 0,400 à 0,470g/cm^3
Dureté (d'après Mohs)	5-6 (valeurs bibliographiques)
Porosité	Jusqu'à 85%
Coefficient de friction interne	
Cohésion	
Température de fusion	La ponce est insensible à la chaleur, seule une légère vitrification apparaît en surface des grains au-delà de 1200°C
Précautions en cours de manipulation	

FICHE TECHNIQUE POUDRE DE PIERRE PONCE TYPE STANDARD (1-250µm)

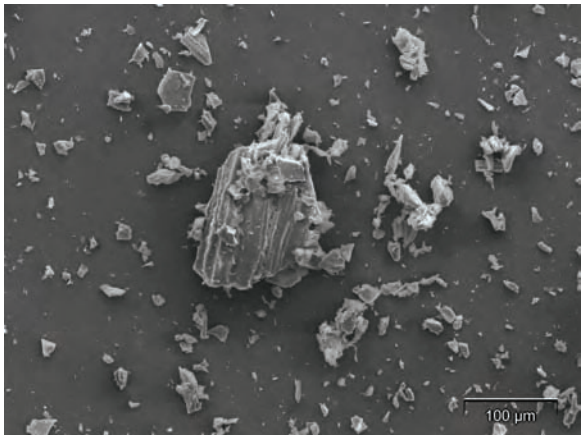

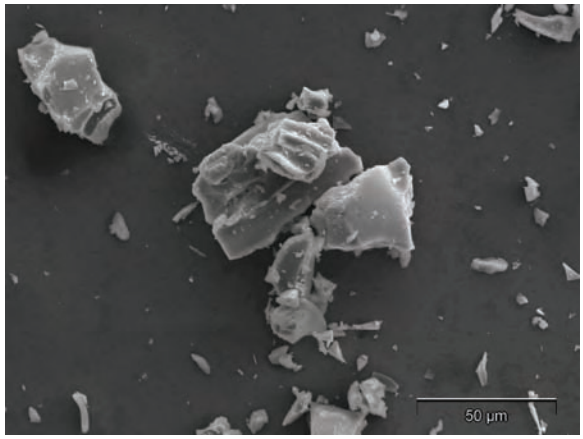

Fournisseur / Références / Emballage	Eyraud S.A. / Type « XXX » / Sacs de 25kg sur palettes
Champ d'application	?
Procédé de fabrication	Lavage et ventilation de la pierre ponce naturelle afin de retirer toute impureté ainsi que l'obsidienne et la magnétite présentes dans le produit volcanique brut
Composition chimique (donnée à titre indicatif puisqu'il s'agit d'un matériau naturel)	SiO_2 71.75% ; Al_2O_3 12.33% ; TiO_2 0.11% ; Fe_2O_3 1.98% ; FeO 0.02% ; MnO 0.07% ; CaO 0.70% ; MgO 0.12% ; Na_2O 3.59% ; K_2O 4.47% ; P_2O_5 0.008% ; CO_2 0.10% ; SO_3 0.18% ; H_2O^+ 3.71%
Propriétés physiques : **- état physique à 20°C** **- couleur**	 - solide - blanc
Granulométrie / Répartition de la taille	1 à 250 microns
Forme des grains / Aspect	Irrégulière, à arêtes vives /
Poids spécifique	
Densité : à sec, réelle et apparente **saturation en eau**	2.31g/cm^3 et 0,400 à 0,470g/cm^3
Dureté (d'après Mohs)	5-6 (valeurs bibliographiques)
Porosité	Jusqu'à 85%
Coefficient de friction interne	
Cohésion	
Température de fusion	La ponce est insensible à la chaleur, seule une légère vitrification apparaît en surface des grains au-delà de 1200°C
Précautions en cours de manipulation	

FICHE TECHNIQUE POUDRE DE SILICE

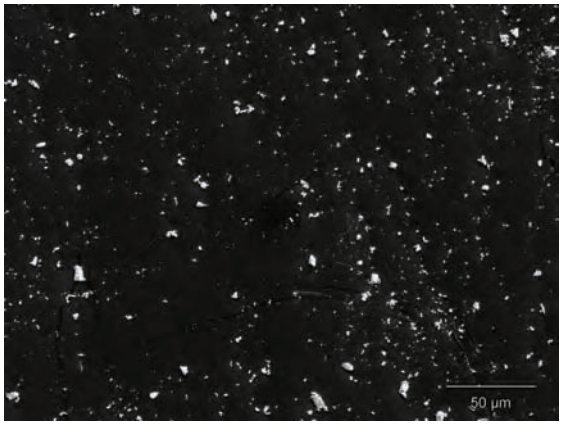

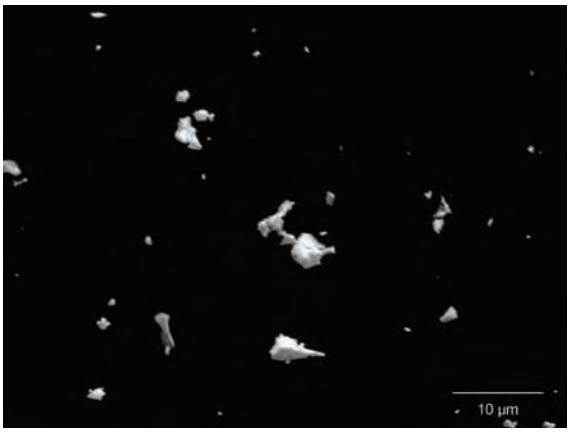

Fournisseur / Références / Emballage	SIFRACO/
Champ d'application	
Procédé de fabrication	
Composition chimique (d'après DIN 8201)	
Propriétés physiques : **- état physique à 20°C** **- couleur**	 - solide - chair
Granulométrie / Répartition de la taille	/ Très étalée
Forme des grains / Aspect	Anguleuse et très variable /
Poids spécifique	
Densité : à sec **saturation en eau**	
Dureté (d'après Mohs)	
Porosité	
Coefficient de friction interne	
Cohésion	Très forte (150 Pa)
Température de fusion	
Précautions en cours de manipulation	Comme pour tout produit pulvérulent non toxique, port d'un masque respiratoire protecteur, de gants et de lunettes

FICHE TECHNIQUE POUDRE DE VERRE (1-80µm)

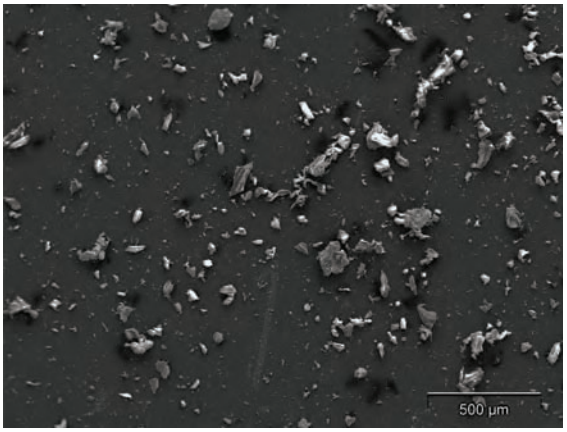

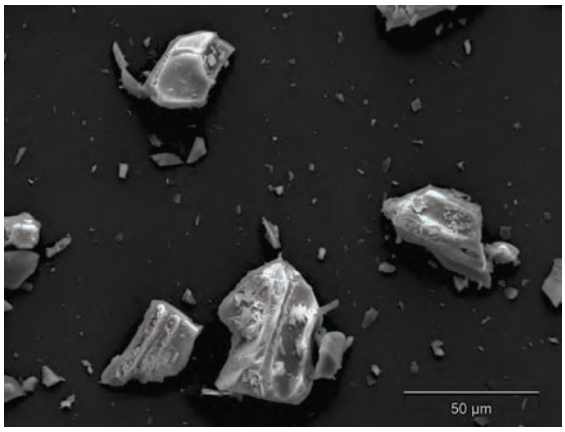

Fournisseur / Références / Emballage	Eyraud S.A./
Champ d'application	Produit de grenaillage de précision pour dérouillage sans dommage, décalaminage, ébavurage et nettoyage de matériaux métalliques pour obtention du plus fin degré de rugosité
Procédé de fabrication	Les éclats de verre sont obtenus à partir de verre blanc broyé et tamisé. Les impuretés étrangères à l'espèce ne sont tolérées qu'à moins de 0.1 % en poids
Composition chimique (d'après DIN 8201)	$SiO_2 \geq 65.0$ % Al_2O_3 de 0.5 à 2.0 % $Fe_2O_3 \leq 0.15$ % $MgO \geq 2.5$ % $CaO \geq 8.0$ % $Na_2O \geq 14.0$ % Autres ≥ 2.0 %
Propriétés physiques : **- état physique à 20°C** **- couleur**	 - solide - chair
Granulométrie / Répartition de la taille	1 à 80 microns /
Forme des grains / Aspect	
Poids spécifique	≈ 2.5
Densité : à sec **saturation en eau**	≈ 1.5
Dureté (d'après Mohs)	?
Porosité	?
Coefficient de friction interne	
Cohésion	Très forte (150 Pa)
Température de fusion	800°C
Précautions en cours de manipulation	Comme pour tout produit pulvérulent non toxique, port d'un masque respiratoire protecteur, de gants et de lunettes

FICHE TECHNIQUE SABLE (100-310µm)

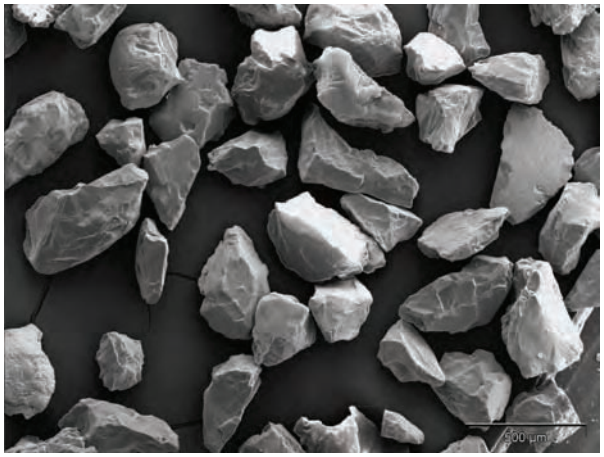

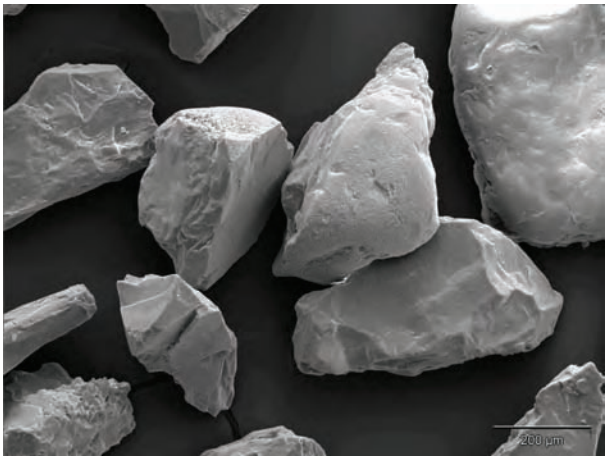

Fournisseur / Références / Emballage	Dousselin Geoffray et Jacquet / HN 31/ Sacs de 40 kg
Champ d'application	Fibre de verre, produits de céramiques et réfractaires, enduits, ciments colles, préfabriqués, sols industriels, sablage, sciage, polissage, potables, de piscines ou résiduaires, caoutchouc industriel, peintures colles, phytosanitaire, sols sportifs, jardins paysagers, golf, aquariophilie
Procédé de fabrication	
Composition chimique (d'après DIN 8201)	SiO_2 = 99.0 ٪ CaO + MgO = 0.15 ٪ Al_2O_3 = 0.4 ٪ Autres = traces $Na_2O + K_2O$ = 0.15 ٪ Fe_2O_3 = 0.1 ٪
Propriétés physiques : **- état physique à 20°C** **- couleur**	 - solide - clair
Granulométrie / Répartition de la taille	0.1 à 0.31 mm /
Forme des grains / Aspect	
Poids spécifique	
Masse volumique : réelle **Apparente sans tassement** **Apparente après tassement**	2.65 g/cm^3 1.20 g/cm^3 1.45 g/cm^3
Dureté (d'après Mohs)	7
Porosité	?
Coefficient de friction interne	0.57
Cohésion	Tamisé : Faible (20 Pa) ; Compacté : forte (100 Pa)
Température de fusion	1750°C
Précautions en cours de manipulation	

FICHE TECHNIQUE TALC

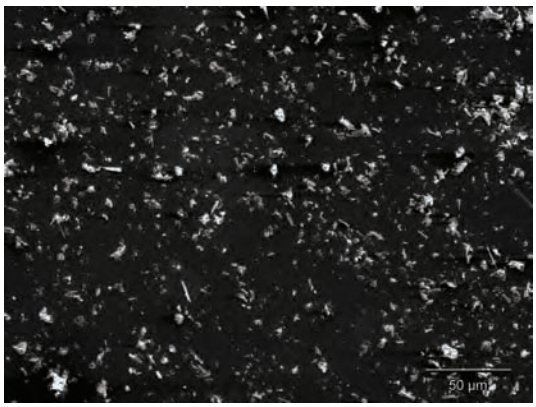

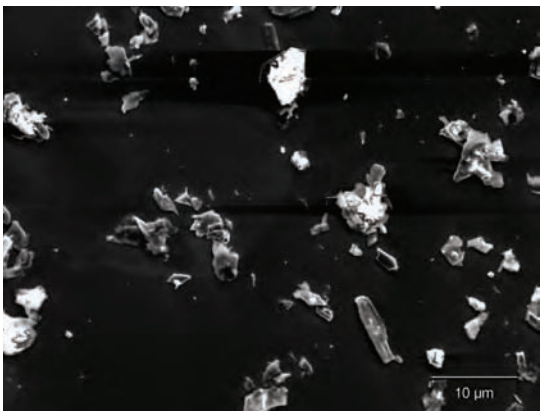

Fournisseur / Références / Emballage	?
Champ d'application	
Procédé de fabrication	
Composition chimique (d'après DIN 8201)	
Granulométrie / Répartition de la taille	
Forme des grains / Aspect	
Poids spécifique	
Densité : à sec saturation en eau	
Dureté (d'après Mohs)	
Porosité	
Coefficient de friction interne	
Cohésion	Très forte
Température de fusion	
Précautions en cours de manipulation	Comme pour tout produit pulvérulent non toxique, port d'un masque respiratoire protecteur, de gants et de lunettes

APPENDIX 7

Structural map of the Western Alpine orogen-foreland system. The location of three sections across the Western Alps and foreland are indicated (profile XX' extends from Jura to Belledonne massif, profile YY' extends from central Jura to Mont-Blanc massif and profile ZZ' extends from Molasse basin to Aar massif), as well as the location of eight smaller sections in the Molasse foreland basin. The anticlinal axes are indicated in the Molasse Plateau. Among the faults fracturing the Prealpes, Molasse Plateau and Jura, the set of large-scale brittle faults is highlighted (thick dark grey lines), with the sense of movement given when possible. The orientation of the conjugate fault systems rotates along strike of the Jura arc from a WNW-ESE orientation to almost N-S. The whole fault system may be interpreted in terms of deformation in a regional transcurrent system (top right scheme).

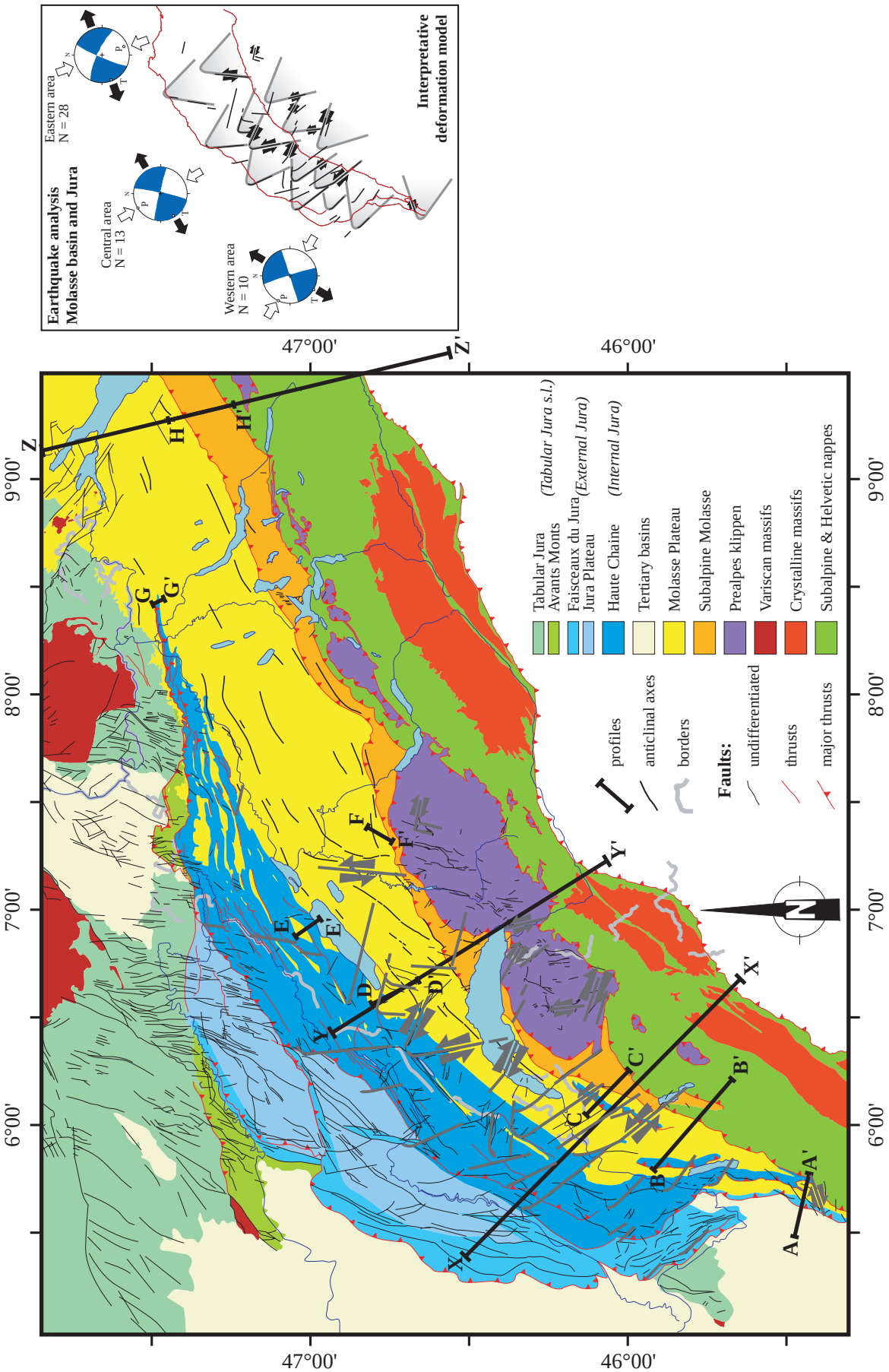
Earthquake analysis
Molasse basin and Jura
Eastern area
N = 28
Central area
N = 13
Western area
N = 10
Interpretative
deformation model
47°00'
46°00'
9°00'
8°00'
7°00'
6°00'
Tabular Jura (Tabular Jura s.l.)
Avants Monts
Faisceaux du Jura (External Jura)
Jura Plateau
Haute Chaine (Internal Jura)
Tertiary basins
Molasse Plateau
Subalpine Molasse
Prealpes klippen
Variscan massifs
Crystalline massifs
Subalpine & Helvetic nappes
profiles
anticlinal axes
borders
Faults:
undifferentiated
thrusts
major thrusts
N
A
A'
B
B'
C
C'
D
D'
E
E'
F
F'
G
G'
H
H'
X
X'
Y
Y'
Z
Z'

CURRICULUM VITAE

Cécile BONNET

cecil-bonnet@caramail.com

Born September 12th, 1979 in Montereau, France

Education

2002-2007	**PhD thesis in Tectonics and Analogue Modelling** Dual-PhD, University of Fribourg (Switzerland) and University Montpellier II, France *"Interactions between tectonics and surface processes in the Alpine foreland: Insights from analogue model and analysis of recent faulting"*
2001-2002	**Master (2nd year) "Structure and Evolution of the Lithosphere"** University Montpellier II "*Morphostructural analysis of surface ruptures due to large magnitude earthquakes: field examples and analogue modelling"* - Multidisciplinary approach using field data, sandbox experiments & aerial photographs
1997-2001	**Bachelor and Master (1st year) in Earth Sciences** University Paris VI, France

Work experience

2002-2007	Assistant in cartography, in analogue modelling and for field trips at the Department of Geosciences, University of Fribourg
2004-2007	Promoter for Fisch.Meier Promotion, Zürich, Switzerland
2002-2005	Webmaster of the Department of Earth Sciences, University of Fribourg

Field experience

2003-2005	Structural & morphological analysis in the Swiss Prealpes
2001 October	Structural analysis of the Alpine Range in Corsica, France
2001 Summer	Structural analysis and mapping in the Ardennes, France
2001 May	Global cross-section of the occidental Alps, France & Italy
2000 June	Structural and paleoenvironmental analysis in the Mesozoic of Barles, French Alps

Skills

Languages	French (mother tongue), English (fluent) and German (read/write/speak)
Softwares	ER Mapper, ArcView GIS, TectonicsFP Microsoft Office, Adobe Photoshop, Illustrator & InDesign, Canvas, EndNote, Macromedia Dreamweaver MX

Publications

C. Bonnet, J. Mosar and J. Malavieille, *Interactions between Tectonics, erosion and sedimentation during the recent evolution of the Alpine orogen - Analogue modeling insights*, Tectonics (submitted 2006).

C. Bonnet, J. Mosar and J. Malavieille, *Surface processes versus kinematics of thrust belts: rates of erosion, sedimentation, and exhumation – Insights from analogue modelling*, Bulletin de la Société Géologique de France (submitted 2007).

J. Mosar, C. Bonnet and J. Malavieille, *Swiss Molasse Basin dynamics: Insights and lessons from analogue modeling*, Basin Research (submitted 2006).

C. Bonnet, J. Mosar and C. Saudan, *Fracture analysis in the Swiss Prealpes Klippen Belt*, Swiss Journal of Geosciences (to be submitted).

Talks

3rd Swiss Geociences Meeting – Zürich, Switzerland (November 2005)
How do uplift, sedimentation and erosion interact in the Alpine evolving orogen from Eocene to Present? – Analogue modelling insights
C. Bonnet, J. Malavieille and J. Mosar

Thrust Belts and Foreland Basins – Rueil-Malmaison, France (December 2005)
How do uplift, sedimentation and erosion interact in the Alpine evolving orogen from Eocene to Present? – Analogue modelling insights
C. Bonnet, J. Malavieille and J. Mosar

Invited talk at the Vrije Universiteit – Amsterdam, Netherlands (February 2006)
Interactions between Tectonics and surface processes in the Alpine evolving orogen during its recent evolution – Analogue modelling insights
C. Bonnet, J. Malavieille and J. Mosar

European Geosciences Union – Vienna, Austria (April 2006)
Influence of erosion and sedimentation on the kinematics of thrust belts: results from sandbox simulations
C. Bonnet, J. Malavieille and J. Mosar

4th Swiss Geociences Meeting – Bern, Switzerland (November 2006)
Tectonics and sedimentation in the Swiss Molasse Basin: Insights and lessons from analogue modelling
C. Bonnet, J. Mosar and J. Malavieille

Posters

GeoMod 2004 – Emmetten, Switzerland (April 2004)
Morphology and structure of active thrust faults surface ruptures: analogue modelling
C. Bonnet, J. Malavieille, S. Dominguez, H. Philip
Landscape, structure and neotectonics in the Swiss and French Prealpes klippen belt
C. Bonnet, J. Mosar

2nd Swiss Geociences Meeting – Lausanne, Switzerland (November 2004)
Fracturing the Prealpes klippen belt
C. Bonnet, J. Mosar, C. Saudan

DRT – Zürich, Switzerland (April 2005)
Transcurrent faulting in the Prealpes klippen belt
C. Bonnet, C. Saudan, J. Mosar

Alpine Workshop – Opatija, Croatia (October 2005)
Transcurrent faulting in the Prealpes klippen belt
C. Bonnet, C. Saudan, J. Mosar

*****

Already published:

Vol. 1 **HILLGÄRTNER, Heiko** (1999) The evolution of the French Jura platform during the Late Berriasian to Early Valanginian: controlling factors and timing (203 pp.).

Vol. 2 **DUPRAZ, Christophe** (1999) Paléontologie, paléoécologie et évolution des faciès récifaux de l'Oxfordien Moyen-Supérieur (Jura suisse et français) (247 pp.).

Vol. 3 **BASSANT, Philip** (1999) The high-resolution stratigraphic architecture and evolution of the Burdigalian carbonate-siliciclastic sedimentary systems of the Mut Basin, Turkey (278 pp.).

Vol. 4 **COLOMBIÉ, Claude** (2002) Sédimentologie, stratigraphie séquentielle et cyclostratigraphie du Kimméridgien du Jura suisse et du Bassin vocontien (France): relations plate-forme – bassin et facteurs déterminants (198 pp.).

Vol. 5 **PICOT, Laurent** (2002) Le Paléogène des synclinaux du Jura et de la bordure sud-rhénane: paléontologie (Ostracodes), paléoécologie, biostratigraphie et paléogéographie (240 pp.).

Vol. 6 **DAPPLES, Florence** (2002) Instabilités de terrain dans les Préalpes fribourgeoises (Suisse) au cours du Tardiglaciaire et de l'Holocène: influence des changements climatiques, des fluctuations de la végétation et de l'activité humaine (158 pp.).

Vol. 7 **HUG, Wolfgang Alexander** (2003) Sequenzielle Faziesentwicklung der Karbonatplattform des Schweizer Jura im Oberoxford und unterstem Kimmeridge (154 pp.).

Vol. 8 **OSWALD, Daniel** (2003) Analyse de l'activité de glissements de terrain et relation avec les conditions climatiques: Exemples dans les Préalpes fribourgeoises (Suisse) (147 pp.).

Vol. 9 **BECKER, Damien** (2003) Paléoécologie et paléoclimats de la Molasse du Jura (Oligo-Miocène): apport des Rhinocerotoidea (Mammalia) et des minéraux argileux (327 pp.).

Vol. 10 **DELALOYE, Reynald** (2005) Contribution à l'étude du pergélisol de montagne en zone marginale (240 pp.).

Vol. 11 **FREUDIGER-BONZON, Jeanne** (2005) Archaeometrical study (petrography, mineralogy and chemistry) of Neolithic Ceramics from Arbon Bleiche 3 (Canton of Thurgau, Switzerland) (187 pp.).

Vol. 12 **STOFFEL, Markus** (2005) Spatio-temporal variations of rockfall activity into forests - results from tree-ring and tree analysis (188 pp.).

Vol. 13 **RAMEIL, Niels** (2005) Carbonate sedimentology, sequence stratigraphy, and cyclostratigraphy of the Tithonian in the Swiss and French Jura Mountains – a high-resolution record of changes in sea level and climate (246 pp.).

Vol. 14 **BRAILLARD, Luc** (2006) Morphogenèse des vallées sèches du Jura tabulaire d'Ajoie (Suisse): rôle de la fracturation et étude des remplissages quaternaires. (226 pp.).

vol. 15 **GOYETTE-PERNOT, Jöelle** (2006) L'Ambroisie: analyse statistique et modélisation numérique de sa trajectoire aérobiologique (274 pp.).

Vol. 16 **TRESCH, Jonas** (2007) History of a Middle Berriasian transgression (Switzerland, France, and southern England) (271 pp.).

GeoFocus is the publication series of the Department of Geosciences, University of Fribourg, Switzerland, and can be ordered at:

Department of Geosciences - Geology and Paleontology
University of Fribourg
1700 Fribourg, Switzerland
http://www.unifr.ch/geoscience/geology

ISSN 1424 - 1463